Improving Immunophenotyping Resolution by Overcoming Autofluorescence with Full Spectrum Flow Cytometry

Article Collection

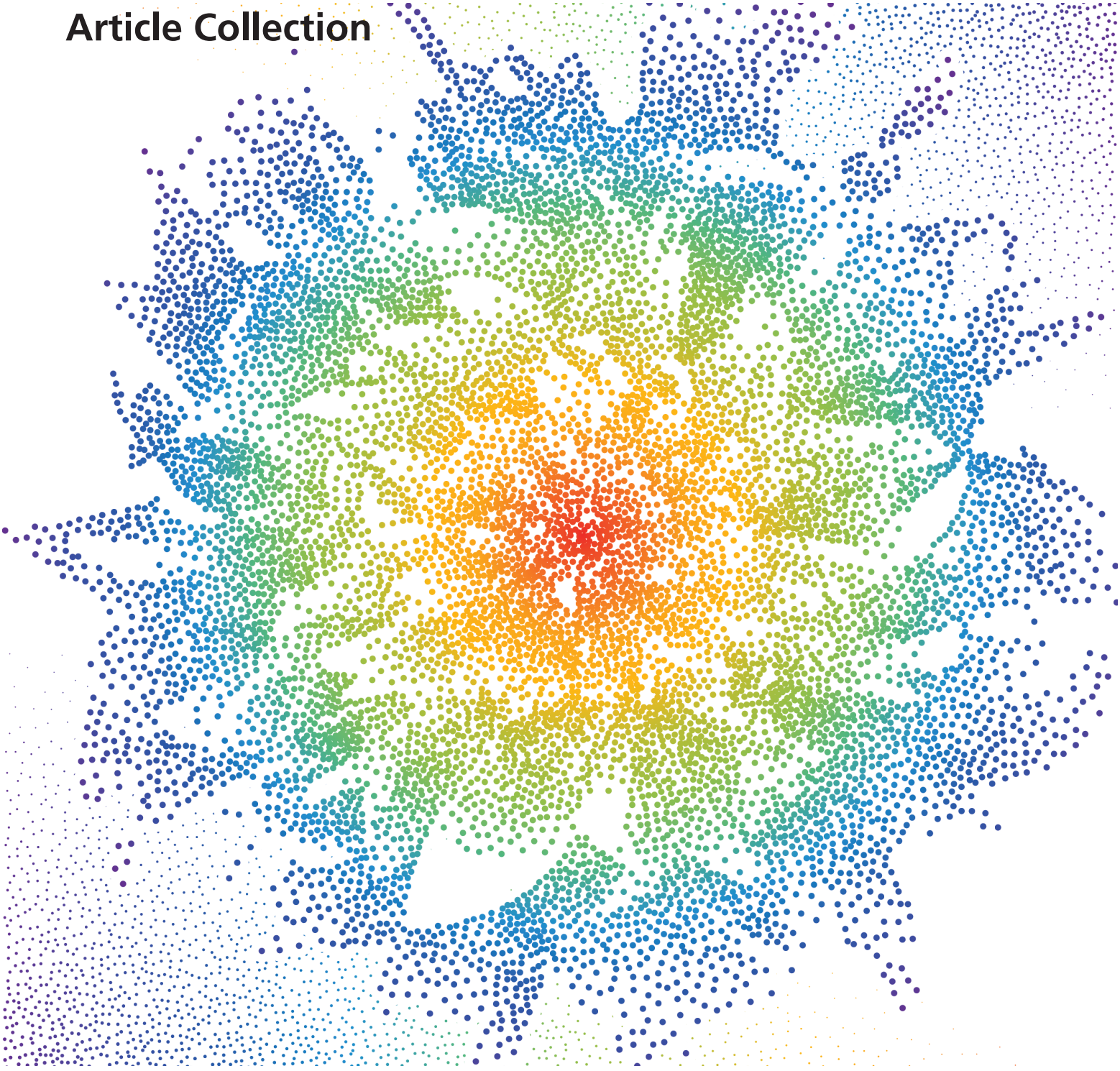

Sponsored by:

WILEY

CURRENT PROTOCOLS
A Wiley Brand

Cytometry PART A
ISAC
Journal of Quantitative Cell Science

CYTEK®
TRANSCEND THE CONVENTIONAL

THE BEAUTY OF EXPRESSION

GIVE YOUR CELLS A VOICE

Your cells have a lot to say. Help them express themselves with high-quality single cell data thanks to Cytek's advanced technology and optimized flow cytometry applications.

- **Streamline** your workflow with highly sensitive, flexible instruments that eliminate the need to reconfigure for every assay
- **Accelerate** discovery with pre-optimized, ready-to-use reagent kits integrated with analysis templates
- **Maximize** efficiency with panel design tools and software that are widget-based and seamless
- **Partner** with highly trained service and application specialists that are ready to assist you with training and support

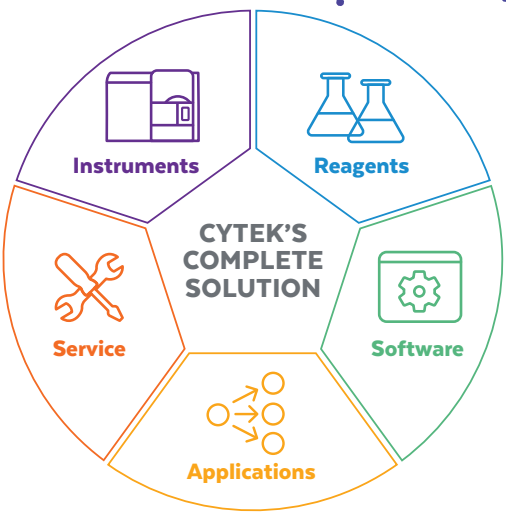

Cytek is committed to providing powerful solutions through scientific innovation. Join the world's most renowned pharmaceutical companies, CRO firms, industrial facilities, and research and academic institutions who have achieved results with our comprehensive approach. **Reveal the Beauty of Cellular Expression.**

CYTEK®
TRANSCEND THE CONVENTIONAL
WWW.CYTEKBIO.COM

Contents

Imprint

© Wiley-VCH GmbH,
Boschstr. 12,
69469 Weinheim, Germany

Senior Account Manager:
Joseph Tomaszewski

Editor:
Róisín Murtagh

Cover image: ©Cytek

Introduction

Spectral flow cytometry has become a game changer in single-cell analysis within research. Early work in measuring cell fluorescence emission spectra led to the development of instruments with improved detection capabilities. These advances included the use of grating-based spectrometers, vidicon detectors, and later multi-anode photomultiplier tubes (PMTs), avalanche photodiodes (APDs), and charge-coupled device (CCD) arrays, which allowed the spectral characteristics of individual cells to be measured. Over time, spectral flow cytometry technology has progressed from a novel approach to a widely spread tool impacting single-cell evaluations.

Spectral flow cytometry is swiftly gaining traction in industrial spheres to tackle challenges, like multicolor immunophenotyping providing processes and superior resolution compared to traditional approaches. This allows greater flexibility in dye selection for multicolor panels and captures autofluorescence from highly fluorescent samples, which can be removed to enhance cell visualization and data analysis. Furthermore, spectral cytometers use a single optical configuration that supports various fluorochromes, reducing the risks of emission mismatch and the need for frequent filter changes typical of conventional cytometers. Additionally, they require fewer lasers, lowering costs and increasing data dimensionality.

APDs are less noisy, improving data clarity and resolution, and are 10 to 100 times more efficient over a wider range of wavelengths. Their compact size also allows for the integration of multiple channels into systems with minimal footprint. These advancements facilitate solutions for the differentiation of overlapping signals and precise assessment of both autofluorescence and external fluorescent markers. In addition, APDs are less expensive, making flow cytometers more affordable.

Cellular autofluorescence has long been considered an unwanted source of background interference, masking signals from weak fluorophores and low abundance markers. Considerable efforts have been made to correct measurements by accounting for autofluorescence signals. Another perspective is that autofluorescence eventually contains rich information about the metabolic or functional state of the cell. Full spectrum flow cytometry (FSFC) provides an opportunity to evaluate the autofluorescent patterns as well as the exogenous fluorescent signals. FSFC provides more sensitive quantitative measurements by accurately accounting for various sources of background noise and autofluorescence [1].

This Article Collection begins with a research paper from Kharraz *et al.* [2] that introduces a novel methodology using FSFC to improve the resolution of myeloid markers in highly autofluorescent biological samples, by extracting multiple autofluorescences. As mentioned above, failure to adequately account for autofluorescence in mixed populations can lead to erroneous conclusions. This is particularly problematic in tissues with high levels of inflammation. The results of this study highlight the potential of FSFC to improve the resolution and accuracy of analysis of highly autofluorescent cells, such as neutrophils, macrophages, and eosinophils.

SpectroFlo software was used in this study as part of a detailed workflow to improve the resolution of the analysis by effectively managing autofluorescence (AF). The software provided a structured approach to handling complex spectral data, facilitating the effective separation of autofluorescence from specific fluorochrome signals. This semi-automated management of autofluorescence allows researchers to gain more precise insights into the phenotypic and functional characteristics of cell populations within complex biological samples. This advancement opens new opportunities for detailed immunophenotyping in areas such as tissue regeneration and inflammation, facilitating a broader understanding of cellular mechanisms and interactions.

Our second publication from Kare *et al*. [3] addresses the challenge of comprehensive immunoprofiling in murine model systems which require advanced immunophenotyping

capabilities that can comprehensively analyze all major leukocyte populations. Existing methods have been limited by the complexity of panel design and the lack of murine-specific tools, preventing a complete understanding of immune dynamics across tissues and treatments. In this context, the study specifically addresses autofluorescence and the implementation of FSFC. These improvements help to effectively separate the fluorescent signal from background autofluorescence.

The development of the OMIP-095 40-color spectral flow cytometry panel addresses these challenges by providing a high-dimensional tool for in-depth immunophenotyping of murine lymphoid tissues. Autofluorescence extraction played a critical role in this study by enhancing the analytical capabilities of the 40-color spectral flow cytometry panel and by improving the clarity and accuracy of the data obtained. It allows the differentiation of leukocyte subsets using a robust set of surface markers, eliminating the need for intracellular staining, and the potential of preserving the analyzed cells for downstream analyses when using a full spectrum sorter. This development represents a significant achievement in FSFC for murine immunophenotyping and has the potential to improve preclinical research and immunophenotyping panel design in the future.

The third research publication presents a protocol for optimizing high-dimensional immunophenotyping with FSFC, developed by Ferrer-Font *et al*. [4]. This protocol addresses the challenges of managing heterogeneous autofluorescence of traditional flow cytometry methods in resolving and differentiating closely related fluorophores, which limits the depth and reliable experimental outcomes of immune system analysis. It further demonstrates how the utilization of FSFC for panel optimization in high-dimensional immunophenotyping assays overcomes these limitations.

The authors provide a comprehensive step-by-step protocol that guides the optimization process, from panel design to troubleshooting. This protocol covers the evaluation of spectral reference controls, antibody titration, adjustment of instrument settings, management of heterogeneous autofluorescence, and evaluation of data quality. Overall, autofluorescence is an important consideration in the study protocols for optimizing the spectral flow cytometry panel, as it directly affects the clarity and accuracy of marker resolution and the overall quality of the data collected.

Our fourth study, published in 2022 by Farrand *et al*. [5] underscores the need for standardized protocols for panel design and analysis, especially for *ex vivo* analysis, where tissue preparation methods must ensure that samples accurately reflect the *in-situ* state of the tissues. The study introduces optimized protocols for processing and phenotyping memory T cells and natural killer T (NKT) cell subsets from different tissues (liver, lung, spleen, lymph node) using FSFC. As previously mentioned, the use of FSFC enables easier characterization and extraction of autofluorescence in difficult-to-analyze tissues.

A detailed 21-color antibody panel is presented for the identification of various memory subsets, including tissue-resident memory (TRM) T cells, which are known to play an important role in adaptive immunity. The protocol also highlights the sensitivity of certain cells, such as liver TRM cells, to processing conditions, advocating for quick processing to maintain cell integrity. It also describes the use of specific autofluorescence tags and autofluorescence extraction techniques to mitigate artifacts caused by autofluorescence. By providing standardized protocols and a comprehensive antibody panel for FSFC, the researchers enable more accurate and detailed analysis of memory T cells and NKT cell subsets in different tissues.

The last study is a protocol for single-cell profiling of microglia that was recently published by Spiteri *et al*. [6]. Microglia, the primary immune cells of the central nervous system, play

a critical role in neuroinflammatory and neurodegenerative diseases. Understanding their function and identification in disease states is essential due to the increasing prevalence of neurodegenerative diseases with societal aging. However, the diagnosis and understanding of those diseases have been hampered by limitations in the accurate identification and analysis of microglia. It has been observed that microglia-specific markers are often downregulated during inflammation, which may have an impact on the autofluorescence characteristics. Autofluorescence can obscure specific signals, compromising the resolution and accuracy of cell population analyses needed to identify and characterize neurological microglia.

To mitigate these issues, the authors recommend the use of autofluorescence extraction techniques. Using spectral cytometry-based technologies and FSFC provides an unprecedented depth of analysis for phenotyping microglia. Spectral cytometry has enhanced the ability to analyze microglial phenotypes by allowing the separation of microglia from monocyte-derived cells, offering improved marker resolution. The authors provide detailed protocols in this study for processing mouse brain tissue for microglia isolation and phenotyping, including steps for single-cell suspension preparation.,—This study represents a significant advance in neuropathologic disease research by introducing high-dimensional methods for single-cell microglial profiling.

Overall, advances in FSFC are set to address significant challenges in high-dimensional cell analysis, with a focus on improving marker resolution and overcoming cellular autofluorescence for more accurate biological insights. FSFC can resolve autofluorescence issues by treating AF as a fluorochrome and separating it from the fluorochrome signal using its inherent ability to measure the entire fluorochrome emission spectrum across multiple lasers and detectors. This has broadened the scope and capability of cytometric analysis in biological research and clinical applications.

We hope that researchers will find this collection of articles useful in their pursuit of knowledge about the latest developments in how spectral flow cytometry has revolutionized the handling of autofluorescence to improve assay resolution. In 2017, Cytek Biosciences introduced Aurora to the flow cytometry community to further support scientific discovery. The Aurora allows users to build larger panels with fewer lasers, thanks to its emission optics design to overcome autofluorescence challenges. For more information, we encourage you to visit Cytek Biosciences to gain a deeper understanding of available options for improving your immunoprofiling process and available applications for FSFC. An Aurora spectral sorter is now available for phenotyping and sorting cells for subsequent assays.

Julian Renpenning, Ph.D.
Scientific Editor

References

[1] Nolan, J.P. (2022). The evolution of spectral flow cytometry. *Cytometry Part A*. DOI: 10.1002/CYTO.A.24566.

[2] Kharraz, Y. *et al*. (2022). Full spectrum cytometry improves the resolution of highly autofluorescent biological samples: Identification of myeloid cells in regenerating skeletal muscles. *Cytometry Part A*. DOI: 10.1002/CYTO.A.24568.

[3] Kare, A.J. *et al*. (2023). OMIP-095: 40-Color spectral flow cytometry delineates all major leukocyte populations in murine lymphoid tissues. *Cytometry Part A*. DOI: 10.1002/CYTO.A.24788.

[4] Ferrer-Font, L. *et al*. (2021). Panel Optimization for High-Dimensional Immunophenotyping Assays Using Full-Spectrum Flow Cytometry. *Current Protocols*. DOI: 10.1002/CPZ1.222.

[5] Farrand, K. *et al*. (2022). Using Full-Spectrum Flow Cytometry to Phenotype Memory T and NKT Cell Subsets with Optimized Tissue-Specific Preparation Protocols. *Current Protocols*. DOI: 10.1002/CPZ1.482.

[6] Spiteri, A.G. *et al*. (2024). High-Dimensional Methods of Single-Cell Microglial Profiling to Enhance Understanding of Neuropathological Disease. *Current Protocols*. DOI: 10.1002/CPZ1.985.

Received: 23 September 2021 | Revised: 30 March 2022 | Accepted: 22 April 2022

DOI: 10.1002/cyto.a.24568

TECHNICAL NOTE

MIFlowCyt

ISAC CYTOMETRY Journal of Quantitative Cell Science PART A

Full spectrum cytometry improves the resolution of highly autofluorescent biological samples: Identification of myeloid cells in regenerating skeletal muscles

Yacine Kharraz[1] | Vera Lukesova[2] | Antonio L. Serrano[2] | Adam Davison[1] | Pura Muñoz-Cánoves[2,3,4]

[1]Application Department, Cytek Biosciences, Inc., Fremont, California, USA

[2]Department of Experimental and Health Sciences, Pompeu Fabra University (UPF), CIBER on Neurodegenerative Diseases (CIBERNED), Barcelona, Spain

[3]Centro Nacional de Investigaciones Cardiovasculares Carlos III, Madrid, Spain

[4]ICREA, Barcelona, Spain

Correspondence
Yacine Kharraz, Cytek Biosciences, Inc., Fremont, CA, USA.
Email: ykharraz@cytekbio.com

Pura Muñoz-Cánoves, Department of Experimental and Health Sciences, Pompeu Fabra University (UPF), CIBER on Neurodegenerative Diseases (CIBERNED), Barcelona, Spain.
Email: pura.munoz@upf.edu

Abstract

Autofluorescence (AF) is an intrinsic characteristic of cells caused by the presence of fluorescent biological compounds within the cell; these can include structural proteins (e.g., collagen and elastin), cellular organelles, and metabolites (e.g., aromatic amino acids). In flow cytometric studies, the presence of AF can lead to reduced antigen and population resolution, as well as the presence of artifacts due to false positive events. Here, we describe a methodology that uses the inherent ability of full spectrum cytometry to treat AF as a fluorochrome and to thereby separate it from the other fluorochromes of the assay. This method can be applied to complex inflamed tissues; for instance, in regenerating skeletal muscle we have developed a 16-color panel targeting highly autofluorescent myeloid cells. This represents a first step toward overcoming technological limitations in flow cytometry due to AF.

KEYWORDS
antigen resolution, Aurora, full spectrum, macrophages, skeletal muscle, tissue regeneration

1 | INTRODUCTION

The inflammatory response initiated by different immune cell types is critical to mediate tissue repair after injury [1]. Although conventional histological methods allow cells within a tissue to be identified and spatially localized, their ability to analyze the full array of phenotypic cell populations and activation states is limited. This constraint can be overcome by using alternative methods, such as flow cytometry, a technique that enables a more in-depth characterization of individual cell populations using multiple surface markers and intracellular proteins. This application also allows cell populations to be sorted and used for further studies.

An important drawback of using flow cytometry for complex tissue samples with high levels of inflammation is the presence of high levels of autofluorescence (AF) of varied spectral output from the constituent cell fractions. This can make it difficult for conventional flow cytometry to appropriately assign photons to a particular dye conjugate or the cell background, thus decreasing the signal-to-noise ratio and leading to a loss in antigen resolution. The failure to adequately account for the impacts of AF can result in erroneous conclusions [2–4]. Current flow cytometry protocols to reduce the impact of AF in complex tissue samples represent an imperfect solution at best [5–7]. The differences in lineages, activation, and differentiation states of cell fractions in inflamed tissues increase the variance of the cellular constituents, thereby escalating the complexity of the AF and complicating the application of current AF management techniques in flow cytometry.

Skeletal muscle shows a remarkable capacity to regenerate after injury and is easily amenable for experimental manipulation [8], making it a particularly appropriate model for assessing the role of inflammation in tissue repair. During regeneration, skeletal muscle undergoes a series of tightly regulated steps that require the coordination of stem cells with several muscle-resident and blood-derived cell populations to restore tissue homeostasis [9]. The hematopoietic system has an essential contribution in this process [10–15]. In particular, the monocyte–macrophage lineage has a critical function,

exemplified by a complete failure of regeneration in injured skeletal muscle of monocyte-depleted mice [16]. Monocytes and macrophages play major roles in phagocytosing tissue debris, contributing to transient matrix support [17] and providing pro-myogenic growth factors and cytokines [18]. Macrophages are highly plastic and change their phenotype quickly in response to different microenvironment cues [1]. For that reason, phenotypical classification of these cells has been controversial over the decades [19], with in vivo profiles that do not match the ones observed in in vitro paradigms. Therefore, understanding the nature and role of each macrophage fraction in tissue regeneration requires using high-dimensional analysis tools to better capture the complexity of this cell lineage.

Despite the advent of new conventional cytometers that enable the simultaneous measurement of up to 30 parameters, there is no study on the role of macrophages in muscle regeneration that have used flow cytometry to detect more than 10 antigens. This can be attributed at least in part to the complexity introduced by AF, which impedes using certain fluorochromes due to the high AF emission at certain wavelengths. Indeed, macrophages produce collagen [17] and express NADPH [20], two highly autofluorescent cellular components that emit mostly in the short wavelength range [21, 22]. In addition, they also take up iron-containing molecules through their expression of CD163 [23]. Iron is then incorporated and stored for further recycling into heme [24], a protein complex that strongly emits in the red and infrared region of the spectrum. Thus, the AF features of macrophages within tissue can vary greatly depending on the activation status and function of the macrophages, with their cellular components emitting across the whole spectrum. Consequently, macrophage AF can potentially interfere with any fluorochrome used in cytometric assays and can therefore compromise the detection of low-density antigens that might be crucial for their identification and classification. This is one of the key reasons why the myeloid compartment has been incompletely characterized by flow cytometry in the context of the inflamed skeletal muscle.

Full spectrum cytometry uses single-stained controls to provide pure spectral signatures of fluorophores as references to an algorithm, which then calculates the contribution of photons from each fluorophore to the signal of the multicolor tube captured across a detector array, a process named spectral unmixing [25]. Because the full spectrum of all cellular AF present in a sample from a given tissue is captured, AF can be isolated and treated as any other fluorochrome within the assay. As with a fluorochrome, it is imperative to use a reference control matching the AF of the cells present in the multicolor sample to accurately reassign the photons to this new autofluorescence parameter during the unmixing process. Because the AF emitted by one cell is the product of the emission spectra of several cellular components with different optical properties and varying concentrations, isolating the AF of a cell population involves working with a combined spectral signature that is the mean of a continuum of slightly different AF spectra.

Here, we describe a methodology in which the multiple AF spectra present in a cell sample are treated in a comparable fashion as the fluorochrome conjugates included in the assay using a full spectrum cytometer. The purpose of this procedure is to capture as many different AF spectra as possible from the unstained sample. These AF spectra are then used in the unmixing algorithm to accurately assign AF produced photons to newly derived AF parameters instead of being misassigned as photons derived from the exogenous fluorochromes on our antibody (Ab) conjugates for a given particle. A simplified model of a highly autofluorescent sample was first created by mimicking AF on compensation beads using fluorochrome-conjugated antibodies, whose emissions were tailored to imitate the AF emission of biological material. These particles were then used to assess and refine an approach to best manage the AF before evaluating this approach on biological models.

2 | MATERIAL AND METHODS

2.1 | Animals

8- to 12-week-old male C57BL/6J mice were used. Each animal procedure used in this work was supervised by the Ethical Committee of Animal Experimentation of the PRBB (CEEA-PRBB) and has been previously authorized by the corresponding Catalan committee, the Section for the Domestic Animal Protection, General Direction of Environmental and Nature Politics, Department of Territory and Sustainability.

2.2 | Induction of muscle regeneration

Mice were anesthetized with ketamine and xylazine (80:10 mg/kg, intraperitoneally). Regeneration of skeletal muscle was induced by intramuscular injection of cardiotoxin (CTX, Latoxan; 10^{-5} M) in the tibialis anterior muscle of the mice as described previously [34]. At 3 days post-injury, mice were euthanized, and the tibialis anterior muscle was collected and prepared for flow cytometric analysis.

2.3 | Cell suspension preparation for analysis by flow cytometry

Muscles were mechanically disaggregated and dissociated in Ham's F10 medium containing Liberase (0.1 mg/g muscle weight; Roche®, 5 mg/mL) at 37°C for 2 h, then successively filtered on 70 and 40 μm nylon filter. Cell suspensions were extensively washed with PBS before being incubated in lysis buffer (BD Pharm Lyse™) for 10 min on ice, re-suspended in PBS with 1% fetal bovine serum (FBS) and counted. Cells were resuspended at 1×10^6 cells in 100 μl. Fc receptors were first blocked for 10 min on ice with mouse BD Fc Block™ (BD Biosciences®). 5 μl of True-Stain Monocyte Blocker™ (Biolegend®) and 10 μl of Brilliant Stain Buffer Plus (BD Biosciences®) were then added to the cell suspension. A first staining step with PE-Cy7-conjugated anti-MertK (Thermofisher®) for 15 min on ice was necessary to cleanly stain macrophages. A mix of the following antibodies was then added to the cell

suspension for 30 additional min on ice: eFluor 450-conjugated anti-CD11b (Thermofisher®), BV570-conjugated anti-Ly6C (Biolegend®), BV605-conjugated anti-CD115 (Biolegend®), BV650-conjugated anti-Siglec-F (BD Biosciences®), BV711-conjugated anti-CX3CR1 (Biolegend®), BV785-conjugated anti-F4/80 (Biolegend®), VioBright FITC-conjugated anti-MHCII (Miltenyi), Spark Blue 550-conjugated anti-Ly6G (Biolegend®), PercP-conjugated anti-CD45 (Biolegend®), PE-conjugated anti-CD163 (Biolegend®), PE-Dazzle 594-conjugated anti CD169 (Biolegend®), PE-Cy5-conjugated anti-CD11c (Thermofisher®), Alexa Fluor 700-conjugated anti-CD3 (Biolegend®), Alexa Fluor 700-conjugated anti-NK1.1 (Biolegend®), Alexa Fluor 700-conjugated anti-CD19 (Biolegend®), APC-eFluor 780-conjugated anti-CD64 (Thermofisher®). Cells were then washed and resuspended in 300 µl PBS with 1% FBS. DAPI was added at a final concentration of 10 ng/mL for 5 min before the acquisition of the samples to mark dead cells. All samples were acquired on a Cytek Aurora® 4 laser (V, B, YG, & R configuration) full spectrum cytometer. Acquisition, spectral unmixing, and analysis were performed using Cytek SpectroFlo® V3.0.1 software.

2.4 | Generation of artificial autofluorescence

UltraComp eBeads™ (Thermofisher®) were stained with the following antibodies to emulate autofluorescence: Alexa Fluor 532-conjugated anti-human CD4 (Thermofisher®), Alexa Fluor 647-conjugated anti-human CD28 (Biolegend®), BV480-conjugated anti-human CD27 (BD Biosciences®). Briefly, stock solutions of antibodies were first diluted at 1-to-100 before being added to 10 different mix cocktails at varied volumes. Volumes of diluted stock solutions are indicated in µl in Table S1. The 10 mix cocktails were then used separately to stain 10 tubes of beads in PBS with 1% FBS for 10 min at room temperature. Beads were extensively washed and pooled together to generate a population of beads bearing 10 different artificial AFs.

2.5 | Staining of beads bearing artificial AF

BV510-conjugated anti-mouse CD3 (Biolegend®), BV785-conjugated anti-mouse F4/80 (Biolegend®), FITC-conjugated anti-mouse CD45 (BD Biosciences®), PE-conjugated anti-mouse CD163 (Biolegend®), and Alexa Fluor 700-conjugated anti-mouse CD3 (Biolegend®) were used to stain separately five tubes of beads bearing artificial AF for 10 min at room temperature (0.25 µg/test). Beads were then washed extensively before being pooled to generate the multicolor tube.

2.6 | Data analysis

All data were analyzed using SpectroFlo® 3.0.1 (Cytek® Biosciences Inc., Fremont, California) or OMIQ® (OMIQ® Inc). When side-by-side comparisons of dot plots were required to assess unmixing quality, bi-exponential scales were manually set with the same values to avoid any scaling artifacts.

2.7 | Statistical analysis

Data were analyzed using GraphPad Prism® 8 (GraphPad® Software). Individual values were plotted as scattered plot with mean and standard deviation displayed on the graph. Mann–Whitney test was performed to compare between two groups. P-value smaller than 0.05 was considered as significant.

3 | RESULTS

3.1 | Bead-based model as a proof of concept

To refine and validate the use of multiple AF as fluorochrome tags, a five-color panel was developed including BV510, BV785, FITC, PE, and Alexa Fluor 700 as reporter labels using universal anti-IgG conjugated beads bearing artificial AF. Artificial AF spectra were generated on compensation beads using a combination of fluorochromes, including those that have spectral profiles overlapping the emission ranges of the reporter labels used in the assay, to emulate how the artificial AF would impact their resolution in a multicolor (MC) sample (Figure S1A). To achieve this, 10 different mix cocktails with varied low concentrations of BV480-, Alexa Fluor 532-, or Alexa Fluor 647-conjugated antibodies were prepared to separately stain 10 tubes of beads (Table S1A). This allowed us to generate bead populations with very close, but unique, autofluorescence spectral signatures (Figure S1B). After staining, the beads were extensively washed and pooled into an individual tube to be acquired as a single sample. This resulted in a bead population with a continuum of AFs approximating those observed in highly autofluorescent biological samples. From this point onwards, this control will be referred to as unlabeled beads with artificial AF. The unlabeled beads without artificial AF are defined as being the same beads without BV480, Alexa Fluor 532, and Alexa Fluor 647 staining. In this model, the fluorochromes used to emulate AF highly overlap with some of the reporter labels incorporated to model antigen (Ag) recognition (BV510, FITC, and Alexa Fluor 700, respectively) while their spectra should affect BV785 and PE resolution to a lesser extent. Half of the unlabeled beads with artificial AF were kept untouched for use as an unstained population, while the other half was distributed into five tubes and stained separately with the reporter labels. These were then washed and pooled back together alongside the unlabeled beads with artificial AF only, before being acquired.

Following sample acquisition, four unmixing strategies were implemented (Figure 1A):

- Strategy 1: Default unmixing in SpectroFlo® (without AF Extraction) using the ordinary least squared (OLS) algorithm: the most negative particles (the unlabeled beads with no artificial AF) were used as the unstained control. The five reporter labels were used as single stained reference controls for spillover calculation.
- Strategy 2: Default unmixing in SpectroFlo® (with single AF Extraction) using the OLS algorithm: the unlabeled beads with artificial

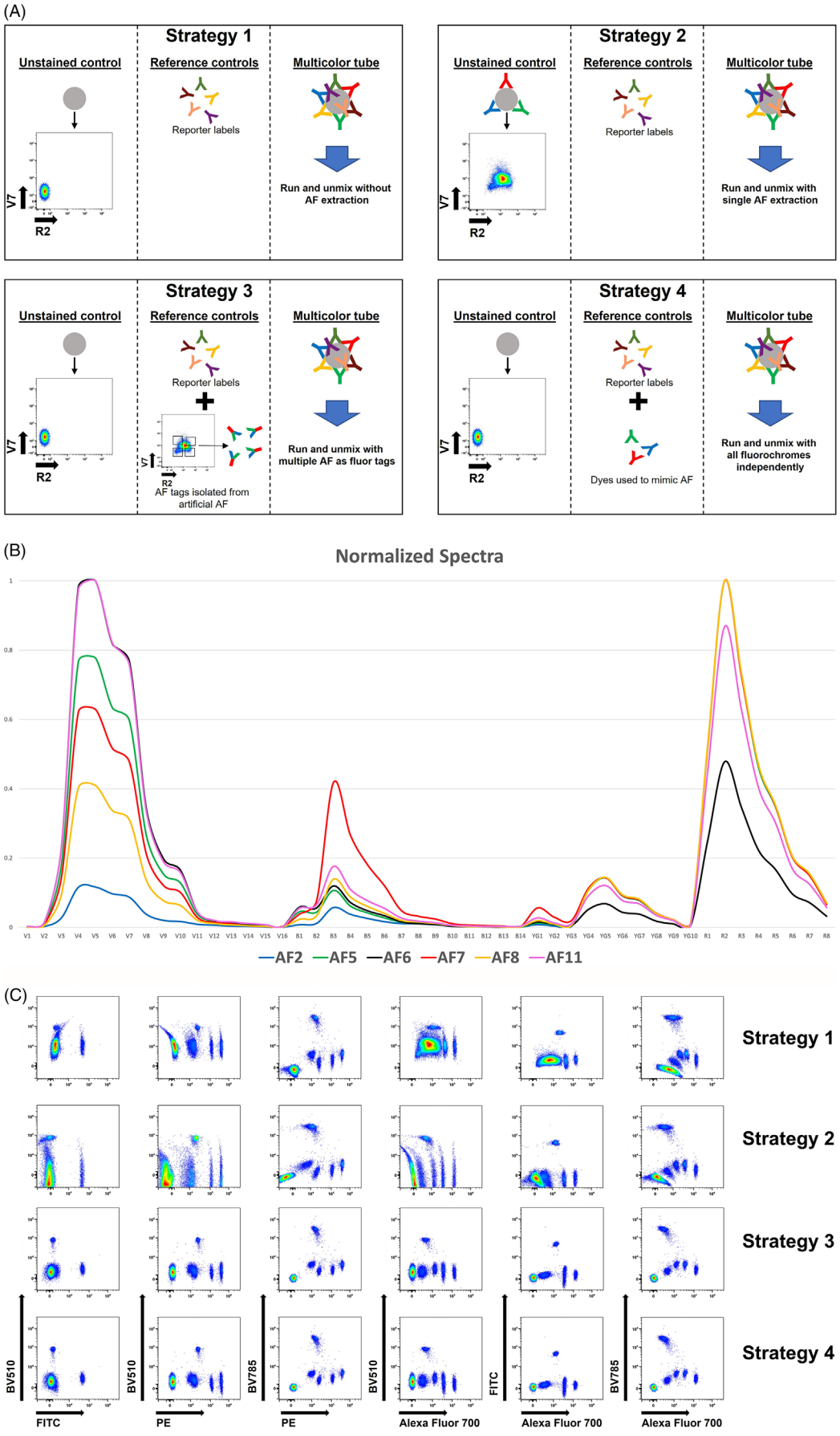

FIGURE 1 Legend on next page.

AF were used as the unstained control for the AF extraction. The five reporter labels were used as single stained reference controls for spillover calculation. Unmixing in this manor would assign photons coming from the single AF spectrum to its own unique parameter.

- Strategy 3: Unmixing with multiple AF as fluorochrome tags using the OLS algorithm: the most negative particles (the unlabeled beads with no artificial AF) were used as the unstained control. Different AF spectra were identified and isolated from the unlabeled beads with artificial AF. These were then introduced into the experiment alongside the five reporter labels as single stained reference controls for spillover calculation. Unmixing in this manor would assign photons coming from each of the AF spectra to their own unique parameters.
- Strategy 4: Experiment control using the OLS algorithm: the most negative particle (the unlabeled beads with no artificial AF) were used as the unstained control. The five reporter labels plus the three fluorochromes used to mimic the AF were separately used as single stained reference controls for spillover calculation. This strategy demonstrates the optimum unmixing based on providing the algorithm with the best possible, "pure", spectra for each of the fluorochrome constituents used to generate the artificial AF.

For strategy 3, it was necessary to first identify, characterize, and extract all the observable spectra found within the unlabeled beads with artificial AF. For this, we examined the signal emitted by our artificially derived autofluorescent particles in all 48 detectors of the system. Here we compared all parameter permutations as bimodal plots, to identify the combination that best separated all the differing AF spectral signatures present within the sample. Each population was independently gated and exported as a derived FCS file containing the pure spectra for these populations. The gating strategy was set with Boolean gates using the NOT operator to avoid capturing the same bead population multiple times (Figure S1C). Through this process, the whole bead population could be divided into 13 subpopulations. The identification of 13 AF signatures in this process rather than 10 (three more than the 10 artificial AF that were assigned to the compensation beads) is likely to be attributed to the potential duplication of some spectra due to the manual identification and extraction of all the different populations. To refine and evaluate the uniqueness of the 13 AF spectral signatures and to remove duplicates, we utilized the QC Controls tool within the unmixing wizard of SpectroFlo® with a specific focus on the Similarity™ Index.

The Similarity™ Index tool within the SpectroFlo® software has been developed by Cytek® Biosciences to determine the degree of similarity, and the ability to mathematically distinguish one spectrum from another, based on the spectral uniqueness of a given pair of signatures. It ranges from 0 to 1 and quantifies how close two spectral signatures are to each other. For instance, two spectral signatures with no spectral overlap, such as BUV395 and APC, have a similarity of 0, while fluorochromes that strongly overlap, such as BB515 and FITC, have a similarity of 0.98, which is considered as a threshold; above this, two spectral signatures cannot be separated by the unmixing algorithm and therefore are considered not to be compatible.

To incorporate these multiple AF into our unmixing assessment, all AF spectral signatures must be introduced into the software as single stained controls in a comparable way to exogenous fluorochromes. Thus (as for any single stained control used in flow cytometry), using AF as a fluorochrome tag requires an appropriate negative population that matches the AF of the particle bearing the spectral signature of the considered fluorophore. In our study, as we were working with the AF itself, we needed to derive a negative control with extremely low AF, as close as possible to that of the detector background noise; for this, we used unlabeled beads without AF (Figure S1D).

Once the AF spectral signatures were reintroduced in the SpectroFlo® software as reference controls, the unmixing wizard provided an easy workflow to access the similarity matrix containing the similarity indices of each reference control paired two-by-two. This facilitates the identification of identical spectral signatures with a Similarity™ Index (SI) above 0.98. The determination of impactful AF spectra to be incorporated into the unmixing process for use in our end analysis was performed as a three-step process:

1. All extracted spectra were ranked based on their equivalency in spectral signature for each AF pairing based on the SI matrix (Figure S1E). We then selected the AF with the lowest number of equivalent spectral signatures. This was followed by selecting,

FIGURE 1 (A) Unmixing strategies used to resolve reporter labels. For all the strategies, single stained beads for the five reporter labels were used as reference controls, and the multicolor sample (MC) is always the same: beads with artificial autofluorescence (AF) stained with five reporter labels (BV510, BV785, FITC, PE, and Alexa Fluor 700). Strategy 1: unlabeled beads without artificial AF were used as the unstained control. Unmixing was performed without AF extraction. Strategy 2: unlabeled beads with artificial AF were used as the unstained control. Unmixing was performed with AF extraction. Strategy 3: unlabeled beads without artificial AF were used as the unstained control. Additionally, distinct AF spectra manually isolated from the population of unlabeled beads with artificial AF were used as reference controls. Unmixing was performed without AF extraction. Strategy 4: unlabeled beads without artificial AF were used as the unstained control. Single stained beads for the three fluorochromes used to mimic AF (BV480, Alexa Fluor 532, and Alexa Fluor 647) were used as reference controls. Unmixing was performed without AF extraction. As this strategy uses the pure spectra for each of the constituent dyes (reporter and artificial AF) it provides more accurate and complete information to unmix the different spectra present in the multicolor tube allowing for optimal unmixing, it was used as experimental control. (B) Normalized spectral signature overlays of the six artificial AFs used along with the single stained reference controls for the label reporters to unmix as described for strategy 3. (C) Comparing the results for each unmixing strategy, strategy 3 is the most similar to the experiment control (strategy 4).

sequentially, the next AF with the next lowest number of equivalent signatures and repeating this process until we vetted the uniqueness of each AF (Figure S1F).

2. When two AF spectra had a SI above 0.98 (therefore are virtually identical) and the same number of equivalent signatures, brightness was then considered as an additional selection criterion. In these circumstances we selected the AF with the highest median fluorescent intensity (MFI) in its primary peak detector as those AFs share the same primary detector. Of the AF spectra pool selected in this and the previous step, we reintroduced these AF spectra as fluorochrome tags into an experiment alongside the single stained reference controls for the reporter labels. The unmixing quality was then evaluated by comparing data resolution with the experimental control (strategy 4).
3. As a supplementary step, through an incremental process, we eliminated the dimmest AF spectra from the experiment and performed a visual assessment of the unmixing quality by comparing the reporter labels' resolution with the experimental control (strategy 4). This process was then repeated until the AF spectra selected stopped providing a comparable outcome in unmixing quality and resolution to that of the experimental control.

It is important to note that the first two AF vetting steps reduced the pool of spectra to be used as AF tags to 6: AF2, AF5, AF6, AF7, AF8, and AF11 (Figure 1B). The selected AFs were then used as reference controls along with the single stained controls for the reporter labels BV510, BV785, FITC, PE, and Alexa Fluor 700 to unmix the data as described for strategy 3. Unmixing strategies 1, 2, and 3 were then assessed by comparing reporter label resolution and unmixing quality with the experimental control (strategy 4).

As expected, the default unmixing with no AF extraction (strategy 1) showed a substantial loss of resolution, especially in the BV510 and Alexa Fluor 700 channels (Figure 1C, strategy 1, column 4), when compared to the experiment controls (Figure 1C, unmixing strategy 4, column 4). The loss in resolution was most clearly visualized in the Alexa Fluor 700 parameter as a complete merging of the two dimmest populations with the artificial AF of the unstained population. This correlates with our expectation that BV510 and Alexa Fluor 700 would be the reporter labels most affected by the artificial AF generated from BV480 and Alexa Fluor 647 staining, respectively, due to their highly overlapping emission spectra. On the other hand, despite substantial overlap between the FITC reporter label and Alexa Fluor 532 (composing the artificial AF), we observed only a minor detrimental impact on FITC resolution. This can be attributed to the dimness of Alexa Fluor 532, which results in less photon contribution from this AF into the FITC emission wavelength range. Treating the whole artificial AF as if it was unique had a poor outcome as default unmixing with a single AF extraction led to a strong distortion of the data that generated super-negative MFI in the BV510 and FITC reporter label parameters (Figure 1C, strategy 2). Unmixing with multiple AF as fluorochrome tags (Figure 1C, strategy 3) was very similar to the experiment control and exhibited few variations regarding the position and resolution of each population. This occurred despite our inability to isolate the 10-bead populations originally used to generate the artificial AF due to the high similarity of some of the AF spectra in the beads with artificial AF. Thus, it demonstrates that even when dealing with the most extreme disparate spectra and brightness, this approach can better resolve populations and achieve results with a high degree of parity to those of the experimental control (Figure 1C, strategy 3 vs. strategy 4).

These data show that unmixing using these six AF tags lead to a resolution very close to that of the experimental control (strategy 4). However, it did not allow us to determine if all six AFs had an equal impact in strategy 3, or, if by removing more AFs we could further improve the resolution. Therefore, in compliance with step 3, we decided to reduce the number of AFs used as fluorochrome tags by iteratively removing AFs one by one. This was implemented through removing the AF with the lowest MFI in its peak channel and observing the impact on unmixing quality and resolution relative to the experimental control. As shown in (Figure S1G), it was found that the two dimmest spectra (AF7 and AF11) could be removed bringing the resolution even closer to that of the experimental control (strategy 4) through small improvements in the BV510 and FITC parameters. Although we could continue this process by further reducing the AF included to three AFs, it was observed that this did not have any detrimental or positive effects on data visualization. Reducing the AFs beyond this point with the inclusion of only two AFs, resulted in an unacceptable loss in data resolution and unmixing quality of the MC sample. At present, we have not yet defined a threshold MFI value for the selection of what AFs to include in strategy three from the vetting process. We believe this threshold is multi-factorial, and considerations require a broader range of controlled testing to establish all the impactful factors. This means that currently we are using imprecise criteria to remove unique but unnecessary AF whose presence could increase the potential spread within the unmixed MC sample and decrease resolution.

Overall, comparing the unmixing strategies, this model shows that using multiple AFs as fluorochrome tags in a sample with a defined, but highly varied AF, provides a robust account of the AF with better antigen resolution than that observed with unmixing strategies 1 and 2. Notably, it suggests that effective unmixing of the complex unstained bead AF spectra does not require the use of all of the AF populations, but rather just those spectra whose exclusion exerts the most negative impact on data resolution in the panel. This is determined based upon the degree of spectral dissimilarity to one another, their brightness, and the distribution of this brightness between each bead particle.

3.2 | Five-color panel to analyze macrophage infiltration into injured skeletal muscle

We used skeletal muscle injury to explore the efficacy of the methodology of using multiple AFs as tags in complex biological samples. Acutely injured muscle is of particular interest, as it is massively infiltrated by inflammatory cells and demonstrates varied and high AF,

when compared to other tissues (such as the myeloid cells from steady state spleen), with most of the AF being emitted following excitation by the violet and blue lasers (Figure S2A). The nature of the injury and the regeneration of the tissue results in highly dynamic changes in the AF spectra present over time. This is determined by the differential in types and activation states of the cells present in the tissue at a given time point. Based on the potential variation of AF by sampling tissue at different time points post-injury, we chose a single time point for all donor mice to minimize this variation. Skeletal muscle at 3 days post-injury was chosen as it is an inflection point in the progression of muscle regeneration. At this point, monocytes start differentiating toward a macrophage phenotype while eosinophils and neutrophils are still present, albeit at a lower frequency than during the prior post-injury stages. This ensured that cells from each myeloid subpopulation could be captured.

To evaluate the robustness and efficacy of the unmixing with multiple AF as fluorochrome tags strategy in highly complex heterogenous tissue with bright AF, we used a small five-color panel. This approach maximally reduces any data spreading that could be attributed to overlap between spectrally close fluorochromes, thereby allowing the impact of complex AF to be more cleanly assessed. The first three unmixing strategies used in the previous bead-based model were compared in the murine injured skeletal muscle model to assess their performance. Performance was determined by the antigen- (Ag) specific marker label's resolution, unmixing quality, and the frequency of immune subsets identified based on gating from the FMO controls. Unlike with the bead-based model, we were not able to set an experimental control listed as strategy 4 in the bead-based model, as it is impossible to have single stain reference controls for all the individual cellular compounds that compose a cell's AF.

To appropriately unmix any unique AF spectrum present in the MC tube, it was essential to identify the dimmest possible spectrum present in the unstained sample. This spectrum would closely reflect the background signal on all 48 fluorescent detectors of the acquisition system and would be defined as the unstained control. This would ensure that as many photons as possible could be assigned appropriately to the relevant AF defined as a fluorochrome tag and not to the background detector noise. This background signal was obtained by gating on the events having the lowest possible signal in the detector V7 and B3 as those are the two detectors with the highest AF signal. They were then extracted as a new FCS file to be used as the unstained control (Figure S2B).

Three unmixing strategies were assessed for unmixing accuracy:

- Strategy 1: Default unmixing in SpectroFlo® (without AF Extraction) using the OLS algorithm: the lowest intensity spectrum in the unstained disaggregated skeletal muscle sample that most closely reflected the background detector signal noise for all 48 fluorescence detectors was used as the reference group unstained control (Figure S2B). Single stained reference controls were all acquired with UltraComp eBeads™ for the five Ag-specific marker labels and used for spillover calculation.
- Strategy 2: Default unmixing in SpectroFlo® (with single AF Extraction) using the OLS algorithm: unstained, disaggregated skeletal muscle was broadly gated based on scatter to be used as the reference group unstained control (Figure S2B). Single stained reference controls were all acquired with UltraComp eBeads™ for the five Ag-specific marker labels and used for spillover calculation. Unmixing in this manor would assign photons coming from the single AF spectrum based on the broad scatter gate to its own parameter.
- Strategy 3: Unmixing with multiple AF as fluorochrome tags using the OLS algorithm: the lowest intensity spectra in the unstained disaggregated skeletal muscle sample that most closely reflected the background detector signal noise for all 48 fluorescence detectors was used as the reference group unstained control (Figure S2B). Distinct AF spectra were identified and isolated from the unstained sample then introduced into the experiment alongside the single stained reference control for the five marker labels and used for spillover calculation. Unmixing in this manor would assign photons coming from each of the AF spectra to their own parameters.

For strategy 3, it was necessary to first identify, characterize and extract all the observable spectra found within the unstained sample. As with the bead-based model this was carried out by assessing all parameter permutations as bimodal plots and identifying the best bimodal pairings to separate the distinct AF spectral signatures present in the unstained sample. Each population was independently gated, and then exported as an FCS file using a Boolean gating NOT operator to minimize spectra duplications until all spectra present had been captured (Figure S2C, step 1). This process was then followed by a further "purification" step: each spectrum was imported back into a new experiment to identify any potential contamination by another spectra. These contaminations are reflected by a high degree of signal intensity variation in some detectors of the system. Where two or more populations were observed, these were then independently gated on and exported as new AF spectra FCS files (Figure S2C, step 2). In this manor, we oversampled the spectra present in the unstained sample but ensured that those taken forwards are as pure as possible with the knowledge that any duplicated AF spectrum would be removed in the vetting process. Following this, we then imported the AF spectra FCS files into a new experiment and used the SI matrix to qualify the different AFs as described previously (Figure S2D). This led us to take forward five AFs (AF1, AF4, AF7, AF9, and AF11) with unique spectra and a low degree of equivalency based on their SI. Each signature corresponded to populations with different morphological features, as visualized by plotting forward scatter (FSC) against side scatter (SSC) (Figure 2A). Overlays of the normalized AF spectra show the differences in AF between subpopulations (Figure 2B). These five spectra were then reintroduced as fluorochrome tags along with the single stained reference controls for the marker labels included in the assay.

As in step 3 of the bead-based model, for the determination of those AF spectra critical for optimal unmixing to be incorporated in

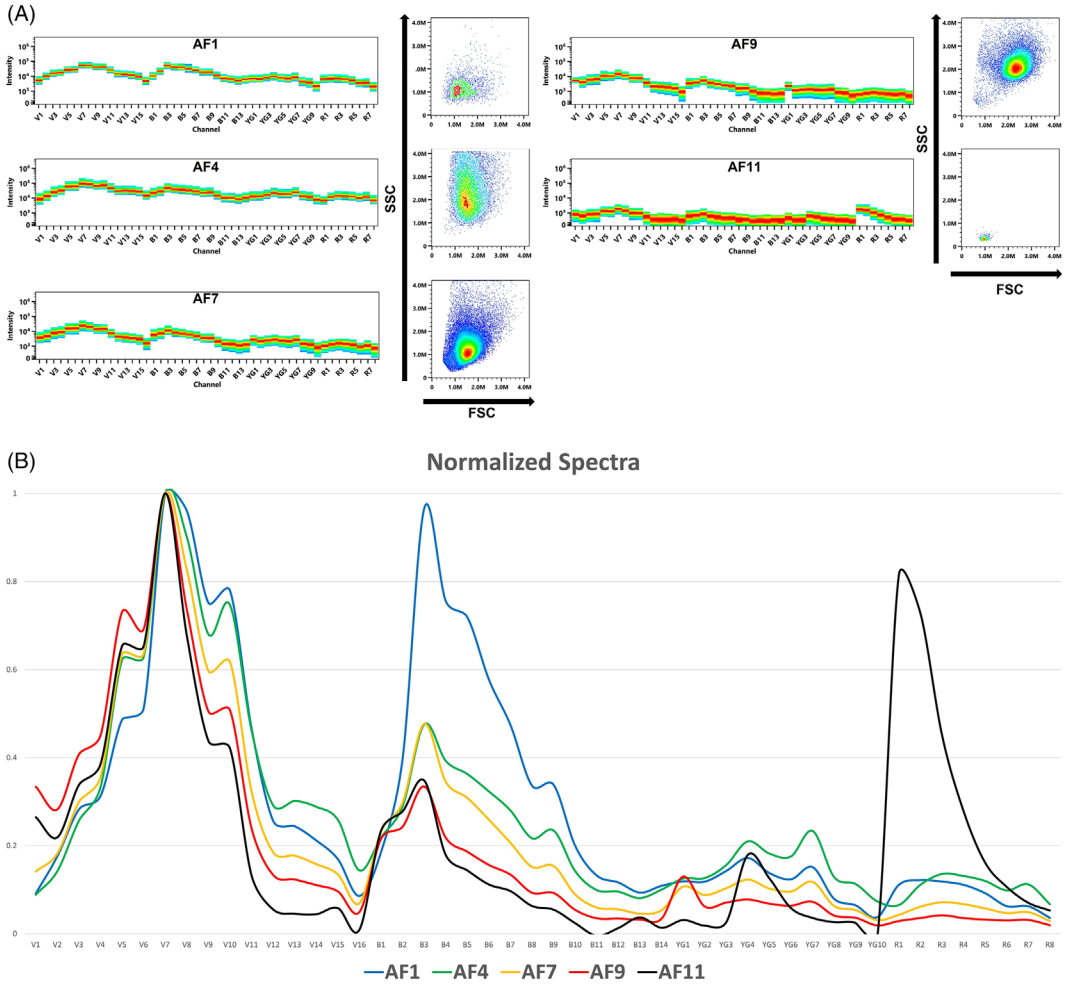

FIGURE 2 (A) Spectral signatures of the distinct AFs extracted from unstained mouse skeletal muscle 3 days post-injury. FSC versus SSC dot plot of the corresponding subpopulation is shown alongside each signature. (B) Normalized spectral signature overlays of the five AF used along with the fluorochrome single stained reference controls to unmix as described for strategy 3. (C) Five-color panel: after gating out doublets and DAPI$^+$ dead cells, macrophages were defined as CD45$^+$ CD11b$^+$ F4/80$^+$ MertK$^+$. For each unmixing strategy, the MertK$^+$ gate was set using the FMO control and adjusted to account for false positive events due to high AF. (D) Quantification of macrophages based on their co-expression of F4/80 and MertK for the three unmixing strategies. Experiment performed in triplicate with $n = 6$. Statistical significance: Mann–Whitney test (*$p < 0.05$; **$p < 0.005$)

unmixing strategy 3, we assessed the unmixing quality using the five selected AFs listed above and then incrementally removed the AFs. These were removed sequentially starting with the spectrum with the dimmest signal on its primary peak detector and then moved to the next dimmest spectrum until there was a loss in the unmixing quality and reporter label resolution. Because we did not have an experimental control as a reference, it was necessary to assess the quality of the unmixing by evaluating the mitigation of spread and the improved resolution, and by using our knowledge of the tissue biology. This third and final selection step is the most complicated to apply as it relies on a subjective manual assessment of the unmixing quality. Through this process, we were able to reduce the number of AF spectra used as tags in the unmixing from 5 to 4. This was achieved by removing AF11, as it had the lowest MFI output in its peak detector, which resulted in no detrimental effects on the unmixing quality and Ag resolution (Figure S2E). This suggests that although the AF11 spectrum was unique, it was not impactful in this experiment. We were able to further reduce the AF spectra included in the unmixing to three AF tags with only minor, but potentially acceptable, reduction in the data resolution by the removal of either AF9 or AF7 (dimmest AF and next dimmest AF, respectively). Removing any further AF tags from the unmixing resulted in an unacceptable loss in Ag resolution and unmixing quality (Figure S2E). This indicated that, in this specific context, step 3 for the determination of critical AF spectra to be incorporated into the unmixing process, identified only one spectrum whose removal neither beneficially nor detrimentally affected data resolution. Consequently, we decided to use all the five AF spectra to compare strategy 3 with strategy 1 and 2.

This panel focused predominantly on macrophages, which we broadly defined as CD45$^+$, CD11b$^+$, and F4/80$^+$. Doublets and dead

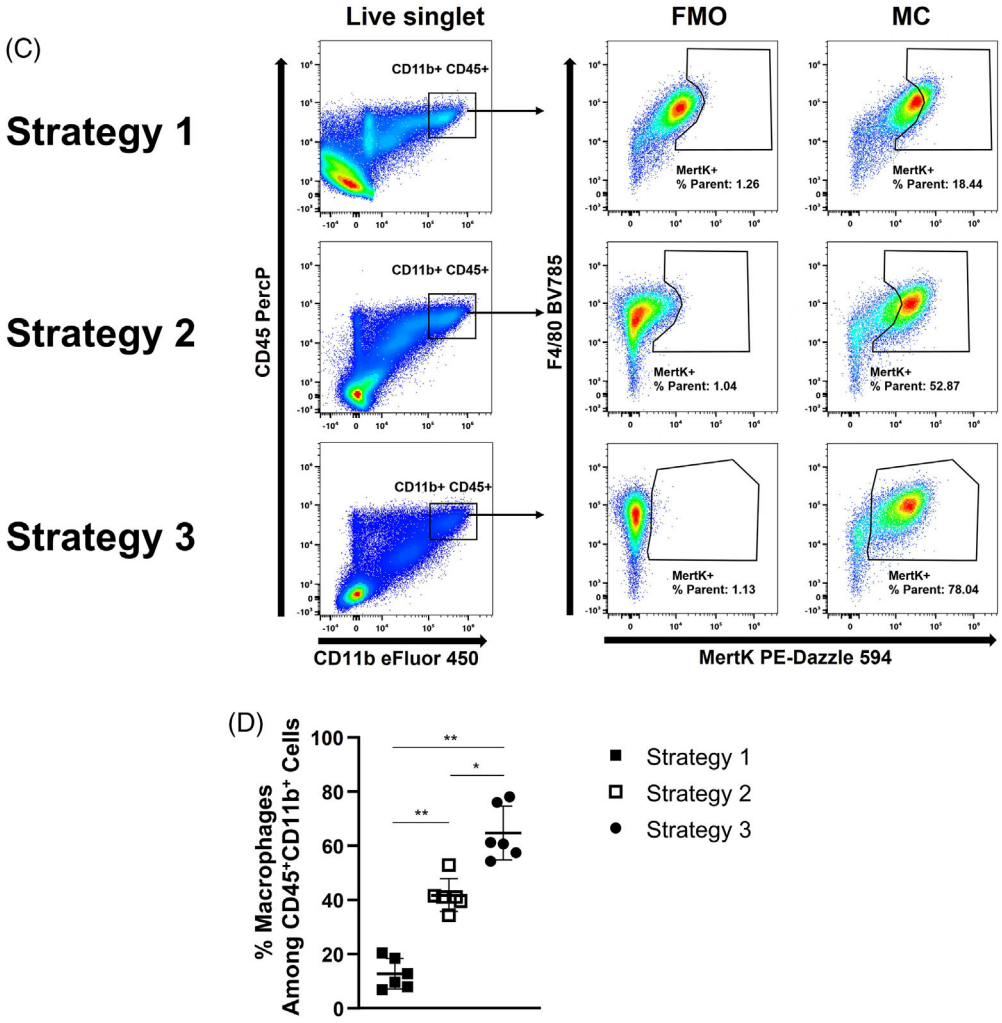

FIGURE 2 (Continued)

cells positive for DAPI were excluded from subsequent analysis. Macrophages were further characterized based on their expression of MertK, a low-density antigen that is essential for macrophage phagocytic activity in both heart and injured skeletal muscles [26, 27]. To detect MertK, PE-Dazzle 594, a bright fluorochrome with an emission spectrum far enough away from the area of the maximal macrophage AF emission, was selected and assigned to this antigen (Figure S2F). Gating was adjusted based on a MertK FMO to avoid defining any highly autofluorescent event as positive for MertK, thereby ensuring antigen resolution (Figure 2C). Using this strategy, we found that default unmixing without AF extraction (strategy 1) identified approximately one-quarter of the total $CD45^+$ $CD11b^+$ population as positive for MertK (~23%). Default unmixing with AF extraction (strategy 2) significantly increased the ability to assess low expression of MertK by partially removing the AF: 52% of the $CD45^+CD11b^+$ population was positive for MertK. Maximal MertK resolution was achieved by unmixing the data with multiple AF as fluorochrome tags (strategy 3) as 74% of the $CD45^+CD11b^+$ population was positive for MertK. To confirm the reproducibility of this result, we replicated the antibody panel and gating strategy in three replicate experiments with samples from six mice. For each experiment, we independently decomposed the combined AF of the unstained sample to unmix with the newly defined AF tags for their relevant donor. The data consistently showed a significant underestimation of macrophages positive for MertK when using the default unmixing with or without AF extraction (strategies 1 and 2) as compared to the method using multiple AF as fluorochromes tags (Figure 2D).

Altogether, these results show that using multiple AFs as fluorochrome tags can significantly improve the resolution of weakly expressed antigens, such as MertK, on highly autofluorescent cells, such as macrophages.

3.3 | Sixteen-color panel to analyze myeloid cell infiltration into injured skeletal muscle

Following successful testing of this approach in a small panel on a biological tissue with complex AF heterogeneity, we applied it to a more challenging panel in the same tissue. To enable some degree of comparability of data between the 5-color (5C) and 16-color (16C) panels,

we used skeletal muscle at 3 days post-injury taken from the same three mice for both panels. Consequently, it was possible to reuse the same AFs (AF1, AF4, AF7, AF9, and AF11) for unmixing strategy 3 in each panel. Because AF11 removal had no impact on data resolution and that using only 3 AFs had a detrimental effect, we elected to unmix the data with five AFs as previously described in the 5C panel to ensure experimental continuity.

For panel optimization and experiment setup, we followed recommendations previously published [25]. To study the myeloid compartment more specifically, a combination of lineage-exclusion antibodies was used to gate out the non-targeted cells. CD3, NK1.1, and CD19 were used to discriminate and remove T cells, NK cells, and B cells, respectively. T cells and NK cells have both been shown to infiltrate skeletal muscle after acute injury [13–15], while early work suggested that B cells could also be important for tissue regeneration [12]. Within the myeloid compartment (defined as $CD11b^{+}$ cells), we used Ly6G to define neutrophils, and Siglec-F for eosinophils [10]. Due to the inherent difficulties in distinguishing between dendritic cells (DCs), macrophages, and monocytes within tissues (as they share many common surface antigens), we followed a gating strategy that has proven to be effective to discriminate those populations in several tissues [28, 29]. Briefly, macrophages were defined by co-expression of CD64 and MertK and DCs were defined by high expression of CD11c and MHCII [30]. Once neutrophils, eosinophils, macrophages, and DCs were removed by gating, cells that expressed low levels of CD64 and F4/80 were classified as monocytes. The macrophage populations were further characterized by the expression of CD163, CD169, Ly6C, and CD115 or CX3CR1 (full gating strategy shown in Figure 3).

Using a gating strategy previously established to define myeloid subpopulations, the gates were set according to the FMOs. After gating out dead cells and $CD3^{+}$, $NK1.1^{+}$, and/or $CD19^{+}$ lymphocytes (Lin^{-}) in the $CD45^{+}$ gate, myeloid cells were gated based on their expression of CD11b. Neutrophils and eosinophils were gated based on their expression of Ly6G and Siglec-F, respectively. Plotting macrophage markers against Ly6G or Siglec-F to identify eosinophils and neutrophils more appropriately was essential for strategies 1 and 2. Indeed, plotting SSC versus Ly6G or Siglec-F would systematically lead to an underestimation of those populations. This was a consequence of gate readjustments to minimize the number of highly autofluorescent events falling into the eosinophil or neutrophil gate of the FMO control (Figure 4A, strategies 1 and 2). This was observed to a lesser extent with strategy 3, as high macrophage AF was more efficiently eliminated by this method (Figure 4A, strategy 3). Therefore, because macrophages have high AF in the area of the spectrum where the fluorochromes assigned to Ly6G and Siglec-F emit, we incorporated a more suitable gating strategy for strategies 1 and 2 by systematically plotting CD64 against non-macrophage markers (Figure 4B) to facilitate the removal of the highly autofluorescent macrophages. Unexpectedly, we observed super-negative MFI values for $CD64^{high}$ macrophages in the Spark Blue 550 channel, where a unique AF was extracted. The same phenomenon occurred for VioBright FITC, another dye emitting in the same area of the spectrum (Figure 4B, strategy 2). These distortions could not be corrected by applying additional compensation, indicating that they were not a consequence of spillover calculation errors but rather were due to an inappropriate management of AF in this area of the spectrum.

We next plotted MertK against CD64 to allow for the discrimination of macrophages. Adjustment of the gating based on FMO controls gave results comparable to those described in Figure 2C. We identified approximately 35% of the cells as macrophages for strategy 1, 50% for strategy 2% and 70% of the cells for strategy 3 (Figure S3A). Note that such discrepancies in frequency between the three strategies was achieved despite the use of PE-Cy7 to detect MertK (PE-Cy7 was selected as it is a brighter fluorochrome than PE-Dazzle 594 and it emits in an area of the spectrum where there is less AF coming from the macrophages). As monocytes are mostly defined by negative or very low expression of antigens common to several subpopulations of myeloid cells, they are the most susceptible population to contamination by macrophages due to inaccurate unmixing or inappropriate gating strategies. Previous studies have shown that $Ly6C^{high}$, but not $Ly6C^{low}$, monocytes can extravasate from the blood to the injured muscle during the first 3 days post-injury [16], and that $Ly6C^{-}$ macrophages are present within the regenerating skeletal muscle in the absence of circulating $Ly6C^{low}$ monocytes [31]. Consequently, most of monocytes within the injured skeletal muscle should express high levels of Ly6C. We therefore evaluated Ly6C expression on monocytes to assess the quality of the three unmixing strategies. Our results for the unmixing strategy 3 show a small proportion of monocytes with low level of Ly6C (Figure 4C, strategy 3); thus, these are likely to be monocytes differentiating into macrophages that have not yet upregulated MertK. The possibility that these cells might also be perivascular $Ly6C^{low}$ monocytes contaminating the sample could not be discarded, as the animals were not perfused before harvesting. However, the pattern of Ly6C expression was completely different after default unmixing with or without AF extraction, with an almost inverted distribution of $Ly6C^{low}$ and $Ly6C^{high}$ monocyte for unmixing without AF extraction (Figure 4C, strategies 1 and 2). This result shows that AF strongly interferes with gating strategies that rely on FMO controls, and that it compromises the analysis and phenotyping of monocytes as macrophages expressing low level of MertK are contaminating this population.

We next compared the resolution of the three unmixing strategies in the macrophage gate itself. Once again, the unmixing using multiple AF as tags gave the best outcome in term of antigen resolution, allowing us to better visualize the exclusive expression of low-density antigens such as CD115 and CD169 with MHCII (Figure 4D, strategy 3). $CD163^{+}$ macrophages were also more clearly identifiable as expressing low level of the chemokine receptor CX3CR1. Altogether, these results show that unmixing with multiple AFs as fluorochrome tags is a reasonable approach to improve resolution in heterogeneous and highly autofluorescent cell samples, such as in regenerating skeletal muscle. This allows clear identification, separation, and characterization of cell populations with different AF characteristics.

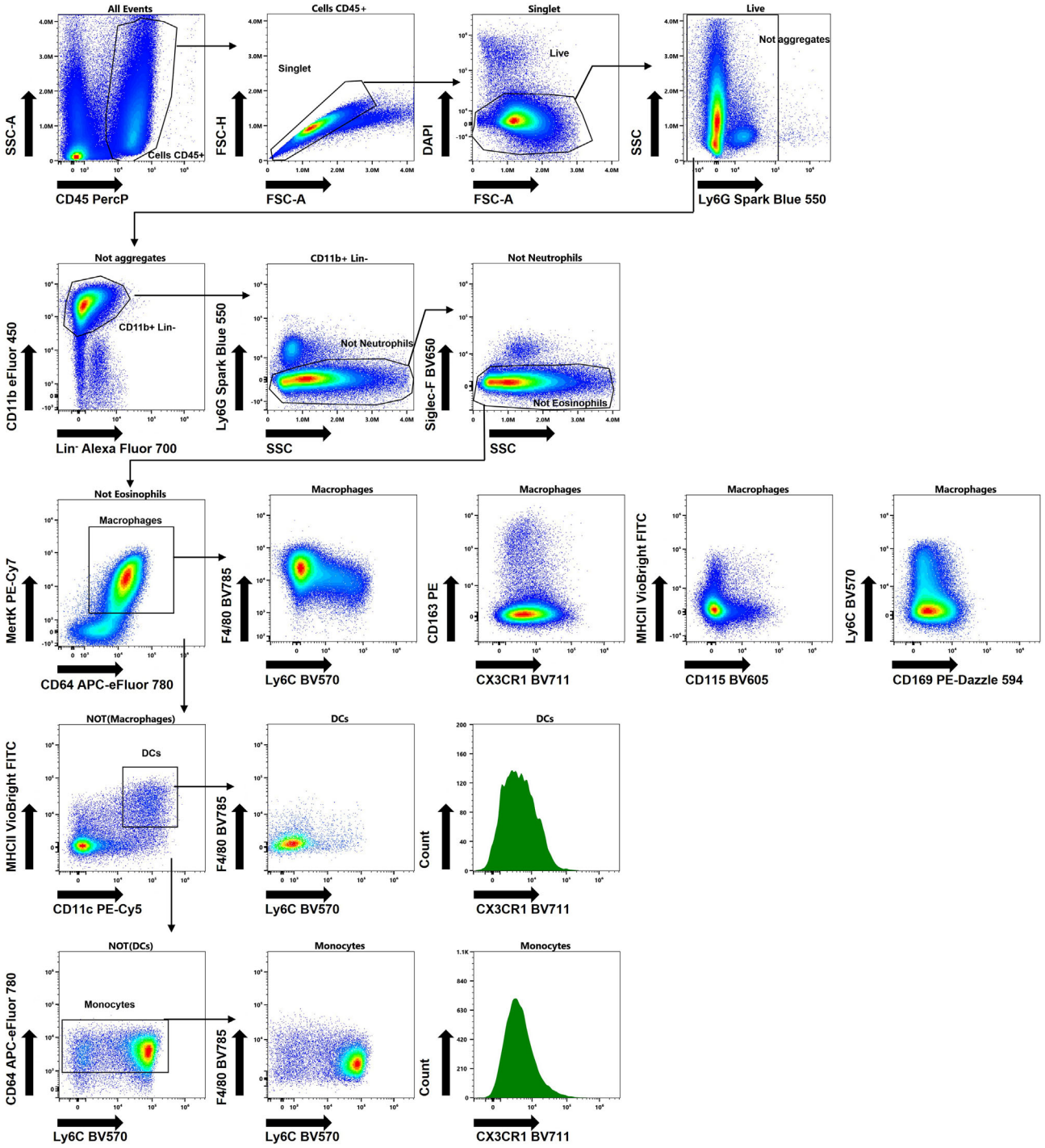

FIGURE 3 Recommended gating strategy for the delineation of key innate immune subpopulations from regenerating skeletal muscle 3 days post-injury. Neutrophils were defined as $CD45^+$ Lin^- $CD11b^+$ $Ly6G^+$. Eosinophils were defined as $CD45^+$ Lin^- $CD11b^+$ $Ly6G^-$ $SiglecF^-$. Macrophages were defined as $CD45^+$ Lin^- $CD11b^+$ $Ly6G^-$ $SiglecF^-$ $CD64^{high}$ $MertK^+$. DCs were defined as $CD45^+$ Lin^- $CD11b^+$ $Ly6G^-$ $SiglecF^-$ $MertK^-$ $MHCII^{high}$ $CD11c^{high}$. Monocytes were classified as $CD45^+$ Lin^- $CD11b^+$ $Ly6G^-$ $SiglecF^-$ $CD64^{low}$ $MertK^-$. Data were unmixed as described in strategy 3. Data are representative of three mice

In this study we used a UMAP dimensionality reduction approach to assess the impact of our three unmixing strategies. As shown in Figure S3B, we see a high degree of comparability between the clustering for all the gated phenotypes, regardless of the unmixing strategy. Although each of the three unmixing strategies segregated into five independent clusters, these clusters' densities and distributions varied depending on the unmixing approach. Based on these UMAP data, we concluded that the unmixing approach affected neither the determination of the total number of identifiable cell clusters nor introduced artifact populations into the sample. The UMAP of the

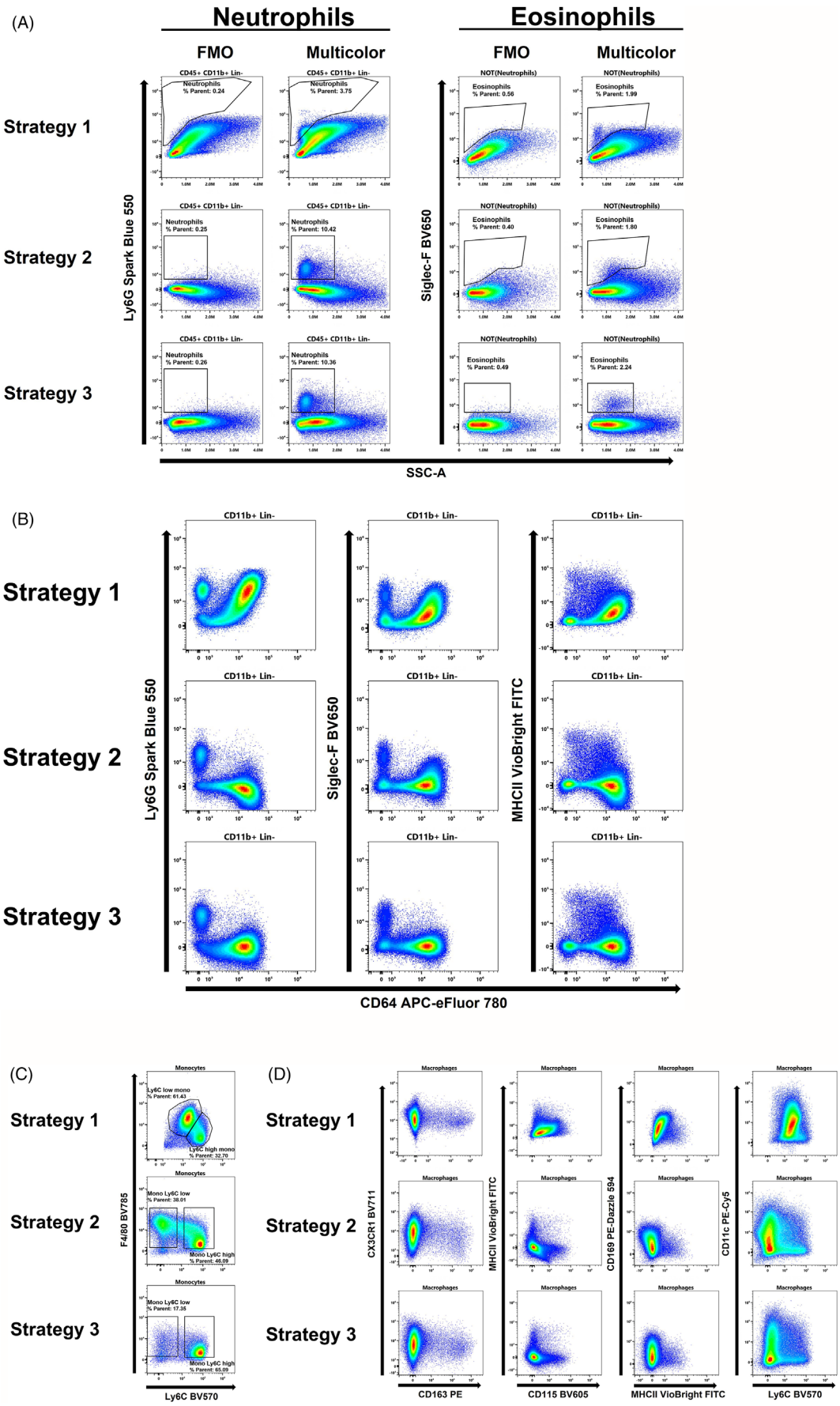

FIGURE 4 Legend on next page.

cells using strategy three generated more discrete clustering of the Ly6C^{low} monocytes, displaying less overlap of these cells with the CD163^{-} and CD163^{+} macrophage clusters. Strategies 1 and 2 were not as effective at separating these phenotypes due to the photon contributions of the AFs, intrinsic to the sample, resulting in a loss in resolution in the marker labels. These data correspond to those observed in our manual gating strategy and clearly show the impact strategy three has in improving resolution in unbiased dimensionality reduction clustering. These improvements emerged purely from the fact that the unmixing method enhanced the resolution of the antigen from the AF background.

Altogether, these data show that unmixing strategy three greatly improves data resolution when compared with strategies 1 and 2.

In a comparable fashion to the 5C panel, we wanted to investigate the assay tolerance to the removal of less impactful AFs in a more complex panel. As with the smaller 5C panel, it was observed that the removal of AF11 had no impact on data resolution (Figure S3C). However, while we could reduce the number of AF spectra to three with a minor, yet acceptable, reduction on the 5C panel's data resolution, this was not possible for the 16C panel. Indeed, regardless of which was the next AF to be removed after AF11, an increase of background signal was observed in the channel of fluorochromes emitting in high AF regions, such as BV650 and Spark Blue 550.

This elevated sensitivity to the removal of certain AF tags is believed to be down to the increased spectral complexity of the expanded panel. Under these conditions there is a greater requirement for robust photon management through their correct assignment, especially in those regions where the signatures of the AF spectra have the highest variation (V10 for BV650 and B3 for Spark Blue 550, see Figure S2B). Of note, because the same mice were used for the 5C and the 16C panels, any discrepancies that might be due to changes in AF between individuals can be discarded. It can therefore be postulated that the AF tag selection for unmixing alongside the reporter labels is determined by the fluorochromes used in the assay. Increasing the panel size may increase the requirement to use more AF tags in the unmixing for the best experimental outcomes.

Overall, these data show that the impact of an AF spectra on data resolution strongly depends on the fluorochrome complexity of the panel. Increasing the number of fluorochromes for a given panel requires better definition of the AF contributions resulting in a requirement to include more AF spectra in the unmixing. This should lead to a reduction in the misassignment of photons to the marker labels and therefore reduce spread in these parameters.

4 | DISCUSSION

Our study describes an approach to modeling AF using a well-defined and easily controlled particle in the form of compensation beads. This model was implemented as a proof-of-concept approach to enable strategies in the identification, vetting, and selection of AF from a complex sample. This was a necessary step as it allowed for more control of key variables to better define their impact, as this is not possible with biological material. This model clearly demonstrated that unmixing differential AFs on a bead standard using a multiple AF extraction approach greatly improves the resolution of the unmixed data when compared to default unmixing with, or without a single AF extraction. Although our manual-based approach for identifying and extracting AF spectra resulted in an oversampling of the AF spectral signatures present in the sample, their appropriate vetting based on the SI and MFI allowed us to discount all but the impactful spectra to use for the unmixing. However, although our assessment involving the reduction of AF based on the SI gave highly comparable results to the experimental control in the bead-based model, this AF selection process and criteria therein is still in its infancy. Consequently, with our manual selection of AF, we cannot completely disregard that another set of AFs than the one we selected would not give a comparable result. In biological samples where it is not possible to generate an experimental control with the pure spectral signatures for each of the chemical components constituting the cells AF, the process of AF spectra selection is more difficult. These questions would need further work to be fully addressed. Regardless, we believe the first two steps of our method allow for the isolation of the most important AFs of the sample, independently of the targeted cells and the fluorochromes included in the assay. Whether further down-sampling of the AF spectra is required to improve resolution, this is likely to be experiment dependent and will continue to require use of an iterative process of manually removing the less critical AF in this specific context. It is important to acknowledge that the impact of the AF tag removal (step 3 of the AF vetting method) on the unmixing and data resolution is largely dependent of the reporter labels used in the assay as seen in the 5-color and 16-color panels. Because this step relies on a visual assessment of data quality that can be highly subjective, there is an important need to work on establishing objective criteria that would make that step more reliable and reproducible between researchers. Similarly, although our proposed method is effective in removing non-essential AFs and extracting only those AFs critical to the unmixing, it is still limited in its application and ease of use. The need to manually gate on fractions to purify populations and their AF spectra also lacks objectivity and robust reproductivity. Therefore, there is a clear

FIGURE 4 Fluorescence minus one-based gating strategy analysis. For all populations, debris, dead cells, and doublets were excluded. (A) Neutrophils were defined as CD45^{+} CD11b^{+} Lin^{-} Ly6G^{+} and eosinophils as CD45^{+} CD11b^{+} Lin^{-} Ly6G^{-} Siglec-F^{+}. (B) In contrast with strategy 3, strategies 1 and 2 required plotting macrophage markers against neutrophil and eosinophil markers to avoid highly autofluorescent macrophages being identified as Siglec-F or Ly6G positive. (C) Monocytes were defined as CD45^{+} CD11b^{+} Ly6G^{-} Siglec-F^{-} MertK^{-} CD64^{low} F4/80^{+} CD11c^{low} MHCII^{low} and further subdivided as Ly6C^{low} and Ly6C^{high} monocytes. (D) Macrophages were defined as CD45^{+} CD11b^{+} Lin^{-} Ly6G^{-} Siglec-F^{-} MertK^{+} CD64^{+} and additional macrophage phenotyping markers are shown

requirement to use an unbiased separation of these spectra using defined rules and distributions. This would be based on variables including emission intensities to incorporate them into the unmixing algorithm in an automated and tightly regulated fashion. Clustering algorithms such as FlowSOM or SPADE could be useful in that regard allowing for a more automated approach throughout.

Using our multiple AF tag strategy, we demonstrated improvements in the correct assignment of AF photons to their particle of origin. The ability to characterize and incorporate AF into spillover calculations is an approach unique to full spectrum cytometry and is not readily achievable on conventional flow cytometers. For this to be possible, it would require detectors dedicated to the measurement of AF at set defined bandwidths and would be extremely limited in its application. The high similarity of the spectral output of these AFs with some fluorochromes (i.e., BV480, BV510 or FITC) makes it virtually impossible to separate these in conventional flow cytometry. This can have important consequences as the proper removal of AF is essential for data analysis and interpretation, especially when cell population definition relies on the negative expression of dim markers. In those cases, accurate gating strategies based on FMOs are of high importance and any interference from AF can compromise their outcome leading to misinterpretation of the data. This is illustrated by the artifact observed in Figure 4C where AF interference with the FMO based gating strategy leads to a misincorporation of the MertK^{low} events into the monocytes gate. As a result, the proportion of Ly6C^{low} monocytes infiltrating the injured skeletal muscle is overestimated and in disagreement with previous observations [16, 31].

To our knowledge, this is the first report using flow cytometry to successfully use 16 fluorescence parameters in mouse skeletal muscle. This lack of other reports highlights the strong limitations of conventional cytometry when analyzing highly autofluorescent cell subpopulations in a solid tissue. Although flow cytometry has been widely used to study skeletal muscle, and especially in the context of inflammation, it is still a very challenging tissue for flow cytometrists. Pitfalls linked to the inherent AF of this tissue and sample preparation compromising sample integrity [32, 33] is likely to explain the lack of flow cytometry reports for high-dimensional analysis of cells populating skeletal muscle. Here we show that full spectrum cytometry, through its ability to account for AF and improve low-density antigen resolution, provides new opportunities for researchers in this field. Our findings indicate that appropriate unmixing methodologies to handle impactful AF spectra from complex samples are a critical component to the precise detection of cell populations, frequency, and antigen density. Accounting for these factors, there are clear implications for the improvement of detection of cell populations in highly autofluorescent tissues, either in steady state or in the context of disease. Additionally, there are clear potential implications in subsequent enrichment of cell fractions from complex autofluorescent tissues through cell sorting applications for downstream genomic studies and functional assays. Yield and purity improvements in cell sorting using correct AF management strategies could greatly improve the outcome of these downstream applications, which are often more costly and time consuming than the cell sorting process itself.

AUTHOR CONTRIBUTIONS

Yacine Kharraz: Conceptualization (equal); data curation (equal); formal analysis (equal); methodology (equal); validation (equal); visualization (equal); writing – original draft (equal). **Vera Lukesova:** Methodology (supporting). **Antonio L. Serrano:** Validation (equal); writing – review and editing (equal). **Adam Davison:** Data curation (equal); writing – review and editing (equal). **Pura Muñoz-Cánoves:** Resources (equal); supervision (equal); validation (equal); writing – review and editing (equal).

ACKNOWLEDGMENTS

We would like to thank Patrick Duncker from Cytek Biosciences for his help with reviewing and editing this manuscript.

CONFLICT OF INTEREST

Yacine Kharraz and Adam Davison are employees of Cytek Biosciences, Inc., the manufacturer of the Aurora full spectrum flow cytometer used in these studies. Vera Lukesova, Antonio Serrano and Pura Munoz-Canoves declare no conflict of interest.

PEER REVIEW

The peer review history for this article is available at https://publons.com/publon/10.1002/cyto.a.24568.

ORCID

Yacine Kharraz https://orcid.org/0000-0001-9172-7624

REFERENCES

1. Vannella KM, Wynn TA. Mechanisms of organ injury and repair by macrophages. Annu Rev Physiol. 2017;79(1):593–617.
2. Zorro Manrique S, Duque Correa MA, Hoelzinger DB, Dominguez AL, Mirza N, Lin H-H, et al. Foxp3-positive macrophages display immunosuppressive properties and promote tumor growth. J Exp Med. 2011 Jun 13;208(7):1485–99.
3. Put S, Avau A, Humblet-Baron S, Schurgers E, Liston A, Matthys P. Macrophages have no lineage history of Foxp3 expression. Blood. 2012 Feb 2;119(5):1316–8.
4. Donnenberg VS, Donnenberg AD. Coping with artifact in the analysis of flow cytometric data. Methods. 2015 Jul;1(82):3–11.
5. Alberti S, Parks DR, Herzenberg LA. A single laser method for subtraction of cell autofluorescence in flow cytometry. Cytometry. 1987 Mar;8(2):114–9.
6. Mosiman VL, Patterson BK, Canterero L, Goolsby CL. Reducing cellular autofluorescence in flow cytometry: an in situ method. Cytometry. 1997 Jun 15;30(3):151–6.
7. Steinkamp JA, Lehnert NM, Keij JF, Lehnert BE. Enhanced immunofluorescence measurement resolution of surface antigens on highly autofluorescent, glutaraldehyde-fixed cells analyzed by phase-sensitive flow cytometry. Cytometry. 1999;37(4):275–83.
8. Muñoz-Cánoves P, Neves J, Sousa-Victor P. Understanding muscle regenerative decline with aging: new approaches to bring back youthfulness to aged stem cells. FEBS J. 2020 Feb;287(3):406–16.
9. Mann CJ, Perdiguero E, Kharraz Y, Aguilar S, Pessina P, Serrano AL, et al. Aberrant repair and fibrosis development in skeletal muscle. Skelet Muscle. 2011 May 4;1(1):21.
10. Heredia JE, Mukundan L, Chen FM, Mueller AA, Deo RC, Locksley RM, et al. Type 2 innate signals stimulate fibro/adipogenic progenitors to facilitate muscle regeneration. Cell. 2013 Apr 11;153(2):376–88.

11. Teixeira CFP, Chaves F, Zamunér SR, Fernandes CM, Zuliani JP, Cruz-Hofling MA, et al. Effects of neutrophil depletion in the local pathological alterations and muscle regeneration in mice injected with Bothrops jararaca snake venom. Int J Exp Pathol. 2005 Apr;86(2):107–15.
12. Long KK, Pavlath GK, Montano M. Sca-1 influences the innate immune response during skeletal muscle regeneration. Am J Physiol Cell Physiol. 2011 Feb;300(2):C287–94.
13. Panduro M, Benoist C, Mathis D. Treg cells limit IFN-γ production to control macrophage accrual and phenotype during skeletal muscle regeneration. Proc Natl Acad Sci USA. 2018 Mar 13;115(11):E2585–93.
14. Burzyn D, Kuswanto W, Kolodin D, Shadrach JL, Cerletti M, Jang Y, et al. A special population of regulatory T cells potentiates muscle repair. Cell. 2013 Dec 5;155(6):1282–95.
15. Wirsdörfer F, Bangen JM, Pastille E, Hansen W, Flohé SB. Breaking the co-operation between bystander T-cells and natural killer cells prevents the development of immunosuppression after traumatic skeletal muscle injury in mice. Clin Sci. 2015 Jun;128(11):825–38.
16. Arnold L, Henry A, Poron F, Baba-Amer Y, van Rooijen N, Plonquet A, et al. Inflammatory monocytes recruited after skeletal muscle injury switch into antiinflammatory macrophages to support myogenesis. J Exp Med. 2007 May 14;204(5):1057–69.
17. Pessina P, Kharraz Y, Jardí M, Fukada S, Serrano AL, Perdiguero E, et al. Fibrogenic cell plasticity blunts tissue regeneration and aggravates muscular dystrophy. Stem Cell Rep. 2015 Jun 9;4(6):1046–60.
18. Kharraz Y, Guerra J, Mann CJ, Serrano AL, Muñoz-Cánoves P. Macrophage plasticity and the role of inflammation in skeletal muscle repair. Mediat Inflamm 2013;2013:491497.
19. Murray PJ, Allen JE, Biswas SK, Fisher EA, Gilroy DW, Goerdt S, et al. Macrophage activation and polarization: nomenclature and experimental guidelines. Immunity. 2014 Jul 17;41(1):14–20.
20. Filippin LI, Moreira AJ, Marroni NP, Xavier RM. Nitric oxide and repair of skeletal muscle injury. Nitric Oxide. 2009 Dec 15;21(3):157–63.
21. Blacker TS, Duchen MR. Investigating mitochondrial redox state using NADH and NADPH autofluorescence. Free Radic Biol Med. 2016 Nov;100:53–65.
22. Shi L, Lu L, Harvey G, Harvey T, Rodríguez-Contreras A, Alfano RR. Label-free fluorescence spectroscopy for detecting key biomolecules in brain tissue from a mouse model of Alzheimer's disease. Sci Rep. 2017 Jun 1;7(1):2599.
23. Akahori H, Karmali V, Polavarapu R, Lyle AN, Weiss D, Shin E, et al. CD163 interacts with TWEAK to regulate tissue regeneration after ischaemic injury. Nat Commun. 2015 Aug;5(6):7792.
24. Winn NC, Volk KM, Hasty AH. Regulation of tissue iron homeostasis: the macrophage "ferrostat". JCI Insight. 2020 Jan 30;5(2):1–14.
25. Park LM, Lannigan J, Jaimes MC. OMIP-069: forty-color full spectrum flow cytometry panel for deep immunophenotyping of major cell subsets in human peripheral blood. Cytometry A. 2020;97(10):1044–51.
26. Nicolás-Ávila JA, Lechuga-Vieco AV, Esteban-Martínez L, Sánchez-Díaz M, Díaz-García E, Santiago DJ, et al. A network of macrophages supports mitochondrial homeostasis in the heart. Cell. 2020 Oct 1;183(1):94–109.
27. Al-Zaeed N, Budai Z, Szondy Z, Sarang Z. TAM kinase signaling is indispensable for proper skeletal muscle regeneration in mice. Cell Death Dis. 2021 Jun 12;12(6):611.
28. Gautier EL, Shay T, Miller J, Greter M, Jakubzick C, Ivanov S, et al. Gene-expression profiles and transcriptional regulatory pathways that underlie the identity and diversity of mouse tissue macrophages. Nat Immunol. 2012 Nov;13(11):1118–28.
29. Jakubzick C, Gautier EL, Gibbings SL, Sojka DK, Schlitzer A, Johnson TE, et al. Minimal differentiation of classical monocytes as they survey steady-state tissues and transport antigen to lymph nodes. Immunity. 2013 Sep 19;39(3):599–610.
30. Brigitte M, Schilte C, Plonquet A, Baba-Amer Y, Henri A, Charlier C, et al. Muscle resident macrophages control the immune cell reaction in a mouse model of notexin-induced myoinjury. Arthritis Rheum. 2010 Jan;62(1):268–79.
31. Varga T, Mounier R, Gogolak P, Poliska S, Chazaud B, Nagy L. Tissue LyC6- macrophages are generated in the absence of circulating LyC6-monocytes and Nur77 in a model of muscle regeneration. J Immunol. 2013 Dec 1;191(11):5695–701.
32. Ford AL, Foulcher E, Goodsall AL, Sedgwick JD. Tissue digestion with dispase substantially reduces lymphocyte and macrophage cell-surface antigen expression. J Immunol Methods. 1996 Jul 17;194(1):71–5.
33. Autengruber A, Gereke M, Hansen G, Hennig C, Bruder D. Impact of enzymatic tissue disintegration on the level of surface molecule expression and immune cell function. Eur J Microbiol Immunol. 2012 Jun;2(2):112–20.
34. Suelves M, Vidal B, Serrano AL, Tjwa M, Roma J, López-Alemany R, et al. uPA deficiency exacerbates muscular dystrophy in MDX mice. J Cell Biol. 2007 Sep 10;178(6):1039–51.

SUPPORTING INFORMATION

Additional supporting information may be found in the online version of the article at the publisher's website.

Received: 24 February 2023 | Revised: 26 July 2023 | Accepted: 18 August 2023

DOI: 10.1002/cyto.a.24788

OMIP

MIFlowCyt

ISAC CYTOMETRY Journal of Quantitative Cell Science PART A

OMIP-095: 40-Color spectral flow cytometry delineates all major leukocyte populations in murine lymphoid tissues

Aris J. Kare[1,2] | Lisa Nichols[3] | Ricardo Zermeno[3] | Marina N. Raie[2] | Spencer K. Tumbale[2] | Katherine W. Ferrara[2]

[1]Department of Bioengineering, Stanford University, Stanford, California, USA

[2]Department of Radiology, Stanford University, Stanford, California, USA

[3]Stanford Shared FACS Facility, Stanford University, Stanford, California, USA

Correspondence
Katherine W. Ferrara, Department of Radiology, Stanford University, Stanford, CA 94305, USA.
Email: kwferrar@stanford.edu

Funding information
National Institute of General Medical Sciences, Grant/Award Number: 5T32GM007276; National Institutes of Health, Grant/Award Numbers: R01CA250557, R01CA253316, R01CA112356, R01EB028646

Abstract

High-dimensional immunoprofiling is essential for studying host response to immunotherapy, infection, and disease in murine model systems. However, the difficulty of multiparameter panel design combined with a lack of existing murine tools has prevented the comprehensive study of all major leukocyte phenotypes in a single assay. Herein, we present a 40-color flow cytometry panel for deep immunophenotyping of murine lymphoid tissues, including the spleen, blood, Peyer's patches, inguinal lymph nodes, bone marrow, and thymus. This panel uses a robust set of surface markers capable of differentiating leukocyte subsets without the use of intracellular staining, thus allowing for the use of cells in downstream functional experiments or multiomic analyses. Our panel classifies T cells, B cells, natural killer cells, innate lymphoid cells, monocytes, macrophages, dendritic cells, basophils, neutrophils, eosinophils, progenitors, and their functional subsets by using a series of co-stimulatory, checkpoint, activation, migration, and maturation markers. This tool has a multitude of systems immunology applications ranging from serial monitoring of circulating blood signatures to complex endpoint analysis, especially in pre-clinical settings where treatments can modulate leukocyte abundance and/or function. Ultimately, this 40-color panel resolves a diverse array of immune cells on the axes of time, tissue, and treatment, filling the niche for a modern tool dedicated to murine immunophenotyping.

KEYWORDS
cell sorting, extracellular staining, full spectrum flow cytometry, innate and adaptive immunity, murine immunophenotyping, pre-clinical research, primary and secondary lymphoid tissues, systems immunology

1 | INTRODUCTION

There currently exists a great need to deeply profile murine leukocytes on the axes of time, tissue, and treatment. For combinatorial cancer immunotherapy, it is crucial to study immune networks to understand how microenvironment remodeling influences survival [1, 2]. Furthermore, synergistic immunotherapies may produce systemic effects due to target or administration route, increasing the value of multi-tissue analyses to fully decipher immune responses [3]. Beyond cancer research, temporal dynamic leukocyte tracking in mouse models of infection [4–6], aging [7, 8], and human disease [9] necessitates novel assays that maximize information from a single sample. Additional applications in atlas construction [10–12] or high-throughput screens [13, 14] also require modular tools that can fully capture leukocyte composition on a tissue by tissue basis.

Full spectrum flow cytometry (FSFC) has matured as a key technology to help fulfill these needs. Advancements in fluorochrome chemistry [15–18], spectral cytometer instrumentation [19, 20], autofluorescence extraction [21–23], and panel complexity [24, 25] have contributed to the maturation of FSFC while redefining traditional

TABLE 1 Summary table for application of OMIP-095.

	Summary table
Purpose	Deep Immunophenotyping of all major leukocyte populations in murine lymphoid tissues
Species	Mouse (C57BL/6)
Cell Type	Spleen, Blood, Bone Marrow, Thymus, Inguinal Lymph Nodes, Peyer's Patches
Cross References	OMIP-031, OMIP-032, OMIP-054, OMIP-057, OMIP-059, OMIP-061, OMIP-076, OMIP-079, OMIP-093

approaches for panel design [26] and computational analysis [27]. Despite this progress, FSFC mouse immunophenotyping panels have been largely undeveloped, as evidenced by the majority of "Optimized Multicolor Immunofluorescence Panels" (OMIPs) published for human samples [28]. Additionally, many initiatives to document immune cell marker expression are focused on human blood [29, 30], further emphasizing the need for a panel that can be used to advance murine systems immunology research.

To supplement the existing literature and fill this niche, we have engineered a high-dimensional, 40-color spectral flow cytometry panel that can deconvolve all major leukocyte populations in primary and secondary lymphoid tissues (Table 1). We systematically selected markers based on current mouse immunology reviews discussing lymphocytes [14, 31–33], myeloid cells [34–39], and granulocytes [40–42] to construct a comprehensive panel while maintaining deep profiling of functional subsets (Table 2). Furthermore, this panel was designed to avoid intracellular staining such that populations could be preserved for downstream functional experiments or multiomic analyses. In the main text, we discuss secondary lymphoid tissues as essential sites in serial or endpoint studies. In the Supporting Information, we provide technical details regarding panel construction and optimization (Figures S1–S12) and briefly highlight lymphocyte development in primary lymphoid tissues (Figure S13). Our lab has successfully used this panel to quantify leukocyte frequencies in the blood, spleen, lymph nodes, and tumors of pancreatic cancer-burdened mice pre- and post-immunotherapy. This application represents just one of many use cases, and we hope by sharing this panel we can enable additional pre-clinical research while informing future FSFC panel design efforts in the cytometry field.

2 | RESULTS

To immunophenotype leukocytes in the spleen, we first used a primary 14-marker gating strategy to identify major lineages, including T cells, B cells, natural killer (NK) cells, myeloid cells (dendritic cells, monocytes, macrophages), and granulocytes (neutrophils, eosinophils, basophils). Using the spleen as a reference, we applied this same strategy to other secondary lymphoid tissues (Figure S14A–C). Briefly, we used scatter signal and viability staining to remove debris, dead cells, and cell aggregates. All leukocytes were then identified using hematopoietic marker, CD45 (Figure 1A). Within the CD45$^+$ gate (Figure 1B), CD45R (B220) and CD19 were first used to separate B-1 and B-2 cells. Afterwards, NK cells and T cells were separated using NK1.1 and CD3ε, respectively.

Next, we proceeded to identify myeloid cells and granulocytes. First, F4/80 and Ly6G were used to separate macrophages and neutrophils, while CD11c and I-A/I-E (MHCII) staining identified classical dendritic cells. Eosinophils and basophils were then gated using markers Siglec-F and FcεR1α, respectively. Finally, CD11b and CX3CR1 were used to distinguish monocytes. Remaining heterogenous cells comprised of various rarer subsets, and additional gating to identity these populations is shown in Figure S14D.

2.1 | Lymphocytes

2.1.1 | B cells

Unlike T cells and other myeloid cells that migrate directly to sites of inflammation, B cells circulate centrally throughout secondary lymphoid tissues. Here, they are responsible for producing secretory antibodies and defending the host via humoral immunity [43, 44]. Under steady state in the spleen, four major populations of CD19$^+$CD45R$^+$ B-2 cells were identified using CD24 by CD38 biaxial gating [45–48] (Figure 1C). Immature CD24^{hi}CD38$^+$ transitional B cells migrate from the bone marrow to differentiate into mature follicular and marginal zone B cells [46, 47]. Using IgD by CD62L biaxial gating on CD24^{hi}CD38$^+$IgM$^+$I-A/I-E$^+$ cells, transitional B cells can be further classified into either early T1 cells or intermediate T2 cells that each have divergent maturation fates upon the quality of B cell receptor (BCR) signaling [46, 49, 50]. CD24$^+$CD38^{hi} marginal zone B cells, which mostly express polyreactive BCRs and possess innate-like functions as first line responders to pathogens [51], have the highest expression of CD38, CD274 (PD-L1), and CD40 compared to other subsets [45, 48, 52]. In contrast, follicular B cells express monoreactive BCRs and produce high-affinity antibodies several days after pathogen exposure [51]. This population has a CD24$^+$CD38$^+$IgD^{hi} phenotype in relation to other B cells and can be separated into two subsets on the basis CD62L expression, likely representing populations with different homing capacities [53]. Lastly, germinal center B cells have a CD38^{lo} phenotype [54] and are the main precursors for long-lived memory B cells and plasma cells [55]. Because we collected data in 8-week-old mice, we did not expect to see high levels of memory or plasma cells given the absence of an immunization event. However, we incorporated co-stimulatory molecules CD80 (upregulated on memory cells [56]) and CD86 to track activation and functional characteristics of B cells [57, 58] (Figure S15A). To provide a benchmark for panel utility, we highlight differences in B cell architecture across all secondary lymphoid tissues in Figure S15B.

2.1.2 | T cells

Similar to B cells, T cells are crucial for adaptive immunity and exhibit remarkable diversity in function, phenotype, and distribution among

TABLE 2 Reagents used for OMIP-095.

Specificity	Fluorochrome	Clone	Purpose
Viability	Live/Dead Blue	-	Cell viability
CD45	AF532	30-F11	Pan leukocytes
CD19	BUV737	1D3	Pan B cells
CD45R	BV570	RA3-6B2	B cells and pDCs
IgM	PE-D594	RMM-1	B cell subsets
IgD	SNIR685	11-26c.2a	B cell subsets
CD24	BUV496	M1/69	B cells, granulocytes, DC subsets
CD38	APC-Fire810	90	B and T cell subsets, macrophages
CD274	BUV395	MIH5	Checkpoint, memory B cells, myeloid subsets
CD11b	BUV661	M1/70	Myeloid cells, granulocytes, and NK subsets
CD26	BUV805	H194-112	DCs, B cells, and T cells
CD3ε	Real Yellow 586	145-2C11	Pan T Cells
CD4	NFB610-70S	GK1.5	CD4 T cell and DC subsets
CD8α	NFY690	53-6.7	CD8α T cells and DC subsets
CD25	BV421	PC61	T regulatory cells and T cell activation
TCRγδ	APC	GL3	Gamma delta T cells
CD62L	BV650	MEL 14	Migration, monocyte, and lymphocyte subsets
CD44	BV510	IM7	Antigen experience, various leukocyte subsets
CD27	SB702	LG.7F9	Lymphocyte co-stimulatory molecule
CD279	BV480	J43	Checkpoint, exhuastion, and other T cell subsets
CD134	BV786	OX-86	T regulatory subsets and T cell activation
NK1.1	BB700	PK136	Natural killer and NKT cells
CD127	R718	A7R34	Various T cell subsets and ILCs
CD11c	eF506	N418	DCs
I-A/I-E	PerCP	M5/114.15.2	B cells and various APC subsets
CD135	PE	A2F10.1	Progenitors and DCs
CD117	BV750	2B8	Progenitors and DCs
CD103	PerCP-eF710	2E7	T cell and DC subsets
CD40	FITC	HM40-3	B cells, APC co-stimulatory molecule
CD80	PE-Cy5	16-10A1	Lymphocyte subsets, APC co-stim molecule
CD86	PE-Cy7	GL-1	Lymphocyte subsets, APC co-stim molecule
Siglec-H	BUV615	440c	Plasmacytoid DCs
Ly6C	BV605	AL-21	Monocytes and lymphocyte subsets, pDCs
CD115	BUV563	T38-320	Monocytes
CX3CR1	PE-Fire700	SA011F11	Migration and monocytes
F4/80	eF450	BM8	Macrophages, eosinophils, DCs, monocytes
FcεR1α	APC-eF780	MAR-1	Pan Basophils
Ly6G	PE-Fire810	1A8	Pan Neutrophils
Siglec-F	eF660	1RNM44N	Pan Eosinophils
CD326	Real Blue 780	G8.8	Epithelial cells and various leukocyte subsets

secondary lymphoid tissues. Among T cells, there is a continuum of populations that vary in antigen experience, activation status, migratory, and functional capacity, all of which have vital roles in host response to disease. We incorporated markers to provide a detailed T cell demographic both in steady state and pathological conditions.

To begin, NK1.1 by TCRγδ biaxial gating was used to separate unconventional NKT cells, γδT cells, and γδNKT cells (Figure 1D). CD49b (clone DX5 on color BB700) can be used as a substitute in non-C57BL/6 mouse strains. Afterwards, conventional T cells were identified using CD4 and CD8, which enhance responses to antigens presented by MHC class II and I complexes, respectively. Within the $CD4^+$ T cells, $CD127^{lo}CD25^{hi}$ gating identified a T regulatory cell enriched (T_{reg}-enriched) population (intracellular FOXP3 staining is necessary for bonafide T_{reg} identification). T_{regs} are responsible for

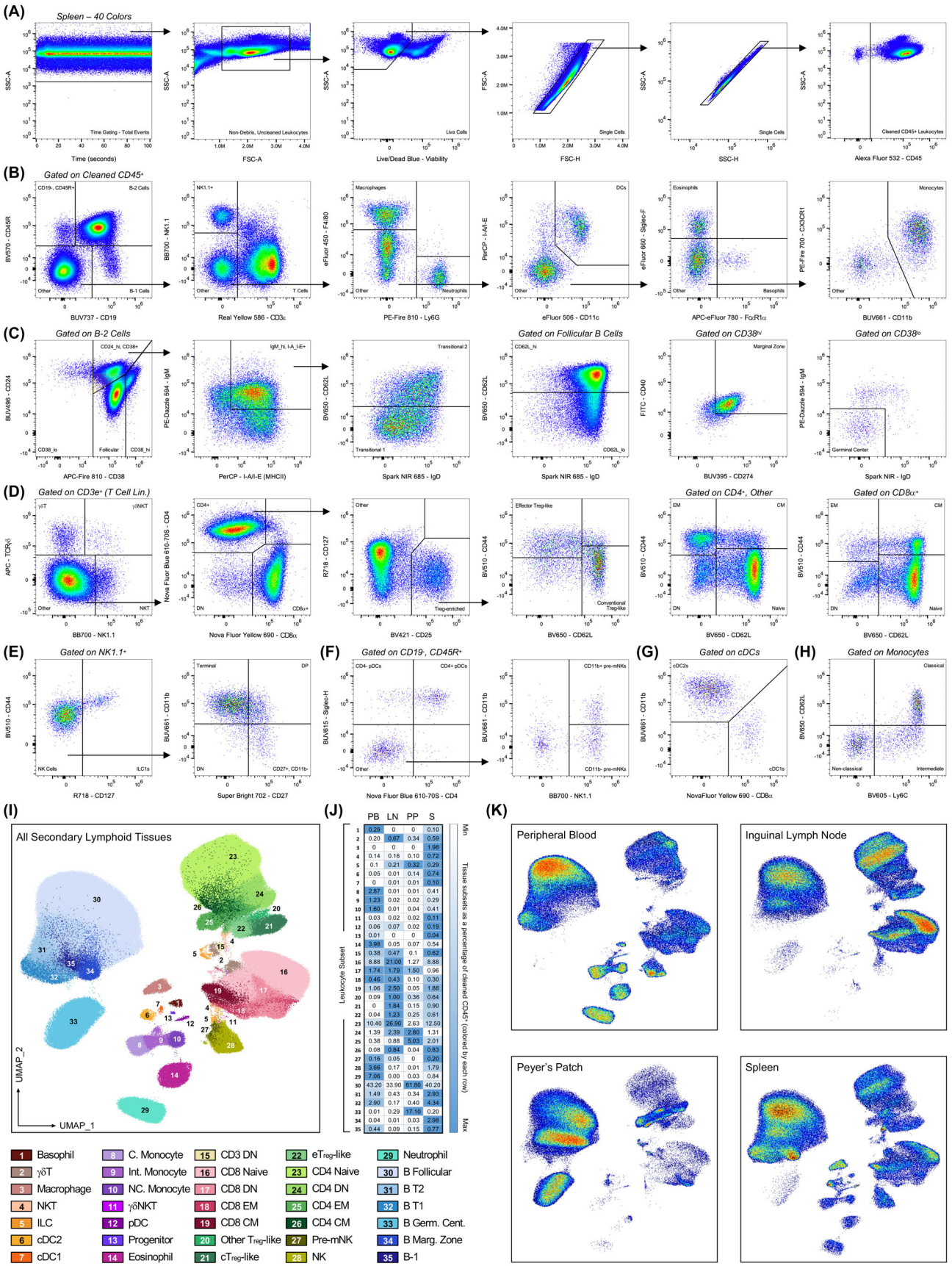

FIGURE 1 Legend on next page.

maintaining homeostasis and self-tolerance [59] but are capable of suppressing anti-tumor immune responses in the context of cancer [60]. As such, we proceeded to assess the migratory capacity and antigen experience of this regulatory enriched population using CD62L and CD44. Adhesion molecule CD62L is a homing receptor that allows cells to migrate from the peripheral blood into secondary lymphoid tissues, and its shedding is often associated with activation upon antigen encounter [61]. CD44 is another adhesion molecule and is highly upregulated upon T cell activation, remaining present on effector and subsequent memory subsets after stimulation [62]. Using this dichotomy, we found two major T_{reg}-enriched subsets, $CD62L^{hi}CD44^{lo}$ conventional T_{reg}-like (cT_{reg}-like), which are derived from the thymus and circulate throughout secondary lymphoid tissues, and $CD62L^{lo}CD44^{hi}$ effector T_{reg}-like (eT_{reg}-like), which are highly activated, proliferative, and immunosuppressive [63, 64]. Indeed, eT_{reg}-like cells express higher levels of regulatory and effector molecules (Figure S16A) and are the dominant T_{reg} population in a variety of cancers [65].

After identifying T_{reg}-like cells, we then applied the same CD44 by CD62L gating strategy to other $CD4^+$ and $CD8\alpha^+$ T cells to identify effector memory (EM), central memory (CM), and naïve cells (Figure 1D, Figure S16B,C). These subsets have distinct phenotypes (Figure S17A,B), and we highlight select markers in the panel for investigating T cell functionality in the tumor microenvironment. Found on almost all T cells, co-stimulatory molecule CD27 promotes survival, expansion, and memory formation upon binding with CD70 on antigen presenting cells [66]. However, cancers that overexpress CD70 can dysregulate the CD70-CD27 signaling axis [67], causing CD27 shedding, effector memory T cell exhaustion [68], increased T_{reg} frequencies [69], and overall immunosuppression. Alternatively, expression of activation marker CD134 reveals extremely potent, tumor-reactive T cells that can secrete cytokine and augment memory generation [70, 71], representing an important subset that has been clinically validated in cancer patients [72]. Other markers also have unique functions in the context of cancer, as Ly6C has been associated with $CD8_{CM}$ homing to lymph nodes and protection against tumor growth [73], while CD103 identifies tumor-infiltrating, resident memory $CD8\alpha^+$ T cells [74].

2.1.3 | NK cells and other innate lymphoid cells

While natural killer (NK) cells serve as the third predominant lymphocyte alongside T and B cells, they are classified as innate lymphoid cells (ILCs) and are heavily recruited during early disease response. NK cells are often viewed as the innate counterpart to $CD8\alpha^+$ T cells due to their similarities in cytokine secretion and cytotoxicity; however, they do not express antigen receptors and cannot be clonally selected upon activation [75]. Despite this, NK cells have the capacity to directly target and kill tumor cells without antigen-education, and as such, we selected surface markers to identify these mature effector populations. Type 1 ILCs (ILC1s) were first removed using CD127 [76] (Figure 1E). Afterwards, we employed a CD11b by CD27 bivariate gating strategy [77] to capture four major NK populations with the following sequential pathway of maturation: precursor $CD11b^-CD27^-$ double negative (DN) → proliferative $CD11b^-CD27^+$ → mature $CD11b^+CD27^+$ double positive (DP) → senescent $CD11b^+CD27^-$. DP NK cells display high effector functions such as in vitro tumor cell lysing and IFN-γ cytokine secretion upon IL-12/IL-18 stimulation [78]. Conversely, terminal $CD11b^+CD27^-$ cells typically have high regulation of activation, a low proliferation potential, and a reduced capacity to produce cytokine [78, 79]; this is further exemplified by $Ly6C^+$ inert/resting NK cells, which are primarily found in this population [80] (Figure S18A). This CD11b/CD27 immunophenotyping strategy has been successfully used in a mouse model of breast cancer [81], as well as human hepatocellular [82] and non-small-cell lung [83] carcinomas, where immature $CD11b^-CD27^-$ NK cells were found to be poorly cytotoxic and disease-promoting.

Finally, one last subset of NK cells called "pre-mature NK cells" (pre-mNK, previously referred to as interferon-producing killer dendritic cells in early reports [84, 85]) can be identified upstream of NK1.1/CD3ε gating. Within the $CD45R^+CD19^-$ cells that were identified in the first set of lineage gates (Figure 1B), we found a population of $NK1.1^+$ cells that corresponded with pre-mNKs (Figure 1F). These cells have been shown to be immediate precursors of $CD27^+CD45R^-$ NK cells, sharing close transcriptional homology [86]. Drawing similarities to human $CD56^{bright}$ NK cells, pre-mNKs have

FIGURE 1 40-Color FSFC characterizes murine secondary lymphoid tissue immune compartments. (A) Representative manual gating strategy for obtaining a clean population of live, single, $CD45^+$ splenic leukocytes from total events. Arrows represent subsequent gating from selected populations. (B) Representative, lineage-based gating scheme for identifying all major leukocyte populations in the spleen. (B–E) Calls on these subsets for further gating. (C) Gating into $CD45R^+CD19^+$ B-2 cells reveals diversity in follicular, transitional, marginal zone, and germinal center subsets. (D) Gating into $CD3\varepsilon^+$ T cells illustrates exceptional heterogeneity with unconventional T cells (γδT, γδNKT, NKT), $CD4^+$ T_{reg}-enriched subsets, and CD4/CD8α effector memory (EM), central memory (CM), naïve, and double negative (DN) populations. (E) After removing type 1 innate lymphoid cells (ILC1s) using CD127 and CD44, NK cells can be divided into four major stages of maturation using CD27 by CD11b biaxial gating. (F) Within the $CD19^-CD45R^+$ population, plasmacytoid dendritic cells (pDCs) and pre-mature natural killer cells (pre-mNKs) can be identified using Siglec-H and NK1.1. (G) Classical DCs (cDCs) can be divided into cDC1 and cDC2 subsets using CD11b and CD8α. (H) Monocytes can be divided into classical, intermediate, and non-classical subsets using Ly6C and CD62L. (I) Dimensionality reduction was achieved via Uniform Manifold Approximation and Projection (UMAP). Details regarding generation can be found in the supplement text. Following UMAP generation, the gating strategies used throughout (B–G) for the spleen were applied to all other tissues (Figure S14), and combined populations were overlaid onto the global UMAP. (J) A population abundance heatmap was generated using all secondary lymphoid tissues. Numbers represent a certain subset (1–35) as a percentage of cleaned $CD45^+$ cells for a given tissue (column). Coloring is applied to each row and is used to show which tissue contains the highest frequency of a given cell subset. (K) Pseudocolor maps for each secondary lymphoid tissue extracted from the global UMAP in (I). [Color figure can be viewed at wileyonlinelibrary.com]

antigen presentation potential and high cytotoxic functionality, representing a hybrid cell type that has been shown to have important implications in tumor response mechanisms [87–89].

2.2 | Myeloid cells (mononuclear phagocyte system)

2.2.1 | Dendritic cells

Dendritic cells (DCs) are professional antigen presenting cells that play vital roles in successful cancer immunotherapy [36], damage/pathogen associated molecular pattern recognition [90], and immune tolerance [91, 92]. Unlike humans, C57BL/6 mice contain few to no mature DCs in the periphery at steady state, but a small reservoir of mature $CD11c^{+}$I-A/I-E^{+} classical DCs (cDCs) occupy the spleen and are responsible for sensing tissue and blood antigens [93]. Because cDCs are heterogeneous, CD8α and CD11b were used to identify $CD8\alpha^{+}$ cDC1s and $CD11b^{+}$ cDC2s (Figure 1G), each representing functionally distinct subsets that preferentially present antigen to CD8 or CD4 T cells respectively [93, 94]. Additionally, we incorporated co-stimulatory and maturation molecules CD40, CD80, and CD86, which reflect activation status (Figure S19A). Phenotypically mature cDCs express high levels of these molecules [95]; however, within the tumor microenvironment, infiltrating cDCs often have dysfunctional antigen presentation and can exhibit tumor tolerogenicity [96], down-regulating expression of CD40/80/86 in the process. These dysregulated, "semi-mature" cDCs have been found in the tumor, spleen, and lymph nodes of pancreatic tumor-burdened mice [97–100] and blood of humans [100, 101], emphasizing the importance of measuring these molecules. For further refinement, we included essential markers CD135 (FLT3) and CD26 to differentiate cDCs from inflammatory monocyte-derived DCs (moDCs), which have poor migratory and antigen presentation potential [102]. Lastly, αE integrin CD103 was incorporated to phenotype migratory DCs in various cancer models, which have been described as key players in potentiating anti-tumor immunity [2, 103, 104].

Plasmacytoid dendritic cells (pDCs) can be readily immunophenotyped due to their expression of Siglec-H on $CD45R^{+}CD19^{-}$ cells (Figure 1B). CD4 expression further divides pDCs into $CD4^{-}$ immature and $CD4^{+}$ mature subsets, the latter of which are potent producers of type 1 interferons upon viral stimulation [105, 106] (Figure 1F). We overlay splenic cDC1s, cDC2s, and pDCs in Figure S19B to highlight differences in expression across 14 markers.

2.2.2 | Monocytes

Monocytes are formed in the bone marrow from unipotent common monocyte progenitors and egress into the periphery as mature $Ly6C^{hi}CD62L^{+}$ classical "inflammatory" monocytes [37–39]. Once in circulation, classical monocytes can either seed organs by differentiating into monocyte-derived cells or repopulate secondary lymphoid tissue monocyte reseviors [107]. Alternatively, they can remain in the peripheral blood by transitioning into $Ly6C^{int/+}CD62L^{-}$ intermediate monocytes and finally $Ly6C^{-}CD62L^{-}$ non-classical "patrolling" monocytes (Figure 1H) that scavenge and monitor the vasculature while maintaining endothelial integrity [38, 39]. To further aid in phenotyping these cells, we included CD115, which is differentially expressed as a function of tissue and monocyte subset (Figure S19C) and is not found on macrophages or DCs. In the setting of cancer immunotherapy, certain drugs such as agonist CD40 can mobilize inflammatory monocytes directly to the tumor microenvironment and reshape their differentiation potential toward antifibrotic, monocyte-derived macrophage phenotypes [108–110]. Consequently, markers such as I-A/I-E, F4/80, CD11c, CD11b, and CD274 can be used with Ly6C to separate inflammatory monocytes from their differentiating counterparts in "monocyte waterfall" plots [99, 111, 112].

2.2.3 | Macrophages

Macrophages (Mφ) are critical regulators of blood homeostasis and innate immune activation, serving as sentinels for blood-borne pathogens [113] and tissue-damage signals [114]. These cells are highly plastic and functionally diverse, but often assume pro-tumor, wound healing roles in the context of cancer. In our experience, F4/80 is a powerful surface molecule for separating Mφs from monocytes, as tissue-resident Mφs constitutively express high levels of this marker (Figure S19D). We also found that red pulp Mφ strongly express CD80 and CD86, as well as activation marker CD38, inhibitory receptor ligand CD274, and I-A/I-E (Figure S19E). In solid cancers, tumor-associated Mφ (TAM) polarization is crucial for tumor response and often studied using the "classically activated, pro-inflammatory M1" and "alternatively activated, anti-inflammatory, wound-healing M2" paradigm [115, 116] (although this definition has now been revised to reflect a spectrum of fluid states [117, 118]). As an alternative to iNOS ("M1") and Arginase-1 ("M2") intracellular staining, upregulation of CD38, CD40, CD80, CD86, and I-A/I-E expression intensity has been associated with an anti-tumor "M1-like" phenotype, while CD206 (used in panel variations) and CD274 are used to identify "M2-like" TAMs [119–121]. It was essential to incorporate these markers to increase the pre-clinical applications of our panel, as $CD38^{+}$ macrophage density has been associated with improved prognosis after surgery in human hepatocellular carcinoma [122] while CD274 mRNA expression was positively correlated with "M2" TAM polarization and poorer outcomes in glioblastoma patients [123].

2.3 | Granulocytes

2.3.1 | Basophils, neutrophils, and eosinophils

In secondary lymphoid tissues, the simple 14-marker gating strategy described previously can completely resolve basophils, neutrophils,

and eosinophils with only FcεR1α, Ly6G, and Siglec-F, respectively (Figure 1B, Figure S20A). Due to their inflammatory roles as first-responding innate immune cells in cancer, we did not dedicate a set of functional markers to these cells but refer the reader to several excellent publications that discuss these granulocytes in detail: basophils [124], neutrophils [125, 126], eosinophils [127, 128].

2.4 | Computational pipeline

2.4.1 | OMIQ workflow

After analyzing our dataset with traditional gating methods, we then implemented computational strategies to visualize population distributions throughout all secondary lymphoid tissues. Using OMIQ (https://www.omiq.ai/), we first uploaded an equal number of cleaned $CD45^+$ leukocytes across all secondary lymphoid tissues and transformed each fluorescent parameter using arcsinh scaling, adjusting each cofactor to compress negative populations unimodally around 0. We then utilized uniform manifold approximation and projection [129] (UMAP) to project 39 parameters (Live/Dead Blue was excluded) into two-dimensional space (Figure S21A). Afterwards, gates applied to the spleen were copied to all other lymphoid tissues and mapped onto the global structure in a single, colored plot (Figure 1I). To compare leukocyte frequencies across all secondary lymphoid tissues, we constructed an abundance heatmap and colored each row according to frequency to quantify compositional heterogeneity (Figure 1J). Afterwards, we extracted each tissue from the global UMAP in Figure 1I and plotted them as pseudocolor dot plots (Figure 1K) to visualize population distributions (thymus and bone marrow are included in Figure S22A,B).

3 | CONCLUSION

In conclusion, we present a full spectrum, 40-color immunophenotyping panel for robust exploration of all major leukocyte populations across primary and secondary lymphoid tissues. While we have personally focused on cancer research, a panel of such complexity is not limited to a single application and will be extremely valuable for studying global immune response in a wide variety of mouse model systems. Additionally, we have shown that a simplified panel of ~14 colors/markers (Figure 1A,B, and potentially less if SSC-A is fully utilized for granulocytes) is sufficient to identify the most major subsets within secondary lymphoid tissues. Such a strategy can easily be adapted to traditional cytometry settings or used as a backbone in more specialized spectral panels to dump unwanted immune cells, allowing researchers to account for a great deal of immune cell complexity with relatively few fluorochromes. In total, the depth and resolution achieved with this panel marks an important milestone within the FSFC murine immunophenotyping literature and will aid both pre-clinical research and panel development in the years to come.

3.1 | Similarity to published OMIPs

Our panel shares similarity to OMIPs −031, −032, −076, and − 079 with the use of CD3ε, CD4, CD8α, CD44, and CD62L to phenotype T cell subsets in the spleen [130–133]. OMIP-054 uses CyTOF in an immunocompetent mouse model of glioblastoma, but shares some similarities in the broad immunophenotyping efforts, spleen and bone marrow tissues studied, and marker choice [134]. OMIPs −057, −059, and − 061 explore γδT cell development in the thymus, progenitor composition in the bone marrow, and antigen presenting cell frequency in virally infected lymph nodes respectively; thus, they share small overlaps in the populations and tissues explored in this work [135–137]. Lastly, OMIP-93 shares similarity in complexity and panel purpose [138].

AUTHOR CONTRIBUTIONS

Aris John Kare: Conceptualization; investigation; writing – original draft; methodology; validation; visualization; writing – review and editing; formal analysis; software; data curation. **Lisa Nichols:** Writing – review and editing; investigation; methodology; resources. **Ricardo Zermeno:** Methodology; investigation. **Marina N. Raie:** Methodology; investigation; writing – review and editing. **Spencer K. Tumbale:** Methodology; investigation; writing – review and editing. **Katherine W. Ferrara:** Writing – review and editing; funding acquisition; project administration; supervision; resources.

ACKNOWLEDGMENTS

The authors would like to thank Christina Giatzikis, Karen Bond, Anisha Madhav, and Kathryn Andrews for helping us to acquire multiple reagents used in this work. The authors would also like to thank Ravi Hingorani for his advice in panel construction and Geoff Kracker for his guidance in using the OMIQ platform for computational analyses. The authors are incredibly grateful to Patrick Duncker and Jonathan Paw for generating figures and their expertise in spectral flow cytometry acquisition, unmixing, and data analysis. The authors also want to thank Dave Parks for his work in optimizing gain settings on Stanford's Cytek Aurora cytometer. Lastly, the authors thank Elizabeth Ingham and James Wang for helping to edit our manuscript.

FUNDING INFORMATION

This research was supported in part by a training grant from NIH Cellular and Molecular Training Grant (NIGMS, grant number 5T32GM007276). Additional funding from the NIH was also used for this work (grant numbers R01CA250557, R01CA253316, R01CA112356, and R01EB028646).

CONFLICT OF INTEREST STATEMENT

The authors declare no conflicts of interest.

DATA AVAILABILITY STATEMENT

Fully stained .fcs files for all primary and secondary lymphoid tissues can be publically accessed at http://flowrepository.org/id/FR-FCM-Z63E. Additional data that support the findings of the study, such as

single stained controls and select FMOs, are available from the lead author upon reasonble request.

ORCID

Aris J. Kare https://orcid.org/0000-0002-4896-2853
Lisa Nichols https://orcid.org/0000-0003-3635-0435
Marina N. Raie https://orcid.org/0000-0002-5549-404X
Spencer K. Tumbale https://orcid.org/0000-0002-0616-8280
Katherine W. Ferrara https://orcid.org/0000-0002-4976-9107

REFERENCES

1. Gubin MM, Esaulova E, Ward JP, Malkova ON, Runci D, Wong P, et al. High-dimensional analysis delineates myeloid and lymphoid compartment remodeling during successful immune-checkpoint cancer therapy. Cell. 2018;175:1014–30. https://doi.org/10.1016/j.cell.2018.09.030
2. Salmon H, Idoyaga J, Rahman A, Leboeuf M, Remark R, Jordan S, et al. Expansion and activation of CD103(+) dendritic cell progenitors at the tumor site enhances tumor responses to therapeutic PD-L1 and BRAF inhibition. Immunity. 2016;44:924–38. https://doi.org/10.1016/j.immuni.2016.03.012
3. Bonilla DL, Reinin G, Chua E. Full Spectrum flow cytometry as a powerful Technology for Cancer Immunotherapy Research. Front Mol Biosci. 2021;7:1–10. https://doi.org/10.3389/fmolb.2020.612801
4. Hotson AN, Gopinath S, Nicolau M, Khasanova A, Finck R, Monack D, et al. Coordinate actions of innate immune responses oppose those of the adaptive immune system during Salmonella infection of mice. Sci Signal. 2016;9:ra4. https://doi.org/10.1126/scisignal.aaa9303
5. Ferrer-Font L, Mehta P, Harmos P, Schmidt AJ, Chappell S, Price KM, et al. High-dimensional analysis of intestinal immune cells during helminth infection. elife. 2020;9:e51678. https://doi.org/10.7554/eLife.51678
6. Tao L, Reese TA. Making mouse models that reflect human immune responses. Trends Immunol. 2017;38:181–93. https://doi.org/10.1016/j.it.2016.12.007
7. Krishnarajah S, Ingelfinger F, Friebel E, Cansever D, Amorim A, Andreadou M, et al. Single-cell profiling of immune system alterations in lymphoid, barrier and solid tissues in aged mice. Nat Aging. 2022;2:74–89. https://doi.org/10.1038/s43587-021-00148-x
8. Nikolaou C, Muehle K, Schlickeiser S, Japp AS, Matzmohr N, Kunkel D, et al. High-dimensional single cell mass cytometry analysis of the murine hematopoietic system reveals signatures induced by ageing and physiological pathogen challenges. Immun Ageing. 2021;18:20. https://doi.org/10.1186/s12979-021-00230-3
9. Rosenthal N, Brown S. The mouse ascending: perspectives for human-disease models. Nat Cell Biol. 2007;9:993–9. https://doi.org/10.1038/ncb437
10. Winkels H, Ehinger E, Vassallo M, Buscher K, Dinh HQ, Kobiyama K, et al. Atlas of the immune cell repertoire in mouse atherosclerosis defined by single-cell RNA-sequencing and mass cytometry. Circ Res. 2018;122:1675–88. https://doi.org/10.1161/circresaha.117.312513
11. Guilliams M, Dutertre CA, Scott CL, McGovern N, Sichien D, Chakarov S, et al. Unsupervised high-dimensional analysis aligns dendritic cells across tissues and species. Immunity. 2016;45:669–84. https://doi.org/10.1016/j.immuni.2016.08.015
12. Korin B, Ben-Shaanan TL, Schiller M, Dubovik T, Azulay-Debby H, Boshnak NT, et al. High-dimensional, single-cell characterization of the brain's immune compartment. Nat Neurosci. 2017;20:1300–9. https://doi.org/10.1038/nn.4610
13. Amir ED, Lee B, Badoual P, Gordon M, Guo XV, Merad M, et al. Development of a comprehensive antibody staining database using a standardized analytics pipeline. Front Immunol. 2019;10:1315. https://doi.org/10.3389/fimmu.2019.01315
14. Weisel NM, Joachim SM, Smita S, Callahan D, Elsner RA, Conter LJ, et al. Surface phenotypes of naive and memory B cells in mouse and human tissues. Nat Immunol. 2022;23:135–45. https://doi.org/10.1038/s41590-021-01078-x
15. Bendall SC, Nolan GP, Roederer M, Chattopadhyay PK. A deep profiler's guide to cytometry. Trends Immunol. 2012;33:323–32. https://doi.org/10.1016/j.it.2012.02.010
16. Telford WG. Near-ultraviolet laser diodes for brilliant ultraviolet fluorophore excitation. Cytometry A. 2015;87:1127–37. https://doi.org/10.1002/cyto.a.22686
17. Chattopadhyay PK, Hogerkorp C-M, Roederer M. A chromatic explosion: the development and future of multiparameter flow cytometry. Immunology. 2008;125:441–9. https://doi.org/10.1111/j.1365-2567.2008.02989.x
18. Mitra-Kaushik S, Mehta-Damani A, Stewart JJ, Green C, Litwin V, Gonneau C. The evolution of single-cell analysis and utility in drug development. AAPS J. 2021;23:98. https://doi.org/10.1208/s12248-021-00633-6
19. Niewold P, Ashhurst TM, Smith AL, King NJC. Evaluating spectral cytometry for immune profiling in viral disease. Cytometry A. 2020;97:1165–79. https://doi.org/10.1002/cyto.a.24211
20. Lawrence W, Varadi G, Entine G, Podniesinski E, Wallace P. A comparison of avalanche photodiode and photomultiplier tube detectors for flow cytometry. Imaging, Manipulation, and Analysis of Biomolecules, Cells, and Tissues VI, vol. 6859, PWB (SPIE, 2008). 2008.
21. Wanner N, Barnhart J, Apostolakis N, Zlojutro V, Asosingh K. Using the autofluorescence finder on the Sony ID7000TM spectral cell analyzer to identify and unmix multiple highly autofluorescent murine lung populations. Front Bioeng Biotechnol. 2022;10:1–12. https://doi.org/10.3389/fbioe.2022.827987
22. Jameson VJ, Luke T, Yan Y, Hind A, Evrard M, Man K, et al. Unlocking autofluorescence in the era of full spectrum analysis: implications for immunophenotype discovery projects. Cytometry A. 2022;101:922–41. https://doi.org/10.1002/cyto.a.24555
23. Lokwani R, Chaudhari R, Wolf MT, Sadtler K. Spectral cytometry on highly autofluorescent samples. Nat Rev Methods Primers. 2022;2:71. https://doi.org/10.1038/s43586-022-00156-0
24. Park LM, Lannigan J, Jaimes MC. OMIP-069: forty-color full Spectrum flow cytometry panel for Deep immunophenotyping of major cell subsets in human peripheral blood. Cytometry A. 2020;97:1044–51. https://doi.org/10.1002/cyto.a.24213
25. Sahir F, Mateo JM, Steinhoff M, Siveen KS. Development of a 43 color panel for the characterization of conventional and unconventional T-cell subsets, B cells, NK cells, monocytes, dendritic cells, and innate lymphoid cells using spectral flow cytometry. Cytometry A. 2020;1–7. https://doi.org/10.1002/cyto.a.24288
26. Ferrer-Font L, Pellefigues C, Mayer JU, Small SJ, Jaimes MC, Price KM. Panel design and optimization for high-dimensional immunophenotyping assays using spectral flow cytometry. Curr Protoc Cytom. 2020;92:e70. https://doi.org/10.1002/cpcy.70
27. Liechti T, Weber LM, Ashhurst TM, Stanley N, Prlic M, Van Gassen S, et al. An updated guide for the perplexed: cytometry in the high-dimensional era. Nat Immunol. 2021;22:1190–7. https://doi.org/10.1038/s41590-021-01006-z
28. Wang W, Creusot RJ. Orchestrating multiplexity in polychromatic science through OMIPs: a decade-old resource to empower biomedical research. Cytometry A. 2021;99:866–74. https://doi.org/10.1002/cyto.a.24471
29. Kalina T, Fišer K, Pérez-Andrés M, Kuzílková D, Cuenca M, Bartol SJW, et al. CD maps-dynamic profiling of CD1-CD100 surface expression on human leukocyte and lymphocyte subsets. Front

Immunol. 2019;10:2434. https://doi.org/10.3389/fimmu.2019.02434

30. Engel P, Boumsell L, Balderas R, Bensussan A, Gattei V, Horejsi V, et al. CD nomenclature 2015: human leukocyte differentiation antigen workshops as a driving force in immunology. J Immunol. 2015;195:4555–63. https://doi.org/10.4049/jimmunol.1502033
31. Pang DJ, Neves JF, Sumaria N, Pennington DJ. Understanding the complexity of γδ T-cell subsets in mouse and human. Immunology. 2012;136:283–90. https://doi.org/10.1111/j.1365-2567.2012.03582.x
32. Abel AM, Yang C, Thakar MS, Malarkannan S. Natural killer cells: development, maturation, and clinical utilization. Front Immunol. 2018;9:1869. https://doi.org/10.3389/fimmu.2018.01869
33. Davenport MP, Smith NL, Rudd BD. Building a T cell compartment: how immune cell development shapes function. Nat Rev Immunol. 2020;20:499–506. https://doi.org/10.1038/s41577-020-0332-3
34. Rose S, Misharin A, Perlman H. A novel Ly6C/Ly6G-based strategy to analyze the mouse splenic myeloid compartment. Cytometry A. 2012;81A:343–50. https://doi.org/10.1002/cyto.a.22012
35. Guilliams M, van de Laar L. A Hitchhiker's guide to myeloid cell subsets: practical implementation of a novel mononuclear phagocyte classification system. Front Immunol. 2015;6:406. https://doi.org/10.3389/fimmu.2015.00406
36. Wculek SK, Cueto FJ, Mujal AM, Melero I, Krummel MF, Sancho D. Dendritic cells in cancer immunology and immunotherapy. Nat Rev Immunol. 2020;20:7–24. https://doi.org/10.1038/s41577-019-0210-z
37. Meghraoui-Kheddar A, Barthelemy S, Boissonnas A, Combadière C. Revising CX3CR1 expression on murine classical and non-classical monocytes. Front Immunol. 2020;11:1117. https://doi.org/10.3389/fimmu.2020.01117
38. Guilliams M, Mildner A, Yona S. Developmental and functional heterogeneity of monocytes. Immunity. 2018;49:595–613. https://doi.org/10.1016/j.immuni.2018.10.005
39. Teh YC, Ding JL, Ng LG, Chong SZ. Capturing the fantastic voyage of monocytes through time and space. Front Immunol. 2019;10:834. https://doi.org/10.3389/fimmu.2019.00834
40. Lee JJ, Jacobsen EA, Ochkur SI, McGarry MP, Condjella RM, Doyle AD, et al. Human versus mouse eosinophils: "that which we call an eosinophil, by any other name would stain as red". J Allergy Clin Immunol. 2012;130:572–84. https://doi.org/10.1016/j.jaci.2012.07.025
41. Stackowicz J, Jönsson F, Reber LL. Mouse models and tools for the in vivo study of neutrophils. Front Immunol. 2019;10:3130. https://doi.org/10.3389/fimmu.2019.03130
42. Chirumbolo S. State-of-the-art review about basophil research in immunology and allergy: is the time right to treat these cells with the respect they deserve? Blood Transfus. 2012;10:148–64. https://doi.org/10.2450/2011.0020-11
43. Hoffman W, Lakkis FG, Chalasani G. B cells, antibodies, and more. Clin J Am Soc Nephrol. 2016;11:137–54. https://doi.org/10.2215/cjn.09430915
44. Akkaya M, Kwak K, Pierce SK. B cell memory: building two walls of protection against pathogens. Nat Rev Immunol. 2020;20:229–38. https://doi.org/10.1038/s41577-019-0244-2
45. Donís-Hernández FR, Parkhouse RM, Santos-Argumedo L. Ontogeny, distribution and function of CD38-expressing B lymphocytes in mice. Eur J Immunol. 2001;31:1261–7. https://doi.org/10.1002/1521-4141(200104)31:4<1261::AID-IMMU1261gt;3.0.CO;2-H
46. Loder F et al. B cell development in the spleen takes place in discrete steps and is determined by the quality of B cell receptor-derived signals. J Exp Med. 1999;190:75–89. https://doi.org/10.1084/jem.190.1.75
47. Benitez A, Weldon AJ, Tatosyan L, Velkuru V, Lee S, Milford TA, et al. Differences in mouse and human nonmemory B cell pools. J Immunol. 2014;192:4610–9. https://doi.org/10.4049/jimmunol.1300692
48. Oliver AM, Martin F, Gartland GL, Carter RH, Kearney JF. Marginal zone B cells exhibit unique activation, proliferative and immunoglobulin secretory responses. Eur J Immunol. 1997;27:2366–74. https://doi.org/10.1002/eji.1830270935
49. Petro JB, Gerstein RM, Lowe J, Carter RS, Shinners N, Khan WN. Transitional type 1 and 2 B lymphocyte subsets are differentially responsive to antigen receptor signaling *. J Biol Chem. 2002;277:48009. https://doi.org/10.1074/jbc.M200305200
50. Allman D, Lindsley RC, DeMuth W, Rudd K, Shinton SA, Hardy RR. Resolution of three nonproliferative immature splenic B cell subsets reveals multiple selection points during peripheral B cell maturation. J Immunol. 2001;167:6834. https://doi.org/10.4049/jimmunol.167.12.6834
51. Cerutti A, Cols M, Puga I. Marginal zone B cells: virtues of innate-like antibody-producing lymphocytes. Nat Rev Immunol. 2013;13:118–32. https://doi.org/10.1038/nri3383
52. Khan AR, Hams E, Floudas A, Sparwasser T, Weaver CT, Fallon PG. PD-L1hi B cells are critical regulators of humoral immunity. Nat Commun. 2015;6:5997. https://doi.org/10.1038/ncomms6997
53. Morrison VL, Barr TA, Brown S, Gray D. TLR-mediated loss of CD62L focuses B cell traffic to the spleen during salmonella typhimurium infection. J Immunol. 2010;185:2737–46. https://doi.org/10.4049/jimmunol.1000758
54. Oliver AM, Martin F, Kearney JF. Mouse CD38 is down-regulated on germinal center B cells and mature plasma cells. J Immunol. 1997;158:1108–15.
55. Young C, Brink R. The unique biology of germinal center B cells. Immunity. 2021;54:1652–64. https://doi.org/10.1016/j.immuni.2021.07.015
56. Zuccarino-Catania GV, Sadanand S, Weisel FJ, Tomayko MM, Meng H, Kleinstein SH, et al. CD80 and PD-L2 define functionally distinct memory B cell subsets that are independent of antibody isotype. Nat Immunol. 2014;15:631–7. https://doi.org/10.1038/ni.2914
57. Suvas S, Singh V, Sahdev S, Vohra H, Agrewala JN. Distinct role of CD80 and CD86 in the regulation of the activation of B cell and B cell lymphoma. J Biol Chem. 2002;277:7766–75. https://doi.org/10.1074/jbc.M105902200
58. Rau FC, Dieter J, Luo Z, Priest SO, Baumgarth N. B7-1/2 (CD80/CD86) direct signaling to B cells enhances IgG secretion. J Immunol. 2009;183:7661–71. https://doi.org/10.4049/jimmunol.0803783
59. Sakaguchi S, Yamaguchi T, Nomura T, Ono M. Regulatory T cells and immune tolerance. Cell. 2008;133:775–87. https://doi.org/10.1016/j.cell.2008.05.009
60. Togashi Y, Shitara K, Nishikawa H. Regulatory T cells in cancer immunosuppression — implications for anticancer therapy. Nat Rev Clin Oncol. 2019;16:356–71. https://doi.org/10.1038/s41571-019-0175-7
61. Ivetic A, Hoskins Green HL, Hart SJ. L-selectin: a major regulator of leukocyte adhesion, migration and signaling. Front Immunol. 2019;10:1068. https://doi.org/10.3389/fimmu.2019.01068
62. Baaten BJ, Tinoco R, Chen AT, Bradley LM. Regulation of antigen-experienced T cells: lessons from the quintessential memory marker CD44. Front Immunol. 2012;3:23. https://doi.org/10.3389/fimmu.2012.00023
63. Vasanthakumar A, Liao Y, Teh P, Pascutti MF, Oja AE, Garnham AL, et al. The TNF receptor superfamily-NF-κB Axis is critical to maintain effector regulatory T cells in lymphoid and non-lymphoid tissues. Cell Rep. 2017;20:2906–20. https://doi.org/10.1016/j.celrep.2017.08.068
64. Koizumi SI, Ishikawa H. Transcriptional regulation of differentiation and functions of effector T regulatory cells. Cell. 2019;8:1–17. https://doi.org/10.3390/cells8080939

65. Tanaka A, Sakaguchi S. Regulatory T cells in cancer immunotherapy. Cell Res. 2017;27:109–18. https://doi.org/10.1038/cr.2016.151
66. Borst J, Hendriks J, Xiao Y. CD27 and CD70 in T cell and B cell activation. Curr Opin Immunol. 2005;17:275–81. https://doi.org/10.1016/j.coi.2005.04.004
67. Flieswasser T, Van Den Eynde A, Van Audenaerde J, De Waele J, Lardon F, Riether C, et al. The CD70-CD27 axis in oncology: the new kids on the block. J Exp Clin Cancer Res. 2022;41:12. https://doi.org/10.1186/s13046-021-02215-y
68. Yang ZZ, Grote DM, Xiu B, Ziesmer SC, Price-Troska TL, Hodge LS, et al. TGF-β upregulates CD70 expression and induces exhaustion of effector memory T cells in B-cell non-Hodgkin's lymphoma. Leukemia. 2014;28:1872–84. https://doi.org/10.1038/leu.2014.84
69. Jak M, Jak M, Mous R, Remmerswaal EBM, Spijker R, Jaspers A, et al. Enhanced formation and survival of CD4+ CD25hi Foxp3+ T-cells in chronic lymphocytic leukemia. Leuk Lymphoma. 2009;50:788–801. https://doi.org/10.1080/10428190902803677
70. Croft M, So T, Duan W, Soroosh P. The significance of OX40 and OX40L to T-cell biology and immune disease. Immunol Rev. 2009;229:173–91. https://doi.org/10.1111/j.1600-065X.2009.00766.x
71. Redmond WL, Ruby CE, Weinberg AD. The role of OX40-mediated co-stimulation in T-cell activation and survival. Crit Rev Immunol. 2009;29:187–201. https://doi.org/10.1615/critrevimmunol.v29.i3.10
72. Curti BD, Kovacsovics-Bankowski M, Morris N, Walker E, Chisholm L, Floyd K, et al. OX40 is a potent immune-stimulating target in late-stage cancer patients. Cancer Res. 2013;73:7189–98. https://doi.org/10.1158/0008-5472.Can-12-4174
73. Hänninen A, Maksimow M, Alam C, Morgan DJ, Jalkanen S. Ly6C supports preferential homing of central memory CD8+ T cells into lymph nodes. Eur J Immunol. 2011;41:634–44. https://doi.org/10.1002/eji.201040760
74. Corgnac S, Boutet M, Kfoury M, Naltet C, Mami-Chouaib F. The emerging role of CD8(+) tissue resident memory T (T(RM)) cells in antitumor immunity: a unique functional contribution of the CD103 integrin. Front Immunol. 2018;9:1904. https://doi.org/10.3389/fimmu.2018.01904
75. Eberl G, Colonna M, Di Santo JP, McKenzie AN. Innate lymphoid cells. Innate lymphoid cells: a new paradigm in immunology. Science. 2015;348:aaa6566. https://doi.org/10.1126/science.aaa6566
76. Robinette ML et al. Transcriptional programs define molecular characteristics of innate lymphoid cell classes and subsets. Nat Immunol. 2015;16:306–17. https://doi.org/10.1038/ni.3094
77. Chiossone L, Chaix J, Fuseri N, Roth C, Vivier E, Walzer T. Maturation of mouse NK cells is a 4-stage developmental program. Blood. 2009;113:5488–96. https://doi.org/10.1182/blood-2008-10-187179
78. Hayakawa Y, Smyth MJ. CD27 dissects mature NK cells into two subsets with distinct responsiveness and migratory Capacity1. J Immunol. 2006;176:1517. https://doi.org/10.4049/jimmunol.176.3.1517
79. Hayakawa Y, Huntington ND, Nutt SL, Smyth MJ. Functional subsets of mouse natural killer cells. Immunol Rev. 2006;214:47–55. https://doi.org/10.1111/j.1600-065X.2006.00454.x
80. Omi A, Enomoto Y, Kiniwa T, Miyata N, Miyajima A. Mature resting Ly6C(high) natural killer cells can be reactivated by IL-15. Eur J Immunol. 2014;44:2638–47. https://doi.org/10.1002/eji.201444570
81. Krneta T, Gillgrass A, Chew M, Ashkar AA. The breast tumor microenvironment alters the phenotype and function of natural killer cells. Cell Mol Immunol. 2016;13:628–39. https://doi.org/10.1038/cmi.2015.42
82. Zhang Q-F, Yin WW, Xia Y, Yi YY, He QF, Wang X, et al. Liver-infiltrating CD11b−CD27− NK subsets account for NK-cell dysfunction in patients with hepatocellular carcinoma and are associated with tumor progression. Cell Mol Immunol. 2017;14:819–29. https://doi.org/10.1038/cmi.2016.28
83. Jin J, Fu B, Mei X, Yue T, Sun R, Tian Z, et al. CD11b(−)CD27(−) NK cells are associated with the progression of lung carcinoma. PLoS One. 2013;8:e61024. https://doi.org/10.1371/journal.pone.0061024
84. Chan CW, Crafton E, Fan HN, Flook J, Yoshimura K, Skarica M, et al. Interferon-producing killer dendritic cells provide a link between innate and adaptive immunity. Nat Med. 2006;12:207–13. https://doi.org/10.1038/nm1352
85. Taieb J, Chaput N, Ménard C, Apetoh L, Ullrich E, Bonmort M, et al. A novel dendritic cell subset involved in tumor immunosurveillance. Nat Med. 2006;12:214–9. https://doi.org/10.1038/nm1356
86. Guimont-Desrochers F, Boucher G, Dong Z, Dupuis M, Veillette A, Lesage S. Redefining interferon-producing killer dendritic cells as a novel intermediate in NK-cell differentiation. Blood. 2012;119:4349–57. https://doi.org/10.1182/blood-2011-11-395954
87. Guimont-Desrochers F, Lesage S. Revisiting the prominent anti-tumoral potential of pre-mNK cells. Front Immunol. 2013;4:446. https://doi.org/10.3389/fimmu.2013.00446
88. Ma Z, Li W, Yoshiya S, Xu Y, Hata M, el-Darawish Y, et al. Augmentation of immune checkpoint cancer immunotherapy with IL18. Clin Cancer Res. 2016;22:2969–80. https://doi.org/10.1158/1078-0432.CCR-15-1655
89. Rosinsky C, Antony PA. A role for pre-mNK cells in tumor progression. J Immunother Cancer. 2016;4:16. https://doi.org/10.1186/s40425-016-0120-6
90. Cabeza-Cabrerizo M, Cardoso A, Minutti CM, Pereira da Costa M, Reis e Sousa C. Dendritic cells revisited. Annu Rev Immunol. 2021;39:131–66. https://doi.org/10.1146/annurev-immunol-061020-053707
91. Audiger C, Rahman MJ, Yun TJ, Tarbell KV, Lesage S. The importance of dendritic cells in maintaining immune tolerance. J Immunol. 2017;198:2223–31. https://doi.org/10.4049/jimmunol.1601629
92. Ari Waisman DL, Clausen BE, Yogev N. Dendritic cells as gatekeepers of tolerance. Semin Immunopathol. 2017;39:153–63. https://doi.org/10.1007/s00281-016-0583-z
93. Merad M, Sathe P, Helft J, Miller J, Mortha A. The dendritic cell lineage: ontogeny and function of dendritic cells and their subsets in the steady state and the inflamed setting. Annu Rev Immunol. 2013;31:563–604. https://doi.org/10.1146/annurev-immunol-020711-074950
94. Brown CC, Gudjonson H, Pritykin Y, Deep D, Lavallée VP, Mendoza A, et al. Transcriptional basis of mouse and human dendritic cell heterogeneity. Cell. 2019;179:846–63. https://doi.org/10.1016/j.cell.2019.09.035
95. Reis e Sousa C. Dendritic cells in a mature age. Nat Rev Immunol. 2006;6:476–83. https://doi.org/10.1038/nri1845
96. Dudek AM, Martin S, Garg AD, Agostinis P. Immature, semi-mature, and fully mature dendritic cells: toward a DC-cancer cells Interface that augments anticancer immunity. Front Immunol. 2013;4:438. https://doi.org/10.3389/fimmu.2013.00438
97. Hegde S, Krisnawan VE, Herzog BH, Zuo C, Breden MA, Knolhoff BL, et al. Dendritic cell paucity leads to dysfunctional immune surveillance in pancreatic cancer. Cancer Cell. 2020;37:289–307. https://doi.org/10.1016/j.ccell.2020.02.008
98. Oba T, Long MD, Keler T, Marsh HC, Minderman H, Abrams SI, et al. Overcoming primary and acquired resistance to anti-PD-L1 therapy by induction and activation of tumor-residing cDC1s. Nat Commun. 2020;11:5415. https://doi.org/10.1038/s41467-020-19192-z
99. Wang J, Fite BZ, Kare AJ, Wu B, Raie M, Tumbale SK, et al. Multiomic analysis for optimization of combined focal and immunotherapy protocols in murine pancreatic cancer. Theranostics. 2022;12:7884–902. https://doi.org/10.7150/thno.73218
100. Lin JH, Huffman AP, Wattenberg MM, Walter DM, Carpenter EL, Feldser DM, et al. Type 1 conventional dendritic cells are

systemically dysregulated early in pancreatic carcinogenesis. J Exp Med. 2020;217:1–20. https://doi.org/10.1084/jem.20190673

101. Tjomsland V, Spångeus A, Sandström P, Borch K, Messmer D, Larsson M. Semi mature blood dendritic cells exist in patients with ductal pancreatic adenocarcinoma owing to inflammatory factors released from the tumor. PLoS One. 2010;5:e13441. https://doi.org/10.1371/journal.pone.0013441
102. Bosteels C, Neyt K, Vanheerswynghels M, Van Helden MJ, Sichien D, Debeuf N, et al. Inflammatory type 2 cDCs acquire features of cDC1s and macrophages to orchestrate immunity to respiratory virus infection. Immunity. 2020;52:1039–56. https://doi.org/10.1016/j.immuni.2020.04.005
103. Williford JM, Ishihara J, Ishihara A, Mansurov A, Hosseinchi P, Marchell TM, et al. Recruitment of CD103(+) dendritic cells via tumor-targeted chemokine delivery enhances efficacy of checkpoint inhibitor immunotherapy. Sci Adv. 2019;5:eaay1357. https://doi.org/10.1126/sciadv.aay1357
104. Flies DB, Higuchi T, Harris JC, Jha V, Gimotty PA, Adams SF. Immune checkpoint blockade reveals the stimulatory capacity of tumor-associated CD103(+) dendritic cells in late-stage ovarian cancer. Onco Targets Ther. 2016;5:e1185583. https://doi.org/10.1080/2162402x.2016.1185583
105. Fujiyama S, Nakahashi-Oda C, Abe F, Wang Y, Sato K, Shibuya A. Identification and isolation of splenic tissue-resident macrophage sub-populations by flow cytometry. Int Immunol. 2018;31:51–6. https://doi.org/10.1093/intimm/dxy064
106. Zhan Y, Chow KV, Soo P, Xu Z, Brady JL, Lawlor KE, et al. Plasmacytoid dendritic cells are short-lived: reappraising the influence of migration, genetic factors and activation on estimation of lifespan. Sci Rep. 2016;6:25060. https://doi.org/10.1038/srep25060
107. Swirski FK, Nahrendorf M, Etzrodt M, Wildgruber M, Cortez-Retamozo V, Panizzi P, et al. Identification of splenic reservoir monocytes and their deployment to inflammatory sites. Science. 2009;325:612–6. https://doi.org/10.1126/science.1175202
108. Beatty GL, Chiorean EG, Fishman MP, Saboury B, Teitelbaum UR, Sun W, et al. CD40 agonists Alter tumor stroma and show efficacy against pancreatic carcinoma in mice and humans. Science. 2011;331:1612–6. https://doi.org/10.1126/science.1198443
109. Long KB, Gladney WL, Tooker GM, Graham K, Fraietta JA, Beatty GL. IFNγ and CCL2 cooperate to redirect tumor-infiltrating monocytes to degrade fibrosis and enhance chemotherapy efficacy in pancreatic carcinoma. Cancer Discov. 2016;6:400–13. https://doi.org/10.1158/2159-8290.Cd-15-1032
110. Wiehagen KR, Girgis NM, Yamada DH, Smith AA, Chan SR, Grewal IS, et al. Combination of CD40 agonism and CSF-1R blockade reconditions tumor-associated macrophages and drives potent antitumor immunity. Cancer Immunol Res. 2017;5:1109–21. https://doi.org/10.1158/2326-6066.Cir-17-0258
111. Tamoutounour S, Henri S, Lelouard H, De Bovis B, De Haar C, Van Der Woude CJ, et al. CD64 distinguishes macrophages from dendritic cells in the gut and reveals the Th1-inducing role of mesenteric lymph node macrophages during colitis. Eur J Immunol. 2012;42:3150–66. https://doi.org/10.1002/eji.201242847
112. Bain CC, Scott CL, Uronen-Hansson H, Gudjonsson S, Jansson O, Grip O, et al. Resident and pro-inflammatory macrophages in the colon represent alternative context-dependent fates of the same Ly6Chi monocyte precursors. Mucosal Immunol. 2013;6:498–510. https://doi.org/10.1038/mi.2012.89
113. Borges da Silva H, Fonseca R, Pereira RM, Cassado AA, Álvarez JM, D'Império Lima MR. Splenic macrophage subsets and their function' during blood-borne infections. Front Immunol. 2015;6:480. https://doi.org/10.3389/fimmu.2015.00480
114. Laskin DL, Sunil VR, Gardner CR, Laskin JD. Macrophages and tissue injury: agents of defense or destruction? Annu Rev Pharmacol Toxicol. 2011;51:267–88. https://doi.org/10.1146/annurev.pharmtox.010909.105812
115. Wang N, Liang H, Zen K. Molecular mechanisms that influence the macrophage m1-m2 polarization balance. Front Immunol. 2014;5:614. https://doi.org/10.3389/fimmu.2014.00614
116. Boutilier AJ, Elsawa SF. Macrophage polarization states in the tumor microenvironment. Int J Mol Sci. 2021;22:6995.
117. Martinez FO, Gordon S. The M1 and M2 paradigm of macrophage activation: time for reassessment. F1000Prime Rep. 2014;6:13. https://doi.org/10.12703/p6-13
118. Xue J, Schmidt SV, Sander J, Draffehn A, Krebs W, Quester I, et al. Transcriptome-based network analysis reveals a spectrum model of human macrophage activation. Immunity. 2014;40:274–88. https://doi.org/10.1016/j.immuni.2014.01.006
119. Li M, He L, Zhu J, Zhang P, Liang S. Targeting tumor-associated macrophages for cancer treatment. Cell Biosci. 2022;12:85. https://doi.org/10.1186/s13578-022-00823-5
120. Jablonski KA, Amici SA, Webb LM, Ruiz-Rosado JD, Popovich PG, Partida-Sanchez S, et al. Novel markers to delineate murine M1 and M2 macrophages. PLoS One. 2015;10:e0145342. https://doi.org/10.1371/journal.pone.0145342
121. Orecchioni M, Ghosheh Y, Pramod AB, Ley K. Macrophage polarization: different gene signatures in M1(LPS+) vs. classically and M2(LPS-) vs. alternatively activated macrophages. Front Immunol. 2019;10:1084. https://doi.org/10.3389/fimmu.2019.01084
122. Lam JH, Ng HHM, Lim CJ, Sim XN, Malavasi F, Li H, et al. Expression of CD38 on macrophages predicts improved prognosis in hepatocellular carcinoma. Front Immunol. 2019;10:2093. https://doi.org/10.3389/fimmu.2019.02093
123. Zhu Z, Zhang H, Chen B, Liu X, Zhang S, Zong Z, et al. PD-L1-mediated immunosuppression in glioblastoma is associated with the infiltration and M2-polarization of tumor-associated macrophages. Front Immunol. 2020;11:1–9. https://doi.org/10.3389/fimmu.2020.588552
124. Marone G, Schroeder JT, Mattei F, Loffredo S, Gambardella AR, Poto R, et al. Is there a role for basophils in cancer? Front Immunol. 2020;11:2103. https://doi.org/10.3389/fimmu.2020.02103
125. Masucci MT, Minopoli M, Carriero MV, Tumor Associated Neutrophils. Their role in tumorigenesis, metastasis, prognosis and therapy. Front Oncol. 2019;9:1146. https://doi.org/10.3389/fonc.2019.01146
126. Xiong S, Dong L, Cheng L. Neutrophils in cancer carcinogenesis and metastasis. J Hematol Oncol. 2021;14:173. https://doi.org/10.1186/s13045-021-01187-y
127. Carretero R, Sektioglu IM, Garbi N, Salgado OC, Beckhove P, Hämmerling GJ. Eosinophils orchestrate cancer rejection by normalizing tumor vessels and enhancing infiltration of CD8(+) T cells. Nat Immunol. 2015;16:609–17. https://doi.org/10.1038/ni.3159
128. Varricchi G, Galdiero MR, Loffredo S, Lucarini V, Marone G, Mattei F, et al. Eosinophils: the unsung heroes in cancer? Onco Targets Ther. 2018;7:e1393134. https://doi.org/10.1080/2162402x.2017.1393134
129. McInnes L, Healy J, Melville J. Umap: uniform manifold approximation and projection for dimension reduction. arXiv preprint. 2018;arXiv:1802.03426.
130. Nemoto S, Mailloux AW, Kroeger J, Mulé JJ. OMIP-031: immunologic checkpoint expression on murine effector and memory T-cell subsets. Cytometry A. 2016;89:427–9. https://doi.org/10.1002/cyto.a.22808
131. Unsworth A, Anderson R, Haynes N, Britt K. OMIP-032: two multicolor immunophenotyping panels for assessing the innate and adaptive immune cells in the mouse mammary gland. Cytometry A. 2016;89:527–30. https://doi.org/10.1002/cyto.a.22867
132. Mincham KT, Young JD, Strickland DH. OMIP 076: high-dimensional immunophenotyping of murine T-cell, B-cell, and antibody secreting cell subsets. Cytometry A. 2021;99:888–92. https://doi.org/10.1002/cyto.a.24474

133. Natalini A, Simonetti S, Favaretto G, Peruzzi G, Antonangeli F, Santoni A, et al. OMIP-079: cell cycle of CD4(+) and CD8(+) naïve/-memory T cell subsets, and of Treg cells from mouse spleen. Cytometry A. 2021;99:1171–5. https://doi.org/10.1002/cyto.a.24509
134. Dusoswa SA, Verhoeff J, Garcia-Vallejo JJ. OMIP-054: broad immune phenotyping of innate and adaptive leukocytes in the brain, spleen, and bone marrow of an orthotopic murine glioblastoma model by mass cytometry. Cytometry A. 2019;95:422–6. https://doi.org/10.1002/cyto.a.23725
135. Buus TB, Jee MH, Ødum N. OMIP-057: mouse γδ T-cell development characterized by a 14 color flow cytometry panel. Cytometry A. 2019;95:726–9. https://doi.org/10.1002/cyto.a.23754
136. Eich M, Trumpp A, Schmitt S. OMIP-059: identification of mouse hematopoietic stem and progenitor cells with simultaneous detection of CD45.1/2 and controllable Green fluorescent protein expression by a single staining panel. Cytometry A. 2019;95:1049–52. https://doi.org/10.1002/cyto.a.23845
137. DiPiazza AT, Hill JP, Graham BS, Ruckwardt TJ. OMIP-061: 20-color flow cytometry panel for high-dimensional characterization of murine antigen-presenting cells. Cytometry A. 2019;95:1226–30. https://doi.org/10.1002/cyto.a.23880
138. Brandi J, Wiethe C, Riehn M, Jacobs T. OMIP-93: a 41-color high parameter panel to characterize various co-inhibitory molecules and their ligands in the lymphoid and myeloid compartment in mice. Cytometry A. 2023;103:624–30. https://doi.org/10.1002/cyto.a.24740

SUPPORTING INFORMATION

Additional supporting information can be found online in the Supporting Information section at the end of this article.

Panel Optimization for High-Dimensional Immunophenotyping Assays Using Full-Spectrum Flow Cytometry

Laura Ferrer-Font,[1,2,6,7] Sam J. Small,[1,6] Brittany Lewer,[1] Katherine R. Pilkington,[3] Laura K. Johnston,[4] Lily M. Park,[3] Joanne Lannigan,[5] Maria C. Jaimes,[3,6] and Kylie M. Price[1,6]

[1]Malaghan Institute of Medical Research, Wellington, New Zealand
[2]Maurice Wilkins Centre for Molecular Biodiscovery, Auckland, New Zealand
[3]Cytek Biosciences, Fremont, California
[4]University of Chicago, Chicago, Illinois
[5]Flow Cytometry Support Services, LLC, Alexandria, Virginia
[6]These authors contributed equally to this work.
[7]Corresponding author: *lferrer@malaghan.org.nz*

Technological advancements in fluorescence flow cytometry and an ever-expanding understanding of the complexity of the immune system have led to the development of large flow cytometry panels reaching up to 43 colors at the single-cell level. However, as panel size and complexity increase, so too does the detail involved in designing and optimizing successful high-quality panels fit for downstream high-dimensional data analysis. In contrast to conventional flow cytometers, full-spectrum flow cytometers measure the entire emission spectrum of each fluorophore across all lasers. This allows for fluorophores with very similar emission maxima but unique overall spectral fingerprints to be used in conjunction, enabling relatively straightforward design of larger panels. Although a protocol for best practices in full-spectrum flow cytometry panel design has been published, there is still a knowledge gap in going from the theoretically designed panel to the necessary steps required for panel optimization. Here, we aim to guide users through the theory of optimizing a high-dimensional full-spectrum flow cytometry panel for immunophenotyping using comprehensive step-by-step protocols. These protocols can also be used to troubleshoot panels when issues arise. A practical application of this approach is exemplified with a 24-color panel designed for identification of conventional T-cell subsets in human peripheral blood. © 2021 Malaghan Institute of Medical Research, Cytek Biosciences. Current Protocols published by Wiley Periodicals LLC.

Keywords: assay optimization and troubleshooting • full-spectrum flow cytometry • high-dimensional flow cytometry panel

CURRENT PROTOCOLS
A Wiley Brand

Current Protocols e222, Volume 1
Published in Wiley Online Library (wileyonlinelibrary.com).
doi: 10.1002/cpz1.222

How to cite this article:
Ferrer-Font, L., Small, S. J., Lewer, B., Pilkington, K. R., Johnston, L. K., Park, L. M., Lannigan, J., Jaimes, M. C., & Price, K. M. (2021). Panel optimization for high-dimensional immunophenotyping assays using full-spectrum flow cytometry. *Current Protocols*, *1*, e222. doi: 10.1002/cpz1.222

INTRODUCTION

Technological advancements in fluorescence flow cytometry and an ever-expanding understanding of the complexity of the immune system have led to the development of large panels reaching 40 fluorophores in the Optimized Multicolor Immunofluorescence Panel (OMIP; Park, Lannigan, & Jaimes, 2020) and 43 colors in a technical note (Sahir, Mateo, Steinhoff, & Siveen, 2020). In contrast to conventional flow cytometry, which primarily measures the peak emission of each fluorophore in a target detector, full-spectrum flow cytometry uses a larger number of detectors with narrow band-pass filters. This allows the entire emission spectrum for every fluorophore to be captured across all laser lines, creating a detailed signature of each fluorophore. This makes it possible to distinguish fluorophores with very similar emission maxima but unique overall spectral fingerprints, increasing the flexibility in fluorophore selection. This feature, coupled with an instrument designed to maximize the detection of emitted light and highly efficient avalanche photodiodes, provides improved detection efficiencies that translate to better detection limits and higher signal resolution (Feher et al., 2016). While these features, unique to full-spectrum flow cytometry, provide the high-quality signals and low noise needed for successful high-dimensional panels, many of the same panel design considerations from conventional flow cytometry still apply. Common characteristics, together with those specific to full-spectrum flow cytometry, have been previously described (Ferrer-Font, Pellefigues, et al., 2020; Park et al., 2020). Now that hardware limitations hindering the use of highly overlapping dyes have been overcome, the main limitations for successful large panel design are the spillover-spreading error inherent to the use of fluorescence and the number of fluorophores available with unique spectral signatures. Many companies have recently begun developing spectrally distinct fluorophores, thus advancing the number of markers available to be analyzed in a single experiment.

Increasing the number of markers in a panel consequently increases the probability of compromising the resolution of the markers and populations of interest. The theoretical approach to panel design aims to avoid issues would that prevent resolution of every marker in the panel; however, in practice it is challenging to perfectly predict the impact of co-expression, variations in marker expression levels, and the performance of each specific reagent. Furthermore, it is difficult to anticipate the accuracy of reference controls for optimal unmixing results. For example, certain fluorophores emit slightly different spectra when bound to compensation beads or in the presence of different buffers.

One obstacle that has always impacted panel design and performance is the unique autofluorescence (AF) signatures of different sample and cell types. Cellular AF levels can vary depending on the type and metabolic state of cells (Mayeno, Hamann, & Gleich, 1992; Roederer, 2016; Shi et al., 2017) as well as sample preparation and staining procedures. This translates into different AF brightness levels and distinct spectral signatures in the samples being analyzed. Full-spectrum flow cytometry can resolve cellular AF signatures and ensure that they are not attributed to any of the fluorophores used. This can improve the signal-to-noise ratio and resolution of markers attached to fluorophores that emit closest to AF maxima (Ferrer-Font, Pellefigues, et al., 2020) in highly

Improving Immunophenotyping Resolution by Overcoming Autofluorescence with Full Spectrum Flow Cytometry

autofluorescent tissues such as brain, lung, skin, intestine, and tumor (Schmutz, Valente, Cumano, & Novault, 2016). It is therefore highly recommended to characterize the AF spectrum of an unstained sample from the tissue or cell type of interest prior to panel design. This will provide useful information during fluorophore selection, ensuring that fluorophores are not allocated to areas of the spectrum where AF dominates.

STRATEGIC PLANNING

Once a high-dimensional full-spectrum flow cytometry panel has been optimally designed (Ferrer-Font, Pellefigues, et al., 2020), the step-by-step protocols presented here provide a series of practical steps for full and successful optimization. As outlined in Figure 1, the main procedures include evaluation of spectral reference controls (SRCs; see Basic Protocol 1), evaluation of unmixing of the fully stained (FS) sample (see Basic Protocol 2), evaluation of marker resolution (see Basic Protocol 3), and assessment of data quality (see Basic Protocol 4). Before any of these methods are performed, it is essential to titrate the antibodies used as well as any viability dye used. This is described in Support Protocol 1. An additional protocol describes changes that can be made to the instrument settings (see Support Protocol 2). Methods for evaluating and mitigating autofluorescence are included in Basic Protocol 3 and Support Protocol 3. Together, these protocols can also be used when troubleshooting a panel to identify sources of problems and provide insights into fixing them.

A 24-color panel optimization for identification of conventional T-cell subsets in human peripheral blood is provided to illustrate these procedures. The protocols were developed using the five-laser (5L) Cytek Aurora (Cytek Biosciences), but should be adaptable to any spectral flow cytometer. The protocols were designed for new full-spectrum flow cytometry users. Once familiarity and experience with specific tissue types is achieved, it is possible to modify the steps and order of the protocols to reduce the overall time

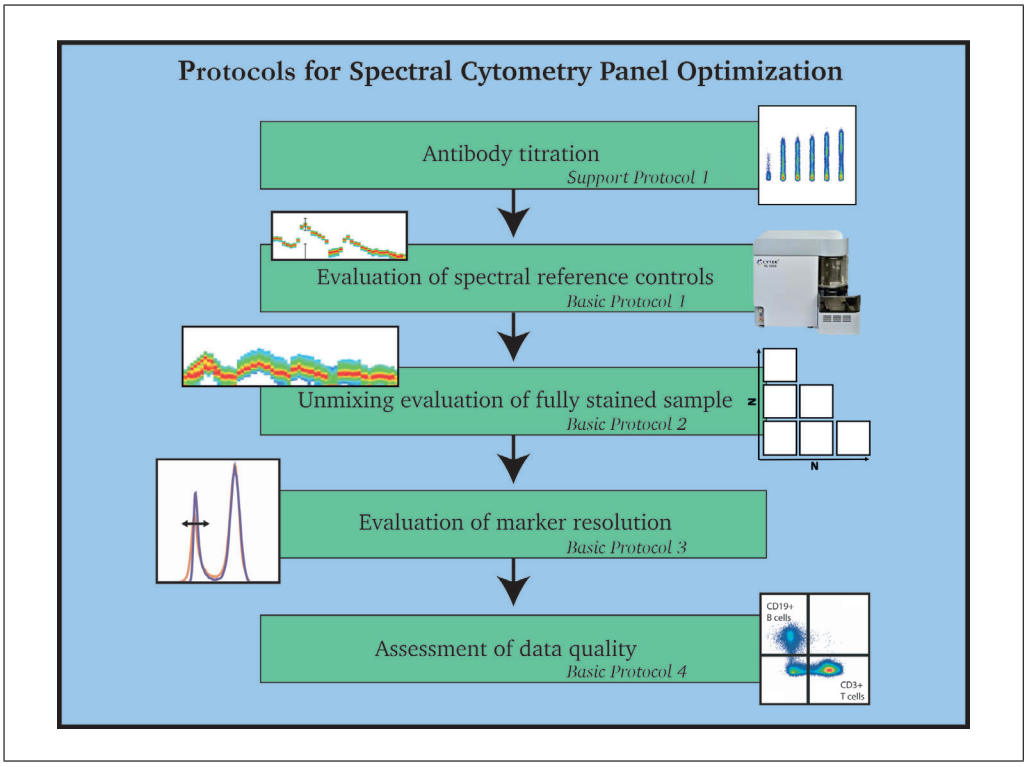

Figure 1 Overview of protocols for successful optimization of a high-dimensional spectral flow cytometry panel.

spent evaluating the panel. If a modified approach is taken, it is recommended that all the overall goals of the protocols (as outlined in Fig. 1) still be carried out.

BASIC PROTOCOL 1

PREPARATION AND EVALUATION OF OPTIMAL SPECTRAL REFERENCE CONTROLS

This protocol is divided in two sections. The first is for preparation of SRCs and ensures generation of the high-quality controls required for accurate unmixing. The steps describe the staining of polystyrene compensation beads and cryopreserved PBMCs with surface-labeling antibodies. They can be adapted for other tissues or staining procedures such as intracellular staining. It is important to mention that the preparation procedure will also guide users to prepare a fully stained (FS) sample and fluorescence minus one (FMO) controls as the protocols are very similar; these will be used later for evaluating the unmixing of the FS sample (see Basic Protocol 2). If preferred, FS and FMO samples can be stained separately, but treatment of samples should be kept identical. Importantly, to successfully complete this protocol, SS and FS cells should also be treated the same (antibody concentration, incubation time/temperature, fixed/unfixed, etc.).

The second section of the protocol is for evaluation. This aims first to check the quality of the acquired SRCs and then to evaluate whether there are any spectral mismatches between beads and cells for each fluorophore, which is accomplished by assessing how well the beads unmix the cells using N × N plots for all markers. Unmixing accuracy must be assessed on the actual sample (cells) to be used in the assay. In some cases beads will be acceptable as SRCs and in other cases it may be necessary to use cells. When this protocol is completed, the optimum SRCs (cells or beads) will be determined for future unmixing. If desired, well-characterized and high-quality controls can be stored for future use.

Materials

Cryopreserved PBMCs
Phosphate-buffered saline (PBS; Gibco, cat. no. 14190-250)
Fetal bovine serum (FBS; Gibco, cat. no. 10091-148)
Polystyrene compensation beads (e.g., UltraComp eBeads, Life Technologies, cat. no. 01-222-42)
FACS staining buffer: PBS with 2% bovine serum albumin (BSA; MP Biochemicals, CAS no. 9048-46-8) and 0.2% sodium azide (Sigma-Aldrich, cat. no. S8032)
Zombie NIR Fixable Viability Kit (BioLegend, cat. no. 423106)
Human TruStain FcX (Fc Receptor Blocking Solution; BioLegend, cat. no. 422301)
Antibodies (see Table 1 for list; see Support Protocol 1 for titration)
Brilliant Stain Buffer Plus (BD Biosciences, cat. no. 566385)

37°C water bath (e.g., Julabo Ecotemp TW12)
Hemocytometer (e.g., Hawksley Counting Chamber) and coverslips
96-well U-bottom plate (In Vitro Technologies, cat. no. 353077)
Filters with 0.65-μm or smaller pore size (*optional*)
Spectral cytometer (e.g., Cytek Aurora)
5-ml polypropylene round-bottom flow tubes (In Vitro Technologies, cat. no. 352008)
Cytek SpectroFlo software
Data analysis software for analyzing FCS files (e.g., FlowJo or FCS Express)

Prepare and acquire samples

1. Thaw PBMCs quickly in a 37°C water bath and add to 5 ml PBS with 2% FBS.

Table 1 Antibodies Used in Example Spectral Flow Cytometry Panel

Fluorophore	Marker	Supplier	Clone	Catalog number	Concentration (mg/ml)
BUV395	HLA-DR	BD Biosciences	G46-6	564040	1
BUV496	CD3	BD Biosciences	UCHT1	612940	1
BUV563	CD27	BD Biosciences	M-T271	741336	1
BUV737	CD45RA	BD Biosciences	HI100	612846	1.25
BV421	CD28	BioLegend	CD28.2	302930	2
Pacific Blue	CRTH2 (CD294)	BioLegend	BM16	350130	8
BV480	CD127	BD Biosciences	HIL-7R-M21	566101	2
BV510	TCRgd	BioLegend	B1	331220	15
BV570	CD4	BioLegend	RPA-T4	300534	1
BV605	CCR4 (CD194)	BioLegend	L291H4	359418	0.6
BV650	CCR6 (CD196)	BD Biosciences	11A9	563922	1
BV785	CD45RO	BioLegend	UCHL1	304234	1
BB515	CD25	BD Biosciences	2A3	564467	8.3
AF488	CCR10	R&D Systems	314305	RDSFAB3478G 0100	0.13
AF532	CD8	Thermo Fisher Scientific	RPA-T8	58-0088-42	0.25
PerCP-Cy5.5	CCR7	BioLegend	G043H7	353220	4
PE	Hu CD1d tetramer	NIH Tetramer Core Facility	PBS-57 loaded		0.81
PE-CF594	PLZF	BD Biosciences	R17-809	565738	0.63
PE-Cy7	CTLA4	eBioscience (TFS)	14D3	25-1529-42	0.2
APC	Hu MR1 tetramer	NIH Tetramer Core Facility	5-OP-RU loaded		0.18
AF647	FoxP3	BioLegend	259D	320214	0.6
APC-Cy7	CXCR3 (CD183)	Biolegend	49801.111	353722	0.13
BV711	CD19	BD Biosciences	SJ25C1	563036	0.25

As the thawing procedure can be critical, we recommend user-specific optimizations to ensure high sample viability (>80%) (Disis, dela Rosa, Goodell, & Ling-Yu, 2006).

CAUTION: *Steps 1-2 should be performed in a biosafety hood.*

2. Centrifuge 5 min at 500 × *g*, room temperature, and carefully flick off the supernatant.
3. Resuspend cells in PBS with 2% FBS and count viable cells on a hemocytometer.
4. Centrifuge as before and carefully flick off the supernatant.

5. Resuspend cells in PBS with 2% FBS to a concentration of 5×10^6 viable cells/ml.
6. Distribute 100 µl suspension per well of a 96-well U-bottom plate, allocating one well per fluorophore in the panel and one well for an unstained sample.

   A FS sample and appropriate FMO controls can be added but are not required for assessing the SRCs at this point. They will be used for assessing unmixing in Basic Protocol 2.

   The number of cells required will differ by tissue type; for PBMCs, ~5×10^5 cells is sufficient.
7. Add one drop of vortexed compensation beads plus 150 µl FACs staining buffer to a second set of wells, allocating one well per fluorophore in the panel except the viability dye.

   Figure 2A shows a typical plate layout. At this stage, the plate should contain unstained and FS sample wells (fully stained beads are not needed) plus two wells per fluorophore in the panel: one with cells and the other with compensation beads (except for the live/dead reagent, which is typically only used on cells). FMO controls should also be included for fluorophores where marker expression is very low or where the positive population is dim and gate placement would be subjective.
8. Centrifuge plate 5 min at 500 × *g*, 4°C, and flick off the supernatant.

   It is recommended to centrifuge samples at 4°C to maintain high viability, but room temperature is acceptable if a refrigerated centrifuge is not available.
9. Prepare viability stain in PBS according to the titration result (see Support Protocol 1) and add 100 µl to the live/dead cell control and FS sample, if included. Resuspend remaining wells with 100 µl PBS. Incubate for 15-30 min at room temperature, protected from light.
10. Centrifuge as above and flick off the supernatant.
11. Block Fc receptors of the cell samples using 100 µl of 1:40 Fc block in FACS staining buffer. Add an equal volume of FACS staining buffer to the beads. Incubate for 10 min at 4°C.

    Fc block should not be used on compensation beads, as all antibody binding sites will become occupied.
12. Centrifuge as above and flick off the supernatant.
13. Remove aggregates from antibody stocks by centrifuging 5 min at 16,000-18,000 × *g*, 4°C (Aass et al., 2011; Ayers et al., 2011; van der Vlist, Nolte-'t Hoen, Stoorvogel, Arkesteijn, & Wauben, 2012) and/or by filtering using a pore size of 0.1-0.65 µm (Inglis et al., 2015).
14. Prepare SS, FS, and FMO control antibody mixes by diluting stocks in FACS staining buffer according to titration results (see Support Protocol 1). Be sure to pipette from the top of the liquid to avoid centrifuged aggregates.

    Prepare enough volume of each antibody mix that two samples can be stained from the same mix. This will reduce differences due to antibody preparation when comparing bead versus cell SRCs. Allow for pipetting errors by making excess antibody mix (e.g., n + 1). Additionally, when more than one Brilliant polymer dye is used at the same time (FS and FMOs), Brilliant Stain Buffer Plus (or equivalent) should be added per manufacturer's instructions to decrease interaction between the dyes. Do not add Brilliant Stain Buffer Plus to compensation beads, as it is known to alter the spectral profile of some beads (Ferrer-Font, Pellefigues, et al., 2020).

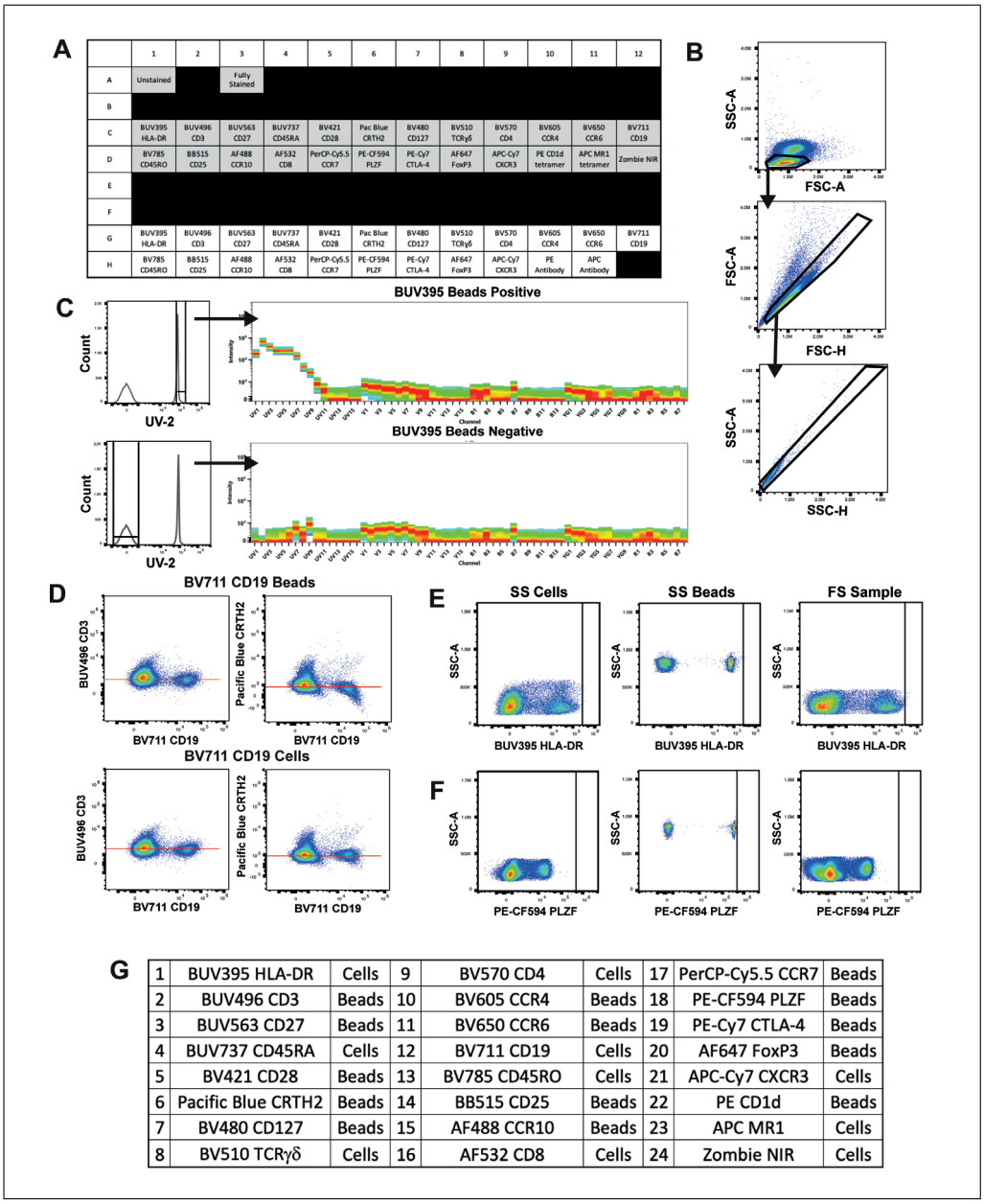

	1	2	3	4	5	6	7	8	9	10	11	12
A	Unstained		Fully Stained									
B												
C	BUV395 HLA-DR	BUV496 CD3	BUV563 CD27	BUV737 CD45RA	BV421 CD28	Pac Blue CRTH2	BV480 CD127	BV510 TCRγδ	BV570 CD4	BV605 CCR4	BV650 CCR6	BV711 CD19
D	BV785 CD45RO	BB515 CD25	AF488 CCR10	AF532 CD8	PerCP-Cy5.5 CCR7	PE-CF594 PLZF	PE-Cy7 CTLA-4	AF647 FoxP3	APC-Cy7 CXCR3	PE CD1d tetramer	APC MR1 tetramer	Zombie NIR
E												
F												
G	BUV395 HLA-DR	BUV496 CD3	BUV563 CD27	BUV737 CD45RA	BV421 CD28	Pac Blue CRTH2	BV480 CD127	BV510 TCRγδ	BV570 CD4	BV605 CCR4	BV650 CCR6	BV711 CD19
H	BV785 CD45RO	BB515 CD25	AF488 CCR10	AF532 CD8	PerCP-Cy5.5 CCR7	PE-CF594 PLZF	PE-Cy7 CTLA-4	AF647 FoxP3	APC-Cy7 CXCR3	PE Antibody	APC Antibody	

1	BUV395 HLA-DR	Cells	9	BV570 CD4	Cells	17	PerCP-Cy5.5 CCR7	Beads
2	BUV496 CD3	Beads	10	BV605 CCR4	Beads	18	PE-CF594 PLZF	Beads
3	BUV563 CD27	Beads	11	BV650 CCR6	Beads	19	PE-Cy7 CTLA-4	Beads
4	BUV737 CD45RA	Cells	12	BV711 CD19	Cells	20	AF647 FoxP3	Beads
5	BV421 CD28	Beads	13	BV785 CD45RO	Cells	21	APC-Cy7 CXCR3	Cells
6	Pacific Blue CRTH2	Beads	14	BB515 CD25	Beads	22	PE CD1d	Beads
7	BV480 CD127	Beads	15	AF488 CCR10	Beads	23	APC MR1	Cells
8	BV510 TCRγδ	Cells	16	AF532 CD8	Cells	24	Zombie NIR	Cells

Figure 2 Evaluation of SRCs and selection of optimal control type. (**A**) Example plate plan. Shaded wells contain cells and unshaded wells contain compensation beads. (**B**) Expert gating of cells of interest and doublet exclusion plots. A well-optimized ASF can be visualized in the second pseudoplot. (**C**) BUV395 bead SRC gating of positive and negative populations and spectral signatures of gated events showing clear positive and negative signals. (**D**) SS cells unmixed with either BV711 CD19-stained compensation beads (top) or cells (bottom). Unmixing of BV711 CD19 is incorrect against certain parameters (e.g., Pacific Blue CRTH2) but not others (e.g., BUV496 CD3) when beads are used. This error is corrected through unmixing with cells with no negative impact to the plot with previously correct unmixing. Red line indicates equal median fluorescence intensity (MdFI) between positive and negative populations. (**E**) Comparison of brightness achieved using SS cells versus beads and the FS sample for BUV395 HLA-DR. Black line shows the maximum fluorescence of positive stained cells. In this example, cells should be used for unmixing as they are brighter than the beads. (**F**) Comparison of brightness achieved using SS cells versus beads as compared to the FS sample for PE-CF594 PLZF. In this example, beads are brighter than cells and should be used for unmixing. Black line shows the maximum fluorescence of positive stained beads is brighter than the FS sample. (**G**) Final decision of optimal SRCs (cells or beads) used for unmixing the panel.

15. Stain all cells and beads with 100 µl of the appropriate antibody mix and incubate in the dark using the incubation time and temperature that will be used in the final assay.
16. Centrifuge as above and flick off the supernatant.
17. Wash twice with 200 µl FACS staining buffer, centrifuging again after each wash.

    At this stage, cells may be fixed (e.g., 1% paraformaldehyde) if required for biosafety or sample longevity. If cells are fixed, beads must also be fixed to ensure equal treatment of fluorophores and to mimic any change to the spectral signature caused by fixation. The fixative must be removed by washing twice with FACS staining buffer before acquisition.
18. Resuspend in 200 µl FACS staining buffer.
19. Acquire on a Cytek Aurora, taking care to meet the following acquisition criteria:
    a. Cytek assay settings are used as a starting point for instrument setup.
    b. The scatter profiles of cells and beads are on scale and the FSC area scaling factor (ASF) is optimized (see example in Fig. 2B).
    c. All fluorescence signals are on scale ($<4 \times 10^6$). This can be assessed in the full-spectrum plot or in individual plots for every detector.
    d. All tubes are recorded with the same fluorescence gain settings for each detector.
    e. Sufficient events are recorded to find a clear positive signal.

    A minimum of 300 events is needed for each positive and negative population. A good starting point is 5000 total events for beads and 30,000-50,000 total events for cell controls, although it may be necessary to record >50,000 cells to get at least 300 positive events of similar fluorescence intensity for rare markers.

Evaluate results (see Video 1)

20. In the SpectroFlo software, check the raw reference control data and verify that the acquisition criteria in the previous steps have been met:
    a. The scatter profiles of the cells and beads are on-scale, clean, and easily gated, and the FSC ASF has been optimized (Fig. 2B).
    b. Cytek assay settings or a close alteration (also see Critical Parameters discussion of Complex Samples and see Support Protocol 2) have been used, and all tubes have been recorded with the same settings.

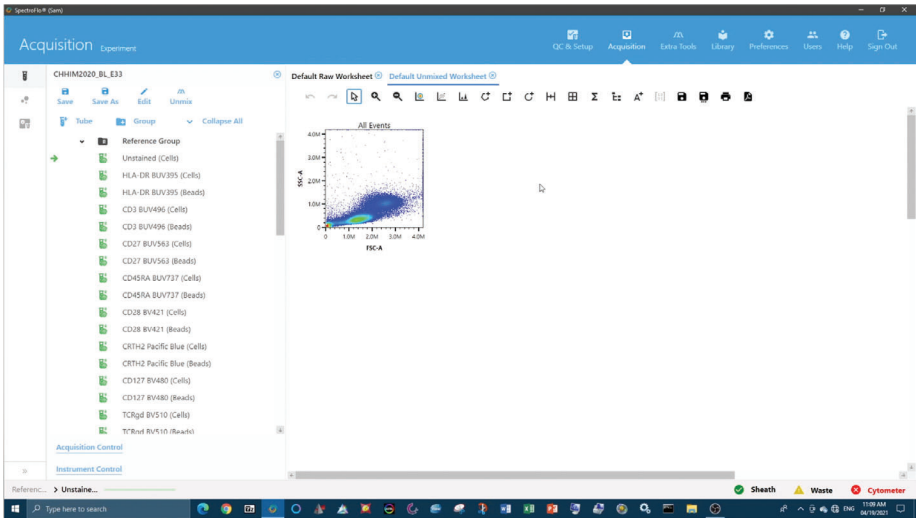

Video 1 Evaluation of optimal spectral reference controls (Basic Protocol 1).

21. Ensure that the unstained sample has no contamination from other fluorophores.

    Unstained cells often have AF signal in the detectors off the UV and violet lasers, which should not be mistaken for contamination.

22. In the SpectroFlo software, step through the Unmixing Wizard and select beads for all SRCs except for unstained and viability controls.

23. Accurately place positive and negative gates for unmixing.

    When setting scatter gates on bead SRCs, it is common to see singlet and doublet populations. Set the scatter gate on the smaller-sized (lower FSC) or more abundant singlet population. Beads should show little variability in staining level when prepared as described above, and thus the positive gate may include the complete positive bead population. If multiple peaks are seen, verify that they are not contaminating fluorophores or sample carryover, and optimize the staining procedure where needed to achieve homogenous staining intensity across all positive beads.

24. Perform quality control (QC) of all spectral signatures by verifying the following criteria:

    a. The peak channel matches that defined in Cytek's Full Spectrum Viewer (*spectrum.cytekbio.com*).
    b. The spectral signature appears as expected based on Cytek's Full Spectrum Viewer, published Cytek fluorophore guidelines, or historical data.
    c. Each channel contains a tight population of events.
    d. All fluorescent signals are on-scale ($<4 \times 10^6$). This can be assessed in the full-spectrum plot or in individual plots for every detector.
    e. Sufficient events have been recorded to find a clear positive signal.

25. Iterating through each fluorophore, place the positive gate over the negative population to verify that there is no fluorophore contamination (Fig. 2C).

26. Under the QC Controls tab, check Similarity Indices to ensure all spectral signatures are unique (i.e., all values within the matrix are ≤ 0.98).

27. Select the Live Unmix button to generate unmixed FCS files.

28. Create N × N plots on an unmixed worksheet (e.g., using software such as FlowJo or FCS Express).

    a. Create as many pseudocolor or dot plots as there are fluorophores in the panel.
    b. Ensure all *x* axes are set to the same fluorophore.
    c. Set each *y* axis to a different fluorophore in the panel.
    d. Change the *x* and *y* axes from manual scaling to autoscaling in the plot properties.
    e. Save this workspace as a template for use in later protocol steps.

29. Select the first SS cell sample.

30. Select all N × N plots. Then, in the Plot Properties window, change the *x*-axis option to the fluorophore matching the selected sample so all plots change simultaneously.

31. Evaluate the unmixing accuracy of the marker on the *x* axis by visually inspecting whether the positive and negative populations are well aligned horizontally along the *x* axis. If unmixing errors are seen in the N × N matrix plots (Fig. 2D, top), make a note of which control was being viewed.

32. Repeat steps 29-31 until the unmixing of all fluorophores has been evaluated.

33. Note which fluorophores require cells to be used for the SRC (i.e., those with identified unmixing errors in step 31). All other controls can remain as beads.

The most likely explanation for bead SRCs not unmixing the cell SRCs correctly is that the signature of the fluorophore on the beads did not match that of the cells. This phenomenon is known to happen but cannot be easily predicted. Another possible cause is that the bead SRC is dimmer than the cell SRC (Fig. 2E,F). If all recommendations for treatment of SS cells have been followed (i.e., identical treatment to FS cells, use of the same number of cells), then the cell SRC should have identical brightness to the FS cells and thus be an appropriate control.

34. Go through the Unmixing Wizard a second time using the controls identified in step 33 as the optimal controls. Unmix again using live unmixing.

35. Follow steps 23-26 for the modified controls to ensure the best unmixing outcome is achieved.

    When setting gates using cells as SRCs, the scatter gate should be placed only on the cells expressing the marker of interest for each control. In cases where there is no negative staining in this population, a universal negative may be used as a surrogate. To ensure the observed negative signal is due to AF rather than contamination, compare it to the matching unstained tube.

36. Repeat steps 29-32 to evaluate the new unmixing for the fluorophores that did not unmix optimally before (Fig. 2D, bottom) and note which fluorophores require cells or beads to be used for the SRC (Fig. 2G).

    Even with high-quality reference controls, unmixing errors may arise if incorrect gates are used in the Unmixing Wizard or if the spectral signatures have mismatches (see troubleshooting Tables 2-5 for more potential issues and how to fix them).

SUPPORT PROTOCOL 1

ANTIBODY TITRATION

Antibody titration is the crucial first step in developing high-dimensional flow cytometry panels. Using the incorrect antibody concentration can increase spread, decrease resolution, increase aggregation of reagents, and give rise to nonspecific binding (Stewart & Stewart, 1997), all of which result in poor panel performance and/or inaccurate results. Ideally, titrations should be carried out in the tissue that will be used in the assay. This is not always feasible, however, if the tissue in question is rare or difficult to work with, or the cells of interest are found at low frequencies within the tissue. In such cases, it is suggested to first add a lineage marker to the mix to help identify the cells that express the rarer marker or to use a surrogate tissue in which the marker is more abundant and simpler to process. Results from this type of titration should always be validated using the tissue of interest.

It is important that readout functional markers are titrated under the maximally activated conditions that will be used in the assay. Staining conditions should also be identical between titration and experiment to prevent spectral pattern mismatches and poor unmixing results.

This protocol describes the preparation of cryopreserved peripheral blood mononuclear cells (PBMCs) for titration of extracellular antibodies. It can be easily adapted and used as a general guideline for antibody titration using other tissues or staining procedures.

Materials

Cryopreserved PBMCs
Phosphate-buffered saline (PBS; Gibco, cat. no. 14190-250)
Fetal bovine serum (FBS; Gibco, cat. no. 10091-148)
Zombie NIR Fixable Viability Kit (BioLegend, cat. no. 423106)
Human TruStain FcX (Fc Receptor Blocking Solution; BioLegend, cat. no. 422301)

Polystyrene compensation beads (e.g., UltraComp eBeads, Life Technologies, cat. no. 01-222-42)
Antibodies (see Table 1)
FACS staining buffer: PBS with 2% bovine serum albumin (BSA; MP Biochemicals, CAS no. 9048-46-8) and 0.2% sodium azide (Sigma-Aldrich, cat. no. S8032)

37°C water bath (e.g., Julabo Ecotemp TW12)
Hemocytometer (e.g., Hawksley Counting Chamber) and coverslips
96-well U-bottom plate (In Vitro Technologies, cat. no. 353077)
Filters with 0.65-μm or smaller pore size (*optional*)
Spectral cytometer (e.g., Cytek Aurora)
5-ml polypropylene round-bottom flow tubes (In Vitro Technologies, cat. no. 352008)
Data analysis software for analyzing FCS files (e.g., FlowJo or FCS Express)

Prepare and acquire samples

1. Thaw PBMCs quickly in a 37°C water bath and add to 5 ml PBS with 2% FBS.

   CAUTION: Steps 1-2 should be performed in a biosafety hood.

2. Centrifuge 5 min at 500 × *g*, room temperature, and carefully flick off the supernatant.
3. Resuspend cells in PBS with 2% FBS and count on a hemocytometer.
4. Centrifuge as before and carefully flick off the supernatant.
5. Resuspend cells in PBS with 2% FBS to a concentration of 5×10^6 cells/ml.
6. Distribute 100 μl suspension per well of a 96-well U-bottom plate, allocating six wells to each antibody being titrated. Include additional wells for unstained and live/dead controls (see example plate plan in Fig. 3A).

   The number of titer points is based on the range of concentrations being tested. The number of cells required will differ by tissue type; for PBMCs, ~5×10^5 cells is sufficient.

7. Centrifuge plate 5 min at 500 × *g*, 4°C, and flick off the supernatant.
8. Stain titration samples and live/dead controls with a viability dye that will not cause significant spillover into the fluorophore being titrated.

   Viability dyes should also be titrated for use in high-dimensional spectral cytometry panels. When titrating a viability dye, skip steps 8-12 for that sample only (adding PBS instead if other samples are being processed simultaneously). If the viability dye has not yet been titrated, follow manufacturer guidelines for concentration and incubation procedures.

9. Centrifuge as above and flick off the supernatant.
10. Block Fc receptors by applying 100 μl of a 1:40 dilution of Human TruStain FcX and incubating 10 min at 4°C.
11. Add one drop of vortexed compensation beads per well for the appropriate single stain (SS) controls.
12. Centrifuge as above and flick off the supernatant.
13. Remove aggregates from antibody stocks by centrifuging the vials 5 min at 16,000-18,000 × *g*, 4°C, or by filtering using a pore size of 0.65 μm or smaller.

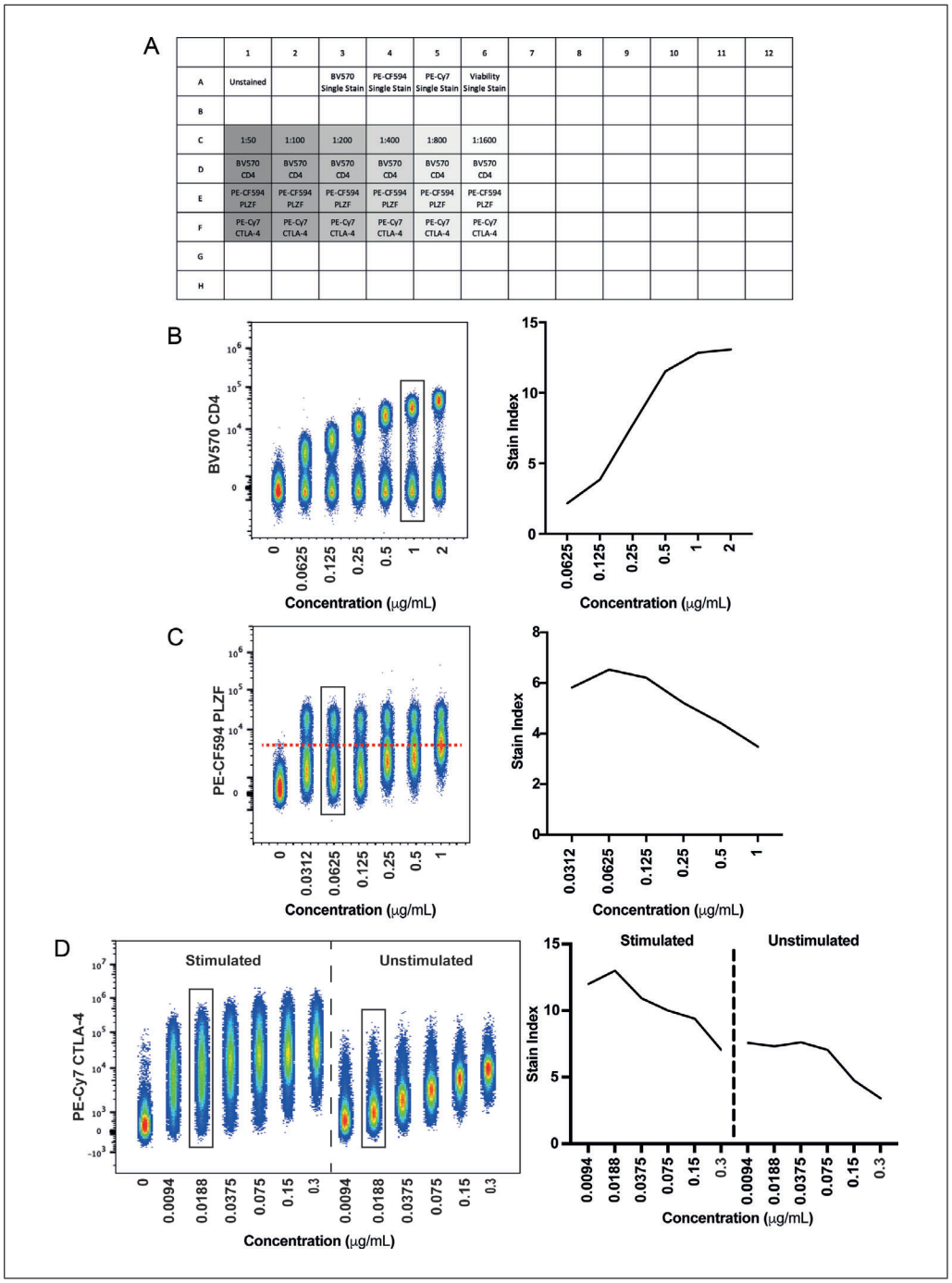

Figure 3 Antibody titration. Example titration of 1:2 serial dilutions for a range of marker subtypes, showing both concatenated flow cytometry data files and the calculated SI. The final dilution selected for the panel is indicated by black boxes. (**A**) Example plate layout. (**B**) T-cell co-receptor CD4 conjugated to BV570. (**C**) Transcription factor PLZF conjugated to PE-CF594. (**D**) Activation marker CTLA-4 conjugated to PE-Cy7 on cells with and without PHA stimulation (5 μg/ml, 2 days).

14. Create a dilution series for each antibody being titrated by diluting stock solutions in FACS staining buffer. Be sure to pipette from the top of the liquid to avoid the spun-down aggregates.

    A suggested dilution series is 1:50, 1:100, 1:200, 1:400, 1:800, 1:1600. This series is broad enough to ensure the likelihood of finding the optimal titer for a range of antibodies. For ease of preparation, concentrations are listed here only in terms of their dilution from stock; actual concentrations (in mg/ml) should be calculated once a titer is selected.

15. Add 100 µl of each antibody dilution to the corresponding sample in the plate. Add FACS staining buffer to unstained and live/dead controls. For compensation beads, use 100 µl of the 1:100 dilution.

    The dilution used for compensation beads should not fall off-scale when using Cytek assay settings, but should be brighter than the samples. A 1:100 dilution is a good starting point, but a lower dilution can be used if some antibodies are too bright.

16. Incubate using the time and temperature that will be used in the final assay.

17. Centrifuge as above and flick off the supernatant.

18. Wash twice with 200 µl FACS staining buffer.

    If fixation will be used for the final samples, titrations should also be determined using fixed samples. For additional details, see Basic Protocol 1, step 17.

19. Resuspend in 200 µl FACS staining buffer and acquire on a Cytek Aurora using Cytek assay settings.

Analyze data

20. Open titration samples in a data analysis software used for analyzing FCS files.

21. Generate median fluorescence intensity (MdFI) values for the positive and negative populations for each concentration.

22. Generate standard deviation (SD) values for the negative population for each concentration.

23. Calculate the stain index (SI) using the equation SI = (MdnFI*pos* – MdnFI*neg*) / (2 × SD*neg*).

    The stain index is a very useful metric of resolution, with a higher value indicating greater resolution. If a lower concentration of antibody produces a reduced positive population MdnFI compared to a higher concentration with no change to the negative population, its stain index is going to decrease, as the separation between the positive and negative populations will be reduced (see example in Fig. 3B). If a higher concentration of antibody gives rise to a similar positive population MdnFI compared to a lower concentration, but has a larger SD of the negative population, its stain index is going to be decreased, as spreading of the negative population reduces the resolution from the positive (see example in Fig. 3C).

24. Select the concentration that gives rise to the best stain index without giving rise to a positive shift of the negative population.

    Such a shift is best visualized by concatenating all FCS files and displaying them on a single plot (as shown in in Fig. 3B-D).

CHANGING INSTRUMENT SETTINGS

SUPPORT PROTOCOL 2

In some cases an adjustment of fluorescent gain settings away from the optimized settings cannot be avoided, for instance, if a bright reporter protein (e.g., eGFP) is off-scale. Such adjustments must be carried out carefully to minimize impact on all spectral signatures within the panel. Adjustments can be made detector by detector or to a whole detector array at one time, where all detectors of a given laser line are changed simultaneously. Reduction of the whole array is the recommended approach, as manual alteration of single detectors is prone to distortion of spectral signatures, where the ratio of brightness from detector to detector is not maintained. Regardless, reducing whole detector arrays can lead to peak emissions of spectral signatures being shifted to an incorrect detector (potentially on a different laser line). Therefore, all changes must be checked to ensure

that signatures remain as expected based on Cytek's Full Spectrum Viewer, published fluorophore guidelines, or historical data.

1. Observe which fluorescent channel(s) has an off-scale signal.
2. Use trial and error to determine the gain setting that is appropriate to bring the emission peak on-scale (i.e., $<4 \times 10^6$ on the Aurora).

   Remember that gain and fluorescence have a linear relationship, so that a 50% reduction in gain will give rise to a 50% reduction in fluorescence signal.

3. Reduce secondary detector arrays with off-scale signals by the same percentage as the reduction made in step 2.
4. Use Cytek's Full Spectrum Viewer, published fluorophore guidelines, or historical data to check that the altered spectral signature retains the correct overall pattern and that the primary emission peak has not been reduced below any secondary emission peaks.

   If the overall pattern is correct, no further steps are required. Record all samples at these adjusted settings. If the overall pattern is not correct, continue to step 5.

5. If adjustments to other laser lines are required, continue reducing the respective detector arrays by the same percentage as in step 2.
6. Repeat steps 4 and 5 until the spectral signature appears as expected or all arrays have been reduced by the same percentage.
7. Record all samples at the adjusted settings.

BASIC PROTOCOL 2

UNMIXING EVALUATION OF FULLY STAINED SAMPLE

Before any analysis can be undertaken, the FS sample must be checked to ensure that clean data can be obtained through removal of artefacts such as doublets, dead cells, and aggregates. It is also necessary to verify that there is positive staining for all markers in the panel, taking into consideration the biology of each marker. Once this has been asserted, it must be determined whether the SRCs selected (either beads or cells) successfully unmix the SS cells in Basic Protocol 1 can also be used to successfully unmix the FS sample (Video 2).

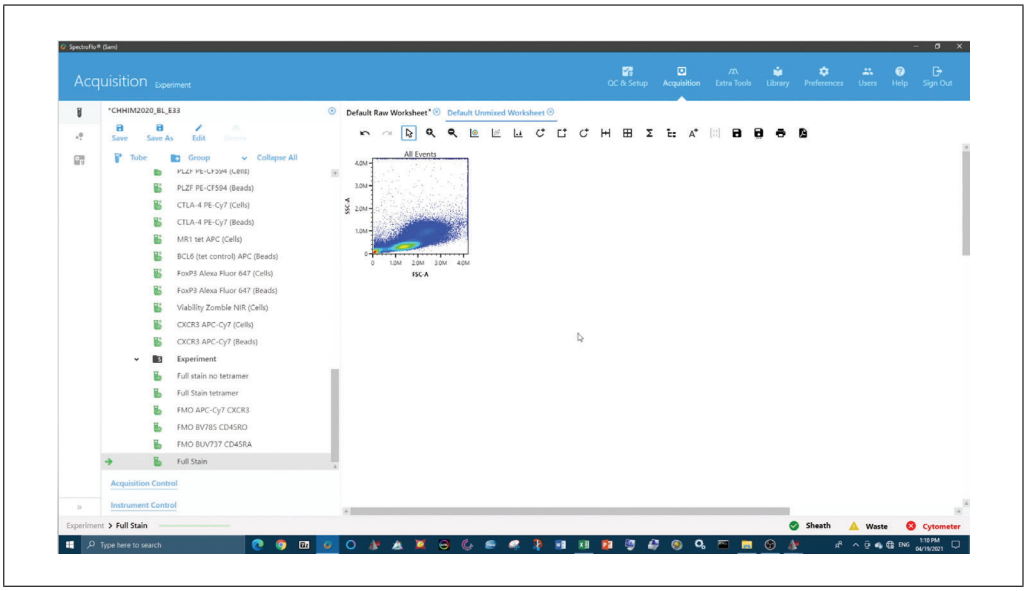

Video 2 Unmixing evaluation of fully stained sample (Basic Protocol 2).

Materials

Cytek SpectroFlo software
FCS files generated in Basic Protocol 1
N × N worksheet template

1. In the SpectroFlo software, work through the Unmixing Wizard and select the SRCs chosen from Basic Protocol 1.
2. In the unmixed workspace, gate on time to remove any events collected during an unstable flow period by plotting time vs. scatter (e.g., FSC-A or FSC-H; Fig. 4A).
3. Gate out doublets by sequentially plotting FSC-H vs. FSC-A and SSC-H vs. SSC-A, and include only the events found in the diagonal population (Fig. 4A).

   If working with whole blood or PBMC samples where incomplete RBC lysis was achieved, unlysed erythrocytes need to be excluded. One method is the blue/violet SSC gating method described by Petriz, Bradford, & Ward (2018).

4. Exclude aggregates through inspection of N × N plots for incorrectly unmixed super-bright events and gate these out of all further analyses (Fig. 4B).
5. Gate out dead cells by including only viability dye negative events (Fig. 4A).

   Viability dyes also need to be titrated (see Support Protocol 1).

6. Gate on cells of interest using FSC-A vs. SSC-A, including only the events required for analysis (Fig. 4A).

   If working with a sample that contains multiple cell types (such as PBMCs), include only the cells that will be involved in downstream analysis. For example, when analyzing a panel that contains only lymphocyte markers, gate out monocytes (validating that T cells are not excluded).

7. Create as many pseudocolor or dot plots as there are fluorophores in the panel. Set the *y* axis to SSC-A and each *x* axis to a different fluorophore (Fig. 4C).
8. Verify that a positive signal can be found for all markers (Fig. 4C).

   For rare or dim markers, FMOs can assist in determining the gating boundaries (Fig. 4D). If no clear signal is observed, take note of that reagent and check the titer and staining protocol. For additional troubleshooting, see Table 3.

9. Open the N × N worksheet template created previously and evaluate how well unmixing was performed for each marker. Inspect the FS sample by assessing whether super-negative events are present (example in Fig. 4E), which can be an indication of unmixing issues.
10. Select all plots making up the matrix. In the Plot Properties window, change the *x* axis option to the next fluorophore down the list so that all plots change simultaneously.
11. Repeat steps 9-10 until all fluorophores have been checked.
12. If there are no major unmixing errors (i.e., the positive and negative populations of each marker in the N × N plots are well aligned), continue to evaluation of marker resolution (see Basic Protocol 3).
13. If there are unmixing issues, even once the unmixing has been performed correctly and optimally, it is possible to make small adjustments (<3%) to the compensation matrix (found in the Tube Properties window).

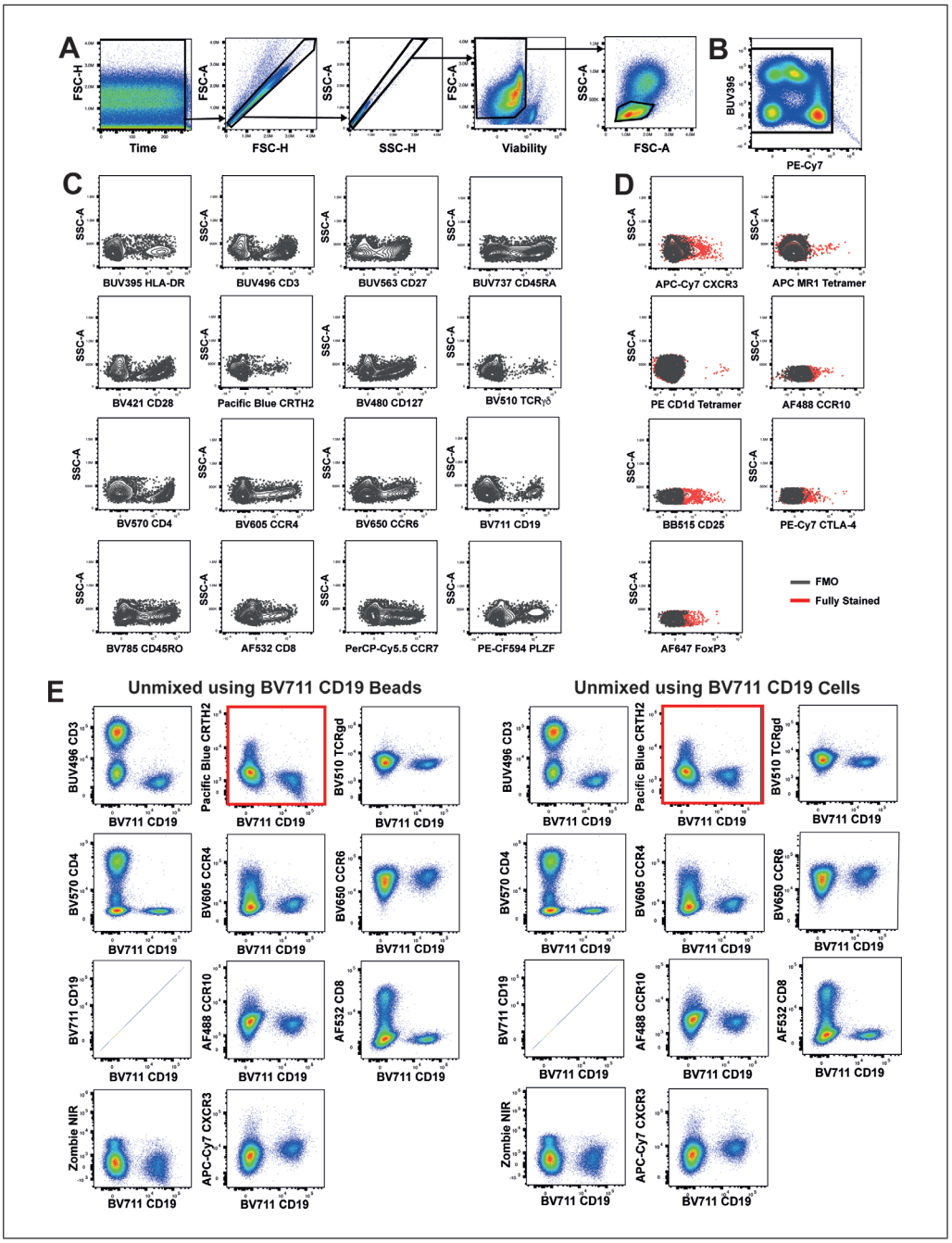

Figure 4 Inspection of the FS sample. (**A**) Gating strategy to gate out inconsistent flow rate events (time gate), doublets, and dead cells and include only cells of interest (lymphocytes). (**B**) Example of aggregates and how to gate them out. (**C**) Dot plots of SSC-A vs. each marker in the panel. (**D**) Dot plots of SSC-A vs. rare/dim markers in the panel, overlaid with FMO controls to show true positive events. (**E**) N × N matrix used to evaluate marker positivity from core panel iteration unmixed using beads (left) or cells (right).

Adjustments to the spillover matrix should be fully justified and the integrity of the data must not be impacted (made with clear knowledge of the biology, such as expression and pattern characteristics). Under-unmixing and over-unmixing issues can be manually adjusted (Ashhurst, Smith, & King, 2017). It is unlikely that there would be a need for more than a 2% to 3% correction. If greater correction is needed, the unmixing accuracy needs to be re-evaluated.

If the samples are something other than PBMCs and significant unmixing issues are still present, more information on how to proceed can be found in the Commentary (see Critical Parameters, Complex Samples).

EVALUATION OF MARKER RESOLUTION

Once the best possible unmixing has been achieved using Basic Protocols 1 and 2, the resolution of each marker in the FS sample must be compared to the SS cell controls. Assessing the spread of the negative population and/or shifts in the positive signal will provide an indication of whether there is any loss of resolution of markers in the panel when fully stained. This assessment is best achieved by overlaying each marker in the SS cell sample onto the FS sample. If any reduction in resolution is seen, the impact of this can be further investigated to identify if it will impact the ability to identify populations of interest using an established gating strategy. Ideally, the same number of cells from the same tissue type should be stained and acquired for all samples. In practice, however, this is not often feasible, and downsampling can be used to achieve identical cell numbers across samples during analysis. In theory, the only difference between the SS and FS cells should be the number of antibodies in the tube (Video 3). Additionally, AF extraction should be tested to determine if marker resolution can be improved (Video 4).

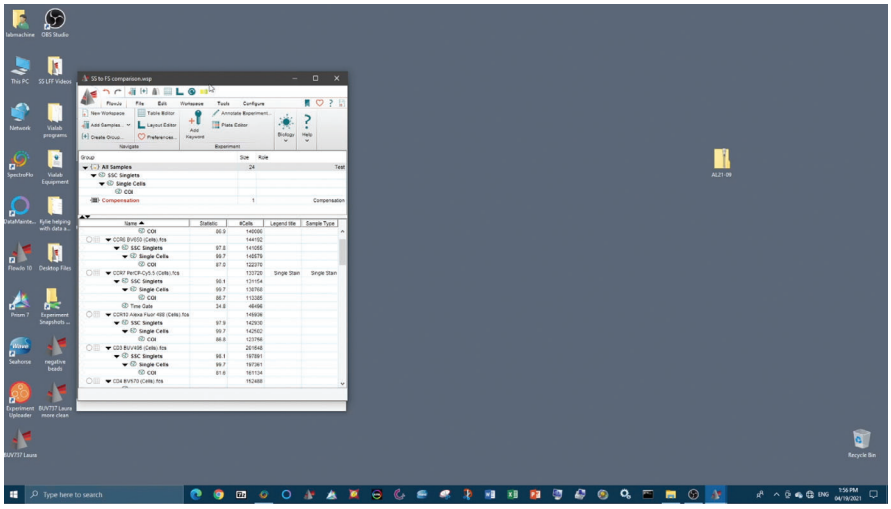

Video 3 Evaluation of marker resolution (Basic Protocol 3).

Video 4 Deciding on an approach for mitigating autofluorescence (Basic Protocol 3) and Support Protocol 3.

Materials

Data analysis software (e.g., FlowJo or FCS Express)
Cytek SpectroFlo software
FCS files generated in Basic Protocol 2
N × N worksheet template

Evaluate marker resolution (Video 3)

1. Open the unmixed FS and SS cell samples in a data analysis software package for analyzing FCS files (e.g., FlowJo or FCS Express).
2. Follow steps 2-6 of Basic Protocol 2.
3. Create a histogram for each fluorophore in the panel (Fig. 5A). If the positive population is rare, use a dot plot for visualization purposes instead of a histogram (Fig. 5B).
4. Overlay the same number of FS and SS cell sample events onto a histogram or dot plot (Fig. 5A,B).

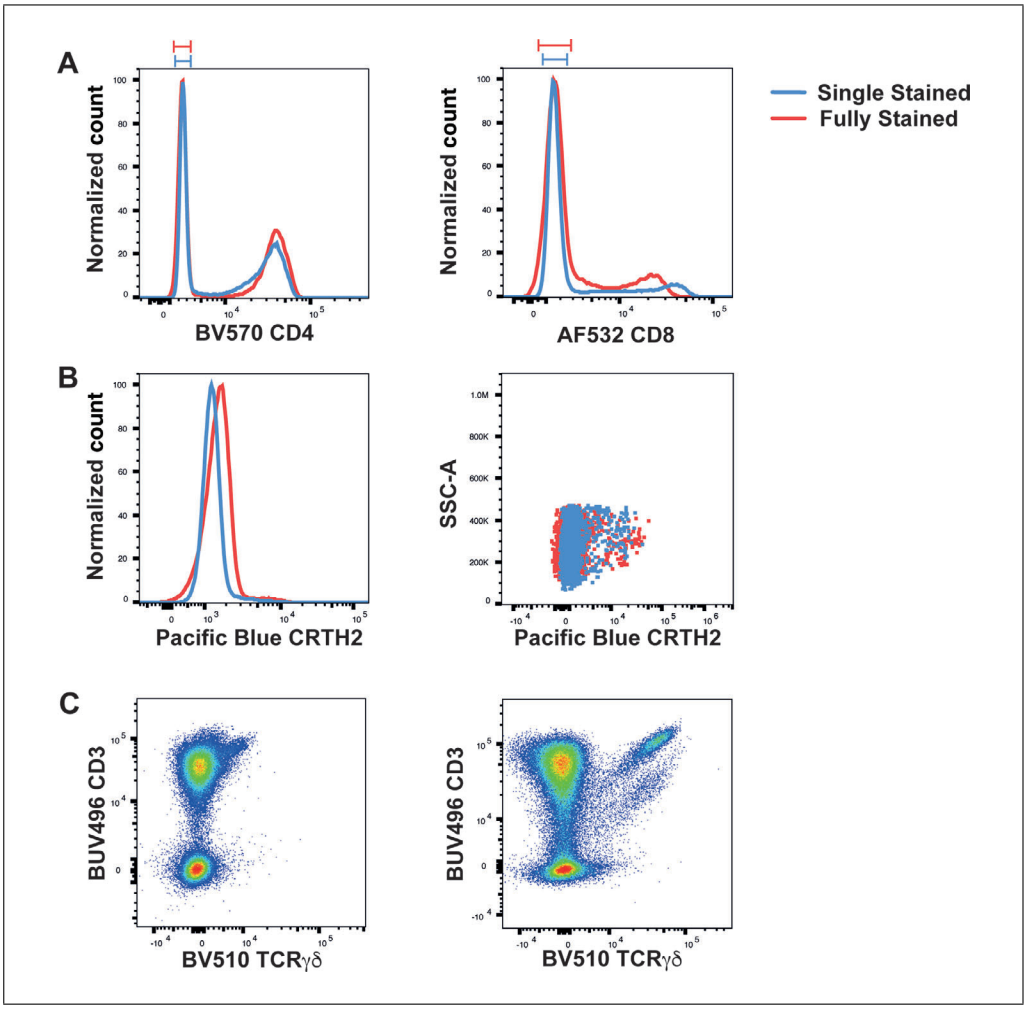

Figure 5 Evaluation of marker resolution. (**A**) A histogram overlay of BV570 CD4 SS cells vs. FS sample (left) provides an example with no additional spread in the negative population, whereas a histogram overlay of AF532 CD8 (right) depicts spreading of the negative population in the FS sample (red) compared to SS cells (blue). (**B**) Histogram and dot plot overlays of Pacific Blue CRTH2. (**C**) Dot plot of BUV496 CD3 vs. BV510 TCR$\gamma\delta$ before (left) and after (right) implementation of sequential staining (Park et al., 2020).

	APC-Cy7-A CXCR3	Alexa Fluor 488-A CCR10	Alexa Fluor 532-A CD8	Alexa Fluor 647-A FoxP3	BB515-A CD25	BUV395-A HLA-DR	BUV496-A CD3	BUV563-A CD27	BUV737-A CD45RA	BV421-A CD28	BV480-A CD127	BV510-A TCRgd	BV570-A CD4	BV605-A CCR4	BV650-A CCR6	BV711-A CD19	BV785-A CD45RO	PE-CF594-A PLZF	PE-Cy7-A CTLA-4	Pacific Blue-A CRTH2	PerCP-Cy5.5-A CCR7	Zombie NIR-A Viability
APC-Cy7-A CXCR3	0	3.57	1.83	23.68	3.33	0.31	7.51	4.04	1.51	0.47	1.34	3.74	0.37	3.00	6.80	1.90	7.39	2.91	5.23	1.11	0.88	6.56
Alexa Fluor 488-A CCR10	0	0	4.87	0.75	22.47	0.62	30.62	7.48	1.20	1.34	3.09	8.22	2.67	2.03	2.41	0.03	1.67	1.45	0.99	2.68	1.26	0.96
Alexa Fluor 532-A CD8	0	5.56	0	0	4.00	0.37	0	0	0	0.39	0	4.88	1.76	1.02	1.34	1.10	1.39	0.38	0.47	0	0.47	0
Alexa Fluor 647-A FoxP3	2.29	0	0	0	0	0	7.48	0	0	0	0	0	0	0	0	0	0	0	0	0.11	0.02	0.07
BB515-A CD25	0.71	14.35	3.27	0	0	0.83	0	0	0	0	0	3.85	1.03	0	0.70	0	0	0	0	2.14	0.75	1.29
BUV395-A HLA-DR	0	1.90	3.64	0.29	3.43	0	0	1.72	0.45	0	1.70	10.54	0	2.20	1.94	0.55	1.57	0.71	0.31	3.08	1.31	0
BUV496-A CD3	0.51	3.18	1.87	0.36	4.92	0.97	0	3.34	0.28	0.86	2.28	6.67	1.41	0.83	1.20	0.94	1.27	1.10	0.47	0.90	0.47	0.33
BUV563-A CD27	0.41	2.53	2.35	0.40	3.88	0.68	9.29	0	0.45	0.62	1.22	5.33	3.28	1.11	1.54	1.13	1.45	1.25	0.53	1.02	0.75	0.37
BUV737-A CD45RA	2.75	0	0	0	0	0	0	0	0	0	0	3.53	0.37	0.47	0	0	0.97	0	1.45	0	0	0
BV421-A CD28	0.42	0.70	1.88	0.29	3.06	1.15	7.93	2.63	0.32	0	2.32	6.60	1.03	0.85	1.16	0.86	1.22	0.72	0.31	5.33	0.54	0.38
BV480-A CD127	1.25	4.28	2.87	0.50	7.26	1.19	20.55	6.43	0.55	1.27	0	8.73	2.50	2.10	2.15	1.62	2.33	1.67	0.53	1.83	0.76	0
BV510-A TCRgd	0	2.10	1.34	0.41	1.51	1.35	0	2.40	0.64	0.52	2.68	0	2.46	3.01	1.02	0.96	0.82	1.86	0.44	4.21	0.62	0
BV570-A CD4	0	2.19	2.14	0.27	3.71	0.64	13.75	6.03	0.43	1.13	1.46	4.25	0	2.64	1.78	0.72	1.02	1.44	0.50	1.45	0.65	0
BV605-A CCR4	0.59	0	2.13	0.53	3.39	0.49	12.30	4.01	0.89	0.93	1.13	5.56	2.13	0	3.04	1.15	1.27	2.92	0.65	1.32	0.85	0.66
BV650-A CCR6	1.19	0.27	0	0.73	0	0	0	0	0.94	0.52	0	0	0	1.02	0	1.13	0	0.70	0.44	1.12	0.43	0.75
BV711-A CD19	2.10	0	0	0.85	0	0	0	0	2.11	0.60	0	0	0	0	0	0	2.22	0	0.35	0	0.63	1.43
BV785-A CD45RO	2.02	0.71	1.09	0.24	1.85	0.44	5.27	1.64	2.01	1.29	0.75	2.84	0.58	0.42	0.48	0.97	0	0.29	0.71	1.07	0.40	1.27
PE-CF594-A PLZF	0.64	3.38	1.65	0.46	3.05	0	0	0	0.51	0.58	0	7.63	0.66	1.96	0.64	0.87	0	0	0.70	0	1.36	0
PE-Cy7-A CTLA-4	2.95	3.82	4.43	0	10.60	0.80	0	4.00	0	1.22	1.85	6.08	4.83	1.69	1.64	2.23	1.92	0.83	0	1.05	0.72	3.04
Pacific Blue-A CRTH2	0.83	1.48	3.69	0	3.95	1.58	0	0	0.64	2.17	6.49	18.71	1.70	0	0	0	0	1.99	0.01	0	0.89	1.07
PerCP-Cy5.5-A CCR7	2.87	0.16	0	2.02	0	0	0	0	1.69	0	0	0	0	1.35	2.86	3.60	2.98	0	1.86	0	0	1.93
Zombie NIR-A Viability	12.39	1.51	1.37	1.53	3.68	0.61	4.65	1.58	1.50	0.56	1.15	3.78	0.82	0.64	0.98	1.52	4.51	0.97	2.29	1.30	0.90	0

Figure 6 Spillover spreading matrix for 24 unique-signature fluorophores used in combination on a panel used to illustrate the protocol. Spread is contributed by fluorophores listed in the rows, impacting the fluorophores listed in the columns. Spillover values are color-coded as follows: white, <3; shades of pink, 3–9; red, >9 (for example, BV480 spreads strongly into BUV496).

To ensure that each sample contains equal events, downsample the cells of interest population from all samples to the same number of events based on the sample with the fewest cells of interest. In FlowJo, for example, select the population of interest, then go to the Workspace tab and select Plugins and then DownSample. Specify the number of events to be downsampled such that all samples can meet the criteria.

5. Determine whether any spreading of the negative population has occurred in the FS sample (Fig. 5A, right).

6. Determine whether such spreading has impacted the resolution of positive and negative populations, either visually or by calculating stain index (SI; see Support Protocol 1, step 22).

7. Create a spillover spreading matrix (SSM) to assess which fluorophores are likely to be introducing spread to the fluorophore of interest (in Fig. 6, find the SSM for the panel used to illustrate the protocol).

In FlowJo, for example, using the SS cells SRCs, navigate through the Compensation Wizard defining positive and negative populations for each fluorophore. The SSM will be automatically generated alongside the compensation matrix and can be displayed or exported from the SSM button.

If the spread of the negative population results in significant loss of resolution such that separation of positive and negative populations becomes difficult, and the marker is

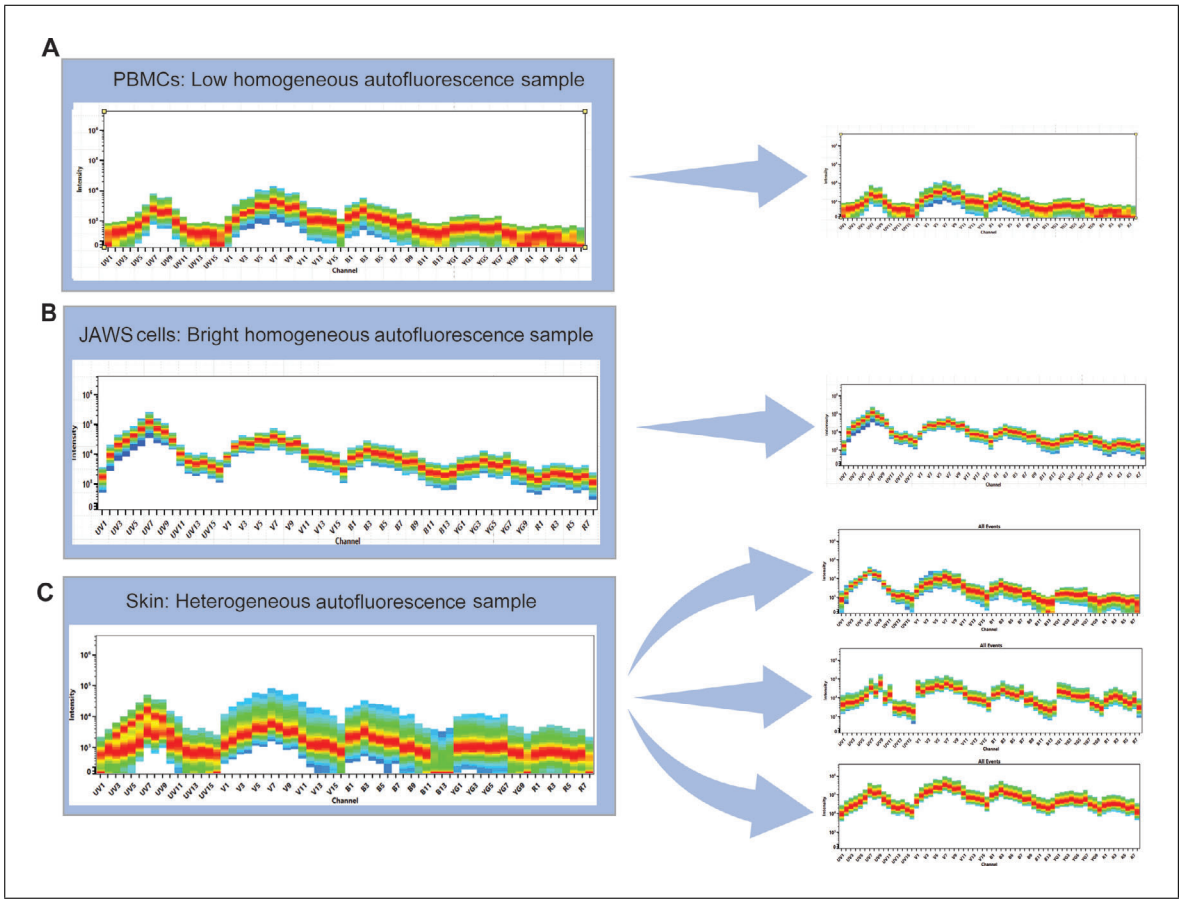

Figure 7 Determination of AF signature type. AF signatures of (**A**) unstained PBMCs, (**B**) unstained JAWS cells (immortalized immature dendritic cell line), and (**C**) unstained skin cells. The latter shows a highly heterogeneous signature that can be split into three unique spectral signatures.

co-expressed in the same cell type as the marker causing the spread, the panel design should be reconsidered and a different fluorophore may be needed to improve resolution.

8. Determine whether any loss in fluorescence intensity of given marker(s) has occurred in the FS when compared to the SS (Fig. 5C).

   Any reduction in positive signal should be investigated. An explanation is offered in Jalbert, Shikuma, Ndhlovu, & Barbour (2013) and Park et al. (2020), where sequential staining of chemokine receptors was required to achieve positive signal in the FS sample comparable to that of the SS cell controls. Sequential staining can also be applied to non-chemokine receptors (Fig. 5C).

Choose approach for mitigating AF (Video 4)

Two scenarios should be considered regarding AF: homogeneous AF, where the whole unstained sample has a single low spectral signature (Fig. 7A) or single bright spectral signature (Fig. 7B), or heterogeneous AF, where there are multiple AF signatures (Fig. 7C). For PBMCs, where the unstained sample has a relatively low homogeneous AF signature, the Simple AF Protocol can be followed to assess whether AF extraction improves marker resolution. AF extraction is particularly helpful in resolving low-expressed markers by lowering the background of the negative population with minimal effect on the positive signal. If samples have heterogeneous or homogeneous but very bright AF, it is likely that AF extraction must be used to obtain unmixing that looks correct in Basic Protocols 1 and 2. In this case, the decision to use AF extraction will be based on unmixing quality instead of improvement of marker resolution. The AF protocol for

heterogeneous AF is explained in detail in Critical Parameters (under Working with Complex Samples) and in Support Protocol 3.

Extract AF

9. Open SpectroFlo and proceed to the Unmixing Wizard.
10. Test the following options for unmixing:
    a. Unmix without AF extraction first. Select live unmixing.
    b. Repeat steps of the Unmixing Wizard with AF extraction, placing the scatter gate on the population of interest only. Select Unmix, Save & Open to generate a separate set of FCS files from step 10a.
11. If there are other cells of interest in the sample that have a brighter spectral signature, try to unmix with the scatter gate on this population in step 10b.
12. Determine the best unmixing outcome comparing the N × N plots by evaluating changes in resolution for the dyes that overlap with the range of emission of AF (e.g., BUV496, BV510, Pac Orange, BV570, FITC, PE).

MANAGING HETEREOGENEOUS AUTOFLUORESCENCE (VIDEO 5)

SUPPORT PROTOCOL 3

The following protocol is divided into three sections: Discover, Distinguish and Designate.

Discover

1. Observe N × N plot permutations of raw channel data.
    a. On the Aurora, draw as many pseudocolor or dot plots as channels.
    b. Leave the *x* axis unchanged.
    c. Set each *y* axis to the different channels, so each plot shows a different raw combination.

    An example of a SpectroFlo N × N raw template is shown in Figure 8.
2. Find a combination that separates the greatest number of populations from one another.

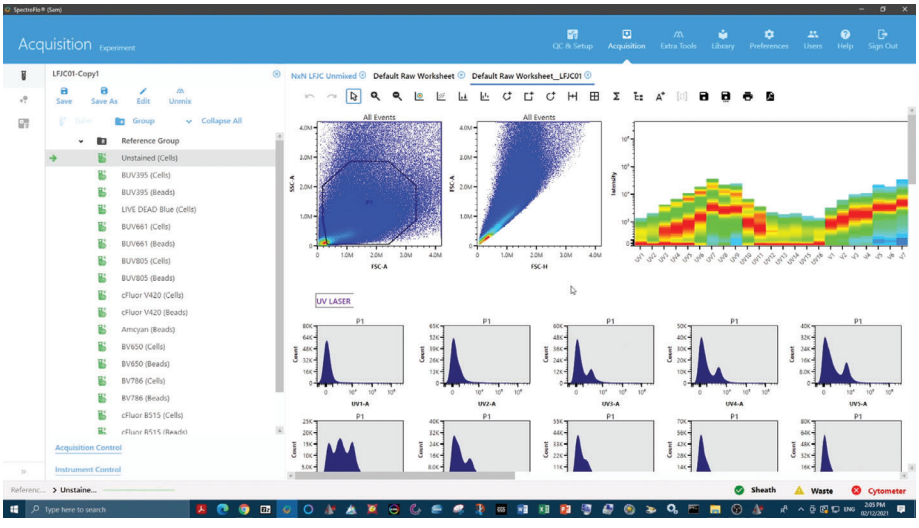

Video 5 Heterogeneous autofluorescence (Support Protocol 3).

Ferrer-Font et al.

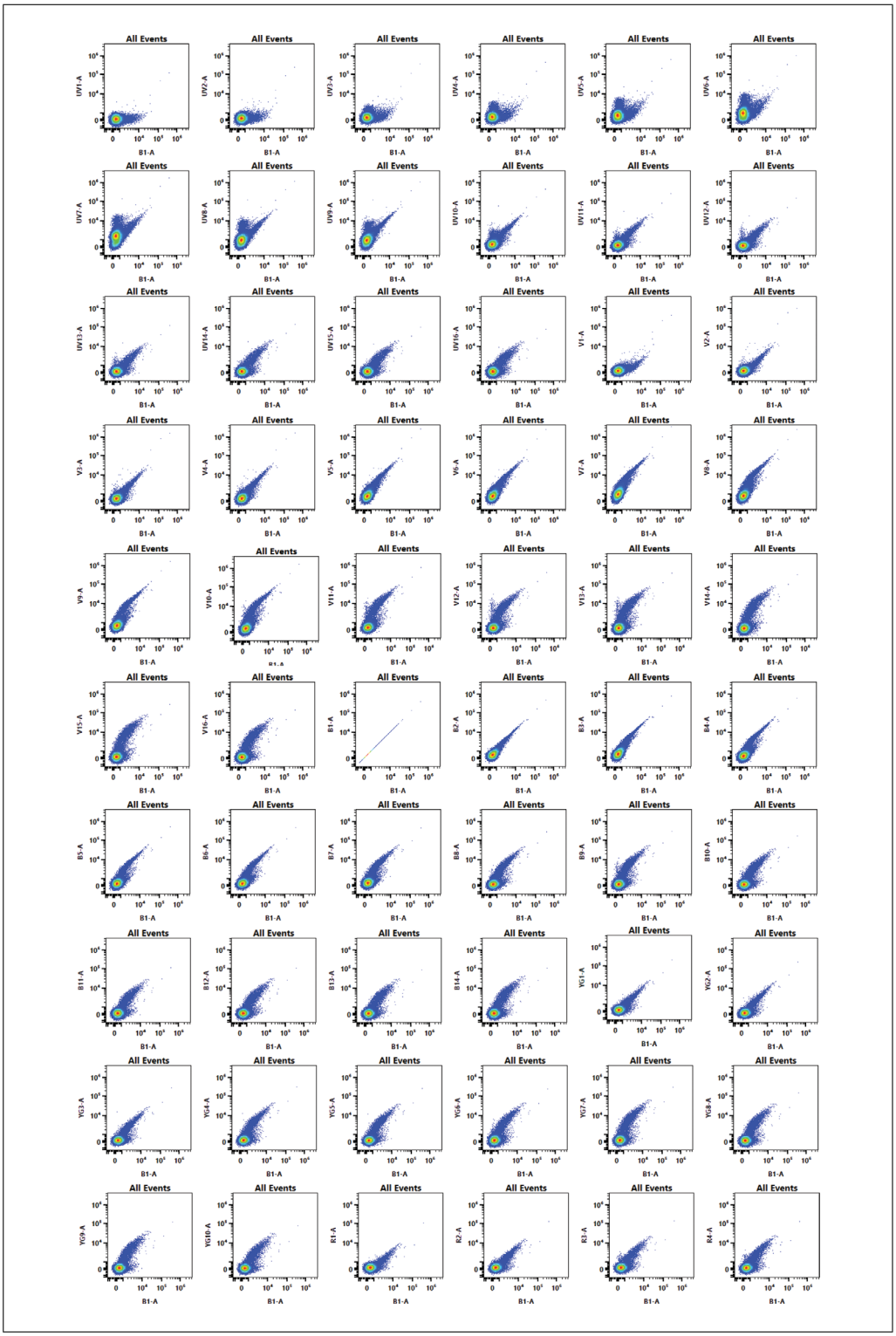

Figure 8 Example of an N × N raw worksheet.

Potential shortcut: Observe spectral plot showing ALL events and find one channel where there is obvious heterogeneity and one channel with similarity. This will immediately pull apart a minimum of two populations. Hint: Mid-range UV channels are most likely to show heterogeneity. If eosinophils are expected, YG1 will assist with isolating eosinophils from other populations.

Distinguish

3. Choose the plot with highest degree of separation.

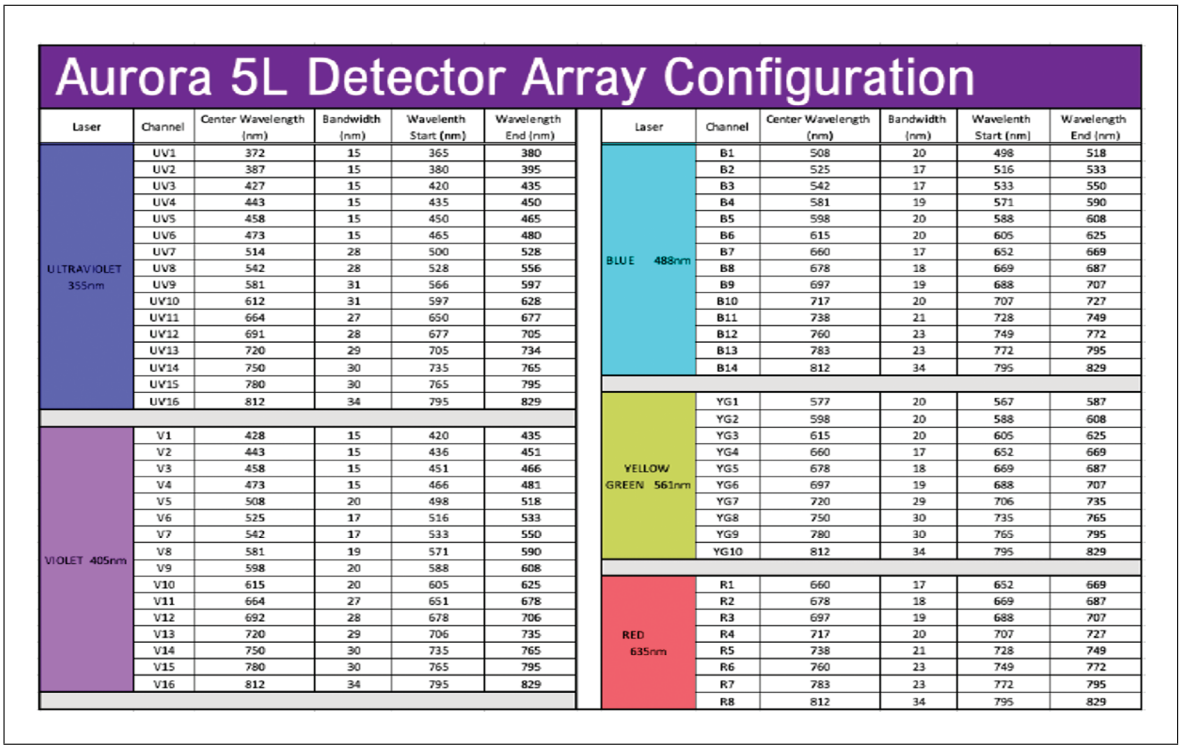

Aurora 5L Detector Array Configuration

Laser	Channel	Center Wavelength (nm)	Bandwidth (nm)	Wavelength Start (nm)	Wavelength End (nm)
ULTRAVIOLET 355nm	UV1	372	15	365	380
	UV2	387	15	380	395
	UV3	427	15	420	435
	UV4	443	15	435	450
	UV5	458	15	450	465
	UV6	473	15	465	480
	UV7	514	28	500	528
	UV8	542	28	528	556
	UV9	581	31	566	597
	UV10	612	31	597	628
	UV11	664	27	650	677
	UV12	691	28	677	705
	UV13	720	29	705	734
	UV14	750	30	735	765
	UV15	780	30	765	795
	UV16	812	34	795	829
VIOLET 405nm	V1	428	15	420	435
	V2	443	15	436	451
	V3	458	15	451	466
	V4	473	15	466	481
	V5	508	20	498	518
	V6	525	17	516	533
	V7	542	17	533	550
	V8	581	19	571	590
	V9	598	20	588	608
	V10	615	20	605	625
	V11	664	27	651	678
	V12	692	28	678	706
	V13	720	29	706	735
	V14	750	30	735	765
	V15	780	30	765	795
	V16	812	34	795	829

Laser	Channel	Center Wavelength (nm)	Bandwidth (nm)	Wavelength Start (nm)	Wavelength End (nm)
BLUE 488nm	B1	508	20	498	518
	B2	525	17	516	533
	B3	542	17	533	550
	B4	581	19	571	590
	B5	598	20	588	608
	B6	615	20	605	625
	B7	660	17	652	669
	B8	678	18	669	687
	B9	697	19	688	707
	B10	717	20	707	727
	B11	738	21	728	749
	B12	760	23	749	772
	B13	783	23	772	795
	B14	812	34	795	829
YELLOW GREEN 561nm	YG1	577	20	567	587
	YG2	598	20	588	608
	YG3	615	20	605	625
	YG4	660	17	652	669
	YG5	678	18	669	687
	YG6	697	19	688	707
	YG7	720	29	706	735
	YG8	750	30	735	765
	YG9	780	30	765	795
	YG10	812	34	795	829
RED 635nm	R1	660	17	652	669
	R2	678	18	669	687
	R3	697	19	688	707
	R4	717	20	707	727
	R5	738	21	728	749
	R6	760	23	749	772
	R7	783	23	772	795
	R8	812	34	795	829

Figure 9 Aurora 5L detector array configuration.

4. Place gates around all unique populations and observe the scatter properties and spectral signatures on adjacent spectral plots and select only the populations that have unique spectral characteristics.
5. Find the peak fluorescent channel for each unique population and then display said population on a histogram using this channel.
6. Gate the brightest 300-500 cells only, in order to derive the brightest AF SS control.
7. Right-click on the gate and export events as a new FCS file.
8. Repeat for all unique populations, producing an FCS file for each.
9. Export an AF dim population (dimmest AF spectral signature found in the sample) to be used as the negative control for the previously exported populations.

Designate

10. Designate these new AF signatures as fluorescence tags in the SpectroFlo Library.
    a. Create a new AF group.

       This will facilitate filtering and exporting these fluorophores for offline analysis, as well as identification when designing experiments.

    b. Assign the AF tag a name, choose the excitation laser, and assign an emission wavelength (use the optical configuration in Figure 9 to determine wavelength based on peak emission channel).
11. Open the experiment of interest and add the new AF tag(s) as if it were a fluorophore in the experiment.
12. In the reference controls tab, add an additional negative for the AF tags that will be the AF dim.

13. Import the populations exported during the Distinguish steps as SRCs for the corresponding tags, and import the AF dim population as an additional negative for the AF SRCs.

14. Use the Unmixing Wizard QC tools to assess AF signature similarity.

    In our experience, a similarity of 0.96 or less indicates that the AF signatures are generally considered to be unique.

15. Unmix the experiment and evaluate the unmixed N × N matrix.

    If unmixing errors are still present, refer to the troubleshooting guide in Table 3.

BASIC PROTOCOL 4

ASSESS DATA QUALITY USING EXPERT GATING AND DIMENSIONALITY REDUCTION ALGORITHMS

Informed gating is a useful way to check panel quality. It is necessary to check that all populations of interest can be identified and to investigate how well they can be resolved (Fig. 10A, Video 6). The biology of the sample should be considered to ensure that populations seen in the sample are as expected and that markers are expressed on all the expected cell types. This protocol indicates whether the panel is ready for use on experimental samples. Additionally, dimensionality reduction algorithms can be useful tools for investigating panel quality, as they simplify the data for visualization while also exposing artefacts that may be missed through expert gating. Using *t*-distributed stochastic neighbor embedding (*t*-SNE; van der Maaten & Hinton, 2008; Fig. 10B), markers that are usually co-expressed should be checked to see they are found in similar regions of the *t*-SNE plot (Brummelman et al., 2019).

Materials

Data analysis software (e.g., FlowJo, FCS Express, or any other software that allows gating of data)
FCS files generated in Basic Protocol 3

Perform expert gating

1. Open the unmixed FS sample in data analysis software used for analyzing FCS files.

2. Follow steps 2-6 of Basic Protocol 2 to gate on live single cells of interest.

3. Gate the rest of the markers based on panel design, prior knowledge, and published literature.

4. Check the gating strategy for unexpected marker combinations or cell populations (Fig. 10A).

   For example, when analyzing PBMCs, a $CD3^+CD19^+$ double-positive population is not expected. If one is found, the source of this staining must be investigated and corrected before the panel is ready for use.

5. Evaluate whether all populations of interest have clear positive signals that can be easily resolved from the negative.

6. Ensure readout markers (used for experimental readout) can be quantified in each of the cell types of interest.

Apply dimensionality reduction algorithm (t-SNE)

7. Using the cleaned data from step 2, run a *t*-SNE at the default settings (iterations: 1000; perplexity: 30) utilizing all fluorescence parameters. Exclude non-informative parameters such as those used in the data cleaning steps (e.g., viability and phenotypic markers for identifying cells of interest).

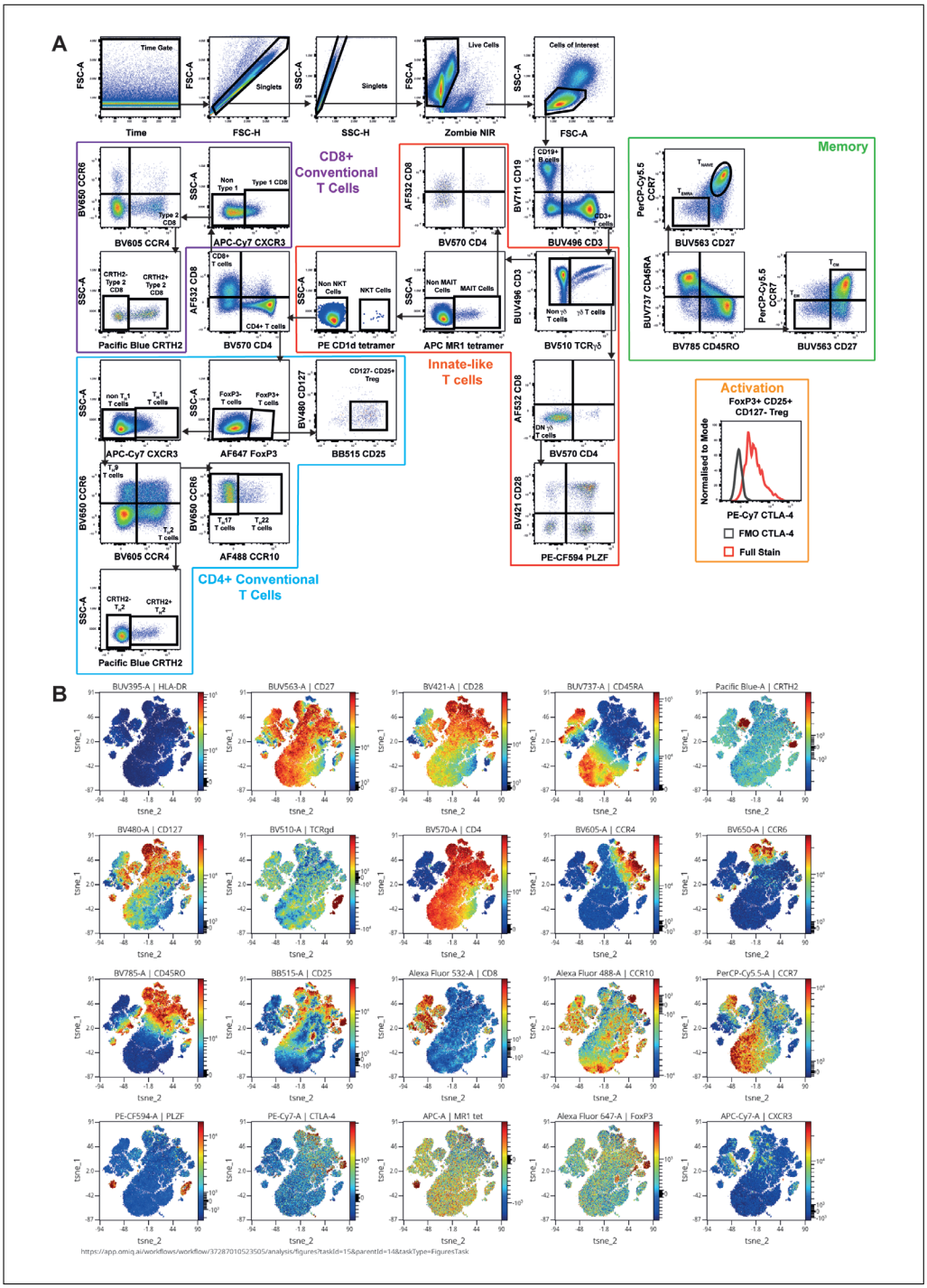

Figure 10 Gating of the FS sample. (**A**) Gating strategy of the panel, including lineage, memory, and activation readouts. (**B**) *t*-SNE as a quality control tool. *t*-SNE analysis was performed with 1000 iterations and perplexity of 30 and displayed in 2D plots using the resultant *t*-SNE 1 and *t*-SNE 2 dimensions according to the per cell expression of 20 proteins. Expression levels of HLA-DR, CD27, CD28, CD45RA, CRTH2, CD127, TCR$\gamma\delta$, CD4, CCR4, CCR6, CD45RO, CD25, CCR10, CD8, CCR7, PLZF, CTLA-4, MR1tet, FoxP3, and CXCR3 are displayed. *t*-SNE scales are shown in each graph and visualized using a rainbow heat scale.

8. Assess marker co-localization one by one in viSNE plots by coloring the *t*-SNE based on the expression of each marker (Fig. 10B).

viSNE is a visualization tool for high-dimensional single-cell data based on t-SNE.

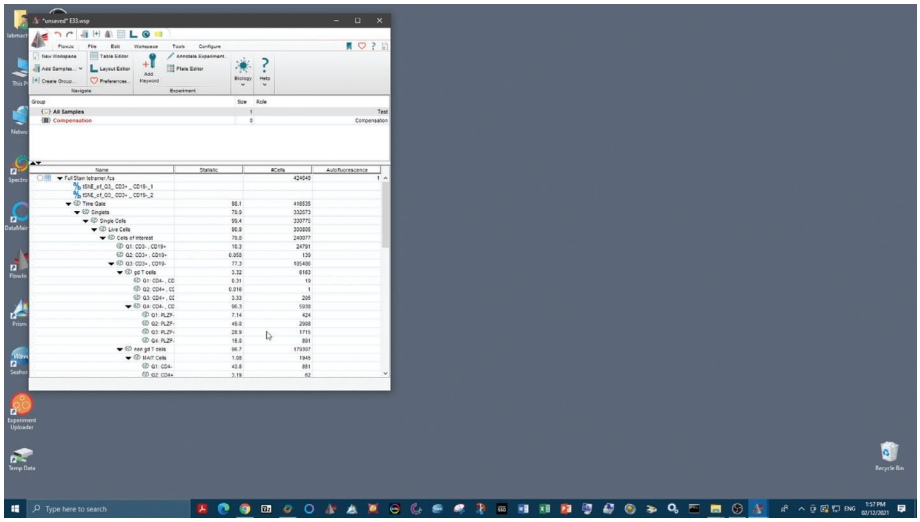

Video 6 Assessment of data quality using expert gating and dimensionality reduction algorithms (Basic Protocol 4).

9. As in step 4, check for the appearance of unexpected marker combinations on specific cell types.

See Figure 11 for a simple checklist to help ensure that all steps have been followed to obtain a high-quality and reliable immunophenotyping panel.

COMMENTARY

Background Information

The first step of building a successful large multicolor panel is good theoretical panel design. Full-spectrum flow cytometry panel design has been previously described (Ferrer-Font, Pellefigues, et al., 2020; Park et al., 2020). In summary, in the context of successful theoretical panel design, it is very important to have a clear experimental question and to know the biology of the markers that are included in the assay, including their expression and co-expression patterns. It is important to understand the instrument configuration (i.e., number of lasers on board) to know what the spectral signatures for each fluorophore will look like with the given configuration, as fluorophore brightness will vary depending on the excitation wavelength available. This information, coupled with the amount of spread (both given and received) of each fluorophore in the panel (detailed in Nguyen, Perfetto, Mahnke, Chattopadhyay, & Roederer, 2013), allows fluorophores to be optimally assigned to the different markers of the immunophenotyping panel.

After the panel has been theoretically designed, performance of QC steps is strongly recommended. This process is necessary to theoretically validate the panel before proceeding to a full experiment in order to reduce preventable issues as much as possible. It is advised to review the panel on a marker-by-marker and population-by-population basis, making sure that fluorophores inducing considerable amounts of spread (which could impair marker resolution) are allocated to non-co-expressed markers, and that dim markers receive a minimal amount of spread, while fluorophore brightness and antigen expression levels are well matched (high-expressing antigens with dim fluorophores and low-expressing antigens with bright fluorophores). To address potential issues, markers that are available with multiple fluorophores can be substituted to see if spillover spread can be minimized. Additionally, fluorophores that create (but do not receive) the most spillover can be designated to dump or viability channels. It is strongly recommended to complete panel optimization before working with an actual biological experiment, as it is a wise investment in terms of time, effort, and cost, without jeopardizing precious experimental samples.

Critical Parameters

Multiple factors influence the success of this protocol. The importance of good sample preparation—addressing sample

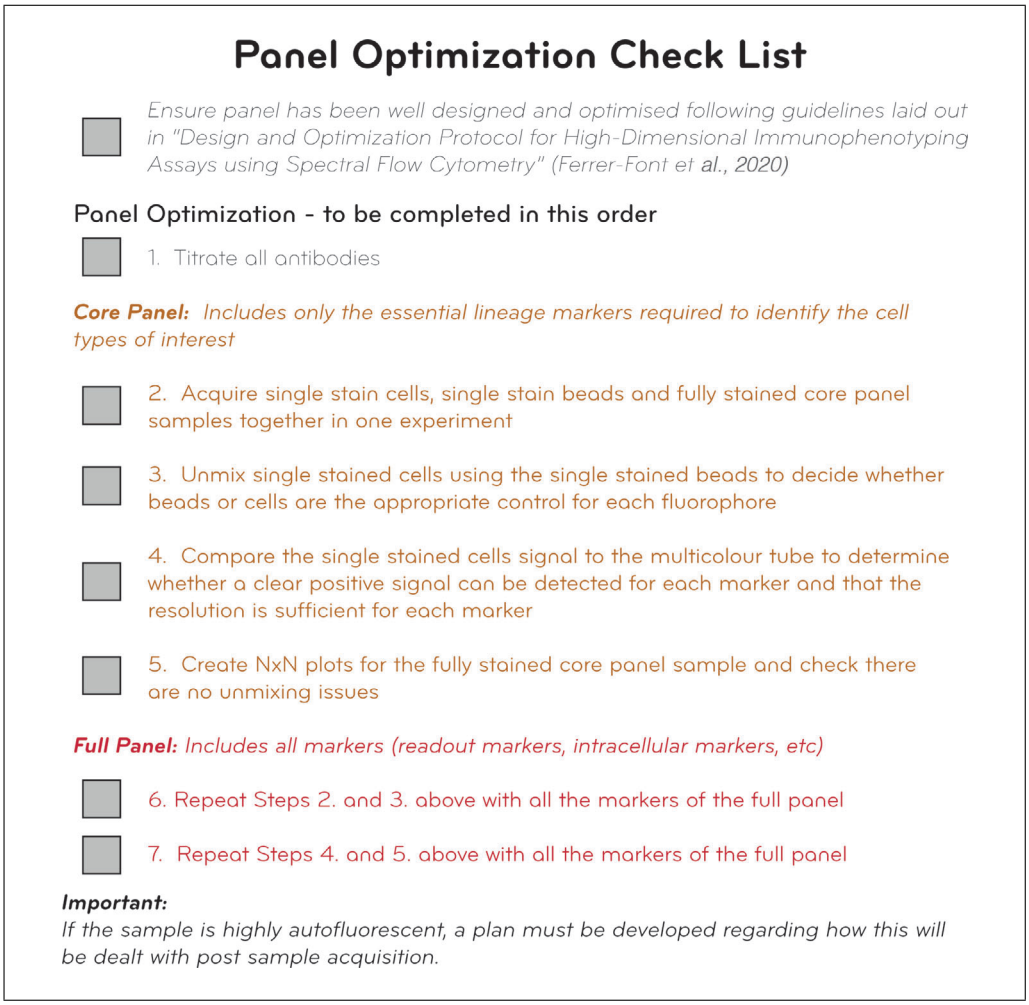

Figure 11 Panel optimization check list. To ensure the rigor and reproducibility of data acquired by spectral cytometry, the following steps are recommended for optimization and validation of each new panel.

complexity issues and the use of high-quality controls—must be emphasized.

Working with complex samples

When working with more complex samples than PBMCs (e.g., skin, tumor, fat tissue), the steps for panel optimization are the same, but there are some extra considerations.

Quality of single-cell suspension. An important consideration that is sometimes underestimated is the quality of the single-cell suspension that will be used to run the immunophenotyping panel. As different immune cell subsets have varying susceptibility to cell death, the single-cell suspension should have a viability of 80% or more to ensure proportional representation of the original sample (Costantini et al., 2003). Cell death can occur for different reasons, including how the sample has been treated before staining. Cryopreservation and harsh digestion protocols can affect sample quality and these procedures also need to be optimized. Indeed, when working with digested tissue, epitopes for the markers of interest should be verified to ensure the digestion protocol has not negatively impacted them. For example, if the same epitopes of interest exist in the spleen, one should compare marker staining and epitope preservation between digested and undigested spleen (Ferrer-Font, Mehta, et al., 2020).

Assessing instrument setup. Wherever possible, the instrument settings for fluorescence detector gains should remain unaltered from the Cytek Assay Settings (CAS). When using fluorescently labeled antibodies, this is achieved by carefully pairing expression levels to fluorophore brightness during panel design, and then by antibody titration to ensure fluorescence signals remain on-scale at the optimized settings. In certain applications where fluorescence intensity is not tunable, such as fluorescent reporter protein expression within

the cells of interest, the instrument settings may need to be adjusted to accommodate off-scale fluorescence signal. Any such change will impact not only the spectral signature being accommodated, but also other signatures with emission in the same area. Reducing fluorescence gains may lead to increased similarity between spectral signatures, which can give rise to more spillover spreading error and thus negatively impact marker resolution (Ferrer-Font, Pellefigues, et al., 2020). See Support Protocol 2 for steps required to alter fluorescence gain settings to accommodate off-scale signals. If using something other than the Cytek Aurora, it will be necessary to optimize the settings based on manufacturer's recommendations.

Autofluorescence. Samples with heterogeneous (Fig. 7C) or very bright homogeneous AF signatures (Fig. 7B) can make unmixing challenging. To improve the accuracy of the unmixing and to improve marker resolution in the case of heterogeneous AF samples, multiple AF reference controls can be created for each of the different AF signatures present in the sample (as if they were individual fluorophores included in the panel). The steps required for this process are divided in three sections called Discover, Distinguish and Designate. The goal is to Discover unique spectral signatures within the unstained control through use of a raw N × N plots; Distinguish these unique signatures into separate SRCs by exporting each population as a new FCS file which can then be reimported; and Designate each signature as unique fluorophores within the software to be unmixed as if they were part of the original panel. Care must be taken to ensure only clearly unique signatures (with similarity index <0.98) with at least 300 events of similar fluorescence intensity are distinguished to ensure high quality SRCs are generated (for a detailed protocol, see Support Protocol 3 and Video 4). For very bright homogeneous AF, the steps outlined in Basic Protocol 3 and Video 4 can be followed to improve unmixing and markers resolution outcomes.

Controls

The quality of controls will directly translate to the quality of unmixing and the data obtained. It is therefore worth investing the time to optimize them. It is of utmost importance to include all necessary controls from the beginning of a project. A complete overview about controls can be found in Maecker & Trotter (2006). Below is a summary of the categories of controls that should be considered when optimizing a flow cytometry panel.

Unstained controls. The unstained control is meant for AF assessment and should have a clean signature with no contamination from other fluorophores and match the tissue or sample type being analyzed. If, for example, different tissue types are used in an experiment, multiple unstained sample controls must be used for each tissue type. Similarly, if samples are being treated differently (e.g., fixed/fresh or stimulated/unstimulated), an unstained control should be included for each condition. It is not advised to mix samples from different conditions and collect only one unstained control, as it may not be possible to have enough events to generate clear AF signatures.

Spectral reference controls. Appropriate single-stained SRC samples are required for optimal unmixing of the fully stained sample. The purpose is to provide a signature of each fluorophore to be used by the unmixing algorithm. Briefly, SRCs should have positive and negative populations that are clearly separated or a universal negative; positive populations should be brighter than the fully stained sample; the negative and positive populations should have identical AF characteristics; sufficient events for both populations should be collected; and the fluorescence spectrum of the positive control needs to be identical to the one in the fully stained sample. To fulfill these best practices, cells and beads should be compared and the best option should be used. Special considerations for viability staining are important, as live and dead cells have different AF signatures, which means the positive and negative controls will not have the same AF signature. To overcome this issue, it is possible to kill all cells in the viability SRC (e.g., heat-killing at 55°-70°C for 5-10 min), stain only half of them, and mix these with the unstained cells. In this case, all the cells will be dead and the AF will be the same for the positive and negative controls.

SS cell controls. SS cell controls are used not only as reference controls but also to assess the performance of each marker compared to the FS tube. SS cells are gold-standard for each antibody performance and are used to quantify the spread of the negative population and/or shifts in the positive signal and thus any subsequent loss of resolution of markers in the panel.

Gating controls. A fluorescence minus one (FMO) control is a sample stained with all

fluorophores used in the experiment except one. Analyzing the FMO control for each fluorophore in the panel is not required for panel optimization, but FMOs can be used as a guide to set the boundary between positive and negative events if it is ambiguous. FMOs also aid in the assessment of spread between positive and negative events and are an important tool for assessing panel performance. A good alternative for large 20+ color spectral panels is the use of fluorescence minus multiple (FMM) controls, as recently described by Jensen & Wnek (2020).

Core versus FS panel

When optimizing a high-dimensional immunophenotyping panel, it is recommended to first complete Basic Protocols 1-4 with a *core panel.* A core panel is limited to only the essential lineage markers required to identify the cell types of interest. This will reduce confounding factors when attempting to understand the source of errors. Once a core panel has been optimized, additional markers can be added (including readout functional markers, intracellular markers, etc.) and optimized with the knowledge that issues are not originating from the core panel.

Fixation/permeabilization buffers

Intracellular staining procedures also require special consideration. It is important to source the fixation/permeabilization reagent that is most appropriate for the markers being detected (e.g., transcription factors, cytokines, or intracellular proteins) while also considering their relative locations (cytosolic or nuclear). The type of fixation buffer can influence the staining of both intracellular and surface markers. The type of fixative can have an impact in many aspects of staining: damaging the epitopes, altering the fluor stability and resulting in a different optimal titer, altering the background fluorescence without altering the positive signal (leading to reduced resolution between positive and negative populations), and altering the fluorescence spectral signatures (causing spectral signature mismatches between FS samples and SRCs, resulting in unmixing issues). It is recommended that antibodies be titrated using the same fixation/permeabilization buffer conditions used for the final staining of FS samples and SRCs.

Troubleshooting

The term troubleshooting is used when one or more issues are found in the panel and the source of these issues needs to be identified and steps included to rectify them. In this regard, the exact steps provided for validating the panel can also be applied for troubleshooting. By following these clear steps, the user will gain a better understanding of the quality of the panel and identify issues prior to acquiring experimental samples.

In general, 80%-90% of unmixing issues that arise can be traced to suboptimal controls. Therefore, it is important to use controls that are well characterized, high quality, and appropriate for the experiment (i.e., matched to the conditions of the experimental sample). This is particularly vital if they are going to be reused.

The checklist provided in Figure 11 aims to help users follow clear steps to optimize and troubleshoot their panels. By following these steps, users should be able to discover issues if they exist and have a pathway and alternatives to address and resolve them. Additional troubleshooting for general issues that may arise during panel optimization can be found in Tables 2-5.

Understanding Results

The example panel optimized using this protocol and presented here aims to identify conventional T cell subsets in peripheral blood of healthy participants. The participants were infected with low-dose human hookworm as part of a longitudinal study. It is well established that during early parasitic infection there is an increase in T-helper Type 2 immune responses (Th2) in the T cell compartments due to the primary role these cells play in host responses to parasites (McSorley & Loukas, 2010). However, the wider effects on the human immune system of long-term chronic parasitic infection with the gut-residing hookworm *Necator americanus (Na)* have not been investigated. Therefore, a panel was designed and optimized to look at the following conventional and unconventional T cell subsets of interest: $CD4^+$ T cells (Th1, Th2, Th17, Th9, Th22, and Tregs), $CD8^+$ T cells (Tc1 and Tc2), and innate-like T cells (γδ T, mucosal associate invariant T [MAIT], and natural killer T [NKT] cells). This panel can assess the frequency of these cell subsets as well as their memory and activation phenotypes, using both expert gating and high-dimensional data analysis.

Some characteristics of the fluorophore selection for a certain panel including the

Table 2 Troubleshooting for Preparation and Evaluation of Optimal SRCs (Basic Protocol 1)

Problem	Cause	Potential solution
Spectral signature of SRC does not match expected signature for fluorophore	Contamination of control with another fluorescent antibody	Preferably prepare new SRC; alternatively, in SpectroFlo software using the raw SRC, exclude the contaminating signature, export the clean file, and import this FCS file as the correct SRC
	Carryover from previous SRCs on the cytometer	Preferably prepare a new SRC; alternatively, in the SpectroFlo software using the raw SRC, exclude the contaminating signature, export the clean file and import this FCS file as the correct SRC
	Tandem dye degradation	Find the cause of degradation (issue with fixative, how long samples are stored in fixative, temperature of incubation, light exposure during protocol, etc.) and make necessary corrections (modifying staining procedure or buy a new vial)
	Brilliant Stain Buffer added to bead controls	Remake bead SRCs without addition of Brilliant Stain Buffer
	Wrong tube was recorded (signature matches different fluorophore)	Read the correct control or import the correct SRC FCS file
More than one spectral signature is visible	Autofluorescence signature	If positive and negative populations have the same secondary signature(s), this may be autofluorescence. See Basic Protocol 3 or Support Protocol 3 to decide on an approach for mitigating AF.
	Contamination of control with another fluorescent antibody	If there are multiple positive populations and gating on each one produces a distinct signature, then it is likely that there are two fluorophores in the SRC. Prepare a new SRC or exclude the signature of the contamination and import this FCS file as the correct SRC, if possible
Fluorescent signal in the negative population of the SRC	Nonspecific binding of antibody to negative beads	Revisit antibody titer to make sure the optimal titration is used; alternatively, use the universal negative feature in the software
	Inadequate sample preparation/wash procedure	Wash SRC controls well in the presence of excess wash solution such as FACS Staining Buffer (see Basic Protocol 1)
	Carryover of samples from previous SRC	Look at time vs. fluorescent signal, export a cleaned FCS file removing the contaminating signal, and import this FCS file as the correct SRC
Unmixing errors in SRCs	Gates were not set correctly in the Unmixing Wizard	Ensure that the P1 gate is set on the population with the highest expression of the marker. Place the positive histogram gate on the brightest signal (this may be different than gating on all positive signals). Better results can be obtained with tighter gates that do not include a side variety of cell sizes and/or fluorescence intensities.
	Contamination of control with another fluorescent antibody	Preferably prepare a new SRC; alternatively, in SpectroFlo software using the raw SRC, exclude the contaminating signature, export the clean file, and import this FCS file as the correct SRC

(*Continued*)

Table 2 Troubleshooting for Preparation and Evaluation of Optimal SRCs (Basic Protocol 1), *continued*

Problem	Cause	Potential solution
No positive signal can be detected	Gates were not set correctly in the Unmixing Wizard	Move P1 gate to population that expresses marker and/or move histogram to peak detector
	Not enough events were recorded	The unmixing algorithm requires a minimum of 300 positive events; record more total events
	Antibody was not added to SRC	Prepare new SRC

Table 3 Troubleshooting for Unmixing Evaluation of Fully Stained Sample (Basic Protocol 2)

Problem	Potential cause	Potential solution
Unmixing Wizard unmixes SRCs cells correctly, but unmixing errors are present in FS cells	SRCs are dimmer than fully stained sample	Use brighter SRCs; ensure staining protocol is exactly the same for SRCs and FS cells (antibody concentration, incubation time/temperature, use of fixative, stimulation of cells, etc.). Note that the optimal antibody concentration for compensation beads is often different than for cells. Pipetting error can easily occur when pipetting small volumes (<1-2 µl) for SRCs compared to using a master mix for FS samples. In this case, it is recommended to dilute antibodies to avoid pipetting small volumes. Other common mistakes include not using fix/perm buffer on compensation beads or using a tissue for SRCs that has lower marker expression than FS sample.
	Beads were used for all the SRCs and there may be a mismatch in the emission spectra between beads and cells	Use SRC stained cells instead.
	Polymer dyes (more than 2) are included in the panel without using Brilliant Stain Buffer or Super Bright Stain Buffer	Use Brilliant Stain Buffer when more than one polymer dye is added in the same tube following manufacturer recommendations.
	AF signature in FS sample is complex and different to the controls	Use AF extraction and see information regarding complex AF samples. Ensure the unstained control used for AF extraction is treated the same as the FS stained sample. AF signature may change with treatment (fixation, stimulation, timepoint, etc.). With human samples there may be patient-to-patient variability in AF signatures, so if using AF extraction for complex AF samples, an unstained control for each patient may be required. Also ensure that enough events are recorded in the unstained control to assess AF.
	Wrong tube was recorded (signature matches different fluorophore)	Read the correct control or import the correct SRC FCS file
Some FS samples unmixed correctly while others have unmixing errors	Biological variation; marker level of expression greatly changes across donors or across experimental conditions.	Try using beads as SRCs. If they are not optimal, use donor with the highest level of expression as control.

Table 4 Troubleshooting for Evaluation of Marker Resolution (Basic Protocol 3)

Problem	Potential cause	Potential solution
Low signal in certain markers (in FS and SS samples)	Marker expression too low or non-existent	Check that the marker is expected to be expressed on the particular cells or animal model of interest. Compare to Technical Data Sheet (TDS) or published literature.
	Experimental design (i.e., timepoint or stimulation) does not elicit certain markers	Stimulate cells with a positive control (e.g., PMC-ionomycin) to ensure cells are capable of expressing the markers of interest.
	Epitope is damaged by digestion procedure	Test different clone or modify digestion conditions
	Epitope is damaged by staining procedure	Test different clone or modify staining conditions
	Fluorophores chosen were too dim	Choose a brighter fluorophore for the specific marker and optimize concentration used
	Tandem dyes have degraded or decoupled	Find cause of degradation (issue with fixative, how long samples are stored in fixative, temperature of incubation, light exposure during protocol, etc.) and replace tandem dye with a new vial
FS sample stained less (lower MFI) than SS sample for a given marker	Binding site blocked by other reagents in the panel or different Ab/receptor binding kinetics	Test sequential staining, perform experiments to identify antibodies that are interfering with each other or try different clones
	Saturation is not achieved at optimal titer for SRCs	Increase titer to reach saturation
	Pipetting error when pipetting antibody cocktails	Repeat experiment to double-check
	Antibody/antibodies were trapped in the column when filtering the antibody cocktail	Optimize centrifuge spinning time and speed
Unstained, SS, and FS cells have high AF background	Cells of interest are highly autofluorescent	Extract autofluorescence
Suboptimal separation/resolution between negative and positive populations	Antibody concentration is too low or too high	Optimize antibody concentration based on antibody titration results
	Spread	Check SSM and use FMOs to confirm source of spread
	Unbound antibodies were not adequately washed from samples	Add additional centrifugation and FACS Staining Buffer wash step
	Viability dye concentration is too high and live cells are stained with dye	If live cells are stained with viability dye, the spreading error from the viability dye must be accounted for and this may cause problems with marker resolution. Ideally, viability dye should be titrated so that live cells do not stain with viability dye.

Table 5 Troubleshooting for Assessment of Data Quality (Basic Protocol 4)

Problem	Potential cause	Potential solution
Appearance of unexpected biological patterns	Inadequate cleaning gates	Make sure you are using time gates, excluding doublets, dead cells, and antibody aggregates, and gating on cells of interest
	Viability dye concentration is too high and live cells are stained with dye	Titrate viability dye to make sure the optimal concentration is used
	Lack of viability dye in panel and dead cells nonspecifically bind to antibodies	Titrate and add viability dye to FS samples
	Lack of addition of Brilliant Stain Buffer	Use Brilliant Stain Buffer when more than one polymer dye is added in the same tube following manufacturer recommendations

similarity and complexity indices of the panel (Fig. 12A) and the spectral signatures of fluorophores used (Fig. 12B) have been included. Although some fluorophores have a high similarity index, they have been allocated to different cell types and therefore the impact of the expected spreading error should be minimal (Fig. 12). A panel distribution table has also been included (Fig. 12C) to show the peak emission wavelengths for the fluorophores and markers assigned to the panel.

After following all the steps of Basic Protocols 1-4 for our panel shown here, and resolving any issues that arose (such as one tandem degradation or implementing the sequential staining for some of the markers), high-quality full-spectrum flow cytometry data as defined by clear resolution of all expected populations was achieved. The optimized staining protocol for this panel is detailed in the Supplementary Material. Sequential staining was applied, following the order given in the protocol, for markers that showed a reduction in positive signal in the FS compared to the SS control, starting at the marker with the greatest reduction and working toward the one with the least reduction. This approach provided satisfactory results and did not require the testing of other combinations. To reduce staining procedure time, further optimization would be required to determine whether some markers could be added at the same time instead of using all of them sequentially.

A clean and clear positive population can be detected for all markers in the panel, with no signal resolution loss when all antibodies are combined. In some cases, such as for the activation markers, the use of FMOs is necessary to assist in evaluating gates to determine positive staining with confidence. All populations of interest could be found using expert gating, and the populations resemble the expected expression patterns and frequencies. Additionally, high-dimensional data analysis algorithms were successfully used without the appearance of artefacts, confirming the high quality of the data.

Time Considerations

The time needed for designing, optimizing, and analyzing a high-dimensional flow cytometry panel can be highly variable and can depend on the assay complexity, number of markers, wait-time required for reagents (geographically dependent), sample access and frequency of sample delivery (particularly for patient samples), duration of the disease model being investigated, and more. As an example, it took five months to optimize the digestion, design, and optimization of a 23-color spectral flow cytometry panel in gut tissue (Ferret-Font, Mehta, et al., 2020), whereas one month may be sufficient for a PBMC panel where digestion does not need optimization. It is therefore advisable to develop certain core panels that can be applied to several experimental questions and models.

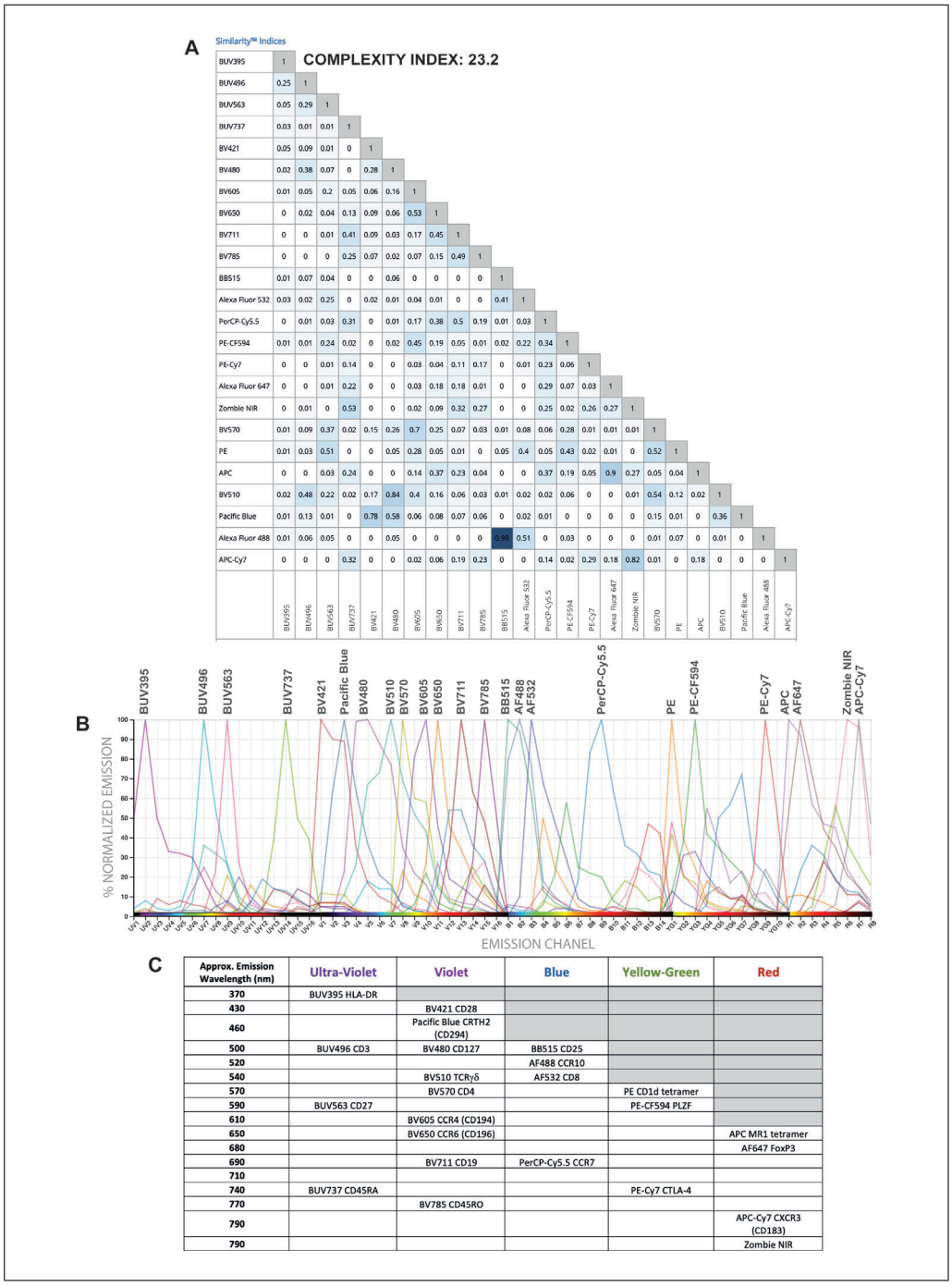

C

Approx. Emission Wavelength (nm)	Ultra-Violet	Violet	Blue	Yellow-Green	Red
370	BUV395 HLA-DR				
430		BV421 CD28			
460		Pacific Blue CRTH2 (CD294)			
500	BUV496 CD3	BV480 CD127	BB515 CD25		
520			AF488 CCR10		
540		BV510 TCRγδ	AF532 CD8		
570		BV570 CD4		PE CD1d tetramer	
590	BUV563 CD27			PE-CF594 PLZF	
610		BV605 CCR4 (CD194)			
650		BV650 CCR6 (CD196)			APC MR1 tetramer
680					AF647 FoxP3
690		BV711 CD19	PerCP-Cy5.5 CCR7		
710					
740	BUV737 CD45RA			PE-Cy7 CTLA-4	
770		BV785 CD45RO			
790					APC-Cy7 CXCR3 (CD183)
790					Zombie NIR

Figure 12 Theoretical panel design. (**A**) Similarity and complexity indices of fluorophores used in the final panel design. (**B**) Cytek Full Spectrum Viewer readout showing the fluorescence signatures of all fluorophores used in the panel, using the 5L Aurora configuration. (**C**) Panel distribution table showing peak emission wavelengths for markers and fluorophores in the panel.

Acknowledgments

This work was enabled by the Hugh Green Cytometry Centre at the Malaghan Institute of Medical Research. We wish to thank the Hugh Green Foundation, the Marjorie Barclay Trust, the Dinies Foundation and the HRC Independent Research Organisation (18/1003) for funding this study. We are also very grateful to the NIH Core Tetramer Facility for supplying the tetramers used in this panel and to Olivia Burn and Kathryn Hally for feedback on the manuscript.

Author Contributions

Laura Ferrer-Font: Conceptualization; investigation; methodology; project administration; writing–original draft; **Sam J. Small:** Investigation; methodology;

writing–original draft; **Brittany Lewer:** Investigation; writing–review & editing; **Katherine R Pilkington:** Resources; writing–review & editing; **Laura K. Johnston:** Writing–review & editing; **Lily M. Park:** Writing–review & editing; **Joanne Lannigan:** Methodology; writing–review & editing; **Maria C. Jaimes:** Conceptualization; methodology; resources; supervision; writing–review & editing; **Kylie M. Price:** Funding acquisition; project administration; supervision; writing–review & editing.

Conflicts of Interest

Kate Pilkington, Lily Park, Maria C. Jaimes are employees of Cytek Biosciences, Inc., the manufacturer of the Aurora full-spectrum flow cytometer used in these studies. Joanne Lannigan is a paid consultant for Cytek Biosciences, Inc.

Data Availability Statement

Data available on request due to privacy/ethical restrictions.

Literature Cited

Aass, H. C. D., Øvstebø, R., Trøseid, A. M. S., Kierulf, P., Berg, J. P., & Henriksson, C. E. (2011). Fluorescent particles in the antibody solution result in false TF- and CD14-positive microparticles in flow cytometric analysis. *Cytometry Part A*, *79 A*, 990–999. doi: 10.1002/cyto.a.21147.

Ashhurst, T. M., Smith, A. L., & King, N. J. C. (2017). High-dimensional fluorescence cytometry. *Current Protocols in Immunology*, *2017*, 5.8.1–5.8.38. doi: 10.1002/cpim.37.

Ayers, L., Kohler, M., Harrison, P., Sargent, I., Dragovic, R., Schaap, M., … Ferry, B. (2011). Measurement of circulating cell-derived microparticles by flow cytometry: Sources of variability within the assay. *Thrombosis Research*, *127*, 370–377. doi: 10.1016/j.thromres.2010.12.014.

Brummelman, J., Haftmann, C., Núñez, N. G., Alvisi, G., Mazza, E. M. C., Becher, B., & Lugli, E. (2019). Development, application and computational analysis of high-dimensional fluorescent antibody panels for single-cell flow cytometry. *Nature Protocols*, *14*, 1946–1969. doi: 10.1038/s41596-019-0166-2.

Costantini, A., Mancini, S., Giuliodoro, S., Butini, L., Regnery, C. M., Silvestri, G., & Montroni, M. (2003). Effects of cryopreservation on lymphocyte immunophenotype and function. *Journal of Immunological Methods*, *278*, 145–155. doi: 10.1016/S0022-1759(03)00202-3.

Disis, M., dela Rosa, C., Goodell, V., & Ling-Yu, K. (2006). Maximizing the retention of antigen specific lymphocyte function after cryopreservation. *Journal of Immunological Methods*, *308*, 13–18. doi: 10.1016/J.JIM.2005.09.011.

Feher, K., von Volkmann, K., Kirsch, J., Radbruch, A., Popien, J., & Kaiser, T. (2016). Multispectral flow cytometry: The consequences of increased light collection. *Cytometry Part A*, *89*, 681–689. doi: 10.1002/cyto.a.22888.

Ferrer-Font, L., Mehta, P., Harmos, P., Schmidt, A. J., Chappell, S., Price, K. M., … Mayer, J. U. (2020). High-dimensional analysis of intestinal immune cells during helminth infection. *eLife*, *9*, e51678. doi: 10.7554/eLife.51678.

Ferrer-Font, L., Pellefigues, C., Mayer, J. U., Small, S. J., Jaimes, M. C., & Price, K. M. (2020). Panel design and optimization for high-dimensional immunophenotyping assays using spectral flow cytometry. *Current Protocols in Cytometry*, *92*, 1–25. doi: 10.1002/cpcy.70.

Inglis, H. C., Danesh, A., Shah, A., Lacroix, J., Spinella, P. C., & Norris, P. J. (2015). Techniques to improve detection and analysis of extracellular vesicles using flow cytometry. *Cytometry Part A*, *87*, 1052–1063. doi: 10.1002/cyto.a.22649.

Jalbert, E., Shikuma, C. M., Ndhlovu, L. C., & Barbour, J. D. (2013). Sequential staining improves detection of CCR2 and CX3CR1 on monocytes when simultaneously evaluating CCR5 by multicolor flow cytometry. *Cytometry Part A*, *83 A*, 280–286. doi: 10.1002/cyto.a.22257.

Jensen, H. A., & Wnek, R. (2020). Analytical performance of a 25-marker spectral cytometry immune monitoring assay in peripheral blood. *Cytometry Part A*, *99*(2), 180-193. doi: 10.1002/cyto.a.24290.

Maecker, H. T., & Trotter, J. (2006). Flow cytometry controls, instrument setup, and the determination of positivity. *Cytometry Part A*, *69*, 1037–1042. doi: 10.1002/cyto.a.20333.

Mayeno, A. N., Hamann, K. J., & Gleich, G. J. (1992). Granule-associated flavin adenine dinucleotide (FAD) is responsible for eosinophil autofluorescence. *Journal of Leukocyte Biology*, *51*, 172–175. doi: 10.1002/jlb.51.2.172.

McSorley, H. J., & Loukas, A. (2010). The immunology of human hookworm infections. *Parasite Immunology*, *32*, 549–559. doi: 10.1111/j.1365-3024.2010.01224.x.

Nguyen, R., Perfetto, S., Mahnke, Y. D., Chattopadhyay, P., & Roederer, M. (2013). Quantifying spillover spreading for comparing instrument performance and aiding in multicolor panel design. *Cytometry Part A*, *83 A*, 306–315. doi: 10.1002/cyto.a.22251.

Park, L. M., Lannigan, J., & Jaimes, M. C. (2020). OMIP-069: Forty-color full spectrum flow cytometry panel for deep immunophenotyping of major cell subsets in human peripheral blood. *Cytometry Part A*, *97*, 1044–1051. doi: 10.1002/cyto.a.22251.

Petriz, J., Bradford, J. A., & Ward, M. D. (2018). No lyse no wash flow cytometry for maximizing minimal sample preparation. *Methods*, *134–135*, 149–163. doi: 10.1016/j.ymeth.2017.12.012.

Roederer, M. (2016). Distributions of autofluorescence after compensation: Be panglossian, fret not. *Cytometry Part A*, *89*, 398–402. doi: 10.1002/cyto.a.22820.

Sahir, F., Mateo, J. M., Steinhoff, M., & Siveen, K. S. (2020). Development of a 43 color panel for the characterization of conventional and unconventional T-cell subsets, B cells, NK cells, monocytes, dendritic cells, and innate lymphoid cells using spectral flow cytometry. *Cytometry Part A*, 2020, Dec 18. doi: 10.1002/cyto.a.24288.

Schmutz, S., Valente, M., Cumano, A., & Novault, S. (2016). Spectral cytometry has unique properties allowing multicolor analysis of cell suspensions isolated from solid tissues. *PLoS One*, *11*, e0159961. doi: 10.1371/journal.pone.0159961.

Shi, L., Lu, L., Harvey, G., Harvey, T., Rodríguez-Contreras, A., & Alfano, R. R. (2017). Label-free fluorescence spectroscopy for detecting key biomolecules in brain tissue from a mouse model of Alzheimer's disease. *Scientific Reports*, *7*, 1–7. doi: 10.1038/s41598-017-02673-5.

Stewart, C. C., & Stewart, S. J. (1997). Titering antibodies. *Current Protocols in Cytometry*, *00(*1*)*, 4.1.1–4.1.13. doi: 10.1002/0471142956.cy0401s14.

van der Maaten, L., & Hinton, G. (2008). Visualizing data using t-SNE. *Journal of Machine Learning Research*, *9*, 2579–2605.

van der Vlist, E. J., Nolte-'t Hoen, E. N. M., Stoorvogel, W., Arkesteijn, G. J. A., & Wauben, M. H. M. (2012). Fluorescent labeling of nano-sized vesicles released by cells and subsequent quantitative and qualitative analysis by high-resolution flow cytometry. *Nature Protocols*, *7*, 1311–1326. doi: 10.1038/nprot.2012.065.

Using Full-Spectrum Flow Cytometry to Phenotype Memory T and NKT Cell Subsets with Optimized Tissue-Specific Preparation Protocols

Kathryn Farrand,[1,5] Lauren E. Holz,[2,5] Laura Ferrer-Font,[1,3] Michael D. Wilson,[1] Mitch Ganley,[4] Jordan J. Minnell,[1] Ching-Wen Tang,[1] Gavin F. Painter,[4] William R. Heath,[2] Ian F. Hermans,[1,3,6] and Olivia K. Burn[1,6,7]

[1]Malaghan Institute of Medical Research, Wellington, New Zealand
[2]Department of Microbiology and Immunology, The Peter Doherty Institute for Infection and Immunity, The University of Melbourne, Victoria, Australia
[3]Maurice Wilkins Centre, Auckland, New Zealand
[4]Ferrier Research Institute, Victoria University of Wellington, Wellington, New Zealand
[5]These authors contributed equally to this work.
[6]These authors share senior authorship.
[7]Corresponding author: *oburn@malaghan.org.nz.*

Published in the Cytometry section

Full-spectrum flow cytometry is now routinely used in many laboratories internationally, and the demand for this technology is rapidly increasing. With capacity to use larger and more complex staining panels, standardized protocols are required for optimal panel design and analysis. Importantly, for *ex vivo* analysis, tissue preparation methods also need to be optimized to ensure samples are truly representative of tissues *in situ.* This is particularly relevant given the recent interest in adaptive immune cells that form residency in specific organs. Here we provide optimized protocols for tissue processing and phenotyping of memory T cells and natural killer T (NKT) cell subsets from liver, lung, spleen, and lymph node using full-spectrum flow cytometry. We provide a 21-color antibody panel for identification of different memory subsets, including tissue-resident memory T (T_{RM}) cells, which are increasingly regarded as important effectors in adaptive immunity. We show that processing procedures can affect outcomes, with liver T_{RM} cells particularly sensitive to heat, such that accurate evaluation requires fast processing at defined temperatures.

Keywords: full-spectrum flow cytometry • high-dimensional flow cytometry panel • memory T cell populations • NKT cells • tissue processing • tissue-resident memory T cells

CURRENT PROTOCOLS
A Wiley Brand
Current Protocols e482, Volume 2
Published in Wiley Online Library (wileyonlinelibrary.com).
doi: 10.1002/cpz1.482

How to cite this article:
Farrand, K., Holz, L. E., Ferrer-Font, L., Wilson, M. D., Ganley, M., Minnell, J. J., Tang, C.-W., Painter, G. F., Heath, W. R., Hermans, I. F., & Burn, O. K. (2022). Using full-spectrum flow cytometry to phenotype memory T and NKT cell subsets with optimized tissue-specific preparation protocols. *Current Protocols*, *2,* e482. doi: 10.1002/cpz1.482

INTRODUCTION

Spectral flow cytometers have facilitated the routine use of large (>20) multicolor flow cytometry panels, enabling phenotypic analysis of multiple cell subsets in a single sample (Hally, Ferrer-Font, Pilkington, & Larsen, 2022; Park, Lannigan, & Jaimes, 2020). Confident data interpretation of spectral flow cytometry experiments is dependent on accurately designed flow cytometry panels and optimal cell sample preparation. Analysis of tissues that are poorly digested or exposed to processing conditions that preferentially remove certain cell types may have a large impact on the experimental readout. Ensuring a sample is truly representative of the source tissue from which it was collected may require trialing various isolation techniques. Indeed, the method of isolation is likely to differ between tissues due to their inherent structural differences or depending on the cell types to be analyzed. Regardless of the method, optimal cell count, viability, and a consistent representation of cell types of interest must be achieved. Only through the combination of optimized processing methods and optimized spectral flow cytometry panels can researchers confidently generate quality data that can be assessed in high-dimensional analysis platforms such as FlowJo, FCS express, and OMIQ.

Mature lymphocytes recirculate between secondary lymphoid organs and gain the capacity to migrate into nonlymphoid tissues after they have been activated. In recent years, a diverse family of noncirculating lymphocytes have also been identified, including tissue-resident memory T (T_{RM}) cells, unconventional T cells such as invariant natural killer T (NKT) cells, intraepithelial lymphocytes, γδ T cells, and an assorted family of innate lymphocytes (Rosato, Beura, & Masopust, 2017; Steinbach, Vincenti, & Merkler, 2018). Depending on their location, these resident cells can contribute significantly to initiation and maintenance of adaptive immune responses and facilitate enhanced secondary responses to antigenic challenge. Recently, we described a vaccine design featuring major histocompatibility complex (MHC)-binding peptide epitopes conjugated to an NKT cell agonist (via a cleavable linker) that specifically induces accumulation of $CD8^+$ T_{RM} cells in the liver, presumably reflecting a unique supportive microenvironment established by activation of liver NKT cells (Holz et al., 2020). This type of immune response is of significant interest, as the presence of antigen-specific liver T_{RM} cells has been correlated with effective prophylaxis in animal models of infection, and in humans the presence of liver T_{RM} cells has been correlated with resolution of chronic infection and liver cancer (Cheng et al., 2021; Fernandez-Ruiz et al., 2016; Holz et al., 2020; Lim et al., 2019; Pallett et al., 2017). To analyze immune responses to vaccines of this kind in mice, we routinely use a five-laser full-spectrum flow cytometer, the Cytek Aurora, as the 64 detectors provide maximum panel design flexibility. Based on previously published guidelines (see *Current Protocols* articles: Ferrer-Font et al., 2020, 2021), we designed and optimized a 21-color full-spectrum T cell immunophenotyping panel that included the analysis of NKT cells and specifically had the capability to assign different T cell phenotypes, including T_{RM} cells. An important first step was to ensure that the sample processing methods

had no effect on T cell viability and expected marker expression patterns, as alterations could influence the conclusions made from the generated data.

The protocols provided here describe optimized sample preparation methods to maintain integrity of memory T cell subsets and NKT cells in liver, spleen, lungs, and lymph node and an optimized full-spectrum flow cytometry panel for their phenotypic analysis. We provide the necessary staining order and controls for optimal panel use and data generation. Importantly, we illustrate the sensitivity of some cells, notably liver T_{RM} cells, to different sample preparation techniques.

NOTE: All protocols involving live animals must first be approved by an Institutional Animal Care and Use Committee (IACUC) or must follow local guidelines for the care and use of live animals.

PROCESSING MOUSE LIVER FOR FLOW CYTOMETRIC ANALYSIS OF MEMORY T AND NKT CELL SUBSETS

BASIC PROTOCOL 1

This protocol describes how to process livers to obtain optimal single-cell suspensions for analysis of memory T cells and NKT cells (Fig. 1). Using our vaccine design, we typically investigate the immune response 28 to 35 days postvaccination, when T cell memory is established and accumulation of liver T_{RM} cells is evident; however, this protocol could be readily used in other treatment regimens or disease conditions.

Materials

Mouse of interest
Liver harvest buffer (see recipe)
Roswell Parks Memorial Institute (RPMI) medium (e.g., Gibco, cat. no. 11875093)
35% Percoll buffer (see recipe)
Red blood cell (RBC) lysis buffer (e.g., Qiagen, cat. no. 158106)
Fluorescence-activated cell sorting (FACS) buffer (see recipe)

24-well plate (e.g., NUNC, cat. no. NUN142475)
70-µm cell strainer (e.g., Falcon, cat. no. BDAA352350)
50-ml centrifuge tube (e.g., Falcon, cat. no. 352070)
1-ml syringe (e.g., BD, cat. no. 302100)
Centrifuge with plate adaptor (e.g., Megafuge 40R)
96-well U-bottom plate (e.g., NUNC, cat. no. NUN163320)

Additional reagents and equipment for mouse euthanasia (see *Current Protocols* article: Donovan & Brown, 2006)

1. Harvest mouse liver following cervical dislocation or CO_2 asphyxiation.

   Remove gall bladder and other connective tissue from the liver.

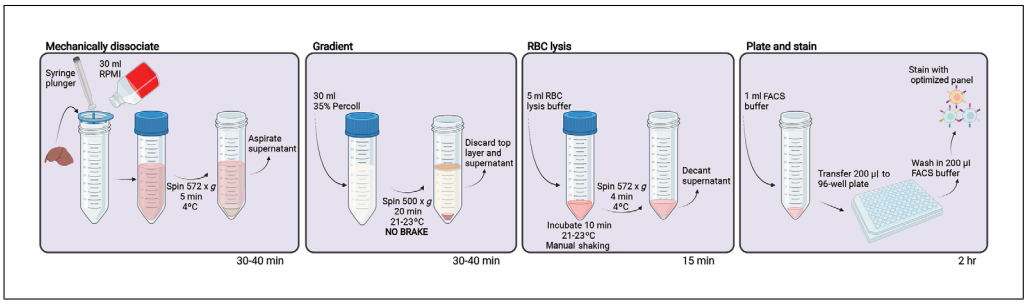

Figure 1 Optimized workflow for liver processing. FACS, fluorescence-activated cell sorting; RBC, red blood cell.

2. Immediately place in 1 ml cold liver harvest buffer in a 24-well plate sitting on ice.
3. Dissociate liver through a 70-µm strainer into a 50-ml tube using the end of a 1-ml syringe plunger and flushing through with RPMI medium periodically until a total suspension of 30 ml is reached.

   Ensure the livers and processed samples stay on ice during this process.

4. Pellet cells by centrifuging 5 min at 572 × *g*, 4°C.
5. Gently aspirate supernatant, being careful as the pellet can be loose. Once aspirated, gently shake tube to dissociate the pellet.
6. Resuspend each tube in 30 ml of 35% Percoll buffer. Invert tubes a few times (do not vortex) to ensure there is no cell pellet, and centrifuge 20 min at 500 × *g*, room temperature, without deceleration brake.
7. Aspirate liver parenchymal cell layer (top) and discard supernatant, leaving only the RBC/white blood cell (WBC) pellet in the tube.
8. Add 5 ml RBC lysis buffer, and leave for 10 min at 21°C to 23°C.

   Gently agitate the tubes during this time. This time interval is dependent on the lysis solution used; some solutions, such as ammonium-chloride-potassium buffer, may only require 5 min.

9. Centrifuge tubes 4 min at 572 × *g*, 4°C.
10. Resuspend cells in 1 ml FACS buffer.
11. Transfer 200 µl of each sample to a 96-well plate (i.e., staining one-fifth of liver).

    The experimenter may pause at this point for a break (1 to 2 hr). Store plate at 4°C during this period.

12. Stain samples according to Basic Protocol 5.

BASIC PROTOCOL 2

PROCESSING MOUSE SPLEEN FOR FLOW CYTOMETRIC ANALYSIS OF MEMORY T AND NKT CELL SUBSETS

This protocol describes how to process spleens to obtain optimal single-cell suspensions for analysis of memory T cell and NKT cell subsets (Fig. 2). Using our vaccine design, we typically investigate the immune response 28 to 35 days postvaccination, when T cell memory is established and accumulation of T_{RM} cells is evident; however, this protocol could be readily used in other treatment regimens or disease conditions.

See Basic Protocol 1 for a list of materials.

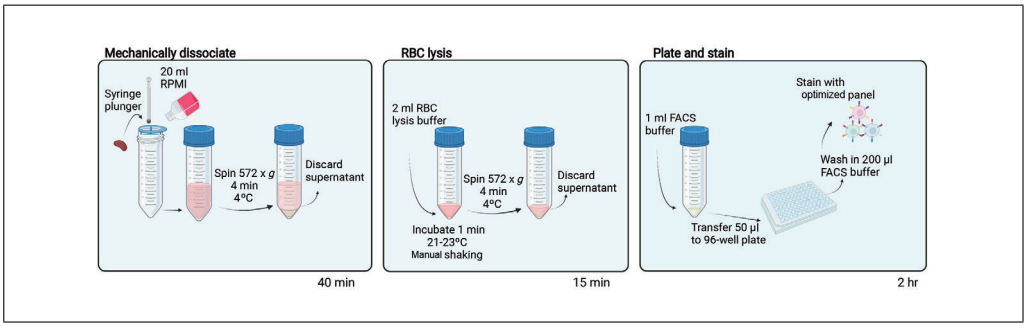

Figure 2 Optimized workflow for spleen processing. FACS, fluorescence-activated cell sorting; RBC, red blood cell.

1. Harvest mouse spleens following cervical dislocation or CO_2 asphyxiation, being sure to remove any connective tissue.
2. Immediately place in 1 ml cold RPMI medium in a 24-well plate sitting on ice.
3. Dissociate spleen through a 70-µm strainer into a 50-ml tube using 20 ml RPMI medium and the plunger end of 1-ml syringe. Transfer each dissociated sample to ice while processing remaining spleens.
4. Pellet cells by centrifuging 4 min at 572 × *g*, 4°C.
5. Decant supernatant and resuspend pellet in 2 ml RBC lysis buffer.
6. Gently agitate tubes for 1 min at room temperature before pelleting WBCs by centrifuging 4 min at 572 × *g*, 4°C.
7. Decant supernatant and resuspend pellet in 1 ml FACS buffer. Transfer 50 µl of each sample to a 96-well plate (i.e., staining one-twentieth of spleen).

   The experimenter may pause at this point for a break (1 to 2 hr). Store plate at 4°C during this period.

8. Stain samples according to Basic Protocol 5.

PROCESSING MOUSE LUNGS FOR FLOW CYTOMETRIC ANALYSIS OF MEMORY T AND NKT CELL SUBSETS

BASIC PROTOCOL 3

This protocol describes how to process lungs to obtain optimal single-cell suspensions for analysis of memory T cells and NKT cells (Fig. 3). Using our vaccine design, we typically investigate the immune response 28 to 35 days postvaccination, when T cell memory is established and accumulation of T_{RM} cells is evident; however, this protocol could be readily used in other treatment regimens or disease conditions.

Materials

Lung digest buffer (see recipe)
Mouse of interest

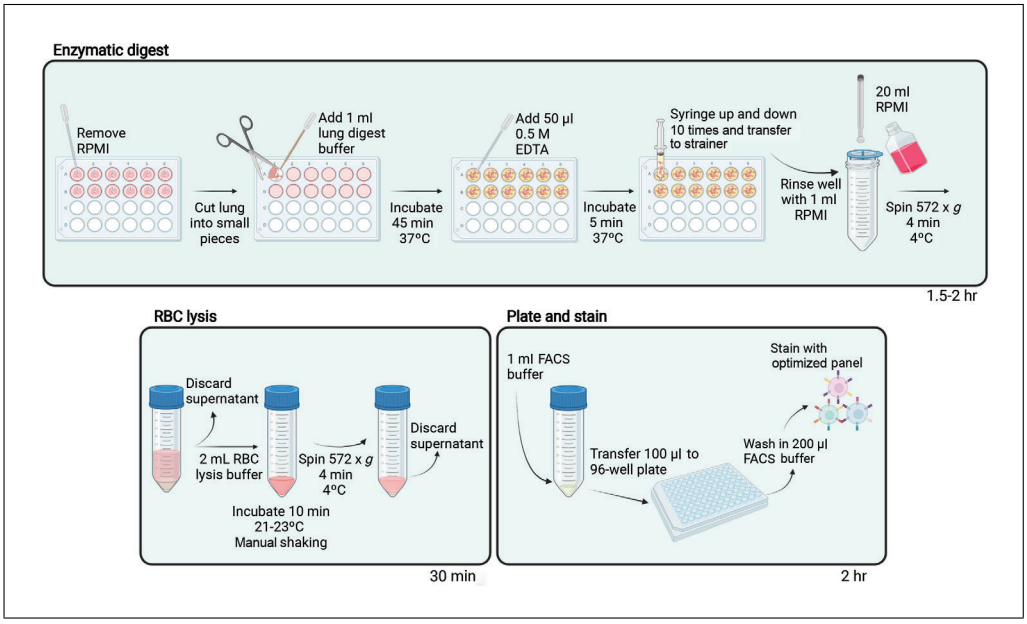

Figure 3 Optimized workflow for processing lungs. FACS, fluorescence-activated cell sorting; RBC, red blood cell.

Farrand et al.

RPMI medium (e.g., Gibco, cat. no. 11875093)
0.5 M EDTA (e.g., Invitrogen, cat. no. AM9260G)
RBC lysis buffer (e.g., Qiagen, cat. no. 158106)
FACS buffer (see recipe)

24-well plate (e.g., NUNC, cat. no. NUN142475)
Dissection scissors or scalpel, to cut lung tissue
37°C, 5% CO_2 incubator
3-ml syringe (e.g., BD, cat. no. 302113)
70-μm cell strainer (e.g., Falcon, cat. no. BDAA352350)
50-ml centrifuge tube (e.g., Falcon, cat. no. 352070)
Centrifuge with plate adaptor (e.g., Megafuge 40R)
96-well U-bottom plate (e.g., NUNC, cat. no. NUN163320)

Additional reagents and equipment for mouse euthanasia (see *Current Protocols* article: Donovan & Brown, 2006)

1. Prepare lung digest buffer fresh before harvest.
2. Harvest lungs following CO_2 asphyxiation of the mouse, being sure to remove any connective tissue.

   Do not perform cervical dislocation.
3. Immediately place in 1 ml cold RPMI medium in a 24-well plate sitting on ice.
4. Remove RPMI medium, and cut lung into very small pieces.
5. Add 1 ml lung digestion buffer, and incubate for 45 min at 37°C.
6. Add 50 μl of 0.5 M EDTA into each well, and incubate for a further 5 min at 37°C.
7. Use a 3-ml syringe to vigorously syringe lung sample up and down in the well to break up lung tissue. Repeat this ten times.

   When filling the syringe, have the tip right at the base of the well to use friction to dissociate the lung tissue. When expelling, lift the syringe only just above the base to use the force of the sample against the base to dissociate.
8. Use syringe to transfer sample through a 70-μm strainer into a 50-ml centrifuge tube. Wash well with 1 ml RPMI medium, and run through strainer. Use the end of a syringe to dissociate lungs through the strainer, periodically adding RPMI medium until a cell suspension of 20 ml is reached.
9. Pellet cells by centrifuging 4 min at 572 × *g*, 4°C.
10. Decant supernatant and resuspend pellet in 2 ml RBC lysis buffer.
11. Agitate tubes for 10 min at 21°C to 23°C before pelleting WBCs by centrifuging 4 min at 572 × *g*, 4°C.
12. Decant supernatant and resuspend pellet in 1 ml FACS buffer. Transfer 100 μl cells to a 96-well plate.

    The experimenter may pause at this point for a break (1 to 2 hr). Store plate at 4°C during this period.
13. Stain samples according to Basic Protocol 5.

PROCESSING MOUSE LYMPH NODES FOR FLOW CYTOMETRIC ANALYSIS OF MEMORY T AND NKT CELL SUBSETS

BASIC PROTOCOL 4

This protocol describes how to process lymph nodes to obtain optimal single-cell suspensions for analysis of memory T cells and NKT cells (Fig. 4). Using our vaccine design, we typically investigate the immune response 28 to 35 days postvaccination, when T cell memory is established and accumulation of T_{RM} cells is evident; however, this protocol could be readily used in other treatment regimens or disease conditions.

Materials

Mouse of interest
RPMI medium (e.g., Gibco, cat. no. 11875093)
RBC lysis buffer (e.g., Qiagen, cat no. 158106)
FACS buffer (see recipe)

24-well plate (e.g., Nunc, cat. no. NUN142475)
Thick gauze
1-ml syringe (e.g., BD, cat. no. 302100)
1.7-ml microcentrifuge tube (e.g., Axygen, cat. no. MCT175C)
Microcentrifuge (e.g., Eppendorf centrifuge 5424R with rotor FA-45-24-11)
96-well U-bottom plate (e.g., Nunc, cat. no. NUN163320)

Additional reagents and equipment for mouse euthanasia (see *Current Protocols* article: Donovan & Brown, 2006)

1. Harvest lymph nodes following cervical dislocation or CO_2 asphyxiation of the mouse, being sure to remove any connective tissue.

   Do not perform cervical dislocation if harvesting cervical or mediastinal lymph nodes.

2. Immediately place in 1 ml cold RPMI medium in a 24-well plate sitting on ice.

3. Place a small piece of thick gauze (~0.5 × 0.5 cm) into each well, and dissociate lymph nodes through the gauze using the plunger end of a 1-ml syringe. Transfer cell suspension to a 1.7-ml microcentrifuge tube.

4. Pellet cells in a microcentrifuge 4 min at 1503 × *g*, 4°C.

5. Aspirate supernatant and resuspend pellet in 500 µl RBC lysis buffer.

6. Agitate tubes for 1 min at 21°C to 23°C before pelleting WBCs by centrifuging 4 min at 1503 × *g*, 4°C.

7. Aspirate supernatant and resuspend pellet in 200 µl FACS buffer before transferring all 200 µl to a 96-well plate for staining.

   The experimenter may pause at this point for a break (~1 to 2 hr). Store plate at 4°C during this period.

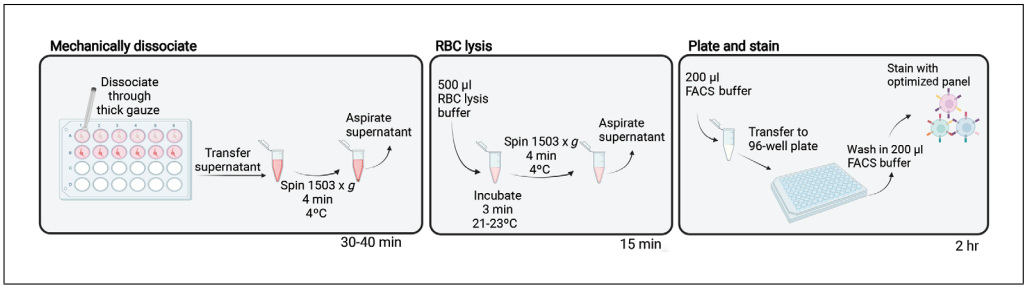

Figure 4 Optimized workflow for lymph node processing. FACS, fluorescence-activated cell sorting; RBC, red blood cell.

8. Stain samples according to Basic Protocol 5.

BASIC PROTOCOL 5

STAINING AND FLOW CYTOMETRIC ANALYSIS OF SAMPLES FOR MEMORY T AND NKT CELL SUBSETS

This protocol describes optimized staining conditions and the full-spectrum flow cytometry panel for assessment of memory T cells and NKT cells. Information for sample acquisition and evaluation is also provided.

Materials

Cells of interest (see Basic Protocols 1 to 4)
Anti-mouse Fc receptor block, clone 2.4G2 (generated from ATCC hybridoma cell line HB-197 or purchased from commercial sources; e.g., BD Biosciences, cat. no. 553142)
Dulbecco's phosphate-buffered saline (PBS; e.g., Gibco, cat. no. 70011-044)
Zombie NIR Fixable Viability Kit (e.g., BioLegend, cat. no. 423106)
Anti-mouse CD62L antibody, Alexa Fluor 700 (e.g., BioLegend, cat. no. 104426)
Antibodies (see Table 1 for list; see Fig. 5 for titration example)
FACS buffer (see recipe)
BD Horizon Brilliant Stain Buffer Plus (BSBP; e.g., BD Biosciences, cat. no. 566385)
4% (w/v) paraformaldehyde (e.g., Sigma-Aldrich, cat. no. HT5012-60)

Centrifuge with plate adaptor
Microcentrifuge
Aluminum foil
Thin gauze, 70 µm (e.g., Sefar Filter Specialists, cat. no. 03-70/41-115)
5-ml round-bottom polystyrene flow tubes (e.g., In Vitro Technologies, cat. no. 352008)
Spectral cytometer (e.g., Cytek Aurora 5 L)
Cytek SpectroFlo software v2.2
Data analysis software for analyzing flow cytometry standard (FCS) files (e.g., FlowJo, FCS express, or OMIQ)

Staining

1. Incubate cells with 100 µl Fc receptor block in PBS (1:100 Fc receptor block:PBS) for 10 min at 4°C. Following incubation, centrifuge plate 2 min at 800 × *g*, 4°C. Discard supernatant by quickly flicking plate upside down into a waste reservoir.

   Make sufficient Fc receptor block in PBS so it can be dispensed using a multichannel pipette: for example, 35 samples × 2 organ types + 4 fluorescence minus one (FMO) controls + 4 spare = 78 wells × 100 µl = 7800 µl. To prepare 1:100 Fc receptor block in PBS, combine 78 µl 2.4G2 supernatant with 7722 µl PBS.

2. Resuspend cells in 100 µl PBS containing Zombie NIR (1:1000) and anti-CD62L (1:300), and incubate for 15 min at 21°C to 23°C in the dark.

   Make sufficient PBS containing Zombie NIR and anti-CD62L so it can be dispensed using a multichannel pipette: for example, 35 samples × 2 organ types + 4 FMO controls + 4 spare = 78 wells × 100 µ l = 7800 µl. To prepare 1:1000 Zombie NIR and 1:300 anti-CD62L in PBS, first combine 7.8 µl Zombie NIR in 7792.2 µl PBS. Then remove 160 µl for anti-CD62L FMO control, and add 25.5 µl anti-CD62L.

   This staining must be performed in PBS as the proteins in fetal bovine serum (a component of FACS buffer) will affect Zombie NIR binding. Be sure to have a well that receives the Zombie NIR stain only, without the anti-CD62L; this will be used as a single-stain reference control during cytometer setup.

Table 1 Full-Spectrum Flow Cytometry Panel

Channel	Antigen	Fluorophore	Clone	Supplier, RRID	Concentration (μg/ml)
UV2	CD8	BUV395	53-6.7	BD Horizon, AB_2732919	0.22
V1	PBS-57-loaded CD1d tetramer	BV421	–	Emory Core facility	1:300 dilution
V3	CD19	eFluor 450	1D3	eBioscience, AB_2734905	0.4
V7	CD44	BV510	IM7	BioLegend, AB_2650923	0.33
V10	CD25	BV605	PC61	BioLegend, AB_2563059	0.67
V11	NK1.1	BV650	PK136	BioLegend, AB_2563159	0.67
V13	CXCR6	BV711	SA05101	BioLegend, AB_2721558	0.67
V15	CX3CR1	BV785	SA011F11	BioLegend, AB_2565938	0.17
B2	TCRβ	FITC	H57-597	BioLegend, AB_313429	2.5
B3	CD4	Alexa Fluor 532	RM4-5	Invitrogen, AB_11218891	0.22
B9	CD49a	BB700	Ha3118	BD OptiBuild, AB_2861198	0.33
B10	PD-1	PerCP-eFluor710	RMP1-30	eBioscience, AB_11151142	2
YG1	$OVA_{257-264}$-loaded H-$2K^b$ pentamer	PE	Batch:VP/8132-07	ProImmune	See Basic Protocol 5
YG3	CD103	PE-Dazzle594	2E7	BioLegend, AB_2566492	2
YG5	CD69	PE-Cy5	H1.2F3, lot: B270768	BioLegend, AB_313112	0.67
YG9	CD101	PE-Cy7	Moushi101, lot: 2191974	Invitrogen, AB_2573378	0.33
R1	KLRG1	APC	2F1/KLRG1, lot: B246931	BioLegend, AB_10641560	0.33
R2	CD64	Alexa Fluor 647	X54-5/7.1, lot: B278887	BioLegend, AB_2566561	1.67
R4	CD62L	Alexa Fluor 700	MEL-14, lot: B244199	BioLegend, AB_493719	1.67
R6	Live cells	Zombie NIR	Lot: B352465	BioLegend	
R7	CD45.2	APC-Fire750	104, lot: B247809	BioLegend, AB_2629723	0.67

3. During incubation, centrifuge antibody tubes (see Table 1) 1 min at 1503 × *g*, 4°C, in a microcentrifuge to remove aggregates. Centrifuge $OVA_{257-264}$-loaded H-$2K^b$ pentamer tube 3 min at 14,000 × *g*, 4°C.
4. When live–dead staining is finished, add 100 μl FACS buffer to each well, and centrifuge plate 2 min at 800 × *g*, 4°C. Flick off supernatant following centrifugation.
5. Repeat wash step in 200 μl FACS buffer.
6. Add 10 μl $OVA_{257-264}$-loaded H-$2K^b$ pentamer mix (follow organ specifications in Table 2) to each well, and incubate for 10 min at 21°C to 23°C in the dark.
7. During incubation, prepare antibody mix following the concentrations in Table 1. Add BD Horizon BSBP to the antibody mix at 1:4 BSBP:antibody mix.

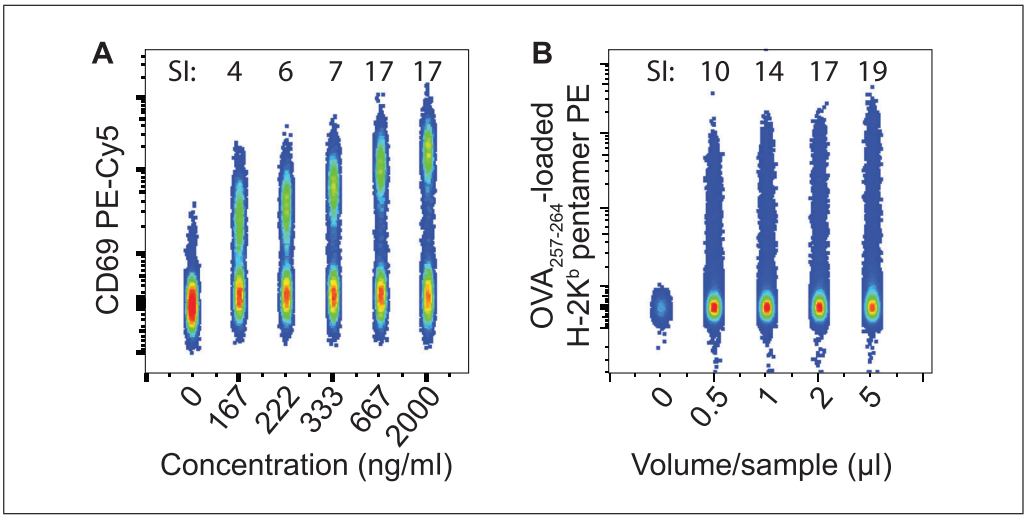

Figure 5 Antibody and multimer example titrations. Flow cytometry standard (FCS) files were concatenated to allow visual display of all concentrations on a single plot. Using this display allows easier interrogation of the negative population spread. The staining index (SI) shown above each concentration is calculated using the equation SI = (MdnFI*pos* – MdnFI*neg*) / (2 × SD*neg*), where MdnFI indicates median fluorescence intensity and SD, standard deviation. (**A**) Titration of anti-CD69 on liver T cells. The ideal concentration is 667 ng/ml as this retains the same SI as the higher concentration of 2000 ng/ml and demonstrates minimal spread of the negative and strong resolution of the positive population. (**B**) Titration of $OVA_{257-264}$-loaded H-2K^b pentamer on liver lymphocytes. The volume added per sample is shown, with the SI value shown above each plot. This plot indicates the ideal volume is between 2 and 5 µl of the $OVA_{257-264}$-loaded H-2K^b pentamer; at a volume of 5 µl, the negative population spreads into the positive, but a drop in SI is seen with a volume of 2 µl. It was recommended that further analysis including 3 and 4 µl volumes was performed.

Table 2 Volumes of $OVA_{257-264}$-Loaded H-2K^b Pentamer for Staining Various Organs

Organ	Volume pentamer per sample (µl)	Volume FACS per sample (µl)	Total volume per sample (µl)
Liver	3	7	10
Spleen	1	9	10
Lungs	1	9	10
Lymph nodes	1	9	10

It is important to include BSBP in panels with more than one Brilliant polymer dye (including FMO controls) to decrease interaction between Brilliant fluorescent polymer dyes, as these may cause staining artefacts that affect data interpretation. However, it is always important to check your panel with and without BSBP to ensure it is not affecting population resolution in the gating strategy.

8. Following incubation with the $OVA_{257-264}$-loaded H-2K^b pentamer mix, add 190 µl FACS buffer to each well. Centrifuge 2 min at 800 × *g*, 4°C, and discard supernatant. Repeat FACS buffer wash step once more.
9. Resuspend in 100 µl antibody/BSBP mix, and incubate for 20 min at 4°C.
10. Centrifuge plate 2 min at 800 × *g*, 4°C, and repeat FACS buffer wash step two times.
11. Fix samples in 100 µl of 1% (w/v) paraformaldehyde for 30 min at 21°C to 23°C in the dark.

Cells can be left fresh if analyzing within ~2 hr and should be stored in the dark at 4°C until analysis.

12. Add 100 µl FACS buffer to each well, and centrifuge plate 2 min at 800 × *g*, 4°C.

13. Resuspend each well in 200 µl FACS buffer, keeping covered in aluminum foil before analyzing on the flow cytometer.

    In our experience, fully stained fixed samples can be left covered in the fridge for up to 2 days before flow cytometric analysis without affecting results. This should be confirmed with your own samples.

Sample acquisition

14. Filter samples before acquisition using thin gauze placed over a 5-ml polystyrene flow tube.

    In replacement of gauze, a 70-µm filter could be used to filter the samples.

15. Acquire spectral reference controls (SRCs) on a Cytek Aurora, using the "Cytek Assay Settings" for the instrument. Adjust scatter profiles to ensure cells and beads are on scale and the forward scatter area (FSC-A) scaling factor is optimal. Adjust threshold to remove debris and any remaining RBCs.

    For more information on SRCs, see Critical Parameters, Controls Required.

16. Perform spectral unmixing using the unmixing Wizard.

    Detailed information is provided in a Current Protocols article by Ferrer-Font et al. (2021). Briefly, it is important to note the following points: (1) Ensure that the unstained cells have no contamination from other fluorophores. They may, however, show autofluorescence (AF) in the detectors of the UV and violet lasers. (2) Ensure the correct control, either beads or single-stained cells, is selected for each fluorophore. (3) Depending on your approach to AF, either ensure you have included AF tags in your reference group, or select "use autofluorescence extraction" within the unmixing wizard. More details are provided in Critical Parameters, Dealing with Autofluorescence. (4) Validate that the spectral signature acquired matches the expected signature, with the marker peaking in the correct channel (defined in Cytek's Full Spectrum viewer: https://spectrum.cytekbio.com).

17. Select the Live Unmix button to generate unmixed FCS files.

18. Create a pairwise (NxN) worksheet to visualize how accurately the SRCs have been unmixed.

19. Once satisfied with unmixing, create a new unmixed worksheet, and generate a gating strategy to reflect that provided in Figure 6.

20. Record 500,000 live events for each sample (i.e., fully stained samples, FMOs, etc.).

    Absolute live cell counts can be achieved using the methods provided in the Support Protocol. If using Calibrite APC counting beads, these should be added to the samples after filtration and just before acquisition.

Results evaluation

The manual gating strategy shown in Figure 6, conducted on liver cells, allows identification of various T cell and NKT cell populations (PBS-57-CD1d-loaded tetramer$^+$, T cell receptor [TCR] β^+). While not the focus of this panel, the included markers also facilitate analysis of B cells (CD19$^+$), monocytes (CD64$^+$), and NK cells (NK1.1$^+$TCRβ^-). T cells can be further differentiated into CD8$^+$ versus CD4$^+$ cells and antigen-specific T cells identified using MHC/peptide multimers; in this example, H-2K^b pentamers loaded with amino acids 257–264 from chicken ovalbumin ($OVA_{257\text{-}264}$) were used to detect CD8$^+$ T cells specific for $OVA_{257\text{-}264}$ peptide, an epitope encoded in the vaccine used. Antigen-experienced cells can be gated based on high CD44 expression (Budd et al., 1987). Broad categorization into different memory populations can be achieved using the markers

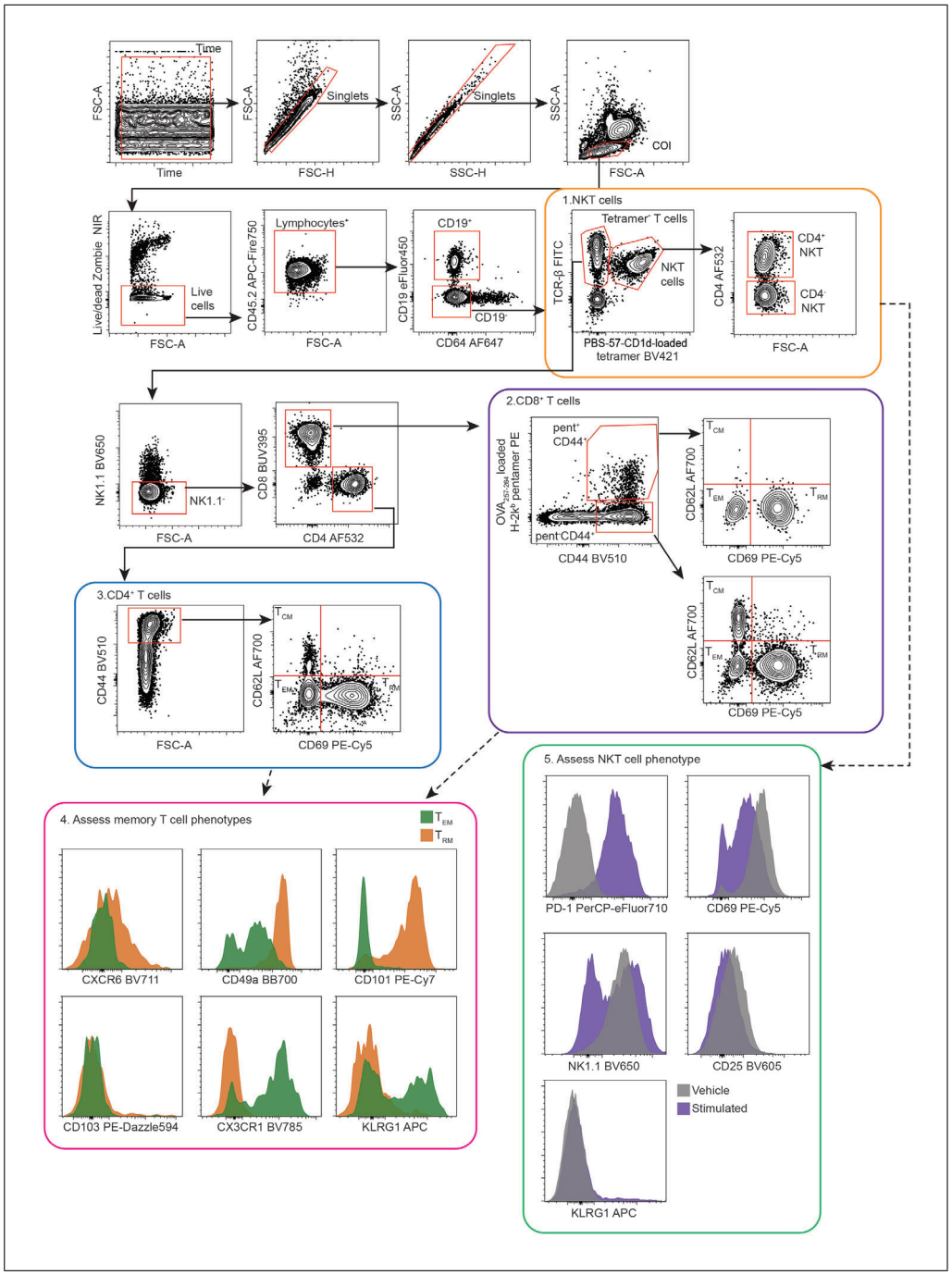

Figure 6 Spectral flow cytometry gating strategy for phenotyping memory T cell subsets and natural killer T (NKT) cells. Example provided is gated on a liver sample 28 days after administration of a glycolipid vaccine specific to the model antigen ovalbumin (OVA). Antibodies used are listed in Table 1. After gating on singlets, cells of interest (COI) and live cells were identified based on CD45.2 expression. To focus on T cell subsets, B cells ($CD19^+$) and monocytes ($CD64^+$) were first excluded. Then NKT cells were identified using the PBS-57-loaded CD1d tetramer ("tetramer") and expression of T cell receptor (TCR) β, which were further defined as $CD4^+$ NKT cells or $CD4^-$ NKT cells. For visualization purposes, staining for NKT cells is shown on an unstimulated sample, as activated NKT cells display downregulation of surface receptors (affecting both TCRβ and CD1d/PBS-57 tetramer binding) resulting in a shift of the NKT cell population toward the negative. To assess conventional T cells, $TCR\beta^+$ $tetramer^-$ cells were gated, $NK1.1^+$ cells excluded, and $CD8^+$ T cells and $CD4^+$ T cells identified. Antigen-specific $CD8^+$ T cells responding to the vaccine were defined as $OVA_{257\text{-}264}$-loaded H-$2K^b$ pentamer ("pent")$^+CD44^+$ cells. The three major memory T cell populations were then gated based on CD62L and CD69 expression, with effector memory T cells

(legend continues on next page)

(T_{EM}) defined as $CD62L^{-}CD69^{-}$ cells, central memory T cells (T_{CM}) as $CD62L^{+}CD69^{-}$ cells, and tissue-resident memory T (T_{RM}) cells as $CD62L^{-}CD69^{+}$ cells. The phenotype of $pentamer^{-}CD44^{+}$ cells was similarly assessed. $CD4^{+}$ T cells were identified as $tetramer^{-}$ $TCR\beta^{+}$ $NK1.1^{-}CD4^{+}$ cells, with the memory $CD4^{+}$ T cell populations defined from $CD44^{+}$ cells using CD62L and CD69. The phenotype of all memory T cell populations was refined by analyzing the expression of CXCR6, CD49a, CD101, CD103, CX3CR1, and KLRG1, with examples of marker expression on T_{EM} and T_{RM} cells in the liver shown. Expression differences in PD-1, CD69, NK1.1, CD25, and KLRG1 were used to assess the activation status of NKT cells, with examples shown from mice injected with vehicle versus vaccine. FSC, forward scatter; FSC-A, FSC area; FSC-H, FSC height; SSC, side scatter; SSC-A, SSC area; SSC-H, SSC height.

CD62L and CD69, with effector memory T cells (T_{EM}) defined as $CD62L^{-}CD69^{-}$ cells, central memory T cells as $CD62L^{+}CD69^{-}$ cells, and T_{RM} cells as $CD62L^{-}CD69^{+}$ cells.

Classification of cells as T_{EM} and T_{RM} cells can be examined further by assessing the mean fluorescence expression of the following markers: CD101, KLRG1, CX3CR1, CXCR6, CD49a, and CD103 (Ghilas, Valencia-Hernandez, Enders, Heath, & Fernandez-Ruiz, 2020; Holz et al., 2020). As shown in the histograms in Figure 6, liver T_{RM} cells show higher expression of CD49a, CXCR6, and CD101 compared with T_{EM} cells, whereas liver T_{EM} cells have higher expression of KLRG1 and CX3CR1 (Fig. 6). Note, although liver T_{RM} do not express high CD103, this is a common T_{RM} marker in other organs such as the lungs and skin. The absolute number of each T cell memory population can be determined using the live cell counts (Support Protocol).

Type I NKT cells, which express stereotyped TCRs that recognize the prototypic NKT cell agonist α-galactosylceramide (α-GalCer) presented on CD1d, can be detected with CD1d tetramers loaded with α-GalCer (or similar derivative, such as PBS-57 used here). NKT cell populations in mice can be split further into $CD4^{+}$ NKT cells and $CD8^{-}CD4^{-}$ NKT cells (double negative; Fig. 5). The activation status of NKT cells can be assessed using PD-1, CD69, NK1.1, CD25, and KLRG1 (Fig. 6), with $NK1.1^{+}$ populations reduced after activation and expression of each of the other markers increased (although following initial activation CD69 eventually returns to a level below baseline; Chang et al., 2008; Van Kaer, Parekh, & Wu, 2015; Wilson et al., 2003). In the example shown in Figure 6, minimal change in CD25 expression was observed, which reflected the time of assessment after administration of a vaccine, which contained a modified derivative of the α-GalCer structure as an NKT cell agonist.

OBTAINING CELL COUNTS FROM FLOW CYTOMETRY DATA

SUPPORT PROTOCOL

Cell counts can be achieved through manual cell counting using a hemocytometer and trypan blue. Alternatively, volume data recorded through the Cytek Aurora cytometers can facilitate calculating the number of live cells, or counting beads can be included in the sample during acquisition.

Using FlowJo export both the volume data (labeled as the keyword $VOL) and the number of events in the live cell gate to a spreadsheet. Then use the following calculation to determine the number of live cells per organ:

$$\text{Live cells} = \frac{\text{volume cells resuspened in plate}}{\text{actual volume recorded}} \times (\text{live cell count}) \times (\text{fraction of organ analyzed}).$$

For example, given 200 µl cells resuspended, 70 µl actual volume, with 500,000 events and one-fifth of the fraction analyzed, the calculation is 200 µl / 70 µl × 500,000 × 5 = 7.1 million live cells.

If you are analyzing samples on a cytometer that does not measure volume, counting beads such as Calibrate APC counting beads can be used instead. Create a stock mixture of the counting beads by adding 100 µl vortexed beads to 5 ml PBS. Calculate the number of beads per 25 µl using a hemocytometer, and note this number for later calculations. During sample acquisition on the cytometer, ensure the APC channel is open, and add 25 µl beads to each sample (which is resuspended in 200 µl FACS buffer). Following acquisition, open the data on your preferred analysis platform, such as FlowJo. Exclude doubles and gate the beads as the positive events in the APC channel with a small FSC-A profile. Also gate the number of live events using the live–dead marker included in your panel (e.g., gating the events negative for Zombie NIR live–dead). Export the event count in each of these two gates to a spreadsheet, and use the following calculation, which is based on a ratio of bead events recorded on the cytometer to the number of beads initially added to the sample tube multiplied by the number of live events:

$$\text{Cell count} = \frac{\text{bead number added to sample}}{\text{bead event count}} \times (\text{live event count}).$$

REAGENTS AND SOLUTIONS

FACS buffer

1 L PBS (e.g., Gibco, cat. no. 70011-044)
1% (v/v) fetal bovine serum (e.g., Gibco, cat. no. 10091-148)
2 mM EDTA (e.g., Ambion, cat. no. AM9260G)
2 mM sodium azide (e.g., Sigma-Aldrich, cat. no. S8032)
Store at 4°C for up to 3 months

Liver harvest buffer

Per liver:
1 ml RPMI medium (e.g., Gibco, cat. no. 11875093)
5% fetal bovine serum
200 U/ml heparin (e.g., STEMCELL Technologies, cat. no. NC0668440)
Store at 4°C for up to 2 weeks

Lung digest buffer

Per lung set:
1 ml RPMI medium (e.g., Gibco, cat. no. 11875093)
0.1 mg/ml Liberase TL (e.g., Roche, cat. no. 5401020001)
0.2 mg/ml DNase I (e.g., Roche, cat. no. 10104159001)
Prepare fresh before use

Percoll buffer, 35%

Per liver:
1.9 ml of 10× PBS (e.g., Gibco, cat. no. 70011-044)
10.5 ml Percoll (e.g., Sigma-Aldrich, cat. no. 17-0891-01)
17.6 ml Hank's balanced salt solution, no phenol red, Ca^{2+}, or Mg^{2+} (e.g., Gibco, cat. no. 14025092)
200 U/ml heparin (e.g., STEMCELL Technologies, cat. no. NC0668440)
Store at 4°C for up to 1 month

Allow solution to reach room temperature immediately before use.

COMMENTARY

Background Information

The information presented in this article is for analysis of memory T and NKT cell subsets in naive and stimulated mouse samples. We provide optimized isolation protocols for the assessment of these cell types in four different organs: liver, lungs, spleen, and lymph node. These differ in the recommended

isolation techniques, with the liver protocol providing an example of density gradient isolation in comparison to the lung protocol, which provides an example of enzymatic digestion. Through highlighting areas where researchers should assess possible effects on their cells of interest, these protocols can also be used as templates for the optimization of isolation methods for other organ types or different immune cell populations.

To accompany these isolation protocols, we designed a multicolor spectral flow cytometry panel to assess memory T and NKT cell subsets *ex vivo*. This was optimized alongside the isolation protocols as it was crucial to consider how the viability and phenotype of the cells of interest were affected by the specific processing methods. This panel presented with many coexpressed markers, which required special consideration when assigning fluorophores to reduce spectral overlap. The resulting panel includes the necessary markers, CD69 and CD62L, to assign cells to three main subsets of memory T cells. Further classification of these memory T cell populations and possible identification of treatment-induced subpopulations can be achieved by assessing the expression of CXCR6, CD101, CX3CR1, CD49a, KLRG1, and CD103. These are a few of the most common memory T cell markers, and others—including but not limited to Ly6C, CXCR3, and CCR7—could be substituted or developed into the panel depending on the required experimental readout. Subsequently, an alternative approach to detecting the expansion of antigen-specific T cells with fluorescent MHC multimers could be to use expression levels of the integrin molecule CD11a. Upon antigen encounter $CD8^+$ T cells have been shown to permanently change their expression of CD11a and CD8α to $CD11a^{high}CD8\alpha^{intermediate}$, allowing tracking of antigen-specific T cells without multimers (Rai, Pham, Harty, & Badovinac, 2009; Schmidt, Butler, Badovinac, & Harty, 2010).

Critical Parameters and Troubleshooting

The success of this protocol is influenced by multiple key factors. Good sample preparation is paramount to generating informative data. We have provided optimized preparation protocols for liver, spleen, lungs, and lymph node in Basic Protocols 1 through 4. There are additional factors that must be taken into account when processing, acquiring, and analyzing your samples. These factors have been extensively covered in a *Current Protocols* article by Ferrer-Font et al. (2021); however, we summarize the key factors for these protocols below.

Processing temperatures

Both T_{RM} and NKT cells express high levels of the extracellular ATP (eATP) receptor P2RX7 in mice (Borges da Silva, Wang, Qian, Hogquist, & Jameson, 2019). In the presence of high eATP or NAD-mediated ribosylation by the enzyme ARTC2.2, an induction of P2RX7 pore formation occurs, and cell death ensues (Borges da Silva et al., 2019). As ribosylation of P2RX7 can occur during manual processing of livers, T_{RM} cells are at potential risk of death. Importantly, pore formation is temperature sensitive, occurring at temperatures above 24°C. Therefore, while many protocols perform RBC lysis at 37°C, we found this had a profound effect on the ability to clearly define T_{RM} cells, resulting in a 20% reduction in the proportion of cells assigned as T_{RM} cells when compared with RBC lysis at 21°C to 23°C (room temperature; Fig. 7A). Indeed, when we assessed cell viability in these samples, additional dead cell populations were visible in the samples incubated at 37°C (Fig. 7B). As a result, we encourage RBC lysis to be performed at 21°C to 23°C.

It has also been shown that CD62L is susceptible to P2RX7-induced activity, with receptor signaling inducing shedding of CD62L from the cell surface (Mahnke et al., 2017; Scheuplein et al., 2009). While processing on ice and lysing at room temperature will also aid in preventing shedding of CD62L, we added an additional change to the protocol where we stained cells for CD62L earlier during the live–dead stain, as sequential staining was found to improve resolution. If this panel was to be used for sorting memory T cells and/or for further incubation of these cells *ex vivo* (which would require temperatures above 24°C), we would recommend researchers follow the advice noted in the publication by Rissiek et al. (2018) and use *in vivo* administration of aARTC2.2-blocking nanobody, s+16a, 30 min prior to organ harvesting to prevent ADP-ribosylation of P2RX7 during the assay.

Antibody titrations

Each new batch of antibody should be titrated on the tissue of interest. An ideal titration shows low spread of the negative population but retains separation of the positive and negative populations as indicated by the maintenance of a high staining index (SI). An

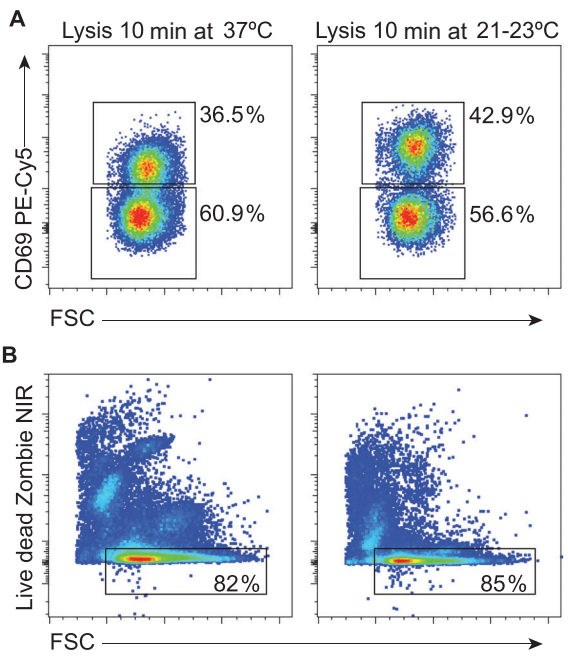

Figure 7 Red blood cell (RBC) lysis temperature affects identification of tissue-resident memory T (T_{RM}) cells. The ability to clearly separate $CD69^+$ T cells from the negative population, an essential step in defining T_{RM} cells (gating strategy provided in Fig. 6), was assessed after RBC lysis was performed at 37°C or room temperature (21°C to 23°C). (**A**) CD69 PE-Cy7 expression of gated $CD8^+$ T cells from liver. (**B**) Zombie NIR staining on liver samples. Shown is the frequency of live singlets (Zombie NIR negative).

example titration is provided for CD69 staining in the liver (Fig. 5A), where a 667 ng/ml concentration is found to be optimal as this maintains a high SI, indicating clear separation of the positive and negative populations with minimal spread of the background, thus providing clear resolution of the positive population.

Fluorescent MHC (or MHC-like) multimers, used to identify antigen-specific cells, must also be titrated on the tissue types of interest. In our protocol, H-$2K^b$ pentamers loaded with the peptide encoding amino acids 257–264 of chicken ovalbumin ($OVA_{257-264}$) were used to identify vaccine-induced $CD8^+$ T cells, and PBS-57-loaded CD1d tetramers were used to identify type I NKT cells. We observed that different concentrations of the H-$2K^b$-$OVA_{257-264}$ pentamer were needed for different organs. A titration series on liver samples is shown in Figure 5B, where an optimal concentration appeared to lie between 2 and 5 µl of the pentamer, as there was a slight drop in the SI when 2 µl was used; however, spread of the negative population upward could be observed with 5 µl. Further analysis confirmed 3 µl was sufficient (data not shown). Multimers specific to other epitopes of interest could be substituted into this panel if they use the fluorophores PE or BV421.

Controls required

Unstained controls: An individual unstained control is required for each tissue type.

SRCs: Unmixing accuracy on full-spectrum flow cytometers is highly dependent on the quality of the reference controls and their ability to accurately represent the spectra of fluorophores present in the fully stained samples. It is well known that fluorescent antibodies can bind beads and cells differently and produce slightly different spectral signatures. To determine which reference control should be used, both beads and cells must be tested in parallel using the same staining conditions as those used on the fully stained samples (i.e., fixative). Upon acquiring these controls, the unmixing accuracy of beads is often tested first by evaluating the unmixing results of single-stained cells. We identified that for some markers/fluorophores, the bead reference control led to unmixing errors; these were CD44, CD25, NK1.1, CXCR6, CX3CR1, PD-1, CD49a, CD69, CD101, and CD64. An example of this is shown in an NxN plot for PD-1 PerCp-eF710, where unmixing with beads or cells is compared

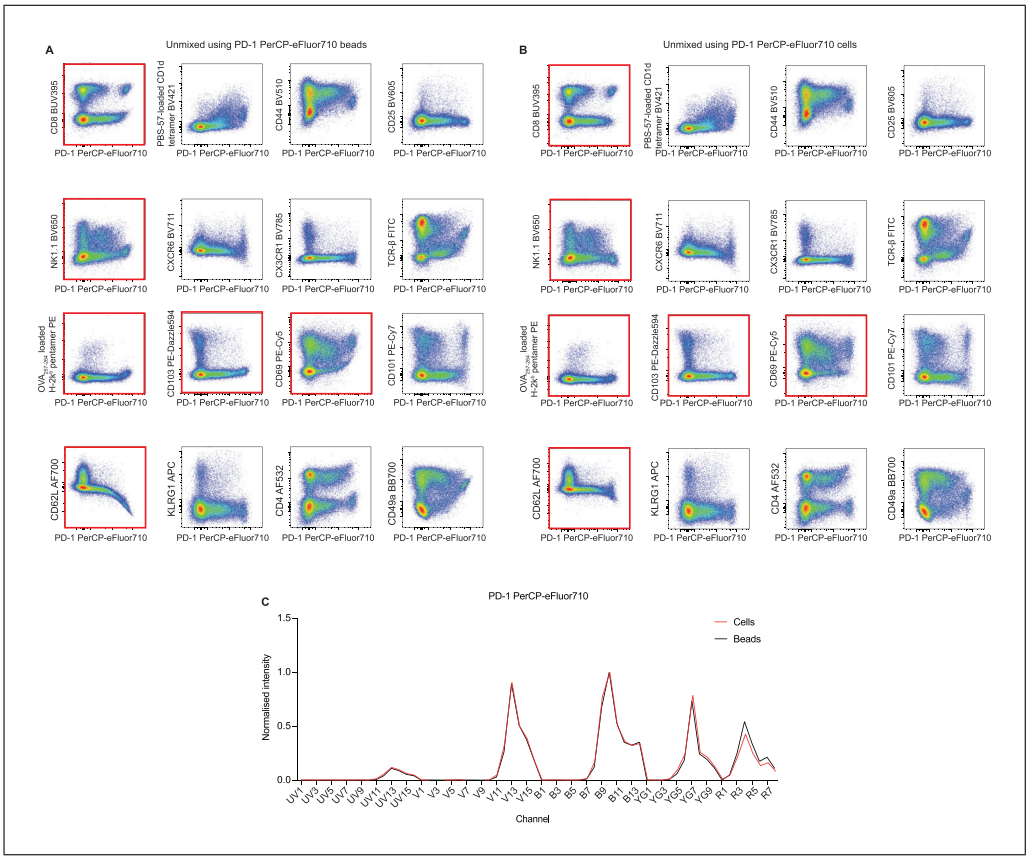

Figure 8 Unmixing accuracy for PD-1 PerCP-eFluor710 when the staining reference control of beads is compared with cells. Boxes with the red border highlight issues in unmixing that are corrected by switching from beads (**A**) to single-stained cells (**B**) for the spectral reference control (SRC). (**C**) Overlaid emission spectra for PD-1 PerCP-eFluor710 SRC on beads and cells. Subtle differences can be seen, which explains the unmixing errors when beads are used as the SRC.

(Fig. 8A,B). Unmixing errors (highlighted in the red squares) were observed when beads were used as the SRC (Fig. 8A). These issues presented either as an upward bend from the horizontal *x*-axis (as seen for CD8 versus PD-1) or a downward bend (dramatically highlighted in CD62L versus PD-1; Fig. 8A). These errors were corrected when the SRC was switched to single-stained cells for PD-1 PerCp-eF710 (Fig. 8B). Investigation as to why the unmixing differed between the two SRC types revealed differences in the emission spectra of the two (Fig. 8C), with the cells emitting at greater intensity at some points and with lower intensity and slightly different spectral patterns in the red channels, particularly in R4. This likely led to the unmixing error observed for PD-1 PerCP-eFluor710 in the red channels and why significant unmixing issues were seen against CD62L Alexa Fluor 700 (a fluorophore that peaks in R4).

Gating controls: FMO controls were included to assist in gating populations where low expression or cell frequency was anticipated. The absence of the fluorophore of interest in these samples aids gate placement by indicating where expression of the negative sits and allowing the positive gate to be placed above this. FMO controls were used to assist gating positive cells for PBS-57-loaded CD1d tetramer BV421, $OVA_{257-264}$-loaded H-$2K^b$ pentamer PE, and CD62L Alexa Fluor 700 (Fig. 9).

Sample quality check

A single-cell suspension should aim to have a viability of 70% or more to ensure proportional representation of the original sample. It is crucial that a dead-cell marker is included in the protocol, as dying cells have increased AF and can display increased nonspecific antibody binding, which can result in false positives and reduced resolution. Assessment of sample viability is shown for each of the four organ types (Fig. 10). The liver, spleen, and lymph node samples have viabilities of over 77%. The lung sample shows more debris and lower viability than the other samples, likely because of the enzymatic digestion required to

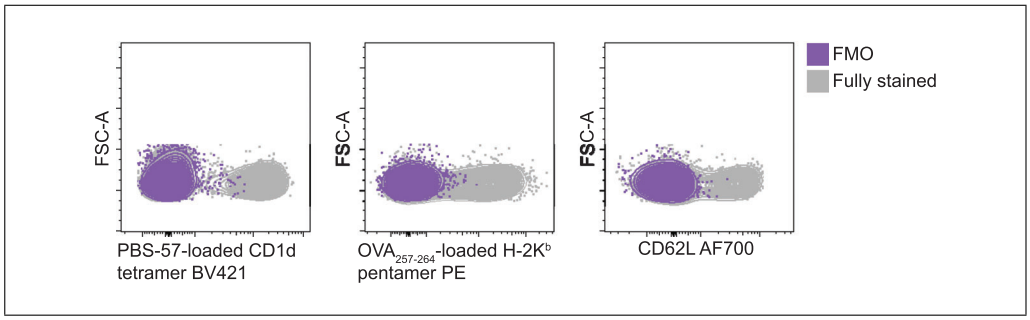

Figure 9 Fluorescence minus one (FMO) controls included in panel to aid gating accuracy and identification of populations. FMO samples were stained with all antibodies except the antibody noted on the *x*-axis. Staining for this marker was then compared with that observed in the fully stained sample. FSC-A, forward scatter area.

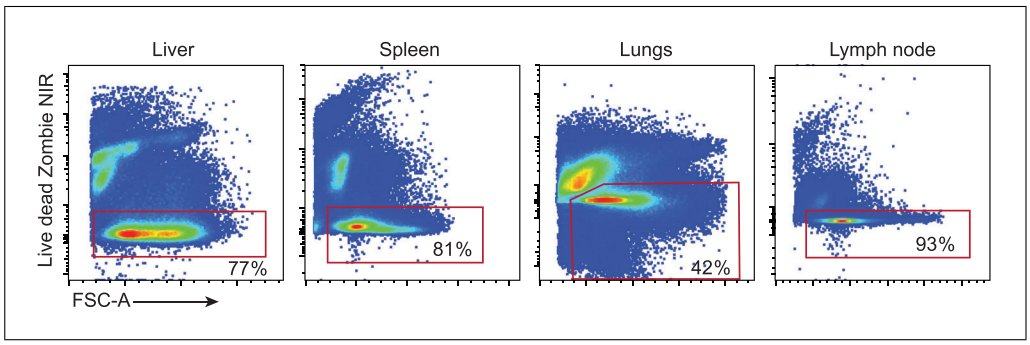

Figure 10 Sample quality assessment for liver, spleen, lungs, and lymph node. The percentage of total live cells following exclusion of doublets is shown for each organ. FSC-A, forward scatter area.

isolate the cells of interest from the lungs. We found a higher concentration of enzymes to remove the debris resulted in greater cell death, but a lower concentration resulted in a lower lymphocyte yield. Optimal enzyme concentrations should be confirmed by the researcher, especially if using new stocks.

Dealing with autofluorescence

This spectral flow cytometry panel is primarily focused on phenotyping T cells in the liver. Unmixing the data without the selection of AF extraction identified significant AF-derived artefacts and unmixing issues, particularly in BV605 as indicated with the red arrows in Figure 11A, highlighting the events appearing on the diagonal in most plots. Selection of AF extraction failed to remove all AF-derived artefacts and unmixing issues, albeit with some improvements in resolution for markers such as CD44 BV510 and CD49a BB700 (Fig. 11B). Further investigation of the unstained liver samples revealed two unique AF signatures, one that peaked in UV7 and another that peaked in V7 (Fig. 11C). We created AF tags for these signatures using the guidelines provided in a *Current Protocols* article by Ferrer-Font et al. (2021). Spectral unmixing with the inclusion of a UV7 tag and V7 signature extraction sufficiently removed the artefacts induced by AF (Fig. 11D).

Note that different organs of interest may have different AF signatures. It is important that unmixing is performed using unstained samples specific to the organ of interest. This can be performed using the SpectroFlo software by right clicking each group during setup and selecting "add unstained control." For both the lung and spleen, we also observed unique AF signatures in the UV7 and V7 channels, and these tags were also included.

Resolution assessment

A comparison of single-stained samples to fully stained samples enables the resolution of each marker in the panel to be assessed (Fig. 12A,B). Importantly, we observed that for most markers the fully stained sample and single-stained samples showed the same resolution, in that the histograms sit near perfectly on top of one another (i.e., TCRβ FITC, CD45.2 APC-AF750; Fig. 12B). For others, such as CD49 BB700 or CD44 BV510, the negative population in the fully stained sample is wider, indicating spread into that channel and a lower SI. However, as this did not affect the ability to resolve the positive and negative populations, no changes were

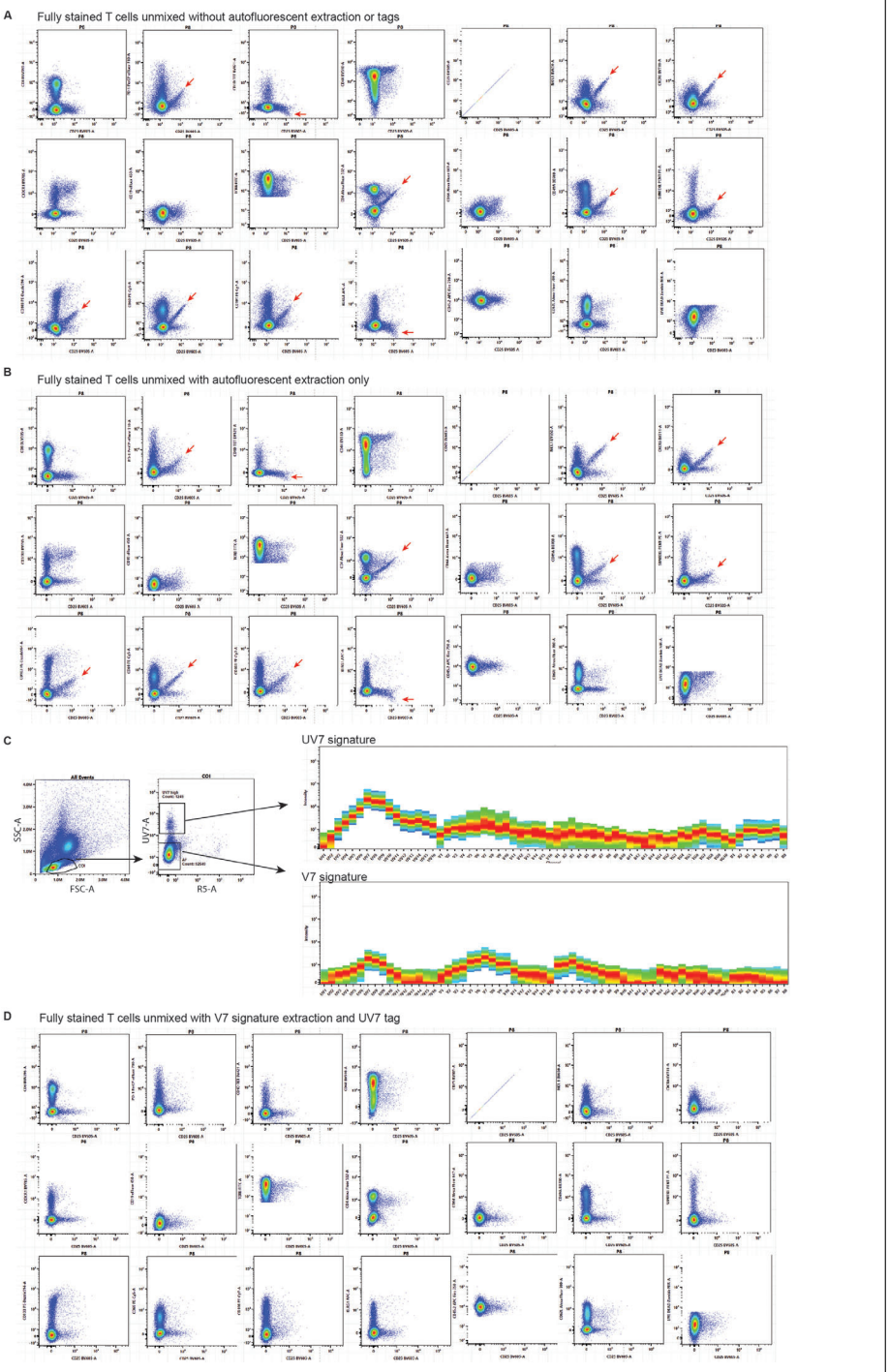

Figure 11 The use of specific autofluorescence (AF) tags and AF extraction removes artefacts in the sample that are induced by AF. (**A**) Sample unmixed without the selection of AF extraction in the unmixing wizard and without any AF tags added. (**B**) Sample unmixed with the selection of AF extraction in the unmixing wizard but without any AF tags added. AF extraction is therefore performed using the signature in the total unstained sample. (**C**) Unique AF signatures identified in the total unstained liver sample. We have commonly seen unstained lymphocytes fluoresce in the UV7 channel and show minimal fluorescence in the R5 channel. Therefore, following gating for cells of interest, $UV7^+$ and $UV7^-$ cells were selected and the signature assessed. In the top panel the $UV7^+$ cells show a unique signature that peaks in UV7. In the bottom panel the $UV7^-$ cells display a signature that peaks in V7. These were signatures captured into AF tags that were added to the reference group. (**D**) Spectral unmixing with the inclusion of a UV7 tag and V7 signature extraction; this sufficiently removed the artefacts induced by AF. FSC-A, forward scatter area; SSC-A, side scatter area.

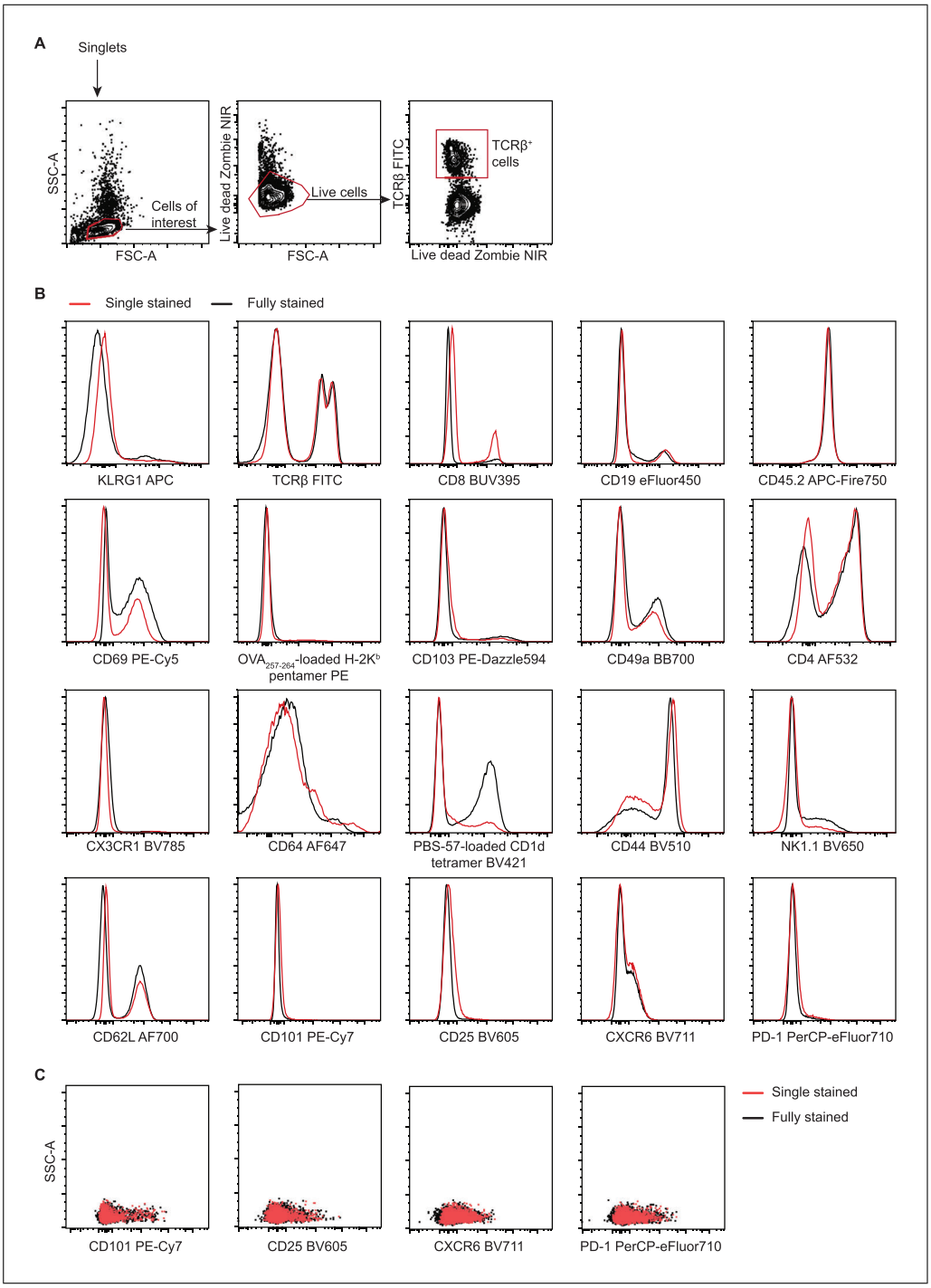

Figure 12 Marker resolution. Comparison of single-stain controls (also stained for viability and T cell receptor [TCR] β) for each fluorophore to the expression on fully stained sample. (**A**) Gating strategy for single, viable cells of interest. (**B**) Histogram overlays of single-stained and fully stained samples for the indicated markers. For CD45.2, TCRβ, and CD64, samples were first gated on live singlets. For all other markers, samples were first gated for live TCRβ$^+$ cells. (**C**) Scatterplots for the indicated markers with single and fully stained samples overlaid. Samples were first gated for live TCRβ$^+$ cells. FSC-A, forward scatter area; SSC-A, side scatter area.

necessary. Alternatively, for markers with very low expression levels or frequencies—such as CD101, CD25, CXCR6, and PD-1—histograms do not provide sufficient detail to investigate changes in resolution. In these instances, scatterplots are more appropriate for determining resolution (Fig. 12C). Here the overlaid samples showed that the signal resolution was retained in the fully stained sample.

Table 3 Breakdown of Marker Expression, Density, and Fluorophore Choice

Antigen	Antigen density	Location	Purpose	Cells expressing marker	Fluorophores available	Fluorophore chosen	Fluorophore brightness
Dead cells	–	Intracellular	Remove dead cells	Viability	Zombie NIR, live–dead fixable blue	Zombie NIR	Moderate
TCRβ	High	Cell surface	Lineage	T cells	FITC, APC, PE	FITC	Moderate
CD19	Medium/high	Cell surface	Lineage	B cells	BV605, eF450, PerCP, PerCP-Cy5.5, FITC, AF488, PE-Cy5, Alexa Fluor 647	eF450	Moderate
CD45.2	High	Cell surface	Lineage	Lymphocytes	APC-Fire750, FITC, PE, PE-Cy5, PE-Cy5.5	APC-Fire750	Moderate
NK1.1	Medium/high	Cell surface	Dump	NK, TCRβ$^+$ cells[a]	BV650, PerCp-Cy5.5, FITC	BV650	Moderate
CD64	Medium	Cell surface	Dump	Monocytes	Alexa Fluor 647, FITC	Alexa Fluor 647	Bright
CD8	Medium	Cell surface	Cells of interest	T cells	BV421, Alexa Fluor 700, BUV395, PerCP, FITC, AF488, PE	BUV395	Dim
$OVA_{257-264}$-loaded H-2K^b pentamer	Low	Cell surface	T cells of interest	T cells	PE	PE	Bright
CD44	Medium	Cell surface	T cells of interest	Activated TCRβ$^+$ cells, CD19$^+$ B cells, CD44$^+$ NK1.1$^+$ cells	PE-Cy5.5, BV605, BV750, BUV737, BV711, PerCP-Cy5.5, APC	BUV737	Moderate bright
KLRG1	Low	Cell surface	Define T_{EM}	OVA$^+$ CD44$^+$ CD8$^+$ KLRG1$^+$ CX3CR1$^+$ CD69$^-$ CD62L$^-$TCRβ$^+$ T cells, NK1.1$^+$ cells	APC	APC	Bright
CD69	Medium	Cell surface	Define T_{RM}	OVA$^+$ CD44$^+$ CD8$^+$ TCRβ$^+$ CD69$^+$ CD103$^+$ CD49a$^+$ CD101$^+$ CXCR6$^+$ T cells, CD19$^+$ B cells, NK1.1$^+$ cells	BB700, PECF594, PE-Cy5, PerCP-Cy5.5, Alexa Fluor 488, FITC, PE-Cy7, Alexa Fluor 647	PE-Cy5	Bright
CD62L	Low/medium	Cell surface	Define T_{CM}	OVA$^+$ CD44$^+$ CD8$^+$ TCRβ$^+$ CD69$^-$ T cells	APC, Alexa Fluor 700, PE-Cy5, PE-Cy7, PE, FITC, Alexa Fluor 488, PerCP-Cy5.5 PacBlue, Alexa Fluor 647	Alexa Fluor 700	Dim moderate
CXCR6	Low	Cell surface	Define T_{RM}	OVA$^+$ CD44$^+$ CD8$^+$ TCRβ$^+$ CD69$^+$ CD103$^+$ CD49a$^+$ CD101$^+$ CXCR6$^+$ T cells, NK1.1$^+$ cells, some CD19$^+$ cells	APC, BV711; commercially available on PE, APC, BV421, PE-Dazzle594, PE-Cy7, Alexa Fluor 647, PerCP-Cy5.5, APC-Cy7	BV711	Moderate bright
CX3CR1	Low	Cell surface	Define T_{EM}	OVA$^+$ CD44$^+$ CD8$^+$ KLRG1$^+$ CX3CR1$^+$ TCRβ$^+$ T cells	BV421, PE-Dazzle594	BV421	Bright
CD101	Low	Cell surface	Define T_{RM}	OVA$^+$ CD44$^+$ CD8$^+$ TCRβ$^+$ CD69$^+$ CD103$^+$ CD49a$^+$ CD101$^+$ CXCR6$^+$ T cells	Commercially available: Alexa Fluor 700, PE-Cy7, PeVio770, APC, Alexa Fluor 594, Alexa Fluor 647	PE-Cy7	Bright
CD103	Low	Cell surface	Define T_{RM}	OVA$^+$ CD44$^+$ CD8$^+$ TCRβ$^+$ CD69$^+$ CD103$^+$ CD49a$^+$ CD101$^+$ CXCR6$^+$ T cells	BV510, APC, BUV395, Alexa Fluor 488; commercially available: BV605, PE-Dazzle594, APC-Cy7, Alexa Fluor 700, FITC, BV421, Alexa Fluor 647, PacBlue, PE-Cy7	PE-Dazzle594	Bright
CD49a	Low	Cell surface	Define T_{RM}	OVA$^+$ CD44$^+$ CD8$^+$ TCRβ$^+$ CD69$^+$ CD103$^+$ CD49a$^+$ CD101$^+$ CXCR6$^+$ T cells	Commercially available: PE-Cy7, PE, APC-Fire750, PerCp-Cy5.5, APC, BUV661, BUV737, BUV615, BB700	BB700	Bright

(*Continued*)

Table 3 Breakdown of Marker Expression, Density, and Fluorophore Choice, *continued*

Antigen	Antigen density	Location	Purpose	Cells expressing marker	Fluorophores available	Fluorophore chosen	Fluorophore brightness
PD-1	Medium	Cell surface	T cell activation	NKT, $CD8^+$, $CD4^+$ T cells	PerCP-eFluor710, PE-Cy7, BUV615	PerCP-eFluor710	Moderate bright
PBS-57-loaded CD1d tetramer	Medium	Cell surface	NKT cells	$TCRB^+$, $NK1.1^+$, $PD\text{-}1^+$, $CD25^+$, $CD4^+$, $KLRG1^+$, $CD69^+$ cells	BV421, PE	BV421	Bright
CD25	Low	Cell surface	Define NKT cells	$TCR\beta^+$, $NK1.1^+$, $PD\text{-}1^+$, PBS-57-loaded CD1d $tetramer^+$, $CD4^+$, $KLRG1^+$, $CD69^+$ cells	FITC, PE, PE-CF594, APC, BV605	BV605	Moderate
CD4	Medium	Cell surface	$CD4^+$ T cells and NKT cells	$CD4^+$ NKT, $CD4^+$ T cells	Alexa Fluor 532, BV711, BV605, BV421, eF450, FITC, PerCP-Cy5.5, PE, APC, Alexa Fluor 700, APC-Alexa Fluor 750	Alexa Fluor 532	Moderate

NK, natural killer; NKT, natural killer T; OVA, ovalbumin; T_{CM}, central memory T cells; TCR, T cell receptor; T_{EM}, effector memory T cells; T_{RM}, tissue-resident memory T cells.
[a] Includes NKT cells that are $NK1.1^+$.

Dump channels

The staining panel described here has been optimized for a five-laser Cytek Aurora system but could be adjusted for use on machines with fewer lasers by incorporating some markers onto the same fluorophore. For instance, $CD19^+$ cells and $CD64^+$ cells may not be of interest and could be merged into the same dump channel. When combining markers onto the same fluorophore for use as a dump channel, it is recommended to select fluorophores with identical spectral signatures and to avoid the use of tandem dyes (i.e., PE-Cy5, BV785, BUV615) as individual differences in donor/acceptor ratios may result in different spectral signatures (see *Current Protocols* article: Ferrer-Font et al., 2020). However, tandem dyes are well suited for use in a streptavidin-biotin setup, where markers are first detected with biotin and then stained with the same secondary tandem dye conjugated to streptavidin.

Understanding Results

The staining panel presented here was designed to identify memory T cell subsets in the liver, spleen, lungs, and lymph node after vaccination. We have previously shown that glycolipid-peptide vaccines comprising MHC-binding epitopes conjugated to a modified version of the prototypic NKT cell agonist α-GalCer induce strong T cell responses and notably accumulation of T_{RM} cells in the liver (Holz et al., 2020). The experiment presented here shows analysis 30 days after a single dose with a glycolipid vaccine targeting the model antigen OVA. The induction of antigen-induced T cells could be detected using H-$2K^b$ pentamers loaded with $OVA_{257\text{-}264}$ peptide, a defined H-$2K^b$-binding epitope in the OVA protein. Various memory markers were used to define different memory T cell populations. Because vaccine efficacy is related to NKT cell function (particularly the T_{RM} cell response), the panel also includes a CD1d tetramer loaded with the α-GalCer analogue PBS-57 to detect NKT cells, along with a variety of markers to assess their activation status.

When designing this panel, we compiled a table containing information about which markers were coexpressed (gathered from the gating strategy shown in Figure 6 and published literature), the density of each marker, which fluorophores were already available in our laboratory, and which markers would need to be purchased (Table 3). Taking all three categories into account, a panel of 21 markers with 21 different fluorophores was designed. The similarity and complexity indices of the panel were determined using the Cytek Spectral viewer tool (Fig. 13A), as well as the spectral signatures of the fluorophores chosen (Fig. 13B). As can be seen, some fluorophores had high similarity but were allocated to different cell types, therefore minimizing the impact of spreading error.

Following optimization of the panel and organ processing conditions, quality control analysis of fully stained samples could be performed. The panel was first examined using the manual gating strategy shown in Figure 6. Dimensionality reduction algorithms can be useful tools for investigating panel quality, as they simplify the data for visualization while also exposing artefacts that may be missed

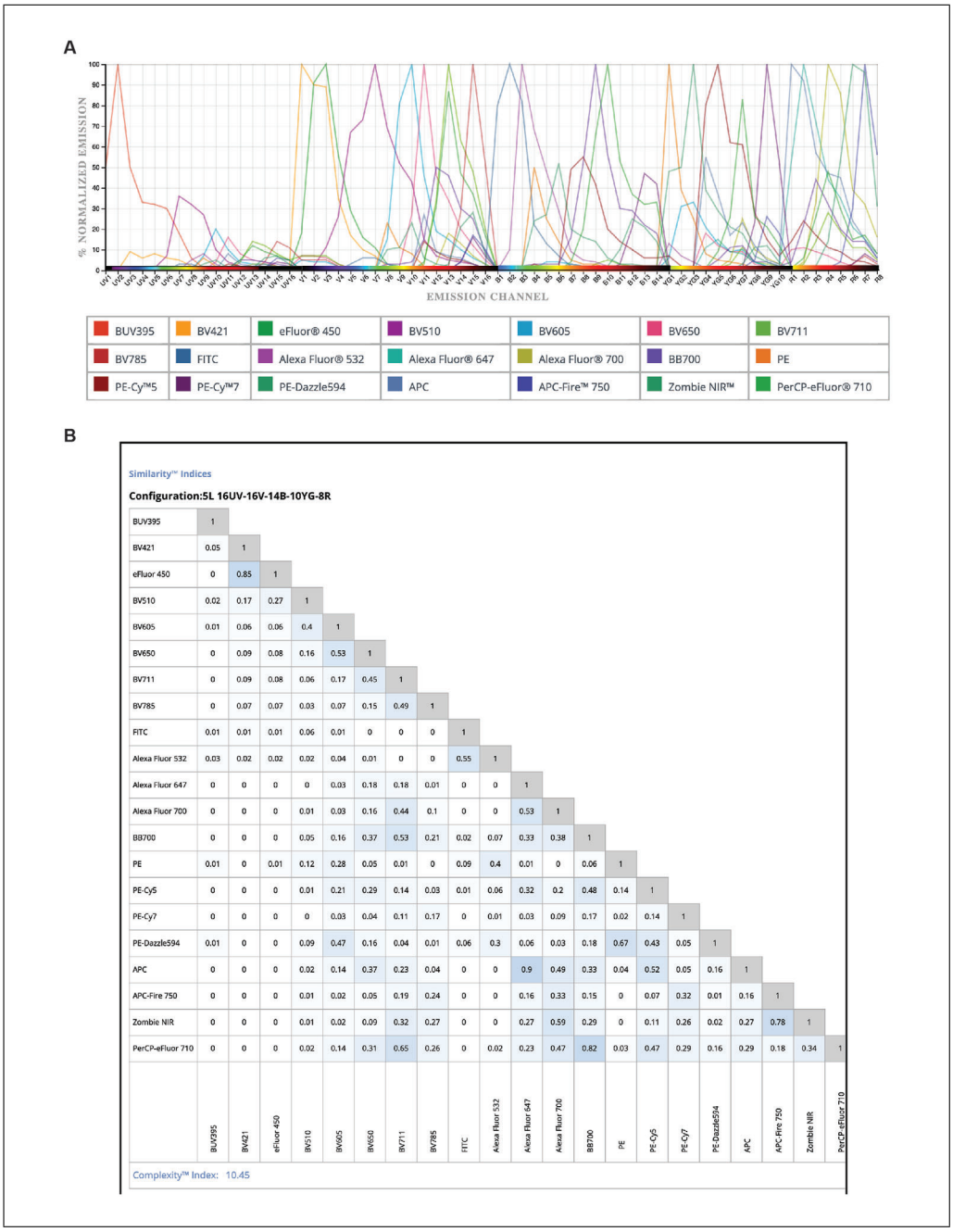

Figure 13 A series of evaluations were conducted to identify the best combination of 21 fluorophores that would provide unique spectral signatures, adequate signal intensities, and minimal spread into neighboring channels. (**A**) Spectral signature of 21 fluorophores visualized using the Cytek Spectrum viewer. All signatures were normalized to peak channels for direct comparison. (**B**) Results of the Similarity Index Matric (SIM), which measures how similar two spectra are to one another. The value "1" indicates virtually no difference between two fluorophores, whereas a value of "0" indicates the two fluorophores are completely unique. Displayed is the numerical value for each pair of fluorophores included in the panel. At the bottom of the matrix is the complexity index, a metric to evaluate the complexity of the entire combination of fluorophores.

through expert gating. Using Uniform Manifold Approximation and Projection (UMAP), markers that are usually coexpressed should be checked to see if they can be found in similar regions of the UMAP plot (Fig. 14A; Becht et al., 2018). For visualization purposes, the UMAP data presented here were performed on a concatenated file containing one unstimulated sample and one stimulated sample, as we anticipated some populations would be present in one sample and not the other (Fig. 14A). To understand the impact of the different conditions, overlaying the expert gated populations on UMAP can be useful

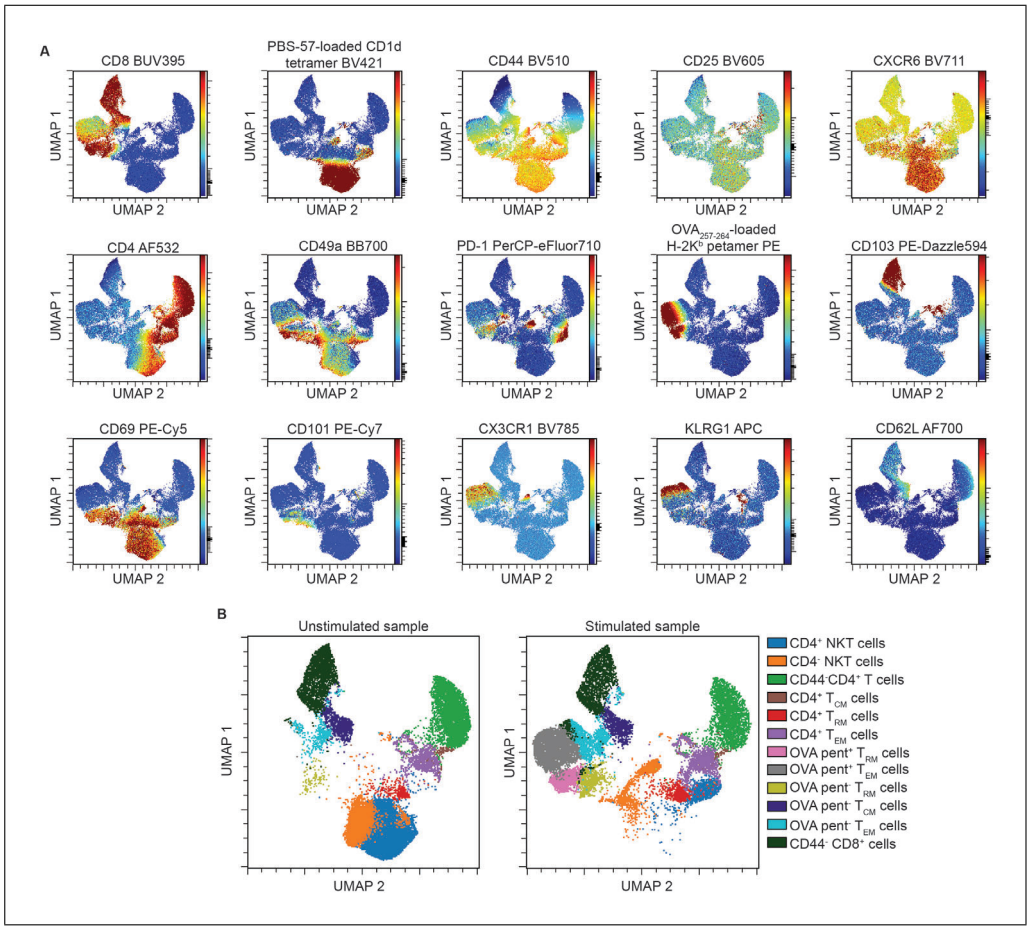

Figure 14 Overview of the 21-marker, 21-fluorophore panel for functional phenotyping of memory T cells and natural killer T (NKT) cells on mouse liver using the dimensionality reduction algorithm Uniform Manifold Approximation and Projection (UMAP). Samples were cleaned by excluding variable flow rate during acquisition, doublets, debris, antibody aggregates, and dead cells. Following cleaning, CD45.2$^+$ TCRβ$^+$ cells were gated and CD64$^-$ and CD19$^-$ cells excluded. (**A**) UMAP analysis was performed using the OMIQ analysis platform with the settings of nearest neighbors at 20 and minimum distance at 0.4 using the Euclidean distance function and displayed as 2D plots using the resultant UMAP 1 and UMAP 2 dimensions according to the per-cell expression of 15 proteins. Expression levels are shown for CD8, PBS-57-loaded CD1d tetramer, CD44, CD25, CXCR6, CD4, CD49a, PD-1, $OVA_{257-264}$-loaded H-2K^b pentamer, CD103, CD69, CD101, CX3CR1, KLRG1, and CD62L. UMAP scales are visualized using a rainbow heat scale (arcsinh). One unstimulated and one stimulated sample have been concatenated for visualization purposes. (**B**) Expert gating overlaid on UMAP dimensions 1 and 2. Vehicle sample and stimulated sample are compared. NKT, natural killer T; T_{CM}, central memory T; TCR, T cell receptor; T_{EM}, effector memory T cells; T_{RM}, tissue-resident memory T.

(Fig. 14B). A shift of the NKT cell population was observed within the stimulated sample owing to the downregulation of surface receptors on activated NKT cells (affecting both TCRβ and CD1d/PBS-57 tetramer binding) after activation. An increase in the H-2K^b/$OVA_{257-264}$ pentamer$^+$ CD8$^+$ T cell population was apparent in the stimulated sample in comparison to the unstimulated sample, as would be expected for a vaccine-induced immune response. Interestingly, there was also a difference in the pentamer-negative T_{EM} and T_{RM} cell populations between these samples, suggesting effects of the vaccine on other CD8$^+$ T cells. Interrogation of the data in this manner allows for the detection of unique changes induced by treatment that would not have otherwise been detected using the expert gating strategy alone, and it is important to assess if the information obtained makes biological sense, otherwise further exploration/optimization of the panel will be required.

Time Considerations

Week 1: Vaccinate mice with desired therapy.

Weeks 1 to 5: Titrate new antibody stocks.

Week 5: Harvest organs of interest and assess response. Harvesting, processing, and staining will take most of the day and will require more than two people if harvesting multiple tissue types from >20 mice. Flow cytometric analysis will take ~6 hr and analysis and interpretation another ~3 hr (subject to change depending on the number of organ types and mice).

Note that this does not include the time to design and optimize the full-spectrum flow cytometry panel, which can take anywhere between 2 and 4 weeks.

Acknowledgments

The authors thank the personnel of the Biomedical Research Unit of the Malaghan Institute of Medical Research for animal husbandry. This research was supported by the Health Research Council of New Zealand (project 20/569 and 14/1003), New Zealand Ministry of Business, Innovation and Employment (Contract RTVU1603), and the Hugh Green Foundation. I. F. Hermans was supported by the Thompson Family Foundation and Hugh Dudley Morgan's Fellowship.

Author Contributions

Kathryn Farrand: conceptualization, investigation, methodology, writing—review and editing; **Lauren Holz**: conceptualization, investigation, methodology, writing—review and editing; **Laura Ferrer-Font**: formal analysis, methodology, visualization, writing—original draft, review, and editing; **Ching-wen Tang**: investigation, methodology; **Michael Wilson**: investigation, writing—review and editing; **Mitch Ganley**: supply of critical reagents, writing—review and editing; **Jordan Minnell**: supply of critical reagents, writing—review and editing; **Gavin Painter**: funding acquisition, supervision, supply of critical reagents, writing—review and editing; **William Heath**: conceptualization, funding acquisition, writing—review and editing; **Ian Hermans**: conceptualization, funding acquisition, supervision, project administration, writing—original draft, review, and editing; **Olivia Burn**: conceptualization, formal analysis, investigation, methodology, visualization, writing—original draft, review, and editing.

Conflict of Interest

I. F. Hermans and G. F. Painter are founding scientists and shareholders of the biotech startup Avalia Immunotherapies Limited.

Data Availability Statement

The data presented in this article are available from the corresponding author on reasonable request.

Literature Cited

Becht, E., McInnes, L., Healy, J., Dutertre, C.-A., Kwok, I. W. H., Ng, L. G., … Newell, E. W. (2018). Dimensionality reduction for visualizing single-cell data using UMAP. *Nature Biotechnology*, *37*, 38–47. doi: 10.1038/NBT.4314

Borges da Silva, H., Wang, H., Qian, L. J., Hogquist, K. A., & Jameson, S. C. (2019). ARTC2.2/P2RX7 signaling during cell isolation distorts function and quantification of tissue-resident CD8$^+$ T cell and invariant NKT subsets. *The Journal of Immunology*, *202*, 2153–2163. doi: 10.4049/jimmunol.1801613

Budd, R. C., Cerottini, J. C., Horvath, C., Bron, C., Pedrazzini, T., Howe, R. C., & MacDonald, H. R. (1987). Distinction of virgin and memory T lymphocytes. Stable acquisition of the Pgp-1 glycoprotein concomitant with antigenic stimulation. *The Journal of Immunology*, *138*, 3120–3129.

Chang, W.-S., Kim, J.-Y., Kim, Y.-J., Kim, Y.-S., Lee, J.-M., Azuma, M., … Kang, C.-Y. (2008). Cutting edge: Programmed death-1/programmed death ligand 1 interaction regulates the induction and maintenance of invariant NKT cell anergy. *The Journal of Immunology*, *181*, 6707–6710. doi: 10.4049/jimmunol.181.10.6707

Cheng, Y., Gunasegaran, B., Singh, H. D., Dutertre, C. A., Loh, C. Y., Lim, J. Q., … Newell, E. W. (2021). Non-terminally exhausted tumor-resident memory HBV-specific T cell responses correlate with relapse-free survival in hepatocellular carcinoma. *Immunity*, *54*, 1825–1840. doi: 10.1016/J.IMMUNI.2021.06.013

Donovan, J., & Brown, P. (2006). Euthanasia. *Current Protocols in Immunology*, *73*, 1.8.1–1.8.4. doi: 10.1002/0471142735.im0108s73

Fernandez-Ruiz, D., Ng, W. Y., Holz, L. E., Ma, J. Z., Zaid, A., Wong, Y. C., … Heath, W. R. (2016). Liver-resident memory CD8$^+$ T cells form a front-line defense against malaria liver-stage infection. *Immunity*, *51*, 889–902. doi: 10.1016/j.immuni.2016.08.011

Ferrer-Font, L., Small, S. J., Lewer, B., Pilkington, K. R., Johnston, L. K., Park, L. M., … Price, K. M. (2021). Panel optimization for high-dimensional immunophenotyping assays using full-spectrum flow cytometry. *Current Protocols*, *1*, e222. doi: 10.1002/cpz1.222

Ferrer-Font, L., Pellefigues, C., Mayer, J. U., Small, S. J., Jaimes, M. C., & Price, K. M. (2020). Panel design and optimization for high-dimensional immunophenotyping assays using spectral flow cytometry. *Current Protocols in Cytometry*, *92*, e70. doi: 10.1002/cpcy.70

Ghilas, S., Valencia-Hernandez, A. M., Enders, M. H., Heath, W. R., & Fernandez-Ruiz, D. (2020). Resident memory T cells and their role within

the liver. *International Journal of Molecular Sciences*, *21*, 8565. doi: 10.3390/ijms21228565

Hally, K. E., Ferrer-Font, L., Pilkington, K. R., & Larsen, P. D. (2022). OMIP 083: A 21-marker 18-color flow cytometry panel for in-depth phenotyping of human peripheral monocytes. *Cytometry Part A*, *101*, 374–379. doi: 10.1002/cyto.a.24545

Holz, L. E., Chua, Y. C., de Menezes, M. N., Anderson, R. J., Draper, S. L., Compton, B. J., … Heath, W. R. (2020). Glycolipid-peptide vaccination induces liver-resident memory $CD8^+$ T cells that protect against rodent malaria. *Science Immunology*, *5*, eaaz8035. doi: 10.1126/sciimmunol.aaz8035

Lim, C. J., Lee, Y. H., Pan, L., Lai, L., Chua, C., Wasser, M., … Chew, V. (2019). Multidimensional analyses reveal distinct immune microenvironment in hepatitis B virus-related hepatocellular carcinoma. *Gut*, *68*, 916–927. doi: 10.1136/gutjnl-2018-316510

Mahnke, K., Useliene, J., Ring, S., Kage, P., Jendrossek, V., Robson, S. C., … Enk, A. H. (2017). Down-regulation of CD62L shedding in T cells by $CD39^+$ regulatory T cells leads to defective sensitization in contact hypersensitivity reactions. *The Journal of Investigative Dermatology*, *137*, 106–114. doi: 10.1016/J.JID.2016.08.023

Pallett, L. J., Davies, J., Colbeck, E. J., Robertson, F., Hansi, N., Easom, N. J. W., … Maini, M. K. (2017). IL-2^{high} tissue-resident T cells in the human liver: Sentinels for hepatotropic infection. *Journal of Experimental Medicine*, *214*, 1567–1580. doi: 10.1084/jem.20162115

Park, L. M., Lannigan, J., & Jaimes, M. C. (2020). OMIP-069: Forty-color full spectrum flow cytometry panel for deep immunophenotyping of major cell subsets in human peripheral blood. *Cytometry Part A*, *97*, 1044–1051. doi: 10.1002/CYTO.A.24213

Rai, D., Pham, N.-L. L., Harty, J. T., & Badovinac, V. P. (2009). Tracking the total CD8 T cell response to infection reveals substantial discordance in magnitude and kinetics between inbred and outbred hosts. *The Journal of Immunology*, *183*, 7672–7681. doi: 10.4049/JIMMUNOL.0902874

Rissiek, B., Lukowiak, M., Raczkowski, F., Magnus, T., Mittrücker, H. W., & Koch-Nolte, F. (2018). In vivo blockade of murine ARTC2.2 during cell preparation preserves the vitality and function of liver tissue-resident memory T cells. *Frontiers in Immunology*, *9*, 1580. doi: 10.3389/fimmu.2018.01580

Rosato, P. C., Beura, L. K., & Masopust, D. (2017). Tissue resident memory T cells and viral immunity. *Current Opinion in Virology*, *22*, 44–50. doi: 10.1016/J.COVIRO.2016.11.011

Scheuplein, F., Schwarz, N., Adriouch, S., Krebs, C., Bannas, P., Rissiek, B., … Koch-Nolte, F. (2009). NAD^+ and ATP released from injured cells induce $P2X_7$-dependent shedding of CD62L and externalization of phosphatidylserine by murine T cells. *The Journal of Immunology*, *182*, 2898–2908. doi: 10.4049/jimmunol.0801711

Schmidt, N. W., Butler, N. S., Badovinac, V. P., & Harty, J. T. (2010). Extreme CD8 T cell requirements for anti-malarial liver-stage immunity following immunization with radiation attenuated sporozoites. *PLoS Pathogens*, *6*, e1000998. doi: 10.1371/JOURNAL.PPAT.1000998

Steinbach, K., Vincenti, I., & Merkler, D. (2018). Resident-memory T cells in tissue-restricted immune responses: For better or worse? *Frontiers in Immunology*, *9*, 2827. doi: 10.3389/fimmu.2018.02827

Van Kaer, L., Parekh, V. V., & Wu, L. (2015). The response of CD1d-restricted invariant NKT cells to microbial pathogens and their products. *Frontiers in Immunology*, *6*, 226. doi: 10.3389/fimmu.2015.00226

Wilson, M. T., Johansson, C., Olivares-Villagómez, D., Singh, A. K., Stanic, A. K., Wang, C.-R., … Van Kaer, L. (2003). The response of natural killer T cells to glycolipid antigens is characterized by surface receptor down-modulation and expansion. *Proceedings of the National Academy of Sciences of the United States of America*, *100*, 10913–10918. doi: 10.1073/pnas.1833166100

High-Dimensional Methods of Single-Cell Microglial Profiling to Enhance Understanding of Neuropathological Disease

Alanna G. Spiteri,[1,2,7] Katherine R. Pilkington,[3] Claire L. Wishart,[1,2] Laurence Macia,[2,4] and Nicholas J.C. King[1,2,4,5,6]

[1]Viral Immunopathology Laboratory, Infection, Immunity and Inflammation Research Theme, School of Medical Sciences, Faculty of Medicine and Health, The University of Sydney, Sydney, Australia
[2]Charles Perkins Centre, The University of Sydney, Sydney, Australia
[3]Cytek Biosciences, Inc., Fremont, California
[4]Sydney Cytometry, The University of Sydney and Centenary Institute, Sydney, Australia
[5]The University of Sydney Institute for Infectious Diseases, The University of Sydney, Sydney, Australia
[6]The University of Sydney Nano Institute, The University of Sydney, Sydney, Australia
[7]Corresponding author: *spiteri.alanna@gmail.com*

Published in the Immunology section

Microglia are the innate myeloid cells of the central nervous system (CNS) parenchyma, functionally implicated in almost every defined neuroinflammatory and neurodegenerative disorder. Current understanding of disease pathogenesis for many neuropathologies is limited and/or lacks reliable diagnostic markers, vaccines, and treatments. With the increasing aging of society and rise in neurogenerative diseases, improving our understanding of their pathogenesis is essential. Analysis of microglia from murine disease models provides an investigative tool to unravel disease processes. In many neuropathologies, bone-marrow-derived monocytes are recruited to the CNS, adopting a phenotype similar to that of microglia. This significantly confounds the accurate identification of cell-type-specific functions and downstream therapeutic targeting. The increased capacity to analyze more phenotypic markers using spectral-cytometry-based technologies allows improved separation of microglia from monocyte-derived cells. Full-spectrum profiling enables enhanced marker resolution, time-efficient analysis of >40 fluorescence parameters, and extraction of cellular autofluorescence parameters. Coupling this system with additional cytometric technologies, including cell sorting and high-parameter imaging, can improve the understanding of microglial phenotypes in disease. To this end, we provide detailed, step-by-step protocols for the analysis of murine brain tissue by high-parameter *ex vivo* cytometric analysis using the Aurora spectral cytometer (Cytek), including best practices for unmixing and autofluorescence extraction, cell sorting for single-cell RNA analysis, and imaging mass cytometry. Together, this provides a toolkit for researchers to comprehensively investigate microglial disease processes at protein, RNA, and spatial levels for the identification of therapeutic targets in neuropathology. © 2024 The Authors. Current Protocols published by Wiley Periodicals LLC.

Basic Protocol 1: Processing the mouse brain into a single-cell suspension for microglia isolation
Basic Protocol 2: Staining single-cell mouse brain suspensions for microglial phenotyping by spectral cytometry
Basic Protocol 3: Flow cytometric sorting of mouse microglia for *ex vivo* analysis

CURRENT PROTOCOLS
A Wiley Brand

Current Protocols e985, Volume 4
Published in Wiley Online Library (wileyonlinelibrary.com).
doi: 10.1002/cpz1.985

Basic Protocol 4: Processing the mouse brain for imaging mass cytometry for spatial microglia analysis

Keywords: autofluorescence • cell sorting • CNS pathology • cytometry • microglia • myeloid • neuroinflammation • single-cell • spectral cytometry

How to cite this article:
Spiteri, A. G., Pilkington, K. R., Wishart, C. L., Macia, L., & King, N. J. (2024). High-dimensional methods of single-cell microglial profiling to enhance understanding of neuropathological disease. *Current Protocols*, *4,* e985. doi: 10.1002/cpz1.985

INTRODUCTION

Diseases affecting the central nervous system (CNS) are collectively the leading cause of disability and second leading cause of death worldwide (Bassetti et al., 2022; Feigin et al., 2020). Often prominent in the pathogenesis of CNS disease are microglia, a remarkable innate myeloid immune cell population that tiles the entire CNS parenchyma, projecting cytoplasmic extensions that constantly survey the microenvironment (Nimmerjahn et al., 2005). Upon perturbation, these cells may proliferate, increase the cross-sectional area of their somata, retract cytoplasmic processes, and express a range of cytokines and signaling molecules. Microglia have been implicated in protective and pathological processes contributing to neuroinflammatory, neurodegenerative, and mental health disorders (McQuade & Blurton-Jones, 2019). As such, they represent an important potential target for immunotherapeutics in CNS disease. Historically, elucidating the specific roles of microglia in pathology has been extremely challenging due to the limited research tools available to identify and target these cells behind the blood-brain barrier (Spiteri, Wishart et al., 2022). In some diseases, identifying microglia becomes further challenged by the infiltration of phenotypically similar myeloid cells from the bone marrow (Getts et al., 2008, 2012; Greter et al., 2015; Lewis et al., 2014; Werner et al., 2020). This has significantly impeded understanding of disease pathogenesis in many neuropathologies and hampered the development of reliable diagnostic markers, vaccines, and treatments.

In recent years, a surge in the development of new experimental tools has enabled more accurate microglia identification and targeting. These include *microglia-specific* identification markers such as P2RY12 and TMEM119 (Bennett et al., 2016; Butovsky et al., 2014) and the CSF1R inhibitor and microglia-depletion drug PLX5622 (Spangenberg et al., 2019). Although these represent significant advances in the field, subsequent work has shown that microglia-specific markers are often downregulated during inflammation, while PLX5622 can also target other cells in the periphery (Depaula-Silva et al., 2019; Greter et al., 2015; Lei et al., 2020; Lewis et al., 2014; Spiteri & King, 2023; Spiteri, Ni et al., 2022; Spiteri et al., 2021; Spiteri, Wishart et al., 2023; Spiteri et al., 2020; Vankriekelsvenne et al., 2022). Moreover, isolated and cultured microglia undergo considerable change from their *in vivo* state (Bennett et al., 2018; Bohlen et al., 2017; Gosselin et al., 2017), significantly limiting the translatability of *in vitro* studies. Thus, examination of microglia from untreated and undepleted brain under minimal experimental intervention is crucial to determine their precise role(s) during the pathogenesis of disease. The prompt *ex vivo* analysis of surface and intracellular protein expression and proliferative status using bromodeoxyuridine (BrdU) or Ki-67, as well as morphology and RNA profile, at various timepoints can together inform detailed understanding of microglial processes.

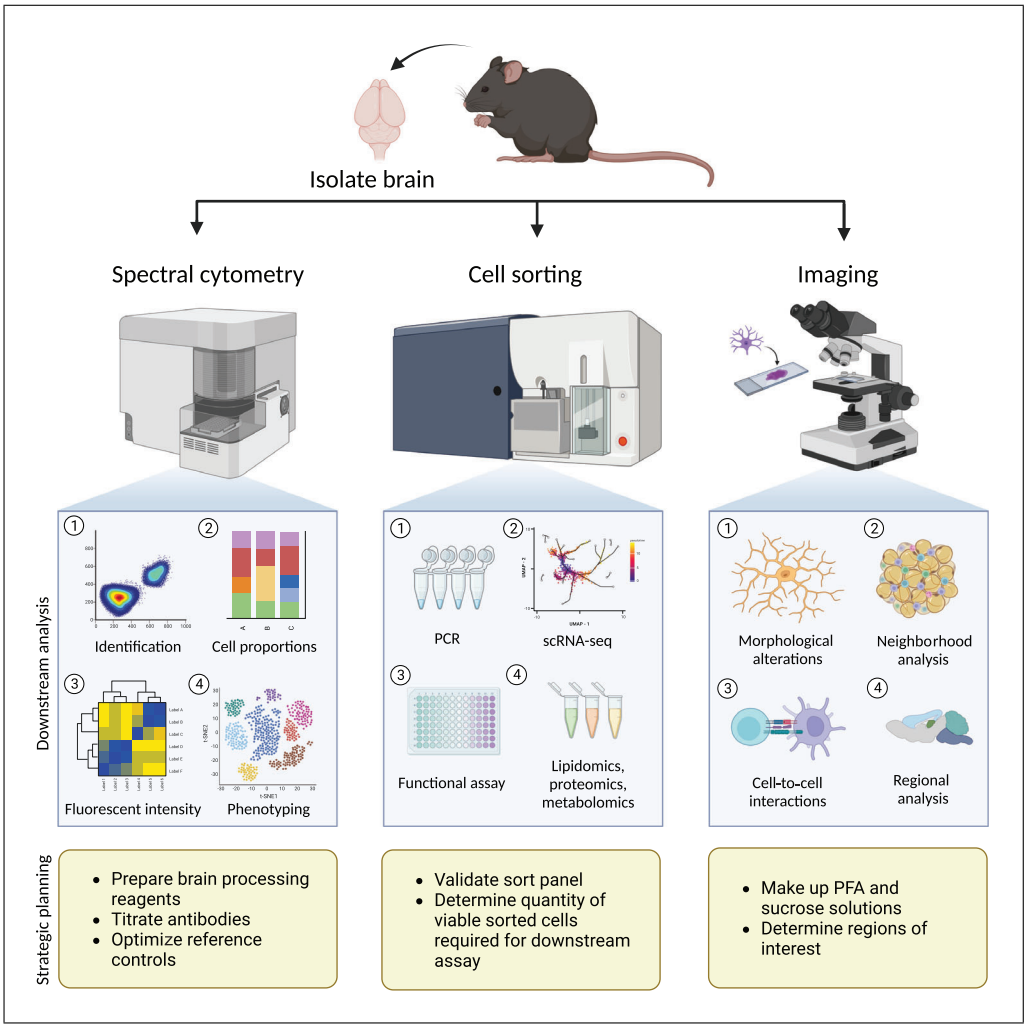

Figure 1 Overview of experimental procedures, analysis outputs, and strategic planning. Created with BioRender.com.

Advances in spectral cytometry, imaging mass cytometry, and single-cell RNA (scRNA) technology have substantially increased the number of parameters that can be analyzed in a single sample. Pairing these with computational analysis approaches allow better discrimination between microglia and other myeloid subsets. This is important to accurately identify their relative contributions to disease pathogenesis. Although the use of single-cell technologies has increased in neuroscience research, consensus on the best cytometric approach for multiple modalities with validated panels remains scant (Sharp et al., 2023). Thus, we detail here single-cell methods of microglia phenotyping to provide a toolkit for researchers to use to examine these cells in molecular detail for the identification of therapeutic targets in murine models of neuropathology (Fig. 1). Specifically, Basic Protocol 1 describes methods to process whole brain tissue into single-cell suspensions. Basic Protocol 2 details surface and intracellular staining steps to phenotype microglia by spectral cytometry using the Aurora. Basic Protocol 3 describes steps to stain and sort microglia for *ex vivo* analysis such as single-cell sequencing. Basic Protocol 4 describes brain-processing methods to obtain high-quality histological images.

NOTE: All protocols involving animals must be reviewed and approved by the appropriate Animal Care and Use Committee and must follow regulations for the care and use of laboratory animals.

BASIC PROTOCOL 1

PROCESSING THE MOUSE BRAIN INTO A SINGLE-CELL SUSPENSION FOR MICROGLIA ISOLATION

Preparing a single-cell suspension is a critical step for single-cell analysis of whole tissues, including for conventional and spectral flow cytometry, cytometry by time of flight (CyTOF), cell sorting, and scRNA analysis. Poor-quality tissue processing impacts cell viability, staining resolution, and the ease of counting, filtering, and running samples on instruments. Conducting the protocol below should yield high-quality data with 85%-90% viability of brain cells.

Various protocols have served as a starting point for the optimized methods described here (Ashhurst et al., 2019; Bohlen et al., 2019; Garcia et al., 2014; Getts et al., 2008; Manglani et al., 2018; Niewold et al., 2020). In this protocol, mice are injected 3 hr before sacrifice with BrdU, an analog of thymidine that is incorporated into DNA during synthesis. Using a fluorochrome-conjugated antibody to label BrdU, it can be determined whether microglia (or other cells) are proliferating *in situ.* Euthanasia procedures should minimize brain anoxia prior to tissue dissociation. The carefully removed brain is cut up into pieces of 0.3-cm diameter or less. Individual cells are dissociated from the whole brain using the GentleMACS (Miltenyi Biotec) dissociator in a cocktail of DNase I and collagenase type IV, and leukocytes are enriched on a Percoll density gradient (Fig. 2). This protocol should be performed efficiently without interruption to enhance yield and viability.

A disadvantage of this enzymatic method is the potential to cleave cell surface markers. From our work, we have shown reductions only in TMEM119 and CD44 expression when using DNase I and collagenase IV (Spiteri et al., 2021). We recommend performing parallel experiments without digestive enzymes to ensure that all surface markers of interest are present. Experiments without enzymes will still yield high-quality data; however, reduced viability and increased debris, should be expected. Digestion with DNase I and collagenase IV, however, is strongly recommended for microglia isolation as it produces high live cell yields ($\sim 5 \times 10^5$ cells from the healthy homeostatic brain). Nevertheless, it should be noted that alternative commercial methods are also available, including the neural tissue dissociation kit from Miltenyi Biotec (Garcia et al., 2014). Additionally, if a GentleMACS dissociator is not available, enzyme-digested brain tissue can be gently mashed through a strainer using a pestle (Manglani et al., 2018).

Materials

10 mg/ml (2×) BrdU stock solution (see recipe; 1 mg per 18-g mouse)
Mice
Isoflurane or equivalent for mouse euthanasia, depending on permitted animal ethics protocols
Ice-cold PBS (~25 ml per sample; see recipe)
70% (v/v) ethanol
10× DNase/collagenase digestion mixture (see recipe; 0.5 ml per sample)

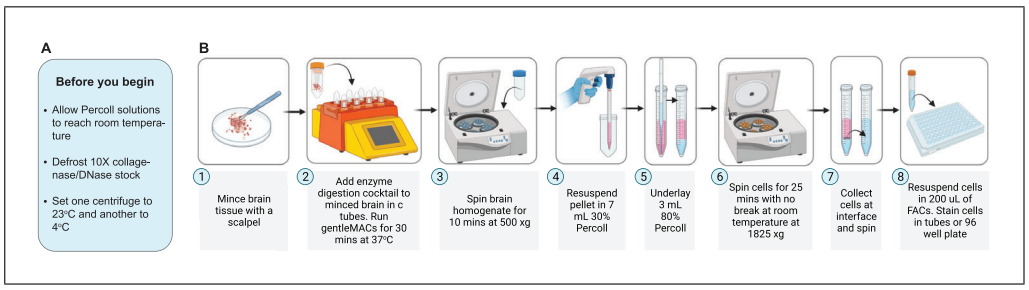

Figure 2 Schematic of brain-processing procedures required to generate a single-cell suspension as described in Basic Protocol 2. Created with BioRender.com.

Staining buffer (see recipe; ~12 ml per sample)
26% (v/v) Percoll solution (see recipe; 7 ml per sample)
73% (v/v) Percoll solution (see recipe; 3 ml per sample)
Trypan blue (Thermo Fischer Scientific, cat. no. 15250061)

Laminar-flow hood (or, if working with PC2 agents, BSC Class II cabinet or equivalent)
Dissection tools: forceps, scissors, and scalpels
10-ml syringe
21-G needle (1 per mouse)
Petri dishes (1 per experimental group)
C tubes (Miltenyi Biotec, cat. no. 130-093-237)
GentleMACS Octo Dissociator with Heaters (Miltenyi Biotec, cat. no. 130-096-427)
50-ml Falcon tube lids (1 per sample)
15-ml tubes (2 per sample)
Centrifuge
Glass pipets
Serological pipets: 1 × 5 ml for each brain, 1 × 25 ml to dispense 26% Percoll, and 1 × 5 ml to dispense 73% Percoll
1-ml and 10-µl micropipets
50-µl multichannel micropipets
96-well round-bottom cell-culture-treated plate (Sigma Aldrich, cat. no. CLS3799)
Hemocytometer
Cell counter
Light microscope

NOTE: If you are not assessing cell proliferation, start from step 4.

1. Defrost 10 mg/ml BrdU stock solution at room temperature and dilute with sterile PBS to make a 5 mg/ml solution.
2. Inject mice intraperitoneally with 55.6 mg/kg BrdU (1 mg per 18-g mouse; 200 µl of a 5 mg/ml solution).

   Record the time when you inject each animal, so you can euthanize each exactly 3 hr later. This is important, as increasing the incubation time may increase BrdU incorporation. However, a 5- to 10-min delay should not be detrimental.

   The interval between injections in subsequent animals depends on the time it will take to harvest organs from each animal later. When collecting extra organs or performing additional procedures, increase the interval time.
3. After 3 hr, anesthetize animals in the order in which you injected them with BrdU.
4. Surgically expose the heart and perfuse mice via the left ventricle with 10 ml ice-cold PBS, using a 21-G needle and a 10-ml syringe, snipping the inferior vena cava to enable complete flushing of the brain vasculature (see Current Protocols, Miller et al., 2010).
5. Decapitate mice with large surgical scissors.
6. Cut the skin sagittally from the base of the neck to the eyes using finer scissors.
7. Peel back the skin laterally to expose the skull.
8. Use finer scissors to gently cut through the midline of the skull from the foramen magnum to the eyes.
9. Make an incision in the nasal process.

10. Using forceps gently pull each side of the skull laterally to expose the brain.
11. Pry the brain out with forceps onto a petri dish containing ~500 µl PBS.

    Clean petri dish with 70% ethanol and Kimwipe between samples, and use a new petri dish for each experimental group.

12. Cut the brain into pieces of 2- to 3-mm diameter or less using a scalpel.

    The smaller the pieces of brain, the better the tissue digestion.

13. Transfer brain pieces into a C tube containing 4.5 ml ice-cold PBS.
14. Place C tube on ice.
15. Collect a spleen and/or bone marrow from one animal for extra cell staining controls for Basic Protocol 2.

    This step is required for Basic Protocol 2 and can be skipped if processed brain cells are not used for cytometry analysis. Spleen and bone marrow collection and processing procedures can be found in Look et al. (2023).

16. Add 0.5 ml of 10× collagenase/DNase mixture into C tubes once all brains have been collected.

    Defrost a 10× stock on ice before you begin euthanizing mice.

17. Load C tubes and heaters onto GentleMACS dissociator.

    Tip the tube upside down and back several times vigorously to ensure all tissue pieces are in the digestion mixture. If tissue is stuck on the side or top of the tube, it will not get digested.

18. Select brain-processing program and run (i.e., 30 min at 37°C, as per Supporting Information 1).
19. Top up with staining buffer and seal with 50-ml Falcon tube lid.
20. Place tubes on ice until ready to process.
21. Spin tubes 10 min at 500 × *g*, 4°C.
22. Carefully pour out supernatant.
23. Resuspend brain samples in 7 ml of 26% Percoll solution using a 5-ml serological pipet and transfer to a 15-ml tube.
24. Place a glass pipet in the center of the tube and pipet 3 ml of 73% Percoll solution into the glass pipet using a 5-ml serological pipet. This should create a sharply defined 26%/73% Percoll fluid interface.

    If the 73% Percoll does not pass through the glass pipet, gently and slowly lift the pipet by ~0.5 mm.

25. Carefully place the tubes in the centrifuge, without disturbing the Percoll interface.
26. Spin tubes for 25 min at 1825 × *g*, room temperature, no brake.
27. Remove upper fat layer using a pipet tip attached to a vacuum aspirator or 1-ml micropipet.
28. Collect leukocytes from the interface layer between the 26% top (pink) and 73% bottom (clear) layers using a glass pipet or a 1-ml pipet until there are no cells left (~3 ml).
29. Transfer collected leukocytes to a 15-ml tube containing 5 ml staining buffer.

Table 1 Expected Cell Counts and Dilutions Factors for Counting

Brain sample	Expected cell count	Staining buffer volume to predilute sample	Total dilution factor
Homeostatic (full brain)	$3.5\text{-}7.5 \times 10^5$	0 µl	2
Moderate chronic neuroinflammation[a]	1×10^6	0 µl	2
Severe acute neuroinflammation[b]	4.5×10^6	40 µl	10

[a] Cerebral interferonopathy modelled in transgenic mice with CNS-targeted chronic production of IFN-α (GFAP-IFN; West et al., 2022) or demyelination modeled in mice treated with cuprizone (Song et al., 2021).
[b] West Nile virus encephalitis (Spiteri, Ni et al., 2022; Spiteri et al., 2021; Spiteri, Wishart et al., 2023; Spiteri, Van Vreden et al., 2023; Wishart et al., 2022).

30. Spin tubes 5 min at 500 × *g*, 4°C.
31. Discard supernatant and resuspend cells in 200 µl staining buffer.
32. Transfer samples into a 96-well plate, or leave in tubes if preferred. Remeasure each sample volume while transferring samples from tubes to wells or resuspending cells in tubes.

    It is important to remeasure to ensure accurate cell counts, as volumes can vary between samples.
33. Transfer 10 µl of each sample into another tube or plate for counting (leave in fridge).

    Counts can be performed during the next incubation period, i.e., the viability and blocking steps (see Basic Protocol 2, step 3).

    Ideally cell counts should be performed within an hour.
34. Pre-dilute counting samples in staining buffer according to Table 1. Add 10 µl trypan blue to 10 µl of pre-diluted sample and load on hemocytometer for counting.

    Only add trypan blue when you begin cell counts. This is to minimize cell death induced by trypan blue toxicity.

STAINING SINGLE-CELL MOUSE BRAIN SUSPENSIONS FOR MICROGLIAL PHENOTYPING BY SPECTRAL CYTOMETRY

BASIC PROTOCOL 2

Depending on the extent of CNS perturbation, microglia upregulate nominal activation markers and produce an array of cytokines and signaling molecules that can dampen or exacerbate pathology. Identifying microglial phenotypes can inform functional processes. However, this must be coupled with additional techniques such as *in vivo* imaging, scRNA analysis, and proteomics to identify their precise contribution to disease processes.

Here we provide a framework for detailed microglial phenotyping involving surface, intracellular, and intranuclear staining and acquisition on a spectral cytometer (5-laser Cytek Aurora). These include myeloid cell markers (CD45, CD11b, F4/80), antigen-presenting and co-stimulation markers (CD86, MHC-II), migration and phagocytosis-related markers (CD11c, CD64, CD68, CD206), the 'inflammatory macrophage' marker Ly6C, markers highly expressed on microglia (P2RY12, CX3CR1), and markers to identify and quantify neutrophils (Ly6G), NK cells (NK1.1), and T cells (CD3ε, CD4, CD8α). To measure proliferation and nitric oxide production, we use BrdU and DAF-FM diacetate, respectively. Production of nitric oxide can enhance CNS pathology and can be targeted therapeutically (Getts et al., 2012). To measure other functional markers, such as

intracellular cytokines, monensin and/or brefeldin A should be added to staining buffers as well as all reagents until cell fixation, including PBS used for perfusion and brain processing reagents, to enhance staining.

During neuroinflammation, monocytes from the bone marrow are recruited to the brain, adopting a similar phenotype to responding microglia. To demonstrate this, we use a mouse model of severe and acute neuroinflammation as seen in West Nile virus (WNV) encephalitis. In this model, there is a 10-fold increase in the number of cells isolated from the brain, with the majority being monocyte-derived cells. To distinguish microglia from infiltrating myeloid cells in the inflamed brain, we used the differential profiles of P2RY12 and CD45. The gating strategy is shown in Figure 3 and can be applied to other inflammatory mouse models as well as the homeostatic brain (Supporting Information 2). Although multiple RNA studies, including our own, have shown that microglia downregulate the expression of the nominal homeostatic microglia-specific markers *P2ry12* and *Tmem119* during neurodegeneration and neuroinflammation (Jordão et al., 2019; Keren-Shaul et al., 2017; Krasemann et al., 2017; Spiteri, Wishart et al., 2023; Wishart et al., 2022), on a protein level, microglia do not downregulate P2RY12 expression in WNE (Spiteri et al., 2021) or alpha-herpesvirus CNS infection (Fekete et al., 2018). As TMEM119 expression is downregulated by microglia in certain inflammatory diseases, such as WNE, P2RY12 enables the separation of microglia from infiltrating myeloid populations when used in combination with CD45. This strategy has been validated with adoptive transfers, monoclonal antibody blocking, and injection of dye to track infiltrating myeloid populations, which could be distinguished from microglia that were depleted with PLX5622 (Spiteri et al., 2021).

All reagents, including those for the controls (see Table 2), should be titrated and tested on the specific tissue in advance of experiments, taking into consideration that increasing the panel size can impact staining resolution and gating accuracy. For panel expansion, a significant portion of the spectrum between 400 and 730 nm is available for UV-excitable dyes, and there are a number of vacant positions from other laser modules. As brain cells are highly autofluorescent in the UV and violet channels, autofluorescence extraction can substantially improve staining resolution in these channels (Supporting Information 3 and 4). Extracting multiple autofluorescent populations from each unstained control per experimental group will further reduce unmixing errors (Supporting Information 3 and 4). Thus, we recommend spectrally unmixing multiple autofluorescence populations from group-specific unstained controls in Spectroflo Software (Fig. 4). Additionally, as only a limited number of cells can be isolated from the healthy brain, we recommend collecting one alternative tissue (spleen or bone marrow) to use for single-color reference controls (see Table 2). More detailed information about flow cytometry staining, acquisition, autofluorescence, staining indices, and spectral cytometry analysis has been extensively published elsewhere (Ashhurst et al., 2019, 2021; Brummelman et al., 2019; Ferrer-Font et al., 2021, 2023; Fox et al., 2020; Kharraz et al., 2022; Maciorowski et al., 2017; Mahnke & Roederer, 2007; Niewold et al., 2020; Nolan & Condello, 2013).

Materials

Single-cell mouse brain samples and staining controls prepared in Basic Protocol 1 (see Table 2 for staining controls)
PBS
Viability/Fc blocking solution (see Table 3) or PBS with Fc block
DAF-FM solution (see Table 3)
Staining buffer (see recipe)
Surface antigen stain mixture (see Table 3)
UltraComp eBeads Compensation Beads (Thermo Fisher Scientific, cat. no. 01-2222-42), if using these as single-color reference controls

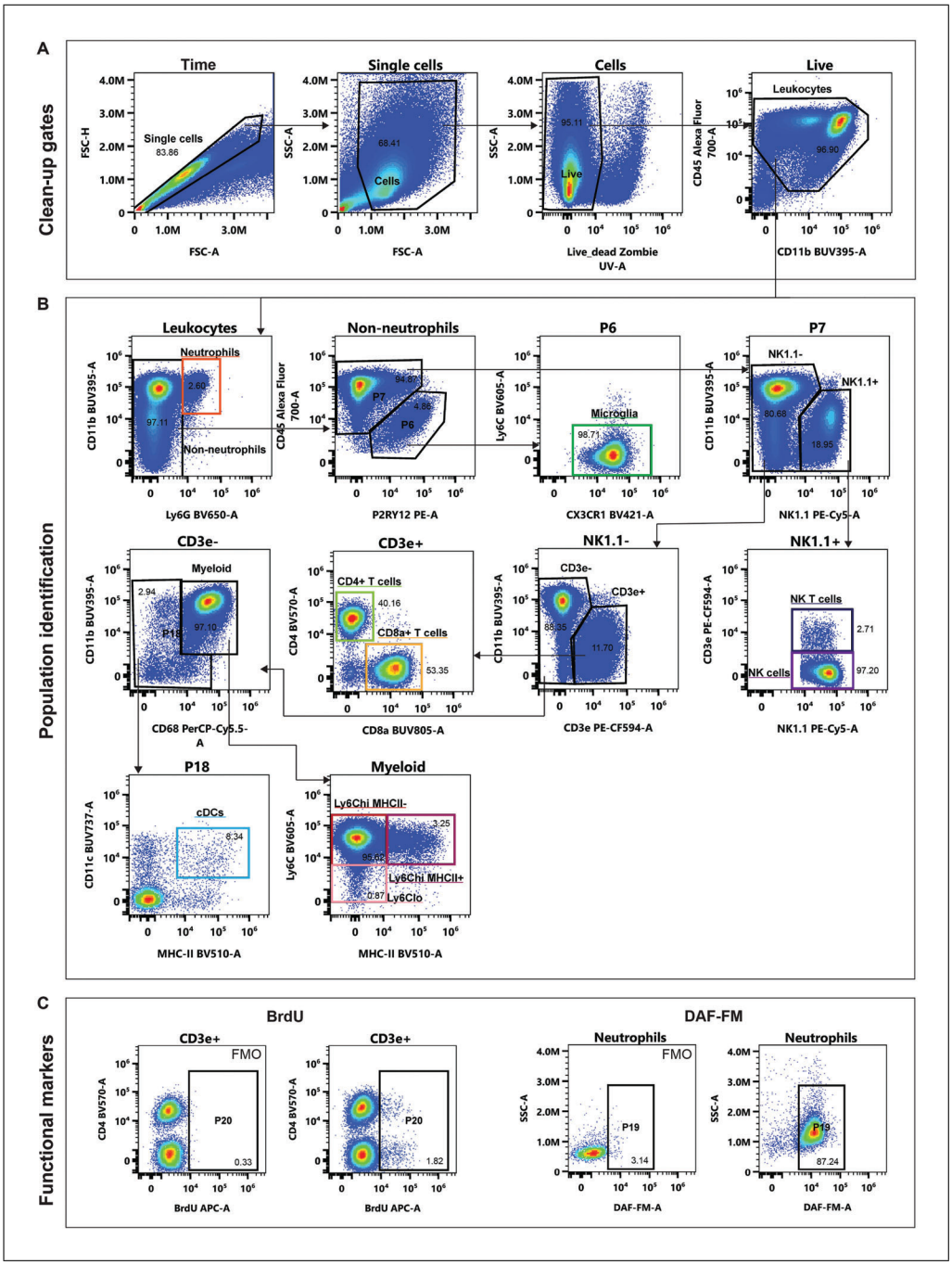

Figure 3 Gating strategy used to identify immune cell populations in the inflamed brain for analysis and cell sorting. (**A**) Quality control gates, including time, single cells, non-debris, and live cell gates, were applied before analyzing cells. (**B**) Identification of neutrophils, microglia, NK cells, T cells, classic dendritic cells (cDC), and infiltrating myeloid cell subsets in the WNV-infected brain. (**C**) Dot plots showing BrdU (measure of proliferation) and DAF-FM (measure of nitric oxide production) staining in T cells and neutrophils isolated from an infected brain. Staining is shown for populations with the highest expression of these markers, with gating based on a fluorescence minus one (FMO) sample. Single-cell brain suspensions from a WNV-infected animal at 7 days post infection were analyzed on the 5-laser Cytek Aurora.

BD Cytofix™ Fixation Buffer (BD Biosciences, cat. no. 554655) or 4% (w/v) paraformaldehyde (PFA) in PBS (see recipe)

BD Cytofix/Cytoperm™ Fixation and Permeabilization Solution (BD Biosciences, cat. no. 554722)

BD Perm/Wash™ Buffer (BD Biosciences, cat. no. 554723)

Table 2 Recommended Staining Controls for Cytometry Experiments

Control	Purpose
Unstained control from each treatment group	Autofluorescence properties of cells can change with treatment. Thus, it is important to pool cells only from the same treatment group (e.g., with two groups, healthy vs. disease, pool only healthy with healthy samples and disease with disease samples; this also applies to cells from wild-type vs. knockout, treated vs. untreated, etc.). If all mice have been injected with a dye/fluorochrome, cells from a non-injected animal will need to be obtained.
Viability control	Any mixture of cells will be sufficient as long as they are unstained. If a sufficient number of brain cells is not available, consider taking spleen or bone marrow cells. Cells can be heat-shocked for 3 min at 60°C to obtain dead cells: divide the heat-shocked tube of cells in half and stain half with viability dye, while keeping the rest as a matched, unstained cell control. However, if using a tissue digest, you should obtain enough dead cells to begin with.
Fluorescence minus one (FMO)	Pool cells only from the same treatment group. If you are performing the protocols for the first time, make FMO controls for each treatment group because staining patterns may differ across groups, with potentially more or less background in the channel of interest, making it difficult to distinguish background from positive signal. This is vital for uncharacterized proteins and/or proteins with a tertiary staining pattern, i.e., a smear with no clear positive and negative population, but is also important for other markers to help identify unexpected antibody interactions that can occur in a multicolor cocktail.
Positive controls	In the healthy brain, BrdU and DAF-FM will be very weakly detected. Therefore, we recommend processing a bone marrow or spleen to provide a positive single-color control for BrdU and DAF-FM staining. These can also serve as reference controls. However, brain samples from inflammatory conditions should be used for reference controls if they show a higher staining intensity for DAF-FM and BrdU compared to the spleen or bone marrow.
Reference controls or single-color controls	Use cell or bead controls, depending on which gives the best unmixing outcome. As only limited cells can be isolated from the brain, consider taking spleens for reference controls where cells provide the best unmixing outcome. See Table 3 for recommendations. However, this must be tested on user samples, as antigen expression will change with disease and treatment conditions. The following points are important for reference controls: (i) They must have the negative and positive populations well separated, while being as bright as, or brighter than, any staining observed in any samples; (ii) the negative and positive particles must have identical autofluorescence characteristics; (iii) the fluorescence spectrum of the reference control must be unique and identical to that of the multicolor sample (some fluorochromes may exhibit spectral shifting when bound to bead controls); and (iv) there must be sufficient events. Control optimization is discussed in detail elsewhere (Ferrer-Font et al., 2021).

BD Cytoperm™ Permeabilization Buffer Plus (BD Biosciences, cat. no. 561651)
3 mg/ml (3×) DNase stock solution (see recipe)

Laminar-flow hood (BSC Class II or equivalent), if working with PC2 agents
Centrifuge
10- and 200-µl pipets
50- and 200-µl multichannel pipets
Aluminum foil
5- or 1.2-ml polypropylene tubes
Falcon® Tube with Cell Strainer Cap (Corning, cat. no. 352235) or equivalent 35 µm nylon mesh
5-laser Cytek® Aurora (or equivalent)
SpectroFlo® Software (or equivalent)

Spiteri et al.

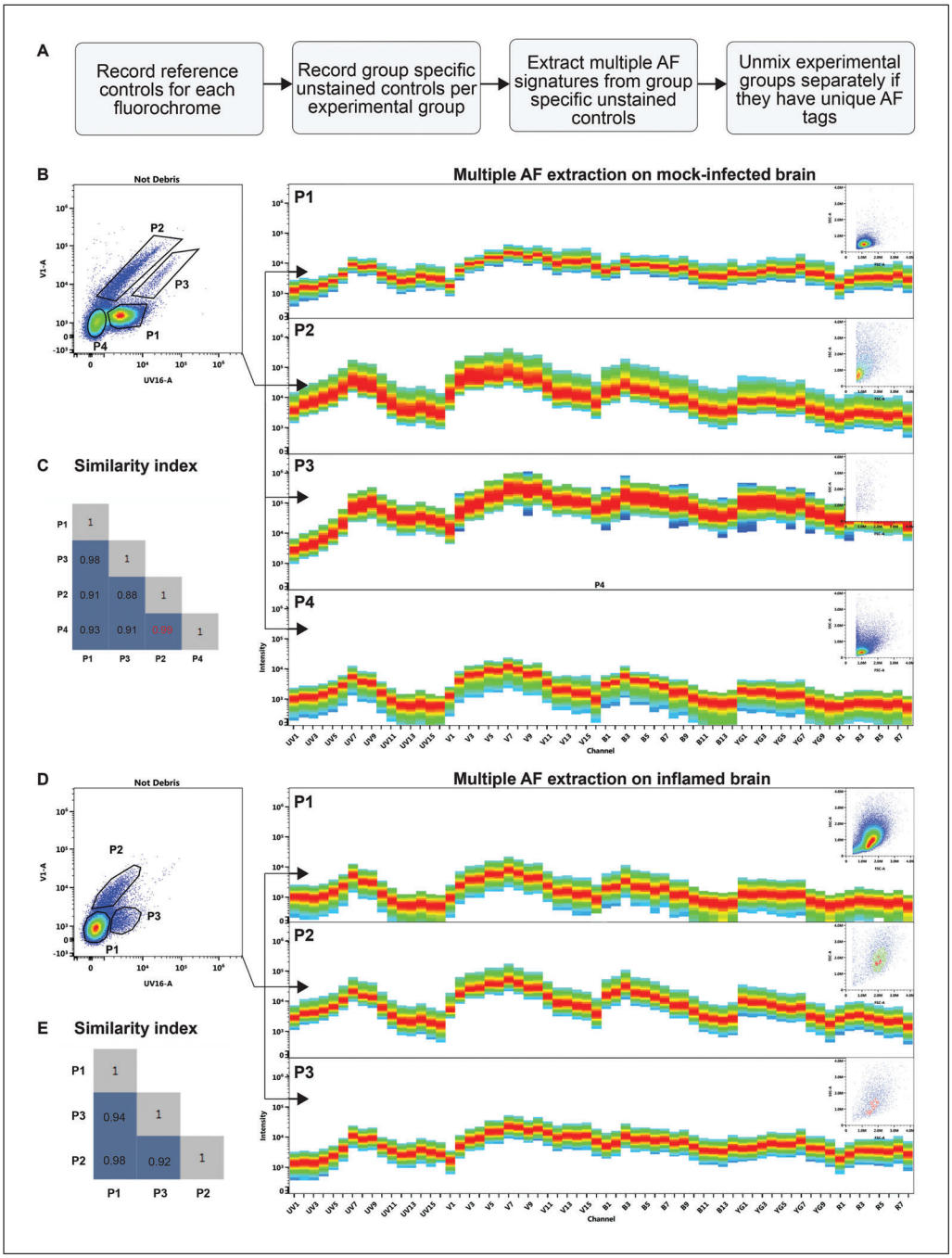

Figure 4 Extraction of multiple autofluorescent (AF) populations in the mock-infected and inflamed brain. (**A**) Overview of optimal spectral unmixing procedure in SpectroFlo®. (**B-E**) Identification of autofluorescent (AF) populations and their unique spectral signatures (**B, D**) and similarity indexes (**C, E**) in unstained cells (single-cells and non-debris gate) from mock- (**B, C**) and WNV-infected brain samples (**D, E**). Gate P4 in the mock-infected brain was not used for AF extraction as it has a similarity index of 0.99 and a lower MFI than P2. See Unmixing in Critical parameters for more information.

Preparation of controls (beginning after step 34 of Basic Protocol 1)

1. Take an aliquot of each brain sample prepared in Basic Protocol 1 and set aside for brain cell controls, including unstained brain cells, single-color reference controls, and fluorescence minus one (FMO) staining controls.

   Brain samples from different animals can be mixed to produce cell controls; however, if samples from individual experimental groups have unique autofluorescence signatures and staining patterns, we recommend having separate unstained and FMO controls for

each of these groups (see Table 2 for more information). A minimum of 2 × 10^5 cells should be used per control. Ideally, more cells should be used, but typically only ~5 × 10^5 cells will be isolated from a healthy brain. In inflammatory conditions, we recommend using a minimum of 1 million cells.

Spleen and/or bone marrow cells (1 million cells is sufficient per control) can be used for single-stained reference controls if the fluorescence spectrum and intensity are identical and equal to or brighter than the one in the multicolor brain sample, respectively. Spleen or bone marrow cells cannot not be used as a substitute for unstained brain cells or FMOs (see Table 2 for more information).

2. Distribute, label, and spin all samples and staining controls in tubes or a plate (whichever is preferred) for 5 min at 500 × *g*, 4°C.

Viability staining and blocking

3. Resuspend samples in 50 µl of viability/Fc blocking solution (see Table 3 for recipe) or 50 µl of PBS with Fc block (for single-color or unstained controls).
4. Incubate for 30 min at 4°C.
5. Top up with 150 µl PBS and spin 5 min at 500 × *g*, 4°C.

DAF-FM staining for nitric oxide production

6. Resuspend cells in 50 µl of DAF-FM DA solution (see Table 3 for recipe; for fully stained samples and single-color DAF-FM control) or PBS (for unstained and viability controls and DAF-FM FMO).
7. Incubate for 30 min at 4°C.
8. Top up with 150 µl PBS.
9. Spin 5 min at 500 × *g*, 4°C.
10. Resuspend cells in 250 µl PBS.
11. Incubate for 15 min at 4°C.
12. Spin 5 min at 500 × *g*, 4°C.
13. Vortex compensation beads and aliquot into tubes or plate for single-color reference controls.

Use cells instead of beads if the fluorescence intensity of a bead control is dimmer than multicolor cell samples, or for fluorochromes that exhibit spectral shifting when bound to bead controls. Spectral shifting will result in unmixing errors in multicolor samples.

Surface staining

14. Flick off supernatant and resuspend samples in 50 µl surface antigen stain mixture (see Table 3 for recipe; for fully stained samples), staining buffer (for unstained controls and single-color controls), and FMO mixtures (for FMO controls).
15. Incubate for 30 min at 4°C.
16. Top wells up with 150 µl staining buffer and spin 5 min at 500 × *g*, 4°C.
17. Wash twice with 250 µl staining buffer.

Fixation

18. Fix cells in 50 µl of either BD Cytofix™ Fixation Buffer or 4% PFA in PBS for 30 min at room temperature.

The fixation incubation time and temperature depend on your facility requirements and whether you are working with infectious agents.

Additionally, some reagents are not fixable, so check this beforehand (all reagents listed in Table 3 are fixable).

Table 3 Preparation of Reagents Used for Flow Cytometry Staining

Viability/Fc block solution

Reagent	Marker	Clone	Company	Cat. no.	Mfr. conc. (mg/ml)	Dilution	Reference control type
Fc block	N/A	93	BioLegend	101302	0.5	100	N/A
Zombie UV™ [a]	Viability	N/A	BioLegend	423108	N/A	500	Spleen

Defrost viability dye immediately before use and add to Fc block/PBS solution. Vortex, spin, and add 50 µl of solution per sample.

DAF-FM staining solution

Reagent	Marker	Clone	Company	Cat. no.	Mfr. conc. (mM)	Final conc. (µM)	Reference control
DAF-FM stock	DAF-FM	N/A	Sigma Aldrich	D2321	5	0.5	Spleen

Defrost DAF-FM DMSO stock (see recipe) immediately before use and dissolve in PBS. Vortex, spin, and add 50 µl of solution per sample.

Surface antigen stain mixture

Fluorophore	Marker	Clone	Company	Cat. no.	Mfr. conc. (mg/ml)	Dilution	Reference control
BUV395	CD11b	M1/70	BD Bioscience	563553	0.2	400	WNV-infected brain[b]
BUV737	CD11c	HL3	BD Bioscience	612796	0.2	100	Spleen
BUV805	CD8α	53-6.7	BD Bioscience	612898	0.2	300	Spleen
BV421	CX3CR1	SA011F11	BioLegend	149023	0.2	300	Mock-infected brain
BV510	MHC-II	M5/114.15.2	BioLegend	107635	0.1	300	Spleen
BV570	CD4	RM4-5	BioLegend	100542	0.2	300	Beads
BV605	Ly6C	HK1.4	BioLegend	128036	0.05	400	WNV-infected brain[b]
BV650	Ly6G	1A8	BioLegend	127641	0.2	200	Beads
BV711	F4/80	BM8	BioLegend	123147	0.2	200	Beads
PE	P2RY12	S16007D	BioLegend	848004	0.2	300	Beads
PE/CF594	CD3ε	145-2C11	BD Bioscience	562286	0.2	200	Beads
PE/Cy5	NK1.1	PK136	BioLegend	108716	0.2	300	Beads
PE/Cy7	CD64	X54-5/7.1	BioLegend	139314	0.2	500	Beads
AF700	CD45	30-F11	BioLegend	103128	0.5	300	Spleen
APC/Cy7	CD86	GL-1	BioLegend	105030	0.2	100	Beads

Centrifuge antibodies for 5 min at 10,000 × *g*, 4°C (to sediment aggregates), before combining the required antibodies as a mixture in BD Horizon™ Brilliant Stain Buffer Plus (10 µl per sample). Top the remaining volume up with staining buffer (see recipe). Add 50 µl of solution per sample.

(*Continued*)

Table 3 Preparation of Reagents Used for Flow Cytometry Staining, *continued*

Intranuclear and intracellular staining mixture

Reagent	Marker	Clone	Company	Cat. no.	Mfr. conc. (mg/ml)	Dilution	Reference control
BV785	CD206	C068C2	BioLegend	141729	0.2	200	Beads
PerCP/Cy5.5	CD68	FA-11	BioLegend	137010	0.2	300	Spleen
APC	BrdU	N/A	BD Bioscience	51-23619L	0.2	100	Spleen

Centrifuge antibodies for 5 min at 10,000 × *g*, 4°C (to sediment aggregates), before combining the required antibodies as a mixture in 1× BD Perm/Wash™ Buffer.

[a] Zombie UV Fixable Viability Kit (reconstitute as per manufacturer instructions and store at −30°C).
[b] Spleen cells can be used instead of WNV brain cells. The reference type will be user specific and depend on the specific experimental model being used, as single-color reference controls must be as bright or brighter than the fluorescence intensity observed in multicolor brain sample.

We recommend fixing cells in BD Cytofix™ Fixation Buffer or 4% PFA prior to permeabilization with BD Cytofix/Cytoperm™ buffer because this increases the staining index of DAF-FM.

19. Top up with 150 µl staining buffer.
20. Spin 3 min at 800 × *g*, 4°C.
21. Resuspend cells in 200 µl staining buffer.

Store overnight.

Next day: Fixation and permeabilization for BrdU detection and intracellular staining

22. Spin 5 min at 800 × *g*, 4°C.
23. Resuspend cells in 50 µl of BD Cytofix/Cytoperm™ buffer.
24. Incubate for 20 min at room temperature in the dark.
25. Top up with 150 µl of 1× BD Perm/Wash™ buffer.
26. Spin 3 min at 800 × *g*, 4°C.

If you are staining for intracellular markers but not assessing cell proliferation (i.e., staining for the intracellular markers CD68 and CD206 but not for BrdU) perform steps 22-26, wash cells twice in 1× BD Perm/Wash™ buffer, and then proceed to steps 40-48 (i.e., skip steps 27-39).

Permeabilization for BrdU detection

27. Resuspend cells in 100 µl of BD Cytoperm™ Permeabilization Buffer Plus.
28. Cover samples with aluminum foil and incubate for 10 min on ice.
29. Top up with 150 µl of 1× BD Perm/Wash™ buffer.
30. Spin 3 min at 800 × *g*, 4°C.

Re-fixation

31. Resuspend cells in 50 µl of BD Cytofix/Cytoperm™ buffer.
32. Incubate for 5 min at room temperature in the dark.
33. Top up with 150 µl of 1× BD Perm/Wash™ buffer.
34. Spin 3 min at 800 × *g*, room temperature.

DNase digestion

35. Defrost 3 mg/ml DNase stock solution at room temperature and add PBS to make a 1 mg/ml solution.

    Defrost DNase during step 34.

36. Resuspend all samples in 100 µl DNase solution.

37. Incubate for 1 hr at 37°C.

38. Top up with 150 µl of 1× BD Perm/Wash™ buffer.

39. Spin 3 min 800 × *g*, room temperature.

Intracellular staining

40. Resuspend cells in 50 µl of intracellular antibody mixture (as per Table 3).

41. Incubate for 45 min at room temperature in the dark.

42. Top up with 150 µl of 1× BD Perm/Wash™ buffer.

43. Spin 3 min at 800 × *g*, room temperature.

44. Resuspend samples in 250 µl of 1× BD Perm/Wash™ buffer.

45. Spin 3 min at 800 × *g*, room temperature.

46. Resuspend samples in 250 µl of 1× BD Perm/Wash™ buffer.

47. Spin 3 min at 800 × *g*, room temperature.

48. Resuspend samples in 150 µl of staining buffer.

Analysis of samples on the spectral cytometer

NOTE: This protocol was developed on a 5-laser Cytek® Aurora; as such, this portion of the method is explicitly described for this instrument and software. If using a different analyzer, use the manufacturer-recommended process for setting up the experiment and optimizing the instrument settings; the controls required will remain the same.

49. Set up experiment in SpectroFlo® by adding fluorescent tags, samples, groups, and marker names in the "Edit experiment" portal. Use CytekAssaySettings for fluorescence detector gains (this does not require alteration if recommended antibody concentrations are used) and optimize FSC and SSC settings as required.

50. Add group-specific unstained reference controls for each treatment group in Spectroflo under the "Groups" in the "Edit experiment" portal. Right click the group folder and select "Unstained control." This is to ensure that you are unmixing with matched autofluorescence properties.

51. Add 50 µl staining buffer to a sample from each treatment group and run at a low flow rate to examine signal intensity to ensure that everything is on scale.

    The addition of staining buffer is to cover the boost volume and minimize cell loss.

52. Record reference controls, and all unstained cell controls.

53. Spectrally unmix by extracting multiple autofluorescent populations from each group-specific unstained controls (see Fig. 4). Right click the group-specific unstained control and follow prompts in SpectroFlo® to identify the unique autofluorescent populations.

    Brain cells are autofluorescent in the UV and violet channels. Autofluorescence extraction with multiple populations substantially improves staining resolution in these channels

as well as reducing unmixing error (Supporting Information 3 and 4). We recommend comparing NxN plots with and without autofluorescence extraction to determine if this improves unmixing for your sample type. See Unmixing in Critical parameters for more information.

In this assay, we identified three unique autofluorescent populations using channels V1 and UV16 in the mock-infected and infected brain (Fig. 4). Additional populations were not spectrally unique and had a lower mean fluorescence intensity (MFI) than their spectrally equivalent population, and thus were not used to extract autofluorescence.

54. Create an unmixed workspace for each experimental group.

As both experimental groups have different unique tags, these were unmixed separately (Supporting Information 5).

55. Record fully stained samples in the appropriate unmixed workspace.

Unmixing can also be performed after sample acquisition.

BASIC PROTOCOL 3

FLOW CYTOMETRIC SORTING OF MOUSE MICROGLIA FOR *EX VIVO* ANALYSIS

Isolating microglia is required for downstream assays requiring a pure population, including bulk RNA and scRNA analysis, proteomics, lipidomics, and functional assays. In this protocol, brain leukocytes are enriched using Basic Protocol 1, i.e., stained with surface markers, and sorted on the 7-laser BD Influx™ cell sorter. It is imperative to work efficiently and continuously (without interruption) to enhance yield and viability of cells. The viability of microglia also substantially decreases after cell sorting; thus, samples must be kept on ice in FBS. Due to the limited number of microglia that can be sorted from a brain, we recommend pooling samples before staining (see Critical Parameters and Troubleshooting for further recommendations). From a single mouse brain, expect to sort $\sim 8 \times 10^4$ according to instrument sort count. However, after spinning and counting cells with trypan blue, this usually equates to $\sim 2.5 \times 10^4$ viable cells.

Other microglial isolation processes, including magnetic separation and immunopanning, have also been described (Bohlen et al., 2019). Although these may be effective for the healthy brain, we do not recommend them for the inflamed brain, as microglia and infiltrating myeloid cells have overlapping expression of many proteins. Thus, it is important to assess the differential expression profiles via flow cytometry to accurately gate each population (see Fig. 3 for gating strategy).

We recommend sorting cells directly into the reagents required for the next steps to avoid cell loss from centrifuging and resuspending cells. For instance, for RNA extraction and lipidomics, we recommend sorting cells directly into TRIzol™ or methanol, respectively. We do not recommend culturing microglia after cell sorting, particularly from adult mice. As well as downregulating genes that inform their *in vivo* state, too few viable cells will remain after culturing. Previously published protocols recommend using juvenile rats for culturing sorted microglia (Bohlen et al., 2019).

If performing scRNA cell capture after sorting, we recommend barcoding microglia and monocyte populations with separate sample tags to ensure that these populations can be accurately identified during analysis. This is because microglia can downregulate microglia-specific genes that clearly distinguish them from non-resident myeloid cells during inflammation, significantly confounding cell type identification (Spiteri, Wishart et al., 2023). Although other scRNA cell capture systems are available, we recommend using the BD Rhapsody™ system and provide modifications to manufacturer protocols prior to cell capture to deal with the low cell numbers obtained from mouse brains.

Table 4 Antibodies Used for Cell Sorting

Surface antigen stain

Fluorophore	Marker	Clone	Company	Cat. no.	Mfr. conc. (mg/ml)	Dilution
BUV395	CD11b	M1/70	BD Bioscience	563553	0.2	400
BV421	CX3CR1	SA011F11	BioLegend	149023	0.2	300
BV605	Ly6C	HK1.4	BioLegend	128036	0.05	400
BV650	Ly6G	1A8	BioLegend	127641	0.2	200
PE	P2RY12	S16007D	BioLegend	848004	0.2	300
PE/Cy5	CD3ε	145-2C11	BioLegend	100310	0.2	200
	NK1.1	PK136	BioLegend	108716	0.2	300
PE/Cy7	CD64	X54-5/7.1	BioLegend	139314	0.2	500
AF700	CD45	30-F11	BioLegend	103128	0.5	300

Centrifuge antibodies for 5 min at 10,000 × *g*, 4°C (to sediment aggregates), before combining the required antibodies as a mixture in BD Horizon™ Brilliant Stain Buffer Plus (10 µl per sample). Top the remaining volume up with staining buffer (see recipe). Add 50 µl of solution per sample.

Materials

Viability/Fc blocking solution (see Table 3)
PBS (see recipe)
Fc block
UltraComp eBeads Compensation Beads (Thermo Fisher Scientific, cat. no. 01-2222-42), if using these as single-color reference controls
Staining buffer (see recipe)
Surface antigen stain mixture (see Table 4)
Fetal bovine serum (FBS), 4°C
BD Mouse Immune Single-Cell Multiplexing Kit (BD Bioscience, cat. no. 633793)
Trypan blue
Calcein AM (Thermo Fisher Scientific, cat. no. C1430)
Draq7™ (BD Bioscience, cat. no. 564904)
BD Rhapsody™ Cartridge Reagent Kit (BD Bioscience, cat. no. 633731)

Falcon® Tube with Cell Strainer Cap (Corning, cat. no. 352235) or equivalent 35-µm nylon mesh
5-ml sort tubes: Round-bottom polypropylene tubes (Corning cat. no. 352063)
7-laser BD Influx™ cell sorter (or equivalent)
INCYTO™ disposable hemocytometer (INCYTO, cat. no. DHC-N01-5)
BD Rhapsody™ Cartridge Kit (BD Bioscience, cat. no. 633733)
BD Rhapsody™ Scanner

Isolation of microglia

1. Perform steps 4-31 of Basic Protocol 1.

   You do not need to remeasure the volume in which your cells are resuspended or count your cells at this stage.

   If you are pooling brain samples to reduce processing time, we recommend adding two brains to a single C tube in 9 ml PBS and 1 ml of 10× collagenase/DNase.

2. Take an aliquot of each sample for staining controls (i.e., unstained brain cells and FMO controls; see Table 2).

Viability staining and blocking

3. Resuspend samples in 50 µl of viability/Fc blocking solution (see Table 3 for recipe) or 50 µl of Fc block in PBS (dilution 1/100; for single-color or unstained controls).

   If you are pooling samples and have >4 million cells, we recommend staining in 100 µl of viability/Fc block solution.

4. Incubate 30 min at 4°C.
5. Top up with 150 µl PBS.
6. Spin 5 min at 500 × *g*, 4°C.
7. If using compensation beads as single-color reference controls, vortex beads and distribute the relevant aliquots into tubes or plate.

Surface staining

8. Flick off supernatant and resuspend samples in 50 µl surface antigen stain mixture (for fully stained samples), staining buffer (for unstained controls and single color controls), or FMO mixtures (for FMO controls).

   If you are pooling samples and have >4 million cells we recommend staining in 100 µl of surface antigen stain mixture.

9. Incubate for 30 min at 4°C.
10. Top wells up with 150 µl staining buffer.
11. Spin 5 min at 500 × *g*, 4°C.
12. Resuspend cells in 250 µl staining buffer.
13. Spin 5 min at 500 × *g*, 4°C.
14. Resuspend cells in 250 µl staining buffer.
15. Filter samples into a 5-ml sort tube through nylon mesh or Falcon® Tube with Cell Strainer Cap.
16. Add 250 µl staining buffer to well plate or tube and transfer remaining cells into 5-ml sort tubes through nylon mesh or strainer cap.

    The final surface stain wash is performed in sort tubes to ensure that cells are sufficiently removed from staining plate or tube and that sorted cells are resuspended in an accurate volume (i.e., as opposed to losing sample when filtering cells in the final step).

17. Spin sort tubes 5 min at 500 × *g*, 4°C.
18. Resuspend cells in 250 µl staining buffer.

    As the number of cells is well below the recommended concentrations for any sort nozzle size, we recommend putting the cells in 250 µl if expecting $<2 \times 10^6$ cells or 500 µl if expecting $>2 \times 10^6$ and $<5 \times 10^6$ cells. Although this volume may take longer to sort due to low cell concentrations, it will reduce cell loss.

    To sort as many cells as possible, as well as be as quick as possible, we do not recommend counting your cells before sorting, as the concentration will always be well below the recommended range.

19. Set up cell sorter instrument, record compensation controls, compensate, and set up gating strategy.

    We recommend adding a final clean-up gate to ensure 100% exclusion of any NK1.1$^+$, CD3e$^+$, and Ly6G$^+$ cells from your microglia gate. If you are doing this for the first time, include FMO controls for these markers to ensure accurate gating. Sort cells from the final clean-up gate.

20. Collect sorted cells in 500 µl 4°C 100% FBS.

    If you are performing RNA extraction or lipidomics on the sorted cells, you can sort them directly into Trizol or methanol, respectively. Use the sort count as a relative cell number for downstream analysis, as re-counting cells after sorting for an accurate cell count will cause cell loss and death with the time and washing steps required. To determine sort efficiency, sort some of one sample into FBS to be re-recorded by the sorter.

21. Place samples on ice.

Single-cell barcoding with single-cell multiplexing kit

If performing scRNA-seq analysis using the BD RhapsodyTM System: Note that the manufacturer's protocol for single-cell multiplexing and staining with viability dyes (steps before cell capture) has been altered to solve the problem of the low cell numbers obtained from brain samples. Please refer to manufacturer documents for further details (Single Cell Labelling with the BD™ Single-Cell Multiplexing Kit and Single Cell Capture and cDNA Synthesis with the BD Rhapsody™ Single-Cell Analysis System).

22. Briefly spin sample tag tubes from BD Mouse Immune Single-Cell Multiplexing Kit.

23. Resuspend sample tags in 180 µl staining buffer.

24. Top up tubes containing sorted cells with 1 ml PBS to dilute FBS, and spin tubes 5 min at 500 × *g*, 4°C.

25. Aspirate supernatant carefully with a pipet or a vacuum on low.

    Leave dead volume to avoid pellet disturbance.

26. Resuspend cells in 0.5 volume of sample tag buffer (~90 µl) and transfer cells to a 96-well plate. Add the rest of the sample tag buffer (~90 µl) to wash and transfer the remaining cells out of the tube and into the well plate.

    Working in plate and flicking the supernatant helps retain cells and reduce cell loss.

    Alternatively, you can sort directly into a plate if the sort volume is <250 µl.

    Sample tag staining can also be performed with membrane staining prior to sorting—this will substantially reduce cell loss that occurs from the additional washes required for sequential staining. However, if two or more cell subsets from the same mouse are being sorted and barcoded uniquely, barcoding must be performed after cell sorting.

27. Incubate at room temperature for 20 min.

28. Top up with 150 µl staining buffer.

    We recommend using staining buffer that contains protein. The addition of FBS helps with cell retention. Do not use PBS alone as you will lose more cells.

29. Spin samples 5 min at 500 × *g*, 4°C.

30. Top up with 250 µl staining buffer.

31. Spin samples 5 min at 500 × *g*, 4°C.

32. Resuspend cells in 110 µl staining buffer.

33. Take 10 µl from each sample and perform a trypan blue count.

    If you do not need to pool samples in a particular ratio, there is no need to count cells at this stage.

34. Pool cells into a single tube in the desired ratio with an excess of the required cells.

Staining cells with viability markers

35. Add Calcein AM (final concentration 10 μM) and Draq7 (final concentration 1.5 μM) to pooled cells and mix with a micropipet.
36. Incubate in the dark for 5 min at 37°C.
37. Filter samples with nylon mesh or Falcon® Tube with Cell Strainer Cap.
38. Count cells using the Rhapsody scanner by pipetting 10 μl of sample into an INCYTO disposable hemocytometer.
39. Dilute or concentrate pooled cells for cartridge loading.

    Pooling cells in the volume required for cartridge loading will prevent the need to spin and reconcentrate cells, minimizing cell loss.

40. Proceed with manufacturer's instructions for cell capture. Details of sample processing for sequencing can be found in Spiteri, Wishart et al. (2023).

BASIC PROTOCOL 4

PROCESSING THE MOUSE BRAIN FOR IMAGING MASS CYTOMETRY FOR SPATIAL MICROGLIA ANALYSIS

The protocols described above involve dissociating the mouse brain into single-cell suspensions, disrupting the tissue microenvironment, and selecting mostly for leukocytes. After CNS perturbation, microglia undergo morphological alterations, including the adoption of a hypertrophied cell soma and shortened and thickened cytoplasmic projections. In addition, these cells can migrate and interact with other cells. Analysis of cell-type-specific interactions, co-localization of markers, and morphological changes, as well as regional analysis from tissue sections, can provide information on additional functional processes that cannot be determined from a single-cell suspension. Thus, below we describe methods to analyze the brain histologically.

The quality of a histological image in a tissue section is dependent on the preservation of cellular morphology, whereas the quality of immunohistochemical labeling depends on the retained or retrievable antigenicity of a tissue section. Satisfactory preservation of cellular morphology can be achieved by fixing tissues in formalin and embedding them in paraffin wax. However, this can significantly challenge the ability to visualize >40 epitopes simultaneously at imaging mass cytometry because this requires antigen-retrieval methods to be optimal for all markers (Ijsselsteijn et al., 2019). Thus, here we suggest freezing tissue to avoid the need for antigen-retrieval processes. We have performed a series of experiments to optimize preparation and fixation conditions on cryosections obtained from frozen mouse brains. The conditions included:

1. The use of PBS versus 2% versus 4% PFA perfused transcardially prior to tissue harvest.
2. The use of cryoprotection (10%, 20%, or 30% sucrose in PBS).
3. The use of a post-fixative (methanol, acetone, or 4% PFA) after cryosectioning.
4. Post-fixation of tissue in methanol/acetone/4% PFA immediately after cutting sections and/or after storing slides in the freezer before staining.

Overall, we found that 2% or 4% PFA perfusion with cryopreservation and section fixation with methanol results in the best morphology and antigenicity compared to all other conditions, although high-quality images can also be obtained without PFA perfusion or overnight fixation but with cryopreservation. The use of cryoprotection substantially increased the tissue quality, reducing the occurrence of holes or a "Swiss cheese" appearance in the brain tissue, as well as preserving the integrity of the cell nuclei. Thus, in instances where other assays need to be performed on the same animal, PFA perfusion can be omitted.

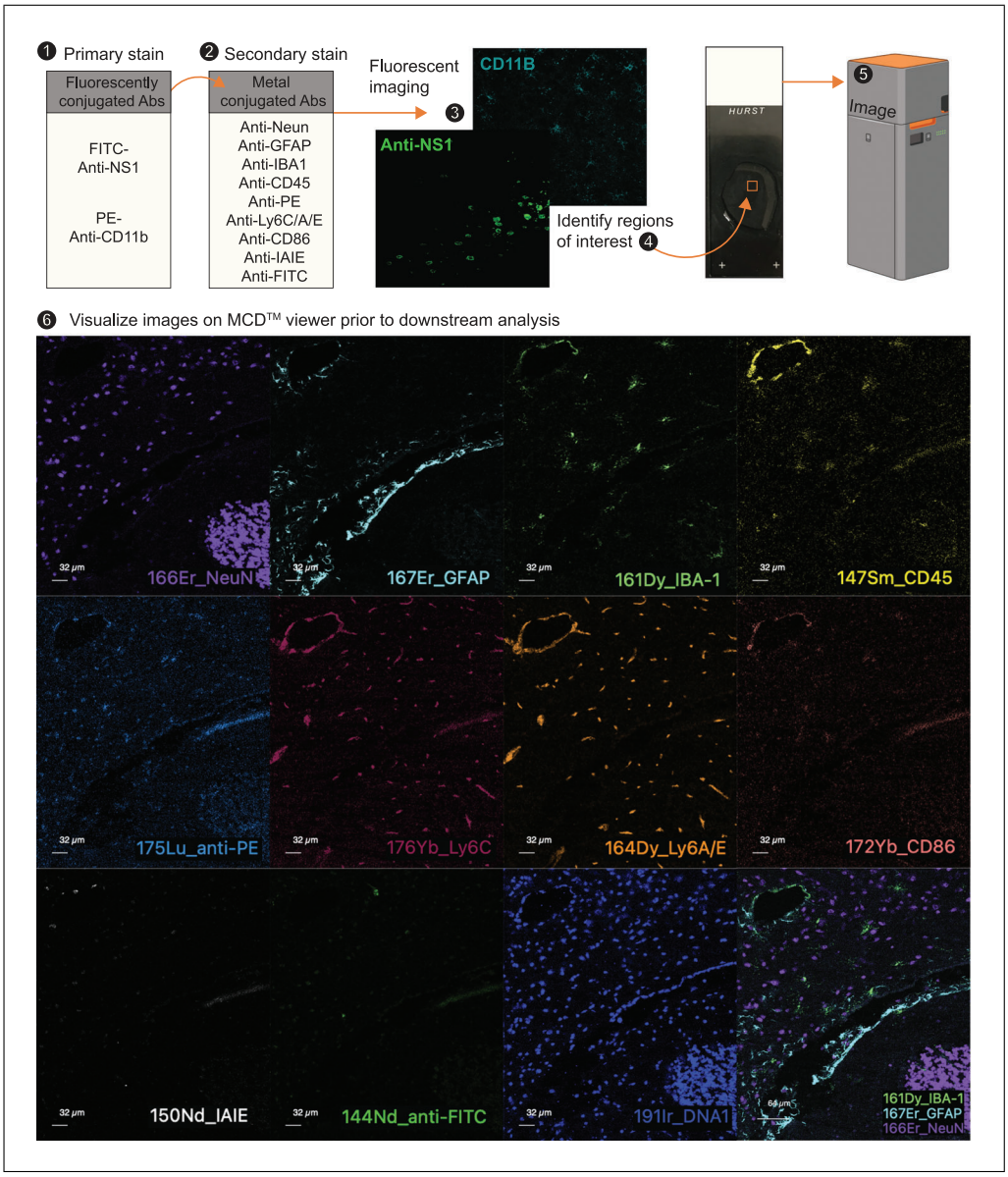

Figure 5 Schematic summarizing imaging mass cytometry protocol for acquisition of high-dimensional brain sections as described in Basic Protocol 4. Images were acquired from a WNV-infected mouse brain at 5 days post infection.

In this protocol, tissue sections are stained with fluorochrome-conjugated antibodies and subsequently labeled with metal-conjugated antibodies (Fig. 5). As such, sections can initially be imaged on a fluorescence microscope to identify regions of interest, before assessment by imaging mass cytometry. The panel of metal-conjugated antibodies described below is simple and intended to be expanded for inclusion of user-specific markers (Table 5).

Materials

Mice
PBS, ice cold
4% (w/v) PFA in PBS (see recipe), ice cold
10%, 20%, and 30% (w/v) sucrose solutions (see recipe), ice cold
Liquid nitrogen
Hexane (Sigma Aldrich, cat. no. 270504-2L)
O.C.T. compound (Tissue-Tek, cat. no. IA018)

Table 5 Reagents Used for Immunohistochemistry and Imaging Mass Cytometry

Primary fluorescent antibody mixture

Fluorophore	Marker	Clone	Company	Cat. no.	Mfr. conc. (mg/ml)	Dilution
PE	CD11b	M1/70	BioLegend	101208	0.2	200
FITC[a]	NS1[a]	N/A	N/A	N/A	N/A	100

Centrifuge antibodies for 5 min at 10,000 × *g*, 4°C (to sediment aggregates), before preparing aliquots of these in blocking buffer (see recipe). Add 150 µl of solution per tissue section.

Metal-conjugated antibody mixture[b]

Metal	Target	Clone	Company	Cat. no.	Mfr. conc. (mg/ml)	Amount per test (µl)
144Nd	FITC	FIT-22	BioLegend	408302	0.5	0.5
150Nd	MHC-II	M5/114.15.2	BD Bioscience	556999	0.5	0.5
153Eu	MAP2	SMI 52	BioLegend	801801	1	2
147Sm	CD45	30-F11	BD Bioscience	553076	0.5	0.5
161Dy	IBA-1	EPR16588	Abcam	AB178846	1.27	2
164Dy	Ly6A/E	D7	BioLegend	108102	0.5	0.5
166Er	NeuN	1B7	BioLegend	834501	1	2
167Er	GFAP	2E1.E9	BioLegend	644702	0.5	1
172Yb	CD86	GL1	BD Bioscience	553689	0.5	1
175Lu	Anti-PE	PE001	BioLegend	408102	0.5	1.3
176Yb	Ly6C	HK1.4	BioLegend	128002	0.5	0.5

Centrifuge antibodies for 5 min at 10,000 × *g*, 4°C (to sediment aggregates), before combining the required antibodies in blocking buffer (see recipe). Add 150 µl of solution per sample.

[a] Primary antibodies will be user specific. In this instance, NS1 was used to detect WNV in infected mice.
[b] Sydney Cytometry core facility conjugated antibodies to metal tags and titrated these as part of the Ramaciotti reagent bank service.

Methanol, prechilled to −30°C
Tris-buffered saline (TBS) solution (see recipe)
TBS/0.05% Tween-20 (TBST) solution (see recipe)
Blocking buffer: TBST (see recipe) with 10% fetal bovine serum (FBS)
Primary staining solution (see Table 5)
Secondary staining solution (see Table 5)
ProLong Gold Antifade Mountant with DAPI (Thermo Fisher Scientific, cat. no. P36931)

Forceps and dissection tools
5-ml tubes (1 per brain, for collection)
50-ml Falcon tube (3 per brain for each sucrose gradient)
Personal protective equipment for procedures
Liquid nitrogen canister
Cryomolds (mold with a well dimension of 25 × 25 × 5 mm for 2 brain sagittal sections and 17 × 17 × 5 mm for 1 sagittal section; Hurst Scientific, cat. no. 31052525 and 31051717)
Aluminum foil
Dry ice
Cryostat

Cryostat blades
Positively charged microscope slides
Slide rack
Hydrophobic pen (Sigma Aldrich, cat. no. Z377821-1EA)
Microscope (Olympus BX-51 microscope or equivalent)
Dark box
Cell-ID™ Iridium DNA intercalator (Standard BioTools, cat. no. 201192A)
Hyperion imaging system (Standard BioTools)

Isolating and fixing tissue

1. Anesthetize mice and then transcardially perfuse each mouse with 10 ml ice-cold PBS.
2. Perfuse mice with ice-cold 4% PFA in PBS.

   Defrost 4% PFA solution (on ice) prior to euthanasia.

   Step 2 can be omitted in instances where half the brain is used for another assay incompatible with fixation.

3. Isolate brain as described in Basic Protocol 1 (steps 5-10).

   Be extra careful to prevent disruption of the integrity of the brain.

4. Cut the brain sagittally in the median plane, and place both halves in ice-cold 4% PFA in a 5-ml tube. Leave at 4°C overnight.

Next day: Cryopreservation

5. Remove any excess 4% PFA by dabbing the brain tissue on a paper towel and transfer it into 15 ml ice-cold 10% sucrose solution.
6. Allow the tissue to sink to the bottom of the tube before transferring it into 15-ml ice-cold 20% sucrose solution.
7. Repeat step 6, but transfer the brain into 15 ml ice-cold 30% sucrose solution.

   The time taken to infiltrate the brain in a graded series of sucrose solutions at 4°C is as follows: 10% for 5-10 min, 20% for 4 hr, and 30% overnight.

Next day: Snap-freezing tissue

8. Fill the metal canister with liquid nitrogen.
9. Half fill a plastic beaker with hexane and place in liquid nitrogen. Allow time for hexane to equilibrate to liquid nitrogen temperature (~4 min).
10. Spread O.C.T. medium in a cryomold.

    Avoid air bubbles in the medium.

11. Blot tissue on a paper towel to remove excess liquid before placing it in the center of the cryomold containing O.C.T.

    Gently press down on the tissue, with each medial sagittal cut surface facing down and the lateral convex surface of the brain hemisphere facing up. Ensure the tissue is placed evenly at the bottom of the cryomold so the sections can be cut on the same plane.

12. Using forceps at room temperature, grasp the cryomold and plunge it into the hexane. Once the block is completely white, remove it.
13. Remove the frozen tissue block from the cryomold, wrap the tissue in foil, and place on dry ice.

14. Store tissue in a −80°C freezer. The tissue should not lose quality for at least 6 months at this temperature.

Sectioning

15. Attach the tissue block to the cryostat chuck by adding a small amount of O.C.T. to the chuck and placing the tissue on top.
16. Place tissue block under the weights on cryobar and allow it to equilibrate to chamber temperature (−30°C; 15 min).
17. Attach the chuck to the cutting head and blade to the blade holder.
18. Section brains in cryostat at 8-10 μm (−16°C tissue head, −30°C cryobar), placing sections on the positively charged slides.
19. Allow the sections to air-dry for 30 min at room temperature.
20. Store sections on the slides in the −80°C freezer or proceed with step 21.

Staining for immunohistochemistry

21. Place the slides containing the tissue sections in cold methanol for 10 min in –30°C freezer.
22. Rinse tissue slides in TBST three times for 3 min per wash.
23. Wipe any excess liquid from slide and around tissue section.
24. Circle the tissue section on the slide with a hydrophobic marker.
25. Add 150 μl blocking buffer within the hydrophobic circle to cover the enclosed section and let it sit for 30 min at room temperature.
26. Shake off excess solution.
27. Add 150 μl of primary fluorescent antibody mixture and let sit for 1 hr at room temperature (Table 5).

    This step can be done overnight at 4°C.

28. Rinse in TBST three times for 3 min per wash.

    Stop at step 28 for IMC staining.

29. Coverslip the section using DAPI antifade mounting medium.
30. Check the slide under microscope—for best images, take micrographs on the day of staining.
31. Store slides in the refrigerator in a dark box.

Staining for IMC

32. Proceed from step 28 if you are using fluorescently conjugated antibodies to define regions of interest for IMC acquisition.
33. Check slides under fluorescence microscope to ensure staining is visible.

    Do this quickly to prevent photobleaching.

34. Add 150 μl of secondary metal-tagged antibody mixture (Table 5) and let sit for 1 hr at room temperature.

    This step can also be done overnight at 4°C.

35. Rinse in TBST three times for 3 min per each wash.

36. Add 150 µl of iridium DNA intercalator (1/2000) in TBST and let sit for 30 min at room temperature.
37. Gently dip tissue slides in Milli-Q water. Repeat.

    Do this step carefully to prevent tissue section from falling off the slide.
38. Examine slides under a fluorescence microscope to determine regions of interest.
39. Air dry slide for 20 min at room temperature.
40. Image on the Hyperion or store in a sealed container at −20°C or room temperature for up to a month.

REAGENTS AND SOLUTIONS

BrdU stock solution, 2× (10 mg/ml)

Dissolve 250 mg 5-bromo-2′-deoxyuridine (BrdU) powder (Sigma Aldrich, cat. no. B5002-250MG) in 25 ml phosphate-buffered saline (PBS). Filter sterilize and prepare 0.5-ml aliquots in 1.5-ml tubes. Store up to 12 months at −80°C.

DNase and collagenase stock, 10×

Dissolve in 50 ml PBS:
0.05 g DNase I (Sigma Aldrich, cat. no. DN25)
0.5 g collagenase, type IV, from *Clostridium histolyticum* (Sigma Aldrich, cat. no. C5138)
Filter sterilize and prepare 5-ml aliquots in 5-ml tubes
Store up to 12 months at −30°C

The 10× stock can be refrozen after being thawed a maximum of two times.

DNase stock solution, 3× (3 mg/ml)

Dissolve 75 g DNase I powder (Sigma Aldrich, cat. no. DN25; 684.69 U/mg) in 25 ml PBS. Prepare 0.5-ml aliquots in 1.5-ml tubes. Store up to 12 months at −80°C.

DAF-FM DA stock solution

5 mM DAF-FM DA solution in DMSO (Sigma Aldrich, cat. no. D2321). Prepare aliquots. Prepare 5-µl aliquots in 0.2-ml tubes. Store up to 12 months at −30°C.

See Table 3 for preparation of DAF-FM working solution.

Paraformaldehyde (PFA) in PBS, 4% (w/v; phosphate-buffered paraformaldehyde)

Weigh out 8 g paraformaldehyde (Sigma Aldrich, cat. no. P6148) in a fume hood. Using a hotplate with integrated magnetic stirrer, combine paraformaldehyde and 100 ml Milli-Q water with a stirring bar and heat to 60°C. Add small pellets of sodium hydroxide (NaOH; Sigma Aldrich, cat. no. 221465), allowing each to dissolve before adding another, until solution clears. Alternatively, using a pipet, add 1 N NaOH dropwise until the solution clears. Cool the mixture and then combine with 100 ml 2× PBS, pH 7.4. Return the pH to 6.9 if necessary, using HCl added dropwise with a pipet. Store up to 2 weeks at 4°C or up to 12 months at −30°C.

Percoll solution, 26%

78.9 ml Percoll (Cytiva, cat. no. 17-0891-01)
30 ml 1.5 M NaCl (Sigma Aldrich, cat. no. 746398)
191.1 ml DMEM (Lonza Australia Pty Ltd, cat. no. 12-604F)
Keep sterile
Store up to 12 months at 4°C

Makes 300 ml, sufficient for 42 brains.

To prepare 1.5 M NaCl, dissolve 87.66 g NaCl in 1 L of Milli-Q water, filter, and keep sterile.

Percoll solution, 73%

73.1 ml Percoll (Cytiva, cat. no. 17-0891-01)
10 ml 1.5 M NaCl
16.9 ml Milli-Q water
Keep sterile
Store up to 12 months at 4°C

Makes 100 ml, sufficient for 33 brains.

To prepare 1.5 M NaCl, dissolve 87.66 g NaCl in 1 L of Milli-Q water, filter, and keep sterile.

Phosphate-buffered saline solution (PBS)

Combine 48 g Dulbecco's Phosphate Buffered-Saline (Sigma Aldrich, cat. no. D5652) with 5 liters Milli-Q water, mix a magnetic stirrer, and filter sterilize. Store up to 12 months at room temperature in 1-liter bottles.

Staining buffer

100 ml EDTA (ChemSupply, cat. no. EL026-2.5l-P)
50 ml fetal bovine serum
850 ml PBS

Sucrose solutions, 10%/20%/30%

10, 20, or 30 g sucrose (Sigma Aldrich, cat. no. S0389)
100 ml PBS

TBST (1× TBS with 0.05% Tween 20)

100 ml 10× TBS (see recipe)
900 ml Milli-Q water
500 µl Tween 20 (Sigma Aldrich, cat. no. P1379)

Tris-buffered saline (TBS), 10×

13.9 g Trizma® Base (Sigma Aldrich, cat. no. T1503)
60.6 g Trizma® hydrochloride (Sigma Aldrich, cat. no. T3253)
60.6 g NaCl
Make up to 1 L with Milli-Q water

Store up to 12 months at 4°C, and dilute to 1× on the day of staining.

COMMENTARY

Background Information

To elucidate the functions of cells in a disease setting, it is important to examine them using multiple modalities. This is because protein and RNA expression do not always correlate, and analysis of morphological data alone does not necessarily reveal precise cellular functions. We hope that the protocols detailed here will serve as a starting point for future experiments to enhance the understanding of microglial biology in disease.

The phenotypic convergence of microglia and monocyte-derived cells in CNS disease (Getts et al., 2008) has historically impeded the ability to accurately discriminate these populations for functional analysis. Advances in cytometry and computational analysis platforms have better elucidated the identities of these cell types (Ashhurst et al., 2021). This has enabled the development of more accurate gating strategies to phenotype and sort microglia and infiltrating myeloid cells (Spiteri, Wishart et al., 2023).

Advances in cell culture protocols that maintain microglial survival, viability, and *in vivo* status post isolation will provide powerful tools to address more mechanistic questions. Until then, other techniques not described here, including intravital imaging, spatial molecular imaging to transcriptionally profile cells *in situ*, and the use of transgenic mice or tissue culture, should also be explored to investigate specific aspects of microglia in disease.

Critical Parameters

Basic Protocol 1

Tissue processing preparation

To work as quickly as possible to prevent tissue degradation, all processing reagents and tubes should be prepared in advance of experiments. This includes preparing the 10× digestion cocktail, Percoll solutions, staining buffer, and PBS. Reagents should be prepared in separate aliquots in bottles/tubes to keep remaining stocks sterile. For every brain, label one C tube and two 15-ml tubes. The day before the experiment, pipet 4.5 ml of PBS into the C tubes and 5 ml of staining buffer into one 15-ml tube. Store these in the refrigerator at 4°C. Leave the other 15-ml tube at room temperature. On the morning of animal euthanasia, remove Percoll solutions from the refrigerator and set one centrifuge to 23°C and another to 4°C. Percoll gradient centrifugation is best performed at room temperature. The 10× enzyme digestion stock should also be thawed and left on ice until use.

Tissue processing

Excepting the Percoll separation centrifugation at room temperature, ensure that tissue and cells are kept on ice during all other processing steps.

Cell counts

It is important to remeasure the volume of staining buffer in which the brain cells are resuspended to get an accurate cell count. Residual volume can affect the final volume and confound cell counts, which are critical for data interpretation.

Basic Protocol 2

Titrating antibodies and optimizing reference controls

Antibodies should be titrated on the exact tissue of interest (including treatment or infection) before the experiment. The cell types infiltrating the brain and their expression profiles will determine the concentration of antibodies required as well as the type of reference control to use (i.e., cells or beads). The age and lot of an antibody may also impact antibody titrations. Although the dilution factors provided here can be used as a starting point, we recommend re-titrating your antibodies on the exact tissue you intend to analyze to achieve saturation labeling, as this enables more accurate quantitative evaluation of antigen expression. Best practices for antibody titration can be found in a number of publications (Brummelman et al., 2019; Ferrer-Font et al., 2021; Maciorowski et al., 2017; Mahnke & Roederer, 2007). As well as titrating antibodies, it is important to determine the type of reference controls to use (i.e., cells or beads) to get the best unmixing result. If you are working on the homeostatic brain and have very limited numbers of cells, consider processing extra brain tissue, collecting alternative tissue(s), or storing good-quality reference controls in reference libraries in the SpectroFlo® Software for use in unmixing future experiments.

Staining mixtures

Prepare staining solutions the day before. For viability/Fc block mixture, prepare PBS and Fc block the day before and add viability dye immediately before staining. To minimize antibody aggregates in premade cocktails, on the day of staining, spin the cocktail staining solution for 5 min at 10,000 rcf and be sure to retrieve the solution from the supernatant carefully, avoiding the bottom of the vial where aggregates could have pelleted.

Staining controls

Accurate assessment of cytometry data requires high-quality controls. Each time a new panel is to be implemented, it is vital to optimize the controls under the specific experimental conditions to be used. If you have not profiled cells from each experimental condition (i.e., untreated vs. treated, disease vs. healthy), we recommend recording unstained and FMO controls for each. Autofluorescence properties can change between experimental conditions, and thus it is important to record an unstained control for each using a group-specific unstained reference control tube. We also recommend using group-specific staining controls such as FMOs, as the staining background can also differ between experimental groups, making it difficult to interpret positive signals for proteins expressed at low levels. If you find no differences between experimental groups in your initial validation experiment, then a single representative of these cells can be used for future experiments.

Unmixing and autofluorescence extraction

Your unmixing results will depend on the quality of reference controls. We recommend control optimization to achieve the best unmixing outcome. Ferrer-Font et al. (2021) contains extensive details and user-friendly videos on troubleshooting and optimizing unmixing. In brief, cleanliness, accuracy of fluorochrome reference spectra, and correct gating in the

unmixing wizard are all critical for optimal unmixing. To evaluate unmixing accuracy, always visualize NxN plots on cleaned data using the gating sequence: time > singlet > non-debris > viable (dead cells will show compensation errors) > leukocytes, and look to ensure orthogonal staining and confirm that no hyper-negative events can be observed in your data (hyper-negative events are the result of over-unmixing from one fluorophore into other fluorophore[s]). If any unmixing errors are found, they must be resolved before you proceed with data analysis pipelines.

Unmixing with autofluorescence extraction substantially improves staining resolution in channels where brain cells are highly autofluorescent. This includes a significant portion of the UV and violet channels (Supporting Information 3 and 4). Although unmixing with group-specific unstained controls will improve population resolution, the best unmixing result with minimal unmixing errors (hyper-negatives, odd-shaped negatives, and compressed populations) can be achieved by extracting the multiple autofluorescent populations from each group-specific unstained control and saving a separate unmixed file for each experimental group (Fig. 4). It is important to note that autofluorescent tags from each brain sample (mock-infected vs. infected) are unique and cannot be used to unmix the non-corresponding sample type (Supporting Information 5). Lastly, although multiple autofluorescence extraction will substantially increase the complexity index of the panel (Supporting Information 5), it will nonetheless improve staining resolution and reduce unmixing errors (Supporting Information 3 and 4). As both mock-infected and infected brains were unmixed with the same number of autofluorescent tags, samples can be exported directly into the desired flow cytometry analysis program for downstream data analysis, including comparison of median fluorescence intensities and dimensionality reduction. If a different number of tags are used for each experimental group, you will need to use a parameter-removal tool after multi-autofluorescence unmixing to ensure files have the same numbers of parameters.

Basic Protocol 3

There are two critical parameters that should be considered prior to sorting cells from the brain: (1) microglia will begin to die as a result of the stresses experienced during sorting and (2) there will be a limited number of cells that can be sorted from a brain.

As such, we recommend pooling brain samples before staining to ensure that you have enough viable sorted cells for downstream assays. Tissue processing, staining, and downstream sorting processes must also be performed quickly and efficiently to maximize acquisition of data from viable cells. In our experience, using a U-bottom 96-well plate and flicking off the supernatant from the cell pellet (i.e., quickly tipping the plate upside down) in the washing and staining steps before and after the sort is the best procedure for reducing cell loss. You can also sort cells directly into a plate for labeling to avoid the extra centrifugation step required to transfer cells from a tube to a plate. If this is not possible because of the sample volume, use a polypropylene tube (5 ml or 1.2 ml) and aspirate the supernatant, ensuring that you leave sufficient residual volume to prevent pellet disturbance. Removing unnecessary steps, including tube changes, is critical to reducing cell loss after sorting. Lastly, we recommend using FBS or BSA in staining buffers before and after the sort. This will improve cell retention and viability.

Basic Protocol 4

Relative to the other protocols, Basic Protocol 4 has fewer critical parameters, as the tissue is fixed and sections from the same block can be recut to optimize staining controls. Following the above protocols should allow robust results. Always include isotype and unstained controls for accurate interpretation of positive signals.

Troubleshooting

See Table 6 for a list of common problems with the protocols, their causes, and potential solutions.

Understanding Results

Expected tissue processing cell counts and viability

Processing healthy murine brains using the protocol detailed here will provide ~500,000 cells with ~95% viability (as determined by trypan blue count immediately after processing). However, the viability will decrease during the staining process. You will typically identify 75%-90% live cells in the analyzed sample as determined with a viability dye. Moreover, cell counts may vary depending on the disease model used.

Table 6 Troubleshooting Guide for Processing Brain Tissue for Cytometric Analysis and Cell sorting

Problem	Possible cause	Solution
No clear Percoll interface	The Percoll interface has been disturbed	Collect liquid near the Percoll interface, and a clearer delineation between the two layers will eventually become visible. Alternatively, if you gently tilt the tube from side to side, you will see where the interface has formed. Collect the entire 26% Percoll layer.
73% Percoll does not pass through glass pipet	Percoll is stuck in the glass pipet	Gently lift up glass pipet slightly, by ~0.5 mm; or, without lifting the pipet, move the pipet around the tube.
Not enough viable sorted cells	Cells were lost during staining and washing steps	Use a U-bottom 96-well plate and a flicking technique to wash and stain. Ensure that you are using staining buffer with FBS or BSA. After processing brain samples, pool the cells into a single well before staining. The more cells in a well, the fewer cells will be lost during staining. Alternatively, to save processing time, process two brains together in a single C tube on the GentleMACS in 9 ml PBS and 1 ml collagenase/DNase mixture. Process all samples in the same way. Minimize time between sorting, staining, and downstream processes. Work as quickly as possible and keep all samples on ice.
Not enough brain cells to generate staining controls	Not enough brain cells were processed	Use cells isolated from the bone marrow or spleen as single-color compensation/reference controls if they are as bright as, or brighter than, staining observed in multicolor brain samples. For unstained controls, FMOs, and isotype controls, you will need to process extra brain tissue.
Collagenase/DNase perturbs expression of specific proteins of interest	Enzymes cleave surface proteins	We advise testing your full panel on enzyme-digested and non-digested tissue before your experiment. We have previously shown that TMEM119 and CD44 detection is reduced with this enzyme cocktail; however, the use of enzymatic dispersion gave us better viability, cell numbers, and staining. Alternatively, other brain processing kits are available from Miltenyi Biotec, including the Neural Tissue Dissociation kit.
Unmixing/ compensation error	Inappropriate reference controls were used	Use reference controls (i.e., beads or cells) that provide antigen expression that is brighter than or equal to that of fully stained samples.Use cells for fluorochromes that exhibit spectral shifting when bound to bead controls.Reference controls must have: (i) negative and positive populations well separated, with the positive cells as bright as or brighter than any staining observed in the samples, (ii) negative and positive particles with identical autofluorescence characteristics, (iii) a unique fluorescence spectrum that is identical to the one in the multicolor sample, and (iv) sufficient events. Unmixing accuracy should be checked on cleaned data using the following gating sequence: time > singlet > non-debris > viable (dead cells will show compensation errors) > leukocytes.
Poor resolution between populations	Antibodies have not been adequately titrated	All reagents should be titrated and tested on the specific tissue in advance of experiments.

Interpreting spectral cytometry results

Compensation

Data should be unmixed in SpectroFlo®, checked for unmixing error in NxN plots on cleaned data, and exported for analysis in the preferred cytometry program. Firstly, as shown in Figure 3, all samples are cleaned up using a time, singlet cell, and non-debris gate. The non-debris gate is then used to examine the compensation matrix. The live leukocyte gate can also be used to inspect the compensation matrix, as dead cells will show errors. The values in the compensation matrix should all be at zero. If you used appropriate reference controls, the unmixing process should be sufficient. However, you may observe compensation errors. Increase matrix numbers when data are under-compensated and reduce numbers when data are over-compensated (see more details at Brummelman et al., 2019; Maciorowski et al., 2017; Mahnke & Roederer, 2007), ensuring that you do not introduce biological error by incorrect spillover correction.

Gating

Once data have been compensated, return to samples and gate data down to populations of interest. Identification of microglia in the homeostatic brain is straight forward: these are "$CD45^{lo}CD11b^{+}P2RY12^{+}CX3CR1^{hi}F4/80^{+}CD64^{+}CD68^{+}$." They can be identified in multiple ways as they have marker profiles that definitively distinguish them from other myeloid cells in the brain ($CD206^{+}$ border-associated macrophages) and lymphocytes (Supporting Information 2). If you are working on an acute and severe inflammatory model, the gating strategy shown in Figure 3 may work for you. However, in neurogenerative conditions, infiltrating myeloid cells may differentiate further with more time spent in the brain, whereas microglia may upregulate so-called "activation markers" (Spiteri, Wishart et al., 2022). We recommend running dimensionality reduction on your data using t-distributed stochastic neighbor embedding (tSNE; van der Maaten & Hinton, 2008) or uniform manifold approximation and projection (UMAP; Mcinnes et al., 2018) visualization and overlaying final gated populations over these to determine if these gates are defined by a cluster. Usually in moderately inflamed conditions, microglia and monocyte-derived cells can be clearly distinguished. Gating strategy accuracy can be validated by (i) using a transgenic animal expressing fluorescent molecules under microglia- and/or monocyte-specific genes (Chen et al., 2020; Kim et al., 2021), (ii) blocking myeloid cell infiltration into the brain, (iii) performing an adoptive transfer of sorted cells, or (iv) injecting a cell tracker dye into the bloodstream to track recently infiltrating cells (Spiteri et al., 2021). To gate BrdU, DAF-FM, or other tertiary proteins of interest, always base this on the FMO for the specific experimental group and gate down to the specific population of interest.

Analysis

There are many great tools to analyze cytometric data, enabling population identification and/or statistics and/or dimensionality reduction in a single package. Firstly, we recommend gating your populations of interest and tabulating cell numbers, cell proportions, and median fluorescence intensity. Secondly, for visualization purposes, we recommend running dimensionality reduction and overlaying gated populations onto these to ensure that they align with your expert gating approach. You can also start with dimensionality reduction and run analysis on the FlowSOM clusters identified; however, we would strongly recommend validating these with expert gating to ensure you are not assessing artefacts. Other visualization approaches include, but are not limited to, heatmaps, bar graphs, bubble plots, and pie charts. High-dimensional analysis can be performed in R with packages such as Spectre (Ashhurst et al., 2021) or Seurat (Reyes et al., 2023) or using browser-based platforms such as the OMIC software from Dotmatics (*www.omiq.ai*, *www.dotmatics.com*) and Cytobank (Kotecha et al., 2010).

Cell sorting

One can expect to sort ~80,000 cells from a single brain of a C57BL/6 mouse, according to instrument sort count. Due to potential inaccuracies with sorting machines and cell loss following centrifuging and counting cells, this is generally reduced by approximately two-thirds (i.e., down to ~25,000 cells). If more cells are required, we recommend pooling samples, as well as having a spare sample to determine the sort accuracy. These sorted cells will need to be recorded to determine the percentage of cells that fall into your selected gate. If you are performing lipidomics, metabolomics, or qPCR, we recommend collecting cells directly into the medium required for cell storage or processing to prevent further cell loss from cell centrifugation. For scRNA-seq, cell sorting accuracy can

be determined by analyzing scRNA-seq data computationally.

Imaging

When imaging brain sections, examine isotype and unstained control samples first to determine whether you are visualizing true staining on fully-stained slides. Decide on the regions of interest and image accordingly. Merging of fluorescence images can be done with a number of programs, including ImageJ or FIJI (Rueden et al., 2017; Schindelin et al., 2012). For high-parameter analysis with multiple markers, particularly if using the Hyperion, cells need to be segmented. This can be done using Elastic (Berg et al., 2019) or Cell Profiler (Stirling et al., 2021). For a detailed review of these processes see (Milosevic, 2023).

Time Considerations

Basic Protocol 1

Preparation of tissue processing reagents and tubes can take some time; thus, it is recommended that reagents, labeled tubes, and antibody-staining cocktails are prepared in advance of experiments. The time required to process brain tissue following dissection will be a minimum of 1.5 hr; however, this will increase with increasing sample numbers and user inexperience. For a sample-number-extrapolated calculation, timing from an experienced technician is as follows: For each brain, it will take 30 min for tissue dissociation on the GentleMACS (max of 8 brains can be processed at a time), 2 min for Percoll layering, ~50 min for centrifugation without brake, 1 min to isolate brains cells per tube, and 15 min for additional spins throughout protocol. Cell counts will take ~3 min per sample, including mixing with trypan blue, loading, and cleaning hemocytometers.

Basic Protocol 2

Surface staining for spectral cytometry or cell sorting will take a minimum of 2 hr; however, this will also depend on the number of samples you are staining. If you are performing intracellular and/or intranuclear staining, that can be done the following day and will take an additional 1 and 3 hr, respectively. Obviously, intracellular and/or intranuclear staining are not compatible with live cell sorting.

To set up your experiment in SpectroFlo® Software, run your reference controls, and unmix will take ~45-60 min. From here, depending on the number of cells you are recording and the volume in which they are resuspended, it will take anywhere from 30 s to a few minutes to record a single sample. We recommend setting up your experiment file in SpectroFlo® Software or Cytek® Cloud in advance to enable prompt sample acquisition.

Basic Protocol 4

In general, we recommend scheduling at least 1.5 hr to set up your sorter, record compensation controls, compensate, and draw your gating strategy. However, increasing the number of fluorochromes and complexity of the gating strategy will add substantially more time. Actual sorting of each sample will take <5 min.

Basic Protocol 5

This protocol is the longest, spanning at least 3 days. On the first day, you will dissect the tissue and leave it overnight in PFA. On the second day, you will submerge the tissue in different concentrations of sucrose: 10% for 10 min, 20% for a few hours, and then 30% brain overnight. The next day (day 3), you will freeze the tissue in liquid nitrogen. You can cryosection the tissue on the same day or store it at −80°C. The efficiency of cryosectioning depends on the user's experience level and the number of sections required, with a minimum of 30 min per block for ~5-10 sections. Staining will take ~3.5 hr (for fixation, blocking, primary and/or secondary staining, and washing), and the time for imaging depends on the number of regions of interest and the fluorochromes.

Acknowledgments

NJCK was supported by National Health and Medical Research Council Project Grant 1088242 and by the Merridew Foundation. AGS was supported by an Australian Government Research Training Stipend Scholarship and The University of Sydney Postgraduate Merit Award. We would also like to acknowledge the Sydney Cytometry Core Research Facility and the University of Sydney's laboratory animal services, as well as Thomas Ashhurst and Steven Allen for assistance with cytometry applications.

Open access publishing facilitated by The University of Sydney, as part of the Wiley - The University of Sydney agreement via the Council of Australian University Librarians.

Author Contributions

Alanna G. Spiteri: Conceptualization; data curation; formal analysis; investigation; methodology; project administration; validation; visualization; writing—original draft; writing—review and editing.

Katherine R. Pilkington: Formal analysis; investigation; validation; visualization; writing—review and editing. **Claire L. Wishart:** Conceptualization; writing—review and editing. **Laurence Macia:** Supervision; writing—review and editing. **Nicholas J.C. King:** Conceptualization; funding acquisition; project administration; resources; supervision; writing—review and editing.

Conflict of Interest

Kate Pilkington is an employee of Cytek Biosciences, Inc., the manufacturer of the Aurora full-spectrum flow cytometer used in these studies.

Data Availability Statement

The datasets used and/or analyzed during the current study are available from the corresponding author upon reasonable request.

Supporting Information

cpz1985-sup-0001-SuppMat.pdf

The Supporting Information consists of the following five parts.

Supporting Information 1 Brain processing program for GentleMacs dissociation.

Supporting Information 2 Gating strategy used to identify immune cell populations in the homeostatic brain for analysis and cell sorting. (A) and (B) Quality control gates, including time, single cells, non-debris, and live cell gates, were applied before analyzing cell subsets. (B) Identification of neutrophils, microglia, NK cells, T cells, classic dendritic cells (cDC), and border-associated macrophages (BAMs) in the homeostatic brain. Single-cell brain suspensions from a healthy animal were analyzed on the 5-laser Cytek Aurora.

Supporting Information 3 Spectral unmixing with multiple autofluorescence extraction substantially improves staining resolution and reduces unmixing error in infected brain samples. (A)-(C) Dot plots showing data spectrally unmixed without autofluorescence (AF) extraction (A), with AF extraction using group-specific unstained controls (B), and with multiple AF extraction (C). Arrows show unmixing error.

Supporting Information 4 Spectral unmixing with multiple autofluorescence extraction substantially improves staining resolution and reduces unmixing error in healthy brain samples. (A)-(C) Dot plots showing data spectrally unmixed without autofluorescence (AF) extraction (A), with AF extraction using group-specific unstained controls (B), and with multiple AF extraction (C). Arrows show unmixing error.

Supporting Information 5 Similarity index for a 19- to 20-color brain panel with and without multiple autofluorescence extraction. (A) Normalized median florescence intensity (MFI) for three distinct autofluorescent (AF) tags in the mock-infected and infected brain. (B)-(E) Similarity and complexity indexes with and without multiple AF extraction and intranuclear staining with BrdU.

Literature Cited

Ashhurst, T. M., Cox, D. A., Smith, A. L., & King, N. J. C. (2019). Analysis of the murine bone marrow hematopoietic system using mass and flow cytometry. *Methods in Molecular Biology*, *1989*, 159–192. https://doi.org/10.1007/978-1-4939-9454-0_12

Ashhurst, T. M., Marsh-Wakefield, F., Putri, G. H., Spiteri, A. G., Shinko, D., Read, M. N., Smith, A. L., & King, N. J. C. (2021). Integration, exploration, and analysis of high-dimensional single-cell cytometry data using Spectre. *Cytometry Part A: The Journal of the International Society for Analytical Cytology*, *101*(3), 237–253. https://doi.org/10.1002/cyto.a.24350

Bassetti, C. L. A., Endres, M., Sander, A., Crean, M., Subramaniam, S., Carvalho, V., Di Liberto, G., Franco, O. H., Pijnenburg, Y., Leonardi, M., & Boon, P. (2022). The European Academy of Neurology Brain Health Strategy: One brain, one life, one approach. *European Journal of Neurology*, *29*, 2559–2566. https://doi.org/10.1111/ene.15391

Bennett, F. C., Bennett, M. L., Yaqoob, F., Mulinyawe, S. B., Grant, G. A., Hayden Gephart, M., Plowey, E. D., & Barres, B. A. (2018). A combination of ontogeny and CNS environment establishes microglial identity. *Neuron*, *98*, 1170–1183.e8. https://doi.org/10.1016/j.neuron.2018.05.014

Bennett, M. L., Bennett, F. C., Liddelow, S. A., Ajami, B., Zamanian, J. L., Fernhoff, N. B., Mulinyawe, S. B., Bohlen, C. J., Adil, A., Tucker, A., Weissman, I. L., Chang, E. F., Li, G., Grant, G. A., Hayden Gephart, M. G., & Barres, B. A. (2016). New tools for studying microglia in the mouse and human CNS. *Proceedings of the National Academy of Sciences of the United States of America*, *113*, E1738–E1746.

Berg, S., Kutra, D., Kroeger, T., Straehle, C. N., Kausler, B. X., Haubold, C., Schiegg, M., Ales, J., Beier, T., Rudy, M., Eren, K., Cervantes, J. I., Xu, B., Beuttenmueller, F., Wolny, A., Zhang, C., Koethe, U., Hamprecht, F. A., & Kreshuk, A. (2019). ilastik: Interactive machine learning for (bio)image analysis. *Nature Methods*, *16*, 1226–1232. https://doi.org/10.1038/s41592-019-0582-9

Bohlen, C. J., Bennett, F. C., & Bennett, M. L. (2019). Isolation and culture of microglia. *Current Protocols in Immunology*, *125*, e70. https://doi.org/10.1002/cpim.70

Bohlen, C. J., Bennett, F. C., Tucker, A. F., Collins, H. Y., Mulinyawe, S. B., & Barres, B. A. (2017). Diverse requirements for microglial survival, specification, and function revealed by defined-medium cultures. *Neuron*, *94*, 759–773.e8. https://doi.org/10.1016/j.neuron.2017.04.043

Brummelman, J., Haftmann, C., Nunez, N. G., Alvisi, G., Mazza, E. M. C., Becher, B., & Lugli, E. (2019). Development, application and computational analysis of high-dimensional fluorescent antibody panels for single-cell flow cytometry. *Nature Protocols*, *14*, 1946–1969. https://doi.org/10.1038/s41596-019-0166-2

Butovsky, O., Jedrychowski, M. P., Moore, C. S., Cialic, R., Lanser, A. J., Gabriely, G., Koeglsperger, T., Dake, B., Wu, P. M., Doykan, C. E., Fanek, Z., Liu, L., Chen, Z., Rothstein, J. D., Ransohoff, R. M., Gygi, S. P., Antel, J. P., & Weiner, H. L. (2014). Identification of a unique TGF-β-dependent molecular and functional signature in microglia. *Nature Neuroscience*, *17*, 131–143. https://doi.org/10.1038/nn.3599

Chen, H.-R., Sun, Y.-Y., Chen, C.-W., Kuo, Y.-M., Kuan, I. S., Tiger Li, Z. R., Short-Miller, J. C., Smucker, M. R., & Kuan, C. Y. (2020). Fate mapping via CCR2-CreER mice reveals monocyte-to-microglia transition in development and neonatal stroke. *Science Advances*, *6*, eabb2119. https://doi.org/10.1126/sciadv.abb2119

Depaula-Silva, A. B., Gorbea, C., Doty, D. J., Libbey, J. E., Sanchez, J. M. S., Hanak, T. J., Cazalla, D., & Fujinami, R. S. (2019). Differential transcriptional profiles identify microglial- and macrophage-specific gene markers expressed during virus-induced neuroinflammation. *Journal of Neuroinflammation*, *16*, 152. https://doi.org/10.1186/s12974-019-1545-x

Feigin, V. L., Vos, T., Nichols, E., Owolabi, M. O., Carroll, W. M., Dichgans, M., Deuschl, G., Parmar, P., Brainin, M., & Murray, C. (2020). The global burden of neurological disorders: Translating evidence into policy. *Lancet Neurology*, *19*, 255–265. https://doi.org/10.1016/S1474-4422(19)30411-9

Fekete, R., Cserep, C., Lenart, N., Toth, K., Orsolits, B., Martinecz, B., Mehes, E., Szabo, B., Nemeth, V., Gonci, B., Sperlagh, B., Boldogkoi, Z., Kittel, A., Baranyi, M., Ferenczi, S., Kovacs, K., Szalay, G., Rozsa, B., Webb, C., … Denes, A. (2018). Microglia control the spread of neurotropic virus infection via P2Y12 signalling and recruit monocytes through P2Y12-independent mechanisms. *Acta Neuropathologica*, *136*, 461–482. https://doi.org/10.1007/s00401-018-1885-0

Ferrer-Font, L., Kraker, G., Hally, K. E., & Price, K. M. (2023). Ensuring full spectrum flow cytometry data quality for high-dimensional data analysis. *Current Protocols*, *3*, e657. https://doi.org/10.1002/cpz1.657

Ferrer-Font, L., Small, S. J., Lewer, B., Pilkington, K. R., Johnston, L. K., Park, L. M., Lannigan, J., Jaimes, M. C., & Price, K. M. (2021). Panel optimization for high-dimensional immunophenotyping assays using full-spectrum flow cytometry. *Current Protocols*, *1*, e222. https://doi.org/10.1002/cpz1.222

Fox, A., Dutt, T. S., Karger, B., Obregon-Henao, A., Anderson, G. B., & Henao-Tamayo, M. (2020). Acquisition of high-quality spectral flow cytometry data. *Current Protocols in Cytometry*, *93*, e74. https://doi.org/10.1002/cpcy.74

Garcia, J. A., Cardona, S. M., & Cardona, A. E. (2014). Isolation and analysis of mouse microglial cells. *Current Protocols in Immunology*, *104*, 14.35.1–14.35.15. https://doi.org/10.1002/0471142735.im1435s104

Getts, D. R., Terry, R. L., Getts, M. T., Müller, M., Rana, S., Deffrasnes, C., Ashhurst, T. M., Radford, J., Hofer, M., & Thomas, S. (2012). Targeted blockade in lethal West Nile virus encephalitis indicates a crucial role for very late antigen (VLA)-4-dependent recruitment of nitric oxide-producing macrophages. *Journal of Neuroinflammation*, *9*, 246. https://doi.org/10.1186/1742-2094-9-246

Getts, D. R., Terry, R. L., Getts, M. T., Müller, M., Rana, S., Shrestha, B., Radford, J., Van Rooijen, N., Campbell, I. L., & King, N. J. C. (2008). Ly6c^{+} "inflammatory monocytes" are microglial precursors recruited in a pathogenic manner in West Nile virus encephalitis. *The Journal of Experimental Medicine*, *205*, 2319–2337. https://doi.org/10.1084/jem.20080421

Gosselin, D., Skola, D., Coufal, N. G., Holtman, I. R., Schlachetzki, J. C. M., Sajti, E., Jaeger, B. N., O'Connor, C., Fitzpatrick, C., Pasillas, M. P., Pena, M., Adair, A., Gonda, D. D., Levy, M. L., Ransohoff, R. M., Gage, F. H., & Glass, C. K. (2017). An environment-dependent transcriptional network specifies human microglia identity. *Science*, *356*, eaal3222. https://doi.org/10.1126/science.aal3222

Greter, M., Lelios, I., & Croxford, A. L. (2015). Microglia versus myeloid cell nomenclature during brain inflammation. *Frontiers in Immunology*, *6*, 249. https://doi.org/10.3389/fimmu.2015.00249

Ijsselsteijn, M. E., Van Der Breggen, R., Farina Sarasqueta, A., Koning, F., & De Miranda, N. (2019). A 40-marker panel for high dimensional characterization of cancer immune microenvironments by imaging mass cytometry. *Frontiers in Immunology*, *10*, 2534. https://doi.org/10.3389/fimmu.2019.02534

Jordão, M. J. C., Sankowski, R., Brendecke, S. M., Sagar, Locatelli, G., Tai, Y. H., Tay, T. L., Schramm, E., Armbruster, S., Hagemeyer, N., Groß, O., Mai, D., Çiçek, Ö., Falk, T., Kerschensteiner, M., Grün, D., & Prinz, M. (2019). Single-cell profiling identifies myeloid cell subsets with distinct fates during neuroinflammation. *Science*, *363*, eaat7554. https://doi.org/10.1126/science.aat7554

Keren-Shaul, H., Spinrad, A., Weiner, A., Matcovitch-Natan, O., Dvir-Szternfeld,

R., Ulland, T. K., David, E., Baruch, K., Lara-Astaiso, D., Toth, B., Itzkovitz, S., Colonna, M., Schwartz, M., & Amit, I. (2017). A unique microglia type associated with restricting development of Alzheimer's disease. *Cell*, *169*, 1276–1290.e17. https://doi.org/10.1016/j.cell.2017.05.018

Kharraz, Y., Lukesova, V., Serrano, A. L., Davison, A., & Munoz-Canoves, P. (2022). Full spectrum cytometry improves the resolution of highly autofluorescent biological samples: Identification of myeloid cells in regenerating skeletal muscles. *Cytometry Part A: The journal of the International Society for Analytical Cytology*, *101*, 862–876. https://doi.org/10.1002/cyto.a.24568

Kim, J. S., Kolesnikov, M., Peled-Hajaj, S., Scheyltjens, I., Xia, Y., Trzebanski, S., Haimon, Z., Shemer, A., Lubart, A., Van Hove, H., Chappell-Maor, L., Boura-Halfon, S., Movahedi, K., Blinder, P., & Jung, S. (2021). A binary cre transgenic approach dissects microglia and CNS border-associated macrophages. *Immunity*, *54*, 176–190.e7. https://doi.org/10.1016/j.immuni.2020.11.007

Kotecha, N., Krutzik, P. O., & Irish, J. M. (2010). Web-based analysis and publication of flow cytometry experiments. *Current Protocols in Cytometry*, *53*, 10.17.1–10.17.24. https://doi.org/10.1002/0471142956.cy1017s53

Krasemann, S., Madore, C., Cialic, R., Baufeld, C., Calcagno, N., El Fatimy, R., Beckers, L., O'Loughlin, E., Xu, Y., Fanek, Z., Greco, D. J., Smith, S. T., Tweet, G., Humulock, Z., Zrzavy, T., Conde-Sanroman, P., Gacias, M., Weng, Z., Chen, H., … Butovsky, O. (2017). The TREM2-APOE pathway drives the transcriptional phenotype of dysfunctional microglia in neurodegenerative diseases. *Immunity*, *47*, 566–581.e9. https://doi.org/10.1016/j.immuni.2017.08.008

Lei, F., Cui, N., Zhou, C., Chodosh, J., Vavvas, D. G., & Paschalis, E. I. (2020). CSF1R inhibition by a small-molecule inhibitor is not microglia specific; affecting hematopoiesis and the function of macrophages. *Proceedings of the National Academy of Sciences of the United States of America*, *117*, 23336–23338. https://doi.org/10.1073/pnas.1922788117

Lewis, N. D., Hill, J. D., Juchem, K. W., Stefanopoulos, D. E., & Modis, L. K. (2014). RNA sequencing of microglia and monocyte-derived macrophages from mice with experimental autoimmune encephalomyelitis illustrates a changing phenotype with disease course. *Journal of Neuroimmunology*, *277*, 26–38. https://doi.org/10.1016/j.jneuroim.2014.09.014

Look, T., Meister, H., Weller, M., & Weiss, T. (2023). Protocol for the expansion of mouse immune effector cells for in vitro and in vivo studies. *STAR Protocols*, *4*, 102700. https://doi.org/10.1016/j.xpro.2023.102700

Maciorowski, Z., Chattopadhyay, P. K., & Jain, P. (2017). Basic multicolor flow cytometry. *Current Protocols in Immunology*, *117*, 5.4.1–5.4.38. https://doi.org/10.1002/cpim.26

Mahnke, Y. D., & Roederer, M. (2007). Optimizing a multicolor immunophenotyping assay. *Clinics in Laboratory Medicine*, *27*, 469–+. https://doi.org/10.1016/j.cll.2007.05.002

Manglani, M., Gossa, S., & McGavern, D. B. (2018). Leukocyte isolation from brain, spinal cord, and meninges for flow cytometric analysis. *Current Protocols in Immunology*, *121*, e44. https://doi.org/10.1002/cpim.44

Mcinnes, L., Healy, J., & Melville, J. (2018). UMAP: Uniform manifold approximation and projection for dimension reduction [Preprint]. *arXiv*, 1802.03426. https://doi.org/10.48550/arXiv.1802.03426

Mcquade, A., & Blurton-Jones, M. (2019). Microglia in Alzheimer's disease: Exploring how genetics and phenotype influence risk. *Journal of Molecular Biology*, *431*, 1805–1817. https://doi.org/10.1016/j.jmb.2019.01.045

Miller, S. D., Karpus, W. J., & Davidson, T. S. (2010). Experimental autoimmune encephalomyelitis in the mouse. *Current Protocols in Immunology*, *Chapter 15*, 15.1.1–15.1.20.

Milosevic, V. (2023). Different approaches to imaging mass cytometry data analysis. *Bioinformatics Advances*, *3*, vbad046. https://doi.org/10.1093/bioadv/vbad046

Niewold, P., Ashhurst, T. M., Smith, A. L., & King, N. J. C. (2020). Evaluating spectral cytometry for immune profiling in viral disease. *Cytometry Part A: The Journal of the International Society for Analytical Cytology*, *97*, 1165–1179. https://doi.org/10.1002/cyto.a.24211

Nimmerjahn, A., Kirchhoff, F., & Helmchen, F. (2005). Resting microglial cells are highly dynamic surveillants of brain parenchyma in vivo. *Science*, *308*, 1314–1318. https://doi.org/10.1126/science.1110647

Nolan, J. P., & Condello, D. (2013). Spectral flow cytometry. *Current Protocols in Cytometry*, *63*, 1.27.1–1.27.13. https://doi.org/10.1002/0471142956.cy0127s63

Reyes, J. G. A., Ni, D., Santner-Nanan, B., Pinget, G. V., Kraftova, L., Ashhurst, T. M., Marsh-Wakefield, F., Wishart, C. L., Tan, J., Hsu, P., King, N. J. C., Macia, L., & Nanan, R. (2023). A unique human cord blood $CD8^+CD45RA^+CD27^+CD161^+$ T cell subset identified by flow cytometric data analysis using Seurat [Preprint]. *BioRxiv*, 2023.08.01.549954. https://doi.org/10.1101/2023.08.01.549954

Rueden, C. T., Schindelin, J., Hiner, M. C., Dezonia, B. E., Walter, A. E., Arena, E. T., & Eliceiri, K. W. (2017). ImageJ2: ImageJ for the next generation of scientific image data. *BMC Bioinformatics*, *18*, 529. https://doi.org/10.1186/s12859-017-1934-z

Schindelin, J., Arganda-Carreras, I., Frise, E., Kaynig, V., Longair, M., Pietzsch, T., Preibisch, S., Rueden, C., Saalfeld, S., Schmid, B., Tinevez, J. Y., White, D. J., Hartenstein, V., Eliceiri, K., Tomancak, P., & Cardona, A. (2012). Fiji: An open-source platform for

biological-image analysis. *Nature Methods*, *9*, 676–682. https://doi.org/10.1038/nmeth.2019

Sharp, R. C., Guenther, D. T., & Farrer, M. J. (2023). Experimental procedures for flow cytometry of wild-type mouse brain: A systematic review. *Frontiers in Immunology*, *14*, 1281705. https://doi.org/10.3389/fimmu.2023.1281705

Song, H., McEwen, H. P., Duncan, T., Lee, J. Y., Teo, J. D., & Don, A. S. (2021). Sphingosine kinase 2 is essential for remyelination following cuprizone intoxication. *Glia*, *69*, 2863–2881. https://doi.org/10.1002/glia.24074

Spangenberg, E., Severson, P. L., Hohsfield, L. A., Crapser, J., Zhang, J., Burton, E. A., Zhang, Y., Spevak, W., Lin, J., Phan, N. Y., Habets, G., Rymar, A., Tsang, G., Walters, J., Nespi, M., Singh, P., Broome, S., Ibrahim, P., Zhang, C., … Green, K. N. (2019). Sustained microglial depletion with CSF1R inhibitor impairs parenchymal plaque development in an Alzheimer's disease model. *Nature Communications*, *10*, 3758. https://doi.org/10.1038/s41467-019-11674-z

Spiteri, A. G., & King, N. J. C. (2023). Putting PLX5622 into perspective: Microglia in central nervous system viral infection. *Neural Regeneration Research*, *18*, 1269–1270.

Spiteri, A. G., Ni, D., Ling, Z. L., Macia, L., Campbell, I. L., Hofer, M. J., & King, N. J. C. (2022). PLX5622 reduces disease severity in lethal CNS infection by off-target inhibition of peripheral inflammatory monocyte production. *Frontiers in Immunology*, *13*, 851556. https://doi.org/10.3389/fimmu.2022.851556

Spiteri, A. G., Terry, R. L., Wishart, C. L., Ashhurst, T. M., Campbell, I. L., Hofer, M. J., & King, N. J. C. (2021). High-parameter cytometry unmasks microglial cell spatio-temporal response kinetics in severe neuroinflammatory disease. *Journal of Neuroinflammation*, *18*, 166. https://doi.org/10.1186/s12974-021-02214-y

Spiteri, A. G., Van Vreden, C., Ashhurst, T. M., Niewold, P., & King, N. J. C. (2023). Clodronate is not protective in lethal viral encephalitis despite substantially reducing inflammatory monocyte infiltration in the CNS. *Frontiers in immunology*, *14*, 1203561. https://doi.org/10.3389/fimmu.2023.1203561

Spiteri, A. G., Wishart, C. L., & King, N. J. C. (2020). Immovable object meets unstoppable force? Dialogue between resident and peripheral myeloid cells in the inflamed brain. *Frontiers in Immunology*, *11*, 600822. https://doi.org/10.3389/fimmu.2020.600822

Spiteri, A. G., Wishart, C. L., Ni, D., Viengkhou, B., Macia, L., Hofer, M. J., & King, N. J. C. (2023). Temporal tracking of microglial and monocyte single-cell transcriptomics in lethal flavivirus infection. *Acta Neuropathologica Communications*, *11*, 60. https://doi.org/10.1186/s40478-023-01547-4

Spiteri, A. G., Wishart, C. L., Pamphlett, R., Locatelli, G., & King, N. J. C. (2022). Microglia and monocytes in inflammatory CNS disease: Integrating phenotype and function. *Acta Neuropathologica*, *143*, 179–224. https://doi.org/10.1007/s00401-021-02384-2

Stirling, D. R., Swain-Bowden, M. J., Lucas, A. M., Carpenter, A. E., Cimini, B. A., & Goodman, A. (2021). CellProfiler 4: Improvements in speed, utility and usability. *BMC Bioinformatics*, *22*, 433. https://doi.org/10.1186/s12859-021-04344-9

Van Der Maaten, L., & Hinton, G. (2008). Visualizing data using t-SNE. *Journal of Machine Learning Research*, *9*, 2579–2605.

Vankriekelsvenne, E., Chrzanowski, U., Manzhula, K., Greiner, T., Wree, A., Hawlitschka, A., Llovera, G., Zhan, J., Joost, S., Schmitz, C., Ponsaerts, P., Amor, S., Nutma, E., Kipp, M., & Kaddatz, H. (2022). Transmembrane protein 119 is neither a specific nor a reliable marker for microglia. *Glia*, *70*, 1170–1190. https://doi.org/10.1002/glia.24164

Werner, Y., Mass, E., Ashok Kumar, P., Ulas, T., Handler, K., Horne, A., Klee, K., Lupp, A., Schutz, D., Saaber, F., Redecker, C., Schultze, J. L., Geissmann, F., & Stumm, R. (2020). Cxcr4 distinguishes HSC-derived monocytes from microglia and reveals monocyte immune responses to experimental stroke. *Nature Neuroscience*, *23*, 351–362. https://doi.org/10.1038/s41593-020-0585-y

West, P. K., Mccorkindale, A. N., Guennewig, B., Ashhurst, T. M., Viengkhou, B., Hayashida, E., Jung, S. R., Butovsky, O., Campbell, I. L., & Hofer, M. J. (2022). The cytokines interleukin-6 and interferon-alpha induce distinct microglia phenotypes. *Journal of Neuroinflammation*, *19*, 96. https://doi.org/10.1186/s12974-022-02441-x

Wishart, C. L., Spiteri, A. G., Locatelli, G., & King, N. J. C. (2022). Integrating transcriptomic datasets across neurological disease identifies unique myeloid subpopulations driving disease-specific signatures. *Glia*, *71*(4), 904–925. https://doi.org/10.1002/glia.24314